Seminar Proceedings

EAWE
European Academy of Wind Energy

NTNU
Norwegian University of Science and Technology

European Academy of Wind Energy

6th PhD Seminar on Wind Energy in Europe

NTNU Trondheim, Norway

30th September and 1st October 2010

Statkraft

NTNU
Norwegian University of Science and Technology

European Academy of Wind Energy

Norwegian University of Science and Technology

Seminar Proceedings

6th EAWE PhD Seminar on Wind Energy in Europe

Norwegian University of Science and Technology (NTNU)

30th September and 1st October 2010

Trondheim, Norway

Organised by NTNU for

European Academy of Wind Energy (EAWE)

Trondheim, September 2010

European Academy of Wind Energy

Norwegian University of Science and Technology

EAWE Steering Committee

President:
Mr. Félix Avia Aranda
National Renewable Energy Centre (CENER), Spain

Vice President:
Prof. Peter Tavner
Durham University, UK

Secretary:
Maren Wagner

Local Organising Committee

Chair:
Prof. Geir Moe
NTNU, Norway

Editors:
Mr. Daniel Zwick
NTNU, Norway

Ms. Marit Irene Kvittem
NTNU, Norway

Mr. Raymundo Torres Olguin
NTNU, Norway

1st Edition, Trondheim, Norwegian University of Science and Technology, 2010

Printed: 150 copies
Press date: September 2010

Contents

Part 1

Session 1 - Introduction to Wind Energy

- Hybrid life-cycle assessment of wind power
  Anders Arvesen, NTNU
- Wind energy research in the age of massively parallel computers
  Michael Muskulus, NTNU
- The correlation between Wind Turbine Turbulence and Failure-Preliminary Work
  Peter Tavner, Durham University
- Forecasting of wind turbine loads based on SCADA data
  Claudia Hofemann, TU Delft

Hybrid life-cycle assessment of wind power

Anders Arvesen, Edgar Hertwich

Industrial Ecology Programme, Norwegian University of Science and Technology

ABSTRACT

Typically foreseen paths to renewable energy supply imply that a massive expansion of the wind power industry and its supply network will take place in coming decades. Despite the renewable nature of wind energy conversion, non-renewable resource inputs and emissions occur in the life-cycle of wind energy systems. Using a hybrid life-cycle assessment methodology, we quantify and assess the environmental impacts associated with the supply of 1 kWh of electricity from wind power. Furthermore, scenario analysis is performed to study economy-wide implications of existing projections for wind power development.

KEYWORDS

Life-cycle assessment (LCA); Wind power; Environmental management; Energy scenarios.

1 INTRODUCTION

Wind power is generally seen as a key technology in achieving the desired shift to renewable energy sources. Despite the renewable nature of wind energy conversion, non-renewable resource inputs and emissions occur in the life-cycle of wind energy systems. Life-cycle assessment (LCA) is the appropriate tool for quantifying and assessing resource use and emissions generated throughout a product's life-cycle. A systematic mapping of resource use and emissions of wind power can be valuable by documenting the technology's environmental performance and, possibly, its superiority over competing options. Furthermore, it may assist in developing system designs and strategies for maximizing the environmental benefits of wind power.

In this work, we employ LCA methodology to analyze emissions associated with supply of 1 kWh electricity from a generic onshore wind farm. By scaling unit-based results according to existing projections of wind power development, we estimate life-cycle carbon dioxide (CO_2) emissions associated with global wind power development towards 2050. The results presented here are preliminary.

2 METHODS AND DATA

2.1 Unit-based analysis

LCA is a standardized and increasingly applied tool to quantify and assess the environmental impacts of products and services [1, 2]. It involves a systematic mapping of resource use and emissions occurring in a network of operations. There are two prevailing approaches to LCA; a bottom-up, engineering approach, and a top-down, economic approach. In this work we combine the two approaches in what is commonly referred to as *hybrid* LCA methodology. Our data sources include miscellaneous industry reports, a commercial LCA database [3], and wind power cost breakdowns [4-6]. The system of analysis includes wind turbines, concrete foundations, electrical connections, transportation activities, installation, maintenance, and decommissioning. Basic assumptions regarding the modeled wind farm are shown in Table 1.

Table 1: Basic assumptions for generic wind farm

Size [MW]	Load factor [%]	Loss transm. [%]	Lifetime [years]	Capital costs [€/MW]	Var. costs [€/kWh]
40x3MW	21	1	20	1250	0.012

2.2 Scenario analysis

Using the International Energy Agency's BLUE Map scenario [7] as a basis, we estimate total global CO_2 emissions associated with wind power development towards 2050. In principle this is achieved by up-scaling the unit-based findings to match the given scenario projections, and assuming that wind energy systems must be replaced at the end-of-life (20 years lifetime). The analysis incorporates increases in load factor and cleaner electricity mix in production with time. In all other aspects, technologies do not change over time. In the BLUE Map scenario, around 2000 GW of wind power will be installed by 2050, supplying 12 % of global electricity demand.

3 RESULTS

3.1 Unit-based analysis

Figure 1 shows life-cycle emissions associated with the delivery of 1 kWh electricity from wind power, according to our results. The life-cycle CO_2 emission is 17.6 g/kWh. The wind turbine is the most important single component, contributing 67 % to the total CO_2 emission. Of this, 40 % is due to the tower, 31 % the nacelle, and 27 % the rotor blades and hub.

Besides the wind turbine, the most important categories in terms of CO_2 emissions are foundation (12 %), other variable costs (8 %), operation and maintenance 4 %, and connection to grid (3 %).

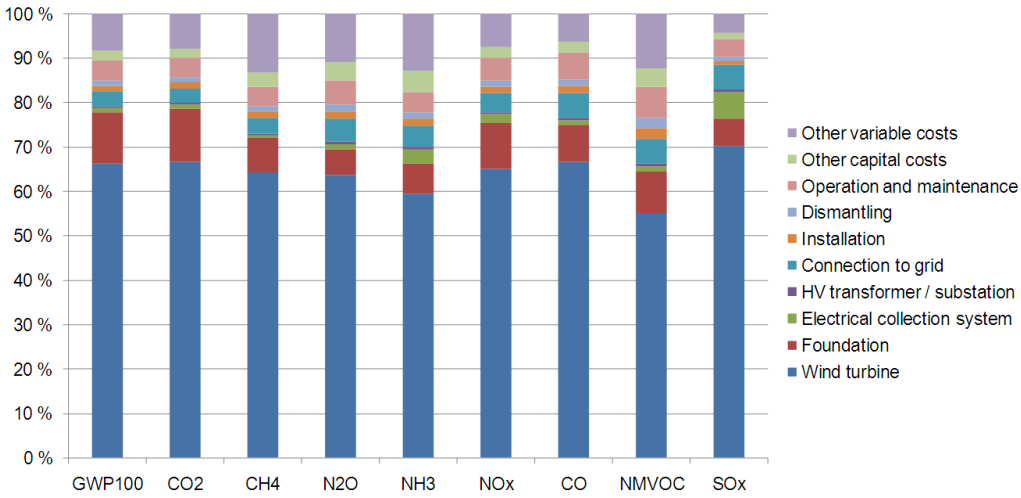

Figure 1: Life-cycle emissions of electricity from wind energy for eight pollutants and global warming impact (GWP100)

3.2 Scenario analysis

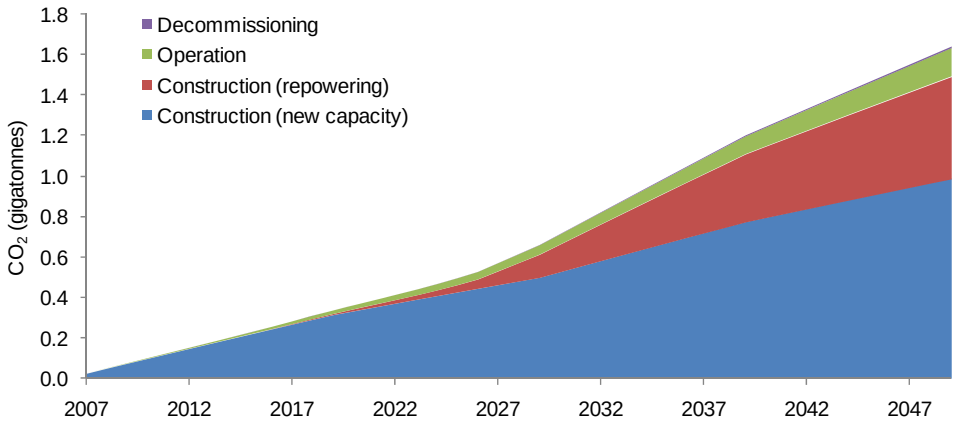

Figure 2: Cumulative emissions of CO_2 caused by wind power development by year

Figure 2 shows cumulative CO_2 emissions associated with wind power development. Total cumulative emissions are 1.6 gigatonnes. This is equivalent to 38 megatonnes per year on average, or 0.13 % of annual CO_2 from global electricity supply in 2007. Construction of new

capacity additions dominates (60 % of cumulative emissions), although replacement of outdated systems becomes increasingly important towards the end of the modeled time period (31 % of cumulative emissions). Due to the combined effects of increased load factor and cleaner electricity mix in production, the relative CO_2 emission is reduced from 17.6 g/kWh in 2007 to 11.1 g/kWh in 2050.

4 CONCLUSIONS

This paper addresses the life-cycle emissions of wind power. Unlike most previous LCA studies on wind power, we employ a hybrid LCA methodology, thereby achieving more complete system coverage, and avoiding the systematic underestimation of impacts that are symptomatic for conventional LCAs. Our unit-based analysis indicates that the life-cycle emissions of wind power are low, compared to existing alternatives. Given the formidable anticipated expansion of wind power in coming decades, it is of interest to quantify aggregated resource use and emissions associated with wind power development. Our scenario analysis provides initial insights regarding the aggregated CO_2 emissions caused by wind power on a global scale. Results indicate that aggregated CO_2 emissions of wind power are very low, compared with emissions from current power generation. In practice, the true climate benefit of wind power will largely depend on the extent to which electricity from wind energy actually replaces fossil-based electricity.

REFERENCES

[1] Finnveden, G.; Hauschild, M. Z.; Ekvall, T.; Guinée, J.; Heijungs, R.; Hellweg, S.; Koehler, A.; Pennington, D.; Suh, S., Recent developments in Life Cycle Assessment. *Journal of Environmental Management* 2009**,** *91*, (1), 1-21.

[2] ISO, Environmental management - Life cycle assessment - Principles and framework (ISO 14040: 2006). International Organization for Standardization: 2006.

[3] Ecoinvent, Life cycle inventory database v2.1. In Swiss Centre for Life Cycle Inventories: 2007.

[4] Blanco, M. I., The economics of wind energy. *Renewable and Sustainable Energy Reviews* 2009**,** *13*, (6-7), 1372-1382.

[5] EWEA *The eonomics of wind energy*; European Wind Energy Association: 2009.

[6] Fingersch, L.; Hand, M.; Laxson, A. *Wind turbine design cost and scaling model*; National Renewable Energy Laboratory. Technical report NREL/TP-500-40566: 2006.

[7] IEA *Energy technology perspectives 2010. Scenarios & strategies to 2050*; International Energy Agency: 2010.

Wind energy research in the age of massively parallel computers

Michael Muskulus[1)]

[1)] Department of Civil and Transport Engineering IVT-BAT, Norwegian University of Science and Technology NTNU, Lerkendalsbygget, 7491 Trondheim, Norway

ABSTRACT

This short note contains some thoughts on future research directions in the field of (offshore) wind energy, taking into account recent developments in computational science. A parallel implementation of an open wind turbine system simulation code will allow to study many interesting problems, of which a few are mentioned. The easy availability of general purpose graphics processor units (GPGPUs) makes this an attractive idea.

KEYWORDS

Wind turbines, computational engineering, fluid dynamics, structural dynamics, GPGPU

1 CHALLENGES IN WIND ENERGY RESEARCH

Wind energy research is a large field with many interdisciplinary aspects, and I will focus on a few challenging problems only. The selection is biased by my own interests in offshore wind turbine systems. As the word “system” suggests, these consist not only of the actual wind turbine, but include both a support structure and a foundation, a control system and a power drive train. The loads in the offshore environment and their interactions with the structure are complex: the aerodynamic forces are history-dependent, nonlinear and stochastic [1], and the hydrodynamic forces are, arguably, even more complicated [2].

1.1 Overview of current modelling practices

Current simulations of the structural dynamics of wind turbine systems are based on either

(1) a flexible multibody formulation or
(2) a finite-element representation with beam elements.

Well-known examples of the former are the computational codes HAWC2 and FAST+AeroDyn; an example of the latter are GH Bladed and ANSYS ASAS+FLEX5. In practice all these models are reduced to a smaller number of dynamic degrees of freedom (modal analysis) for computational reasons. Due to nonlinearities in aerodynamics and the engineering practice of modelling the foundation as a nonlinear spring-dashpot system (F-y

and T-z curves), simulations beyond preliminary design are almost exclusively executed in the time-domain. Given the large number of design load cases prescribed by current standards [3] it is clear that such approximations are necessary with current single-CPU implementations.

1.2 Sequential or fully-coupled analyses

The offshore environment has put many interesting problems into focus. The substructures used are often not developed by wind turbine manufacturers. Due to sensitive commercial interests the structural analysis of wind turbine systems has commonly been done in a sequential way for these individual components, e.g., with time series of prescribed displacements that are exchanged between different analysis teams. In recent years it has been realized that there might be subtle dynamical effects in the fully coupled system that are not present in a sequential analysis [4] and could influence fatigue lifetime significantly [5]. Although this is not fully understood at present, it seems nevertheless sensible to perform a fully coupled analysis whenever feasible.

This is unfortunately hampered by the difficulty of coupling different computational codes together. One issue is that the simulation methods need to be compatible. If closed software codes are used, it might not even be possible to implement such a coupling, or only under degradation of performance (e.g., with fixed time step integration instead of more efficient adaptive methods). Quite a few PhDs were gained by working on this problem.

2 COMPUTATIONAL WIND ENERGY RESEARCH

2.1 Possibilities for future developments

Many topics of present interest are related to details of the modelling. The soil-structure interaction is an area of active research. Although commonly used in engineering practice, it is interesting to ask how useful current soil models (as given in standards and working practices) are. Comparing their predictions with more complex two- and three-dimensional finite-element soil simulations and, ultimately, with real-world measurement data, is one important development (see the contribution of Eric van Buren in this volume).

Regarding the hydrodynamics, it is presently unclear how to precisely account for marine growth, hydrodynamic damping, sea ice, and forces resulting from breaking waves (wave slamming). Of course there exist established approaches and validated software tools to deal with these issues, but current wind turbine system computational codes often lag considerably behind these ideas.

From the above it seems that the wind energy research community is really in need of

(1) an open software code that can be modified freely and easily, and that furthermore
(2) is sufficiently fast to allow for realistic simulations of much increased complexity than are being done routinely nowadays.

Whereas FAST+AeroDyn is a candidate for (1), it does not take enough advantage of current computer technology.

2.2 Computational speed and parallelization

Why is computational speed so important? I once heard someone remark that “if you cannot wait three weeks for the results of a calculation, then you are working on the wrong problem”. I do not agree with this statement. Not only is research often an iterative process (in general, not only in preliminary design studies), but a speed-up of a factor of 100x or more allows one to study problems that have simply not been possible before. Although a clever algorithmic idea is still of utmost importance, there are limits to what is possible with a single traditional processor. The only way to achieve significant speed-up beyond this is parallelization. It is fortunate that there now exist very powerful general-purpose parallel computing processors realized as graphical processing units (GPUs). The current generation NVIDIA Tesla C2050 GPU features 448 processing cores running at 1.15 GHz. Paired with a memory bandwidth of 144 GB/s and affordable even on a meagre budget, it has been marketed as the “supercomputer in a desktop” [6]. Rewriting computational codes to take advantage of this architecture results in a speed-up factor of 10x easily, and gains up to three orders of magnitude in speed when fully optimized. These developments have influenced many research areas (e.g., see [7]), and it seems that the field of wind energy research is now due. Without going into too many details, let us remark that the computational vibration analysis of structures, at least in the time-domain, is almost exclusively based on linear algebra [8] and is therefore an excellent candidate for extreme parallelization under the GPU programming model [9]. Mass and stiffness matrices are sparse (banded) and iterative solution methods are almost “embarassingly parallel”; and the common Basic Linear Algebra Subprograms (BLAS) library is available in an optimized GPU version. Subspace iteration to determine the dynamical degrees of freedom in the Rayleigh-Ritz method, or the calculation of Lanczos coordinates [8] can all be efficiently realized.

3 OUTLOOK

Such parallel implementations will also allow to address interesting issues in turbulence modelling and the analysis of wind farms. The effect of replacing the wind turbine monopile tower (commonly used for aesthetic reasons onshore) with an alternative truss tower offshore (see the contribution of Marit Reiso in this volume) can be studied in detail. The

generation of three-dimensional turbulence wind fields can be realized with improved resolution. And parallel implementation would make it possible to study complete wind parks in much greater detail than currently possible. Finally, structural optimization will be another interesting field of application.

Given the need for improved, innovative and customized designs of wind turbine systems (with the goal of reducing the cost) in the offshore environment, parallel simulation might offer the computational capacity needed to address many important issues.

Our group has therefore recently acquired a Tesla C2050 GPU system and is working together with the High Performance Computing lab at NTNU [10] to realize some of the ideas mentioned. The Offshore Code Comparison Continuation Project [11] will be an excellent forum for validating some of this work.

BIBLIOGRAPHY

[1] Leishman, J.G.: *Principles of helicopter aerodynamics.* Cambridge University Press 2006.

[2] Sarpkaya, T.: *Wave forces on offshore structures.* Cambridge University Press 2010.

[3] IEC 61400-3. Wind turbines Part 3: Design requirements for offshore wind turbines. International electrotechnical commission 2009.

[4] Böker, C.: Load simulation and local dynamics of support structures for offshore wind turbines. PhD thesis, Fakultät für Bauingenieurwesen und Geodäsie, Gottfried Wilhelm Leibniz Universität Hannover, Germany, 2010.

[5] Kjetså, A.; Saaghus, L.J.: Local dynamics of offshore wind turbine jacket sub-structures. Master's thesis, Faculty of Engineering Science and Technology, NTNU, Norway, 2010.

[6] http://www.nvidia.com/object/personal_supercomputing.html [accessed 16-09-2010]

[7] Walsh, S.D.C.; Saar, M.O.; Bailey, P.; Lilja, D.J.: Accelerating geoscience and engineering system simulations on graphics hardware. *Computers & Geosciences* 35 (2009), 2354-2364.

[8] Clough, R.W.; Penzien, J.: *Dynamics of structures.* McGraw-Hill 1993.

[9] Kirk, D.; Hwu, W.-M.W.: *Programming massively parallel processors.* Morgan Kaufmann 2010.

[10] http://research.idi.ntnu.no/hpc-lab/ [accessed 16-09-2010]

[11] http://www.ieawind.org/Task_30/Task30_Public.html [accessed 14-09-2010]

European Academy of Wind Energy

Norwegian University of Science and Technology

The Correlation between Wind Turbine Turbulence and Failure-Preliminary Work

Professor Peter Tavner [1], Athanasios Korogiannos [1], Dr Yingning Qiu [1]

[1] Durham University, DH1 3LE, UK

ABSTRACT

Work at Oldenburg University in EAWE has shown the vital importance of wind turbulence on the power curve of Wind Turbines. But turbulence not only affects the control behavior of the turbine it also drives turbine failure root causes, particularly in the aerodynamic components, the blades and their pitch mechanism. This paper presents an early attempt to extract turbulence information from the slow SCADA data, available to operators, correlating it with known failures. The results clearly show that turbulence is a root cause for pitch mechanism faults and the work presents ideas for future study to improve our understanding in this area and mitigate the effects observed.

1 INTRODUCTION

1.1 Introduction to Wind Turbine Reliability

Wind Turbine (WT) reliability has been investigated by the lead author and others [1] [2] [3] over a number of years and clear information is now available of the distribution of location of major faults as exemplified in Figure 1.

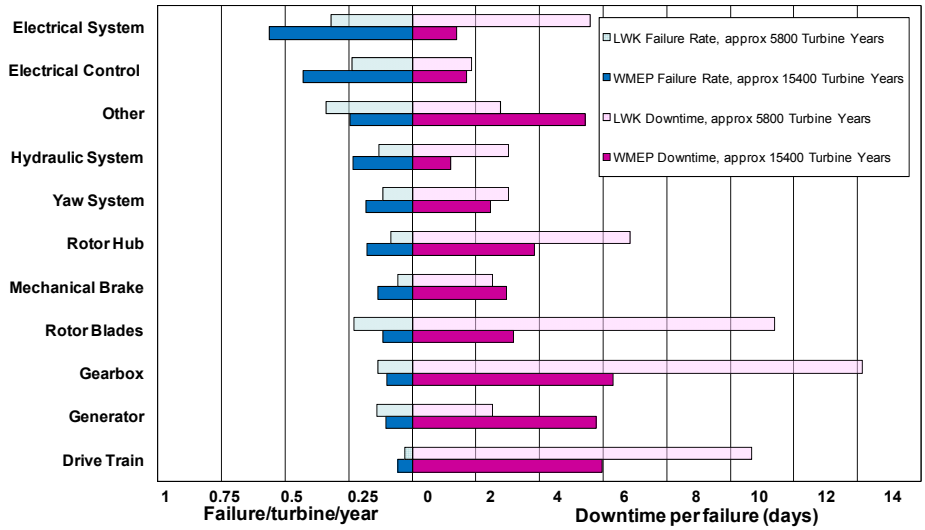

Figure 1: Failure/turbine/year and Downtime from 2 European WT Surveys over 13 years.

It is clear from Figure 1 that the rotor, its hub, blades and pitch mechanism, are an important area of turbine unreliability. However, this represents the fault locations not their failure mode or indeed root cause.

1.2 Wind Turbulence and its Effect on WT Reliability

The turbulence of wind has been investigated by a number of researchers [4][5][6][7][8][9]. To investigate that turbulence it is necessary to make rapid and accurate spatial and temporal wind speed measurements, see Figure 1. From a reading of this material it is clear that turbulence must be a significant driver of the root causes of WT failure particularly in those parts of the WT which are exposed to aerodynamic effects, such as the blades and pitch mechanism.

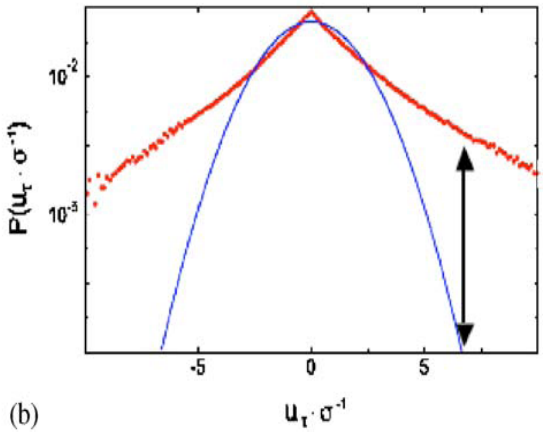

Figure 2: Probability density function (PDF) of spatial transversal velocity increments over a distance of 10 m, for τ=4 s is compared to a Gaussian distribution (solid line) [7].

1.3 SCADA Data

The majority of operational WTs are fitted with instrumentation from which data, including wind speed, is collected by the turbine Supervisory Control and Data Acquisition (SCADA) system, usually at 10 min intervals. Turbulence studies[8][9]suggest that wind speed data must be collected at least at 1 min intervals to resolve wind turbulence structures. However, recent work by the authors using data from a large number of 1.5 MW, variable speed, WTs in a Spanish Wind Farm (WF) has demonstrated that turbulent structures are clearly visible even in 10 min SCADA wind speed data, see Figure 2.

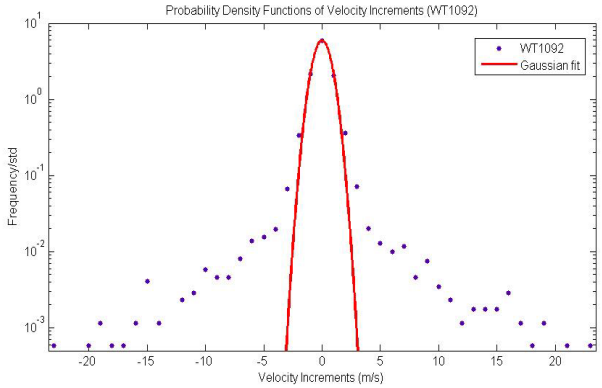

Figure 3: Probability density function of wind speed from a WT SCADA

1.4 Failure Data from SCADA

As a result of work done by the EU FP7 ReliaWind Consortium data from these three Spanish WFs has been analysed to determine the failures occurring in the Pitch Mechanism of these turbines. This area of the WT has been shown by earlier work, described above, to be significant and is exposed to the turbulence of the wind. This failure data is available daily from specific WTs at 3 separate WFs in different locations with varying wind conditions.

2 WIND TURBINE TURBULENCE ANALYSIS

2.1 Wind Turbulence Model

A simple statistical method has been used to identify the turbulence in the wind speed time series with a 10 min sampling interval, based on a method described in [8]. In order to obtain a numerical turbulence measure, which could be averaged daily, as the failure data above is recorded, the standard deviation of the velocity increments can be used to quantify how widely spread the velocity increments are. A difficulty with this method was that the majority of the wind speed changes were in the region ±2m/s around the mean so that of the velocity standard deviation alone does not give a convincing measure of turbulence during a specific time interval. To overcome this, a novel method was introduced. A representation of the turbulence was obtained by taking the mean of the standard deviation of wind speed variations, over a period of time t, with cuts for wind speed variations δ_{uT} about the mean wind speed, u_w see Figure 3. This will be called 'wind speed turbulence coefficient' defined as $ku_{\delta uT}$ for a mean wind speed u_w. An example of this representation for a cut of ±5 m/s about the mean wind speed u_w can be seen in Figure 4.

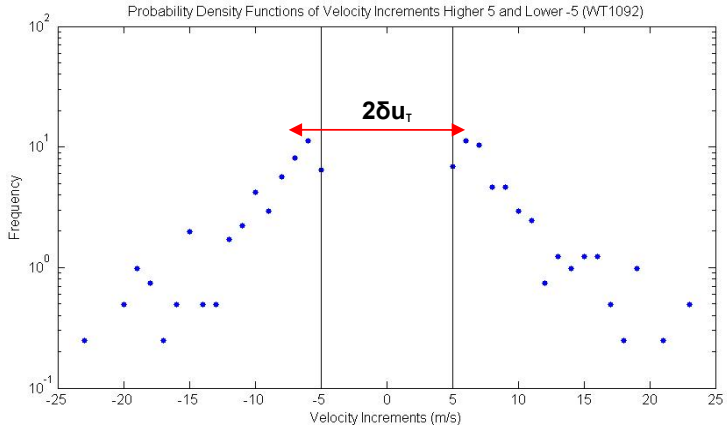

Figure 4: Probability density function of velocity increments higher than 5m/s and lower than -5m/s

A time series of the daily wind turbulence coefficient for wind speed deviations of ±2, ±5 and ±10 m/s were obtained from the wind speed time series at each of the three WFs.

2.2 Wind Turbulence Effects on Pitch Mechanism

To identify whether WT pitch mechanism failures are caused by wind turbulence the failure and wind turbulence coefficient time series for WTs with known pitch mechanism failures were cross-correlated using the methods described in [10][11].

3 RESULTS

The wind turbulence coefficients, k_{u2}, k_{u5}, k_{u10}, for ±2, ±5 and ±10 m/s deviations in wind speed respectively over the whole period of the study are shown in Figure 5 for six WTs with known pitch mechanism failures.

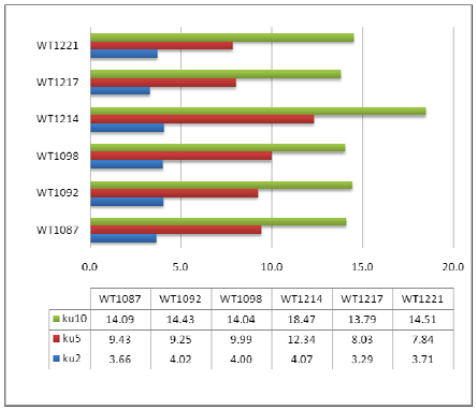

	WT1087	WT1092	WT1098	WT1214	WT1217	WT1221
ku10	14.09	14.43	14.04	18.47	13.79	14.51
ku5	9.43	9.25	9.99	12.34	8.03	7.84
ku2	3.66	4.02	4.00	4.07	3.29	3.71

Figure 5: Wind Speed Turbulence Coefficient over the total length of wind speed data

The results of the cross-corelation between the pitch mechanism failures and wind turbulence coefficient time series for those six WTs are shown in Figure 5, together with their cross-correlations to the mean wind speed and the wind speed standard deviation in each case.

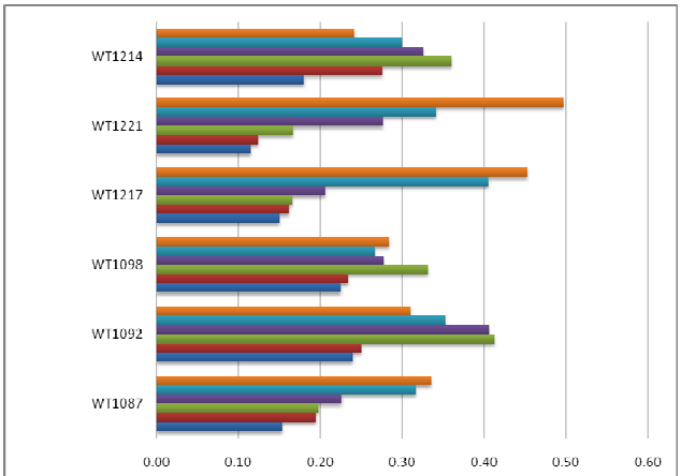

	WT1087	WT1092	WT1098	WT1217	WT1221	WT1214
ku10	0.34	0.31	0.28	0.45	0.50	0.24
ku8	0.32	0.35	0.27	0.41	0.34	0.30
ku5	0.23	0.41	0.28	0.21	0.28	0.33
ku2	0.20	0.41	0.33	0.17	0.17	0.36
Standard Deviation	0.19	0.25	0.23	0.16	0.12	0.28
Mean	0.15	0.24	0.23	0.15	0.11	0.18

Figure 6: Cross-correlation results of Pitch Mechanism Failures with Wind Speed Turbulence Coefficients

4 DISCUSSION

It can be seen from Figure 5 that there is a significant degree of wind turbulence visible at the sites of all six WTs and that the value of $k_{u10} > k_{u5} > k_{u10}$ in all six cases.

Figure 5 shows that for all six WTs there was a greater cross-correlation between failures and the wind speed turbulence coefficients than there was to mean wind speed or wind speed standard deviation, as had been studied in [10][11]. The cross-correlations between failures and wind turbulence coefficients generally exceeded 30% and showed a Pearson test statistical significance for the sample size taken in excess of 99.9%.

5 CONCLUSIONS

- 10 min S CADA wind speed data yields significant wind turbulence data despite its long sampling interval.

- Six WTs from 3 WFs with pitch mechanism failures clearly showed a higher cross-correlation between failure and wind turbulence coefficient time series than with wind speed and wind speed standard deviation.
- The statistical significnace of these results was inexcess of 99.9%.
- This confirms that for WT pitch mechanism failures wind speed turbulence is a very significant root cause.

BIBLIOGRAPHY

[1] Tavner P.J., Xiang J., Spinato F.: *Reliability analysis for wind turbines*, Wind Energy, 2007, 10, pp. 1–18.

[2] Spinato, F. Tavner, P.J., van Bussel, G.J.W., Koutoulakos, E.: *Reliability of wind turbine subassemblies*, IET Renew. Power Gener., 2009, Vol. 3, Iss. 4, pp. 1–15.

[3] Faulstich S., Hahn B.: *Comparison of different wind turbine concepts due to their effects on reliability*, UpWind, EU supported project nr. 019945(SES6), deliverable WP7.3.2, public report, Kassel, 2009.

[4] Madsen, P, Frandsen, S, *Wind induced failure of wind turbines*, Eng. Struct., Vol. 6, October 1984.

[5] Mouzakis, F, Morfiadakis, E, Dellaportas, P,*Fatigue loading parameter identification of a wind turbine operating in complex terrain*, Journal of Wind Engineering & Industrial Aerodynamics, Vol 82, 1999, pp69-88.

[6] Riziotis, V, Voutsinas, S, *Fatigue loads on wind turbines of different control strategies operating in complex terrain*, Journal of Wind Engineering & Industrial Aerodynamics, Vol 85, 2000, pp211-240.

[7] Peinke, J, Barth, S, Bottcher, F, Heinemann, D, Lange, B, *Turbulence, a challenging problem for wind energy*, Physica A 338, 2004, p187-193.

[8] Gottschall, J, Peinke, J, *Stochastic modeling of a wind turbine's power output with Special Respect to turbulent dynamics*, Journal of Physics: Conference Series 75, IOP Publishing, 2007.

[9] Peinke, J, Anahua, E, Barth, S, Gontier, H, Schaffarczyk, A.P, Kleinhans, D, Friedrich, R, *Turbulence a challenging issue for the wind energy conversion*, European Wind Energy Conference, April 2008.

[10] Tavner, P.J., Edwards, C., Brinkman, A., Spinato, F., *Influence of wind speed on wind turbine reliability*, Wind Engineering, 2006, Vol. 30, No. 1, pp 55-72.

[11] Tavner, P J, Gindele, R, Faulstich, S, Hahn, B, Whittle, M W G, Greenwood, D M, *Study of effects of weather & location on wind turbine failure rates*, EWEC, Warsaw, 2010.

Forecasting of wind turbine loads based on SCADA data

Claudia Hofemann, Gerard van Bussel, Herman Veldkamp

DUWIND, Delft University of Technology, the Netherlands

ABSTRACT

If at least one reference wind turbine, providing sufficient information about the wind turbine loads is available an artificial neural network (ANN) can be implemented to monitor the loads acting on the neighboring wind turbines. This research explores the possibility's to apply such a network not only within a wind park but on turbines located at different sites. Following the idea to develop a tool allowing to monitor and forecast the particular loads of any wind turbine in the field without the need to install additional measuring systems a model has been developed in such a fashion that only signals contained in the Supervisory Control and Data Acquisition (SCADA) data are needed as input signals. While SCADA data is used as input parameters data from load measurements is used to train and verify the generated model. SCADA data, is on-line data describing the turbine state as well as the environmental conditions, it is comparably easy to access and recorded for all commercial wind turbines.

KEYWORDS

SCADA Data, Load Forecasting, Artificial Neural Networks

1 INTRODUCTION

The presented study is part of a project investigating the potential of data provided by the SCADA system to forecast the side dependent mechanical loading of wind turbines over their lifetime. Standard signals, providing on-line information, are available for nearly all commercial wind turbines. Those signals, obtained by the SCADA system, provide turbine manufactures and operators with online information of the wind turbine state, the state of turbine components and environmental conditions as temperature or wind speed. Such information can be used to estimate the loads acting on a particular wind turbine [1] or to access the performance of a wind farm [8] if verification data to train and verify the model is available. The referred models use artificial neural networks (ANN's) to estimate the experienced loads. Here as well an ANN has been trained, but this time not only the capability of the system to reconstruct the loads is tested but its transferability. Bringing us a step closer to the idea behind those projects: to establish a system allowing to estimate the loads without the need to install additional measurement equipment. Up to know such models have been only tested going back and forth in time or within one wind park, the here established model is trained for one turbine and tested on a different turbine located at a

different site. The by the ANN established empirical relationships are based on SCADA data as input data and tested by data obtained from load measurements, verification data, representing the actual loads measured on the turbine. Verification data is only needed to validate the code. Once the ANN is trained predictions are performed using only the input data; hence signals which are included in the standard SCADA data. Implying that the loads acting on a particular wind turbine can be estimate without the need to

2 ARTIFICIAL NEURAL NETWORKS

ANN's can be used for a wide range of applications. Up to know ANN's are not that common in the wind turbine industry but are applied successful on other forecasting problems as the development of the stock market or the energy price. This section provides a principle explanation on the basic concepts and architecture of ANN's. From an engineering point of view most of the ANN's can be seen as a black box. They are inspired by the mechanism of the brain ANN's and can be classified by different categories as for example the learning mechanism or how they are trained (supervised n unsupervised) [3]. ANN's accept inputs, process them, and produce outputs according to a nonlinear transfer function [11]. The modern age of ANN's began 1943, with the paper "A logical calculus of the ideas immanent in nervous activity" written by McCulloch and Pitts [6]. Five assumptions governing the operations of neurons were presented. By then it was not possible to train the neurons, the neurons could act according to certain logic functions. In 1949, Donald Hebb made one of the first hypotheses for a mechanism of neural learning, the Hebbian learning. He described the learning process from a microbiological viewpoint. He was the first to state that information can stored in the weighted connections between the neurons and developed the first learning strategy allowing to adjust those connections. His paper "The organization of behavior" published in 1949 had a major impact on the later work in this field [4]. The first defined computationally oriented neural network, the precepton, was defined in 1958 by Frank Rosenblatt; it was a machine that could be trained to classify certain parameters [9]. A reassembly of this precepton to Adaline (adaptive linear element) marks the next step in the evolution of artificial neural networks [10]. When in 1969 Marvin Minsky and Seymour Papert pointed out that single layer neural networks have limited capabilities, the research slowed down [7]. The revival of ANN's began in 1982 when the first working recurrent neural network, the Hopefield-network, was presented, a network allowing to store information and to perform a function of data storage and retrieval [5]. Today a broad range of neural

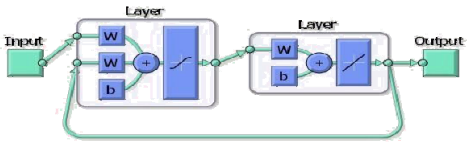

Figure 1: View of the implemented network

networks can be found, applied for tasks as system identification and control, game-playing, decision making, pattern recognition, medical diagnosis and data mining. For the described forecasting problem a nonlinear autoregressive exogenous model (NARX) has been chosen. Those network types are typically applied to problems dealing with time-series predictions. They are recurrent feed forward neural networks. Here a NARX network consisting out of two layers has been implemented, the layers of the network are connected unidirectional, and each of the neuron of each layer is connected with branches to all of the neurons of the next layer. The architecture of feed-forward networks does not foresee connections between the neurons of one layer. The connections between the neurons (of different layers) are unidirectional; information is only transported in one direction (feed-forward). At every level represented by the different layers of neurons an output is generated that serves as input for the next layer of neurons. The neuron output serves as an input to a nonlinear activation function whose output is the response of the neuron. The output of the network is fed back to the input of the feed-forward network, as shown in figure 1. Even if there is no limit for the number of layers, in general only two or three layers are used. In fact it can be shown that a multi-layer preceptor (MLP) that has only one hidden layer, with a sufficient number of neurons, acts as a universal approximator of nonlinear mapping [3].

3 TRAINING OF THE ANN

The network is trained to predict the blade root moments of two wind turbines located at different sites. A supervised ANN has been chosen, implementing that load data has to be provided to train the network to establish the relationship between the SCADA data and the measured loads. The data describing the measured loads, the target data of the network, is used to train the network as well as to verify the made predictions. Training an ANN is a trade of between computation time, accuracy and over fitting. The more parameters are feed into the network the more accurate is the reproduction of the target data. A modern wind turbine transmits between 130 and 380 statistical parameters. A lot of those parameters are hour counters and temperature sensors, whose influence on the accuracy of the forecasting are of no significance. Of more interest are signals as wind speed and wind direction, power output, pitch angle or yaw moment. Those parameters are used as input data. The predictions are performed by dynamic recurrent feed forward neural network trained with the Bayesian regulation back propagation, a network training function that updates the weight and bias values according to Levenberg-Marquardt optimization. It minimizes a combination of squared errors and weights, and then determines the correct combination to produce a network that generalizes well [2]. Each of the training routines performs about 1000 passes. The network has been trained with 10 minutes statistics, generated from time series. The

data is presented to the network in a chronological order. A period of 10 minutes has been chosen for the simple reason that the signals recorded by the SCADA system, are computed over a period of 10.

4 SCADA AND VERIFICATION DATA

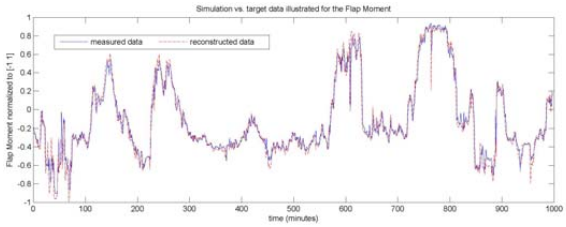

Figure 2: Time series of a predicted and a measured blade bending moment

The developed model shall be able to perform predictions of the wind turbine loads of all wind turbines of at least one fleet. At the moment the model has been tested on three different turbines. The results regarding the forecasting of the loads on one particular turbine are promising. Until now the transferability of the developed model has been tested on two wind turbines, located in a similar environment. The reference turbine for which the model is developed and verified is located in Denmark. The second turbine, on which the developed model has been tested, is located in Sweden. Both turbines are equipped with load sensors. The load sensors have been installed for a different purpose and not all sensors which can be found on the reference turbine are as well installed on turbines chosen to test the model, respectively similar sensors might be installed on both turbines, but mounted at different locations. About 7 load sensors are installed on the reference wind turbine, describing the loads acting on the wind turbine blades. At the moment the model is trained with all of the available sensors and tested with the available set from the test turbine, taking in account inaccuracies due to the different mounting of the sensors. The signals form missing sensors are set to zero. From the available set of signals representing the SCADA data, 18 different input parameters as wind speed, wind direction and turbine state have been chosen to train the neural network.

5 PERFORMANCE OF THE MODEL

The developed model has been tested on three different turbines. The reconstruction of the blade bending moments for one particular wind turbine are accurate. If the model has been trained with sufficient data a correlation coefficient between R=0.95 and R=0.99 can be reached for short term forecasts. Figure 2 illustrates a plot of two time series, the blue line here representing the measured blade bending moments, the target data of the network and the red dashed line the simulated output from the model, normalized between -1 and 1. The in figure 2 illustrated case has an R-value of 0.976. The network has been trained with 20000 data points. The visualized test has been performed with an additional data set, consisting

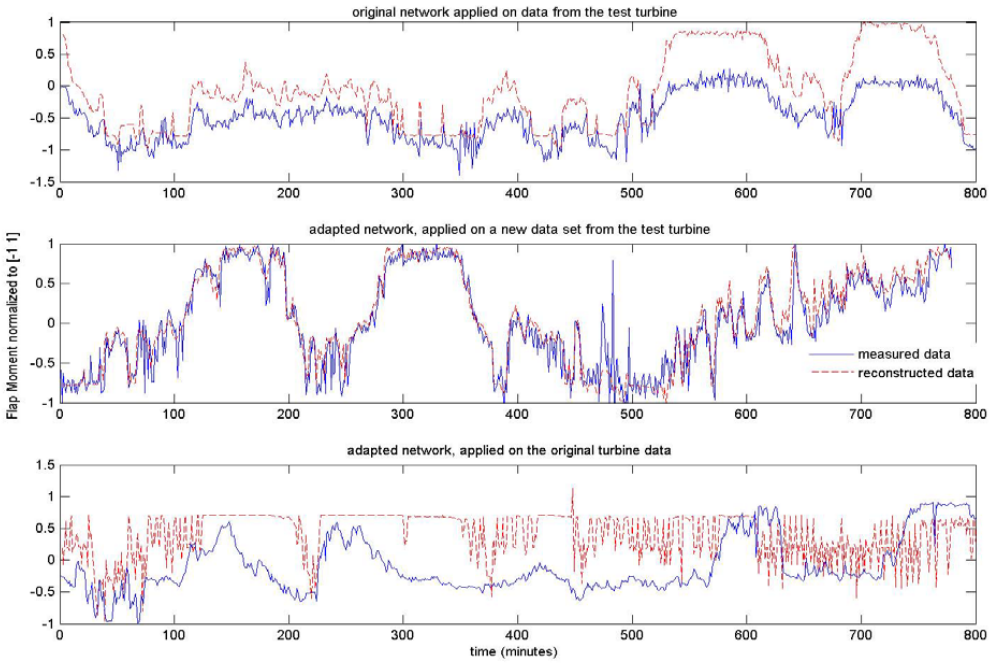

Figure 3: The original network and an adapted version tested on two different wind turbines

out 1000 data points which are completely unknown for the network. The data which has been used is not filtered or sorted, the sets have divided into training and test data depending on the time stamp to be able to present a consistent time line to the network. If the established relationships are transferred from one turbine to another the correlation factor decreases. The quality of the predictions is directly related to the training as well as to the quality and quantity of the available data. Transferring the established relationships from the reference turbine to the test turbine, by applying the original network one new data from the test turbine, a correlation coefficient of R=0.93 has been reached, whereas no additional training with the data from the test turbine has been performed. If additional training is performed the correlation coefficient increases as visualized in figure 3. As illustrated in the third plot of figure 3 is the transferability not always as unproblematic as from the reference turbine to the test turbine. The third plot illustrates the inverse transfer of the knowledge structures, here the network has been trained by additional 800 data points form the test turbine and is applied on 800 new data points of the reference turbine. Due to a too huge variation in the data as well as insufficient training and memory functions of the network, are the predictions for this specific case poor.

6 OUTLOOK

The model is still in a developing phase, if it is once fully tested it shall be applicable to a range of turbines representing different environments. At the moment only a basic set of sensors is used for the forecasting. To predict the loads in different environments the integration of parameters characterizing the site might be needed. The memory of the network has to be increased to as well as an adaption of the training mechanism is needed to guard against the in figure 3 visualized problem.

7 ACKNOWLEDGMENTS

I would like to thank Vestas for supporting this project, in particular Srikar Vulli and Karl H. Svendsen.

BIBLIOGRAPHY

[1] N. Cosack and M. Kuhn. An Approach for Fatigue Load Monitoring without Load Measurement Devices.

[2] Howard Demuth, Mark Beale, and Martin Hagan. Neural network toolbox TM 6, user's guide.

[3] F.M. Ham, I. Kostanic, F.M. Ham, and F. Ham. Principles of neurocomputing for science and engineering, McGraw-Hill New York, 2001.

[4] D.O. Hebb. The organization of behavior: A neuropsychological theory. Lawrence Erlbaum, 2002.

[5] J.J. Hopfield. Neural networks and physical systems with emergent collective computational abilities, Proceedings of the National Academy of Sciences of the United States of America, 79(8):2554, 1982.

[6] W.S. McCulloch and W. Pitts. A logical calculus of the ideas immanent in nervous activity. Bulletin of Mathematical Biology, 5(4):115{133, 1943.

[7] M. Minsk and S. Papert. Perceptrons, 1969.

[8] TS Obdam, L. Rademakers, and H. Braam. Flight Leader Concept for Wind Farm Load Counting: First Offshore Implementation. Technical report, ECN-M-09-114, 2009.

[9] F. Rosenblatt. The perceptron: A probabilistic model for information storage and organization in the brain. Psychological review, 65(6):386{408, 1958.

[10] B. Widrow and ME Ho_. Adaptive switching circuits. 1960 IRE WESCON Convention Record. New York: IRE, 4:96{104, 1960.

[11] A. Zaknich. Neural networks for intelligent signal processing. World Scientific Pub Co Inc, 2003.

Part 2

Session 2 - Control and Design of Wind Turbines

- Optimal Operation Planning for Wind Farms
  Natalia Moskalenko, Otto-von-Guericke-University
- Yaw stability of a free-yawing 3-bladed downwind wind turbine
  David R.S. Verelst, Risø DTU
- Aerodynamics of Diffuser-Augmented Wind Turbines
  Ben M. Geurts, TU Delft

Optimal Operation Planning for Wind Farms

N. Moskalenko, K. Rudion

Otto-von-Guericke-University Magdeburg, Germany

ABSTRACT

The main task of this work is to investigate the possibilities of optimal operation planning to maximize the energy yield from a wind farm. In general, maximization of energy yield could be reached by an appropriate adjustment of the pitch angle in different wind turbines within the farm as well as through the adjustment of the yaw angle of individual wind turbines. The current status of the work is the research and comparison of existing wake models as well as the selection of an appropriate model or program system for solving this task. After selection of the appropriate wake model, the necessary extensions of the model will be implemented and the analysis of the wind farm operation will be carried out.

KEYWORDS

Wind energy, wind farm, energy yield, wake effect, pitch angle, yaw angle.

1 INTRODUCTION

Wind energy has a stochastic character that can worsen the voltage and power quality in the power grid. The efficiency of wind power utilization depends on many parameters such as non-zero aerodynamic resistance, the finite number of blades and due to this fact tip losses, and the positioning of wind turbines in relation to each other because of turbulence rotation behind the wind turbine rotor. During the wind farm planning various aspects have to be considered:

- The optimal wind farm layout for energy yield maximization and minimal area usage;
- Optimal integration of a large number of wind turbines into the power system (compliance with the Grid Code) with appropriate operation management;
- Optimal integration into the environment for minimal influence on the nature and surrounding landscape.

An important task of the wind farm planning is to get as much energy as possible from the minimal number of wind turbines and with a minimal space between the turbines. However, minimization of the distance between single wind turbines within a wind farm causes an increase in the wake effect, which consequently leads to the reduction of energy yield in the shadowed units.

natalia.moskalenko@ovgu.de

2 WAKE EFFECT - GENERAL CHARACTERISTICS

2.1 Wake formation

Wake effect can have a significant influence on the total energy yield, on the variable wind loads and vibration induced fatigue on the rotors, and can even cause a short circuit at the neighboring transmission lines when the wakes swing back and forth in opposite phases.

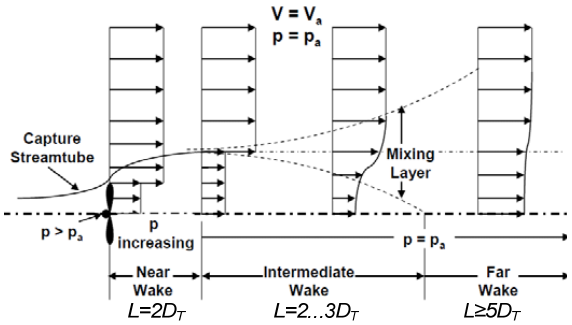

Figure 1: Wake flow structure of horizontal-axis wind turbine [1]

The wake's structure consists of several zones (Figure 1): near, intermediate and far wake [2]. The length of each of these zones depends on the rotor diameter and has its own properties that are determined by the values of pressure *p* and wind speed *V*. According to the properties of each zone the optimal distance between the wind turbines can be chosen to minimize the influence of the turbines on each other.

2.2 Wake modelling

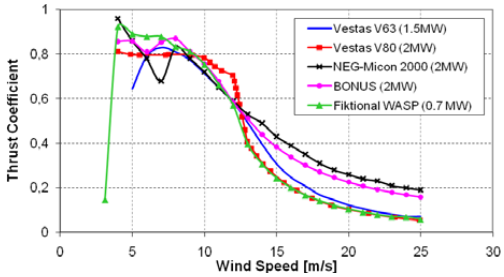

Figure 2: Thrust coefficient c_T for different wind turbines (based on [3], [4])

For wake effect analysis and optimal wind farm planning a wake model was developed that is based on Jensen's model, since this one is simpler than other models, e.g. by Lissaman, Larsen or Ainslie, and requires a shorter time for calculations. In this program wake flow is controlled by the entrainment constant *k* [2], [5], and by the thrust coefficient c_T, which depends on the wind speed and wind turbine type (Figure 2). The wake flow is assumed to be linear and the near-wake region is neglected.

2.3 Influencing wake intensity

A wind turbine operates in a non-uniform and continually variable wind field, where wind speed and its direction change every moment. The inability of a wind turbine to be oriented by the wind at every moment leads to considerable power losses. To decrease wake effect and thereby increase energy production it is necessary that the wind turbine is able to accommodate to such a changeable situation and adjust its parameters, such as pitch and yaw angles, to the optimal position according to the wind. Thus, the pitch angle of wind turbine has to be optimal in an acceptable wind speed range (4-25 m/s) at every moment. Also, it is necessary to provide the alignment of the axes of the wind turbine nacelle with the wind direction. So, the sensor should constantly determine the direction in which the air flow has the maximal wind speed, and orient the wind turbine in this direction in order to avoid the turbulence flow.

3 ENERGY YIELD IMPROVEMENT IN WIND FARM

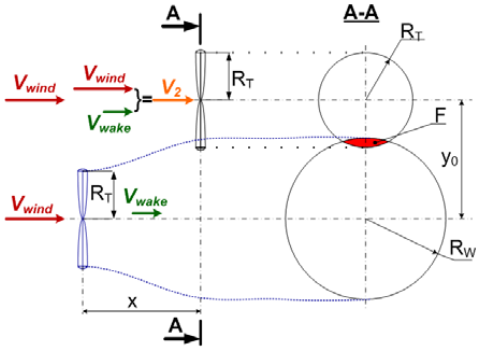

Figure 3: Wind turbines with the same yaw angle

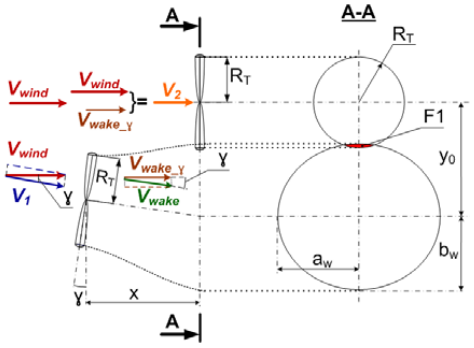

Figure 4: WT1 was rotated at yaw angle γ to the wind flow

The calculation of the energy yield of two wind turbines depending on their yaw angle adjustment is presented here. The cross-sections of air flows from turbines at the sectional view A-A are shown (Figure 3, Figure 4). The shadowing area where these cross-sections intersect, the speed of the second wind turbine and its energy production, and the total energy yield were obtained. In the first case, both wind turbines are directly oriented to the wind flow with the same yaw angle. In the second case, the wind turbine WT1 has been rotated at some yaw angle γ (here γ=10°) in order to reduce the shadowing of second wind turbine (WT2) and to increase its initial wind speed. The assumed type of wind turbine is Repower MM82 with 3 blades and maximal power of 2 MW. The energy production from the k-th WT can be obtain using Eq. (1), [2]:

$$P_k = \frac{1}{2} \cdot \rho_{air} \cdot A \cdot V_{0,k}^3 \cdot C_{p\_rated} \quad (1)$$

The wind speed of wind turbine WT2 and the speed of wake flow from the WT1 can be determined using Eq. (2), where $\beta_{T2,T1} = \frac{F_{T2,T1}}{\pi \cdot R_T^2}$ is the shadow coefficient:

$$V_{T2} = V_{wind} \cdot \left[1 - \sqrt{\beta_{T2,T1} \left(1 - \frac{V_{wake}}{V_{wind}} \right)^2} \right]; \; V_{wake}(x) = V_{wind} \left[1 - \left(1 - \sqrt{1 - c_T} \right) \cdot \left(\frac{R_T}{R_T + k \cdot x} \right)^2 \right] \quad (2)$$

Table 1 shows that the energy production in case 1 is larger than in case 2, but the shadowing area and the wake speed are smaller in second case. So in a wind farm structure with many wind turbines the second method could be a useful way to reduce the overall influence of the wake effect.

Table 1: Summary concerning the shadowed area and wake speed

Case	Shadow Area, $F_{T2,T1}$ [m^2]	WT1 Wind Speed V_{wind}	Wake Speed V_{wake}	WT2 Wind Speed V_2	WT1 Energy Yield	WT2 Energy Yield	Total Energy Yield
		[m/s]			[W]		
1	212,1	14,50	13,68	14,34	$2{,}05 \cdot 10^6$	$1{,}981 \cdot 10^6$	$4{,}031 \cdot 10^6$
2	174,4	14,28	13,27	14,28	$1{,}958 \cdot 10^6$	$1{,}957 \cdot 10^6$	$3{,}915 \cdot 10^6$

4 CONCLUSIONS

In this paper chosen aspects of wind farm planning were discussed with a focus on the mutual interaction between the wind turbines that are specified by the wake effect. Some methods for wind farm structure optimization are the adjustment of the yaw angle of individual wind turbines within the farm as well as the optimization of the pitch angle settings in the individual wind turbines. In a future study, the investigation of the latter method has to be carried out and the performance compared with the method based on optimally adjusting the yaw angle of individual WTs.

BIBLIOGRAPHY

[1] Werl, M. J.: A New Analytical Model for Wind Turbine Wakes, FloDesign Inc. Wilbraham, MA 01095, Wilbraham USA, 1 June, 2008. Available at www.flodesign.org/pdf/fdwt200801.pdf.

[2] Rudion, K.: „Aggregated Modelling of Wind Farms"; Otto-von-Guericke-Universität Magdeburg; Magdeburg 2008.

[3] VanLuvanee, D. R.: Investigation of Observed and Modeled Wake Effects at Horns Rev using WindPRO. Master Thesis at the Technical University of Denmark, 25 August 2006. Available at www.fm.mek.dtu.dk/English/Publications/ Mastertheses.aspx.

[4] www.wasp.dk/Download/PowerCurves.html.

[5] Jensen, N. O.: „A Note on Wind Generator Interaktion"; Technical Raport RISO-M-2411; Denmark November 1983.

European Academy of Wind Energy

Norwegian University of Science and Technology

Yaw stability of a free-yawing 3-bladed downwind wind turbine

David R.S. Verelst[1)], Torben J. Larsen[1)]

[1)] Risø-DTU, Denmark

ABSTRACT

A passive free yawing configuration can reduce complexity, maintenance costs and downtime of a wind turbine, due to the absence of an active yawing mechanism. However this concept is often unstable in yaw rotation and therefore rarely used. In this paper, a free-yawing, 3-bladed, stall-regulated, downwind medium sized wind turbine is investigated with respect to static yaw stability. Different blade coning angles under yawed inflow conditions are considered for some exploratory stability calculations, using the aeroelastic code HAWC2.

KEYWORDS

Wind turbines, yaw stability, passive yaw, coned rotor

1 INTRODUCTION AND BACKGROUND

A detailed description of a coned wind turbine rotor concept is discussed in [1] (ex. free yaw). Yaw stability of a free yawing turbine is always problematic (see for instance chapter 4.3.3.10 of [2]) and requires extensive analysis. For this paper, only the static yaw stability is considered (no yaw degree of freedom present). Note that a free yawing configuration can only be stable dynamically in yaw (see figure 1) when there is at least static stability. One of the key parameters which can influence yaw stability is blade coning angle (see figure 2).

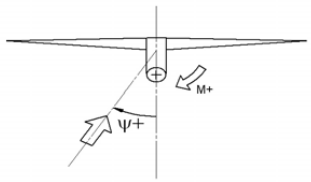

Figure 1

Static stability requirement: for positive yaw error Ψ, the yaw moment should be as indicated (positive). For a negative yaw error, the yaw moment should be negative to in this frame of reference. In the stable case, the yaw moment will realign the turbine again with the flow (Ψ to 0).

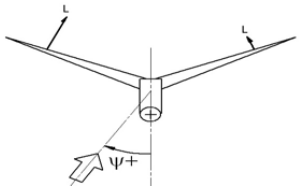

Figure 2

For a coned rotor, depending on the azimuth position, there will always be one blade which is better aligned with the flow compared to the others, resulting in different aerodynamic loading (i.e. lift). This difference in lift on the left and right part of the rotor results in a stabilizing yaw moment.

dave@risoe.dtu.dk

A coned rotor can be achieved by either having a stiff blade under a constant coning angle (set at the hub), a flexible blade which deforms significantly in flap-wise direction or a combination of both. For this study, a stiff blade with a constant coning angle is considered (as illustrated in figure 2).

2 METHODOLOGY AND SIMULATION MODEL

HAWC2 [2] is used to perform time domain simulations, using a medium sized, 3 bladed, downwind wind turbine (see table 1). From the steady state results of the time domain simulations, the average values over a 50 second period are considered in this paper. Both the tower and the blades have a quite stiff structural layout. The generator torque can be varied to a certain extent, resulting in a variation in rotational speed in low wind speeds. A deterministic wind field with shear (power law, exponent 0.2) and a tower shadow model is used for all simulations.

Table 1: Key parameters of the considered wind turbine model

Configuration	3 blades, downwind, stall controlled	**Cut in- cut out wind speeds**	3 – 25 m/s
Rated power	140 kW	**Rated wind speed**	12 m/s
Blade length	10 m	**Hub radius**	0.5 m
Tower Height	30 m	**Rated RPM**	57 rpm

By performing simulations for each coning angle and yaw error from cut-in to cut-out wind speed, a complete picture of the static yaw stability can be drafted. The yaw moment at the virtual yaw bearing (fixed in yaw) determines the stability: stable when yaw error and moment have the same sign (see figures 1 and 2).

In order to assess how different radial positions contribute to the yaw moment, the blade loadings at different radial positions are evaluated. They are summed up over all 3 blades and their moment contribution around the yaw bearing point is calculated. In doing so, contributions of both structural- and aerodynamic forces and moments at the blade are taken into account. This approach provides some first insight in what part of the rotor destabilizes the yawing behaviour.

3 RESULTS

3.1 Power output and flap-wise blade root bending moment as function of coning angle

Figure 3 (left) outlines the dependency of the power output on wind speed and coning angle. For especially large coning angles (larger than 20 deg), the drop in rated power is significant. Further, the additional introduced centrifugal forces due to the coning angle will alleviate the blade root bending moments. Theoretically, one could consider changing coning angle during

operation so that the flap-wise blade root bending moment is always close to zero. In figure 3 (right), the blade root bending moment is plotted for different wind speeds and coning angles. Note that the average blade root bending moments are affected significantly as function of coning angle.

Based on figure 3, one could intuitively say that a coning angle in the range 10-20 degrees could mean a close to zero blade root bending moment for some wind speeds while having a not too high penalty on the power output.

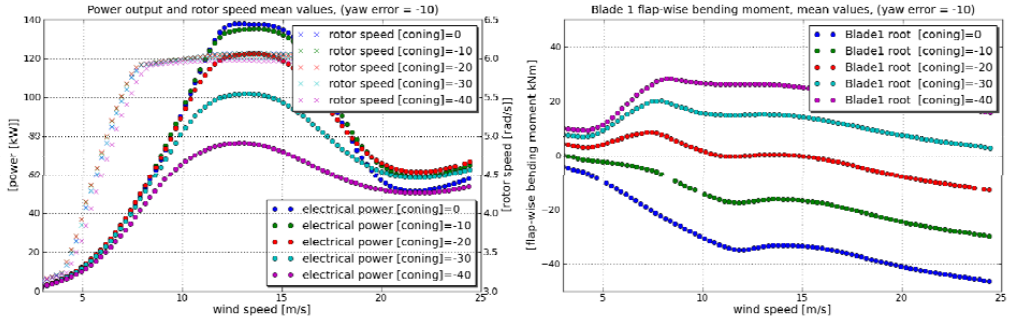

Figure 3: Power output (left) and blade root bending moments (right) as function of wind speed and coning angle

3.2 Yaw moment as function coning angle

A turbine under yawed inflow conditions behaves asymmetrically with respect to the yaw moment: wind coming from the right or left results in non symmetric loadings (see figure 4). In order to have static stability, a negative (positive) yaw error requires a negative (positive) yaw moment. From figure 4, it can be concluded that positive yaw angles are not problematic with respect to static yaw stability for a coned rotor, since at all times the yaw moment is larger than zero. For a negative yaw error on the other hand, between 11 and 16 m/s (depending on the cone angle) there exists a destabilizing yawing moment.

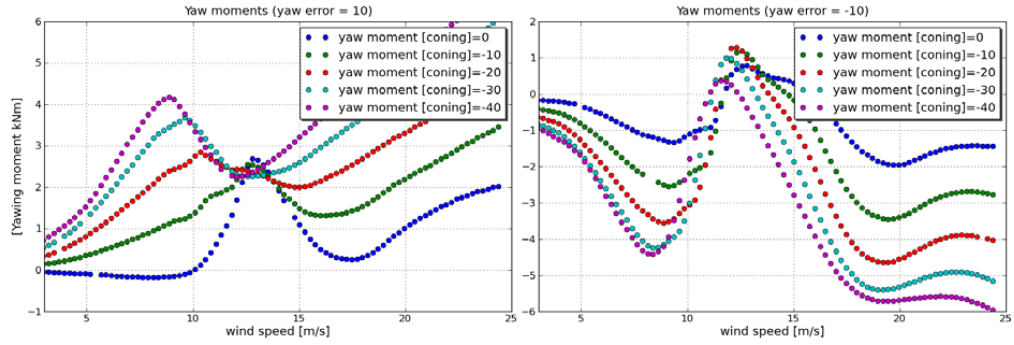

Figure 4: Yaw moment for different coning angles, while subject to a yaw error of 10 and -10 degrees. Static stability for positive (negative) yaw error when yaw moment positive (negative)

3.3 Radial blade load yawing contributions

In order to identify which airfoil sections are responsible for the unstable yaw moment contribution in the negative yaw error cases, yaw moment contributions for different radial positions of the blade are evaluated. The average yaw moment contribution of each node (considering the 3 blades) is plotted for different coning angles and wind speeds in figure 5. Especially the inner part of the blade (relative radius of 15-45%) contributes to a destabilizing yaw moment.

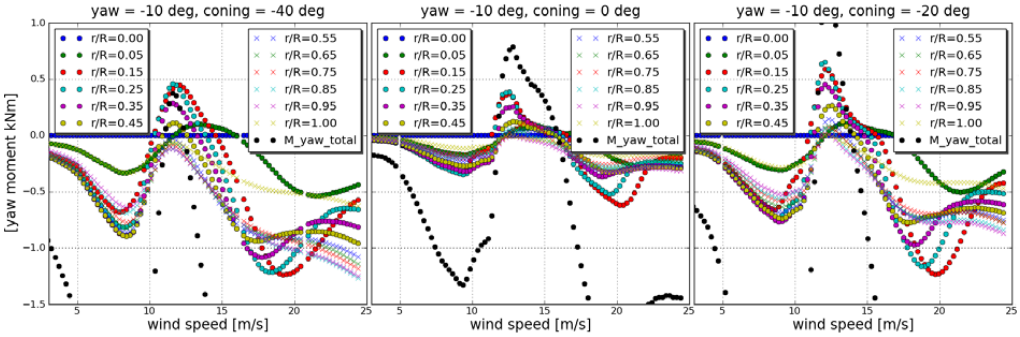

Figure 5: Yaw moment contributions per 3 blades radial positions, ranging from root to tip

4 CONCLUSIONS AND FUTURE WORK

Static yaw stability seems to be achievable for a downwind, coned rotor. However, an unstable region around 11-16 m/s (depending on coning angle) remains for negative yaw errors. The inner part of the blade is responsible for these small unstable regions and it is suggested to further investigate the influence of lift/drag contributions, airfoil selection and 3D aerodynamic correction methods on the yawing moment.

5 ACKNOWLEDGEMENTS

The authors wish to express their appreciation for the funding of this work by the EU. Details regarding the Marie Curie funded project are: WINDLFOWER, Aeroelastic tailoring of a passive wind turbine rotor and validation of design code. Grant number 230698.

6 REFERENCES

[1] Curran Crawford and Jim Platts, “Updating and Optimization of a Coning Rotor Concept,” *Journal of Solar Energy Engineering* 130, no. 3 (2008): 031002-8. [DOI: 10.1115/1.2931497]

[2] Manwell, McGowan, Rogers, Wind Energy Explained, Wiley 2002, ISBN: 0-470-84612-7

[3] Torben J. Larsen, “HAWC2 user manual”, Tech. Report Ris-R-1597(ver. 3-9)(EN), Risø National Laboratory, Denmark, September 2009.

Aerodynamics of Diffuser-Augmented Wind Turbines

B.M. Geurts[1)], C. Simão Ferreira[1)], G.J.W. van Bussel[1)]

[1)] Technical University Delft, The Netherlands

ABSTRACT

My PhD work at the TU Delft is funded by a European Framework-7 project. The aim of the project is the development of a roof-mounted system combining solar-thermal, PV, and wind energy. To maximize the wind power potential, the roof-mounted construction will feature a diffuser type of structure around the turbines. My contribution involves the aerodynamics of the diffuser-turbine-combination. In this context, I simulated a 2D VAWT in a diffuser and performed basic experiments with HAWT's in straight and circular diffusers. In the future these experiments and simulations will be extended to other methods and setups.

KEYWORDS

Diffuser, HAWT, VAWT, Flow augmentation.

1 INTRODUCTION

The RoofCapture project is a Framework-7 project. This means that a number of small and medium-sized companies get financial support from the European Commission to spend on scientific support for a proposed development project. In the RoofCapture project, the target is to design, build, test and market a roof-mounted setup combining different sustainable energy generation components. The wind energy department at the TU Delft contributes to this scientific support in the form of my PhD position. My main assignment is therefore to provide knowledge from simulations and experiments to base the aerodynamics of the RoofCapture design on. In my position as a PhD-student, however, I also want to perform research which can be of value from an academic point of view. This brings along consequences for both the choice of the research topic and the time allocation.

The initial RoofCapture concept featured a diffuser ring around an Eclectic D400 turbine as well as a 2D diffuser (half), both shown in figure 1. The initial test results with the prototype-diffusers were disappointing, and suggested that there is more to a diffuser than meets the eye. As there exist different diffuser-theories, and they hardly ever concur with each other, my efforts are now directed at the aerodynamic research on diffuser-augmented wind turbines.

2 EXISTING DIFFUSER THEORY

Diffuser research has been on-going since the 50's and the research from the early days is still highly referenced although diffuser-augmented turbines have never really found their way to commercial applications up until recent years. In the seventies, Foreman, Gilbert and Oman [1] estimated the power augmentation using one-dimensional momentum theory with loss factors and a dependency on the thrust coefficient C_T which they validate with wind tunnel tests. These tests, however, are conducted in a very small wind tunnel, resulting in questionable Reynolds numbers. The turbine is simulated using a drag-screen, omitting the possible interaction of the tip-vortices with the diffuser. In the eighties, Igra [2] avoids the vague loss factors and introduces a turbine load factor, diffuser pressure recovery and shroud exit pressure. In similar experiments as those performed by Forman, Gilbert and Oman, Igra starts with long diffusers to combine a descent area ratio with very low wall angles. Subsequently, he tries to shorten the diffuser by adding detached flap sections behind the diffuser shroud. These tests also feature a screen setup and questionable Reynolds numbers. In the later researches by van Bussel [3], Lawn [4] and Werle and Presz [5], similar issues occur in various combinations. The main goal is generally to be able to predict the performance of the augmented turbine, but the understanding of the actual aerodynamics, and the interaction between the diffuser and the turbine and its tip vortices remain mostly covered in mist.

Figure 1: Prototype of the diffuser-augmented Eclectic D400 turbine during wind-tunnel tests

3 CURRENT RESEARCH

With the testing of the prototype diffuser setups in combination with the Eclectic D400 turbine shown in figure 1, a first orientation took place. From the disappointing test results, the question rose whether a crosswind turbine could maybe be more appropriate for the RoofCapture application. Using a 2D panel code, an initial investigation showed promising power increases for the augmented VAWT, but also gave rise to some very interesting

questions. A higher velocity increase through the empty diffuser did not necessarily result in a higher power output from a turbine installed in this diffuser. Figure 2 shows the averaged velocity induction field for two different diffuser nozzle areas with an identical VAWT inside. It is possible to come up with different reasons for this phenomenon, but more research is needed to pinpoint the exact aerodynamics behind the observed flow behavior.

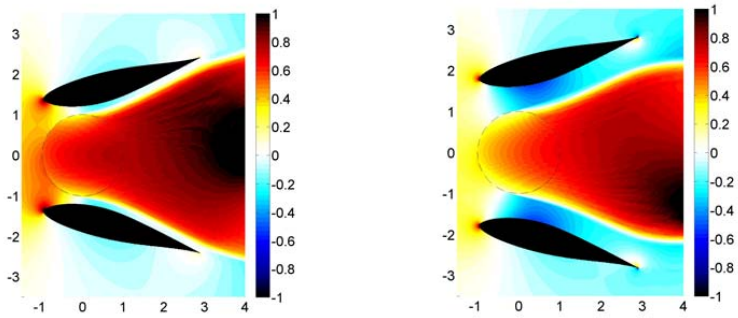

Figure 2: Velocity induction distribution for two different diffusers with identical VAWTs

4 FOLLOWING STEPS

With more time allocated to real research for the remainder of my PhD, a whole list of logical next steps is worked out as shown in table 1. Some of the steps will be taken in parallel, while some have to be taken in series.

Table 1: Summary of the planned future research steps

More extensive 2D vortex code – VAWT	3D Vortex Code – VAWT
2D CFD calculations – VAWT	3D Vortex Code – HAWT
Experiments – VAWT	Experiments – HAWT

The clear first step is to expand the 2D vortex code simulations of the VAWT in order to form a clear and complete image of the situation. As a check, 2D CFD calculations can be of use. In order to extend the gathered knowledge and generalize a possible theory, the case of the diffuser-augmented HAWT also has to be investigated. To avoid pitfalls associated with 2D (actuator disc) approaches, a 3D vortex code will be used. Simultaneously, this same simulation code will be used to expand the VAWT-case with a third dimension. Unquestionably, this theoretical research has to be checked and validated with experiments. To this extend, wind tunnel tests will be performed with both diffuser-augmented HAWTs and VAWTs along the course of my PhD. The timing, however, will be determined by the available resources.

BIBLIOGRAPHY

[1] Foreman, K.M.; Gilbert, B.; Oman, R.A.: Diffuser augmentation of wind turbines. Joint conf. Of american Section int. Solar Energy soc. & Solar Energy soc. Canada. 1976

[2] Igra, O.: Research and development for shrouded wind turbines. European Wind Energy Congference, 1984

[3] Van Bussel, G.J.W.: An assessment of the performance of diffuser augmented wind turbines (dawt's). 3rd ASME/JSME Fluid Engineering Conference San Fransisco. 1999

[4] Lawn, C.J.: Optimization of the power output from ducted turbines. Proceedings of the Institution of Mechanical Engineers, Part A: Journal of Power and Energy. 2003

[5] Werle, M.J.; Presz W.M.: New Developments in Shrouds and Augmentors for subsonic Propulsion Systems. 44th AIAA Joint Propulsion Conference & Exhibit. 2008

Part 3

Session 3A - Rotor Design I

- Bond Graph Modelling of Wind Turbine Rotor
  Yihan Xing, NTNU
- Modelling the Aerodynamics of Vertical-Axis Wind Turbines in Urban Wind Conditions
  Frank Scheurich, University of Glasgow
- Comparative Study of Distributed Active Load Control Concepts for Wind Turbine Blades
  Peter Bæk, LM Wind Power and Risø DTU
- Root Flow Aerodynamic Investigation of a HAWT
  Busra Akay, TU Delft

Bond Graph Modelling of Wind Turbine Rotor

Yihan Xing[1)], Eilif Pedersen[2)], Torgeir Moan[1)]

[1)] CeSOS, NTNU, Trondheim, [2)] IMT, NTNU, Trondheim

ABSTRACT

This paper presents the application of a graphical modelling method, the bond graph method, to the mathematical modelling of the wind turbine rotor. A multi-body approach is adopted where the rotor is divided into rigid hub and elastic blade bodies. The individual bodies are modelled separately and then interconnected using spring-damper systems to give the complete rotor model. This is developed using the bond graph specific software *20Sim* and verified for steady state conditions. The motivation is to demonstrate the application of an easy-to-use and systematic tool for modelling and simulation of large, complex engineering systems, e.g. the wind turbine.

KEYWORDS

Bond Graph, System Modelling, Wind Turbine

1 INTRODUCTION

The bond graph method is an intuitive representation of the physical system. It consists of an energy-conserving network of bonds (represented by lines) and lumped parameter elements of resistance, capacitance and inductance (represented by symbols). Energy is exchanged between the elements through the bonds as a combination of effort (force) and flow (velocity). The system equations are then derived automatically from the bond graph representation and then used for the simulation process. For an extensive and detailed overview of this method, see Karnopp [3]. In this paper, the bond graph technique will be applied to model the NREL 5MW offshore baseline wind turbine rotor [2].

2 BOND GRAPH MODEL OF WIND TURBINE ROTOR

2.1 System Overview (see Figure 1)

The rotor is modelled in four degrees of freedom, three translational dofs and one rotational dof about the rotor spin axis (also the direction of incoming wind). The rotor is divided into four bodies; one hub body and three blade bodies. The hub is represented as a rigid body mounted on spring-damper systems (representing bearings) and the blade body is

represented as a rigid body with superimposed elastic modes. The Karnopp-Margolis method [3] is used for the connection between the hub and the blades. Four different types of bond graphs sub-models, (i) to (iv), are required here. To ease understanding, simplified bond graphs of these sub-models will be presented in this paper.

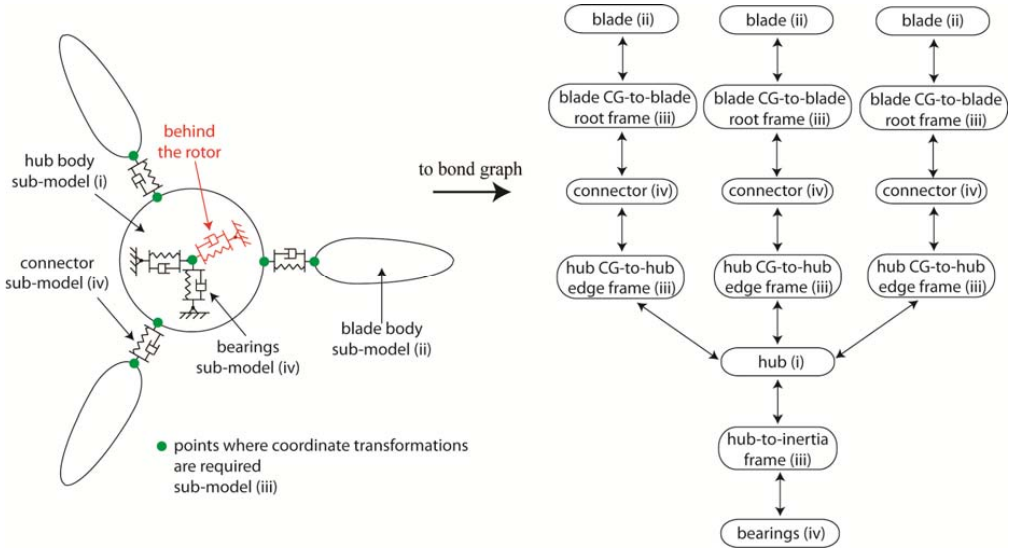

Figure 1: System Overview of the Wind Turbine Rotor

The individual sub-models are then interconnected to give the complete bond graph from which the system equations are derived and then used for simulation.

2.2 Bond Graph Sub-Models

(i) Rigid Hub Body

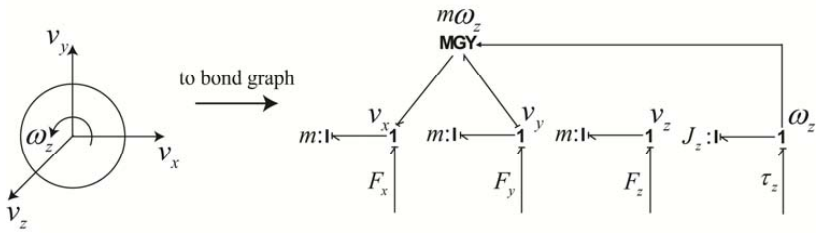

Figure 2: Bond Graph of Rigid Body Dynamics

This bond graph corresponds to the hub in the Eulerian (CG-fixed) coordinate system and thus requires coordinate transformations to the inertia frame.

(ii) Elastic Blade

The blade is modelled as a pre-twisted beam with free-free ends. The bond graph of a simpler case of a uniform elastic beam is shown. There are three groups of elements shown

corresponding to the rigid body modes, the first elastic mode and the second elastic mode. It is possible to include additional modes if desired. One of the free ends will be connected to the hub in the complete bond graph.

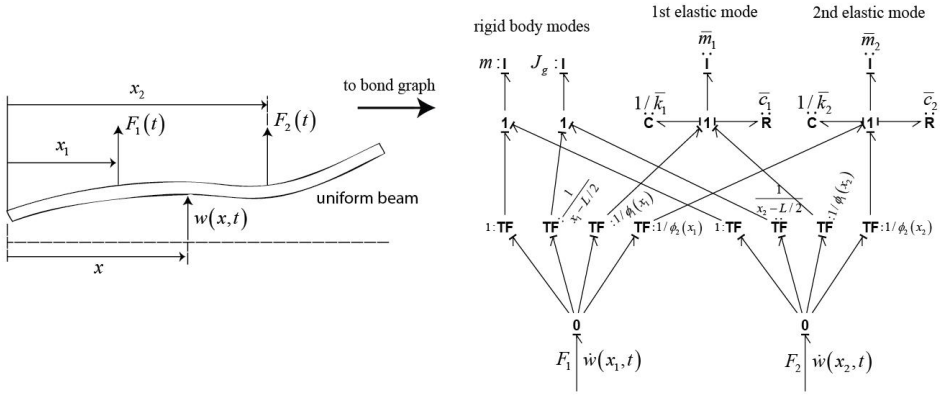

Figure 3: Bond Graph of Elastic Beam

(iii) Coordinate Transformations

The green points in Figure 1 are points where coordinate transformations are required. The bond graph equivalent is the modulated transformer (MTF) element. $\underset{\sim}{m}(\theta)$ is the transformation matrix.

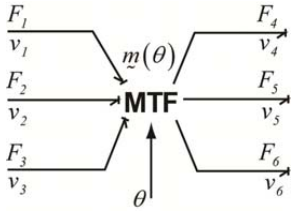

Figure 4: Transformer Element for Coordinate Transformations

The TF-element relates efforts (forces) and flows (velocities) between the original and the transformed coordinates.

(iv) The Karnopp-Margolis method [3] - Spring-Damper System (Connector/Bearings)

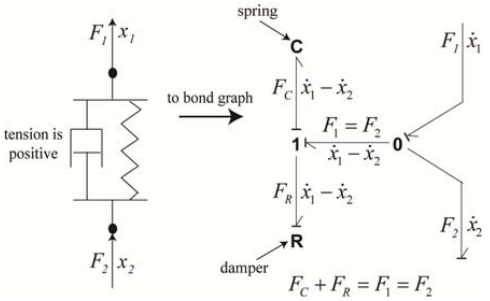

Figure 5: Bond Graph of Spring-Damper System

2.3 Aerodynamic Loads

The aerodynamic load calculations are based on the blade element momentum (BEM) method. Details of the BEM method can be found in Hansen [1].

3 RESULTS AT STEADY STATE CONDITIONS

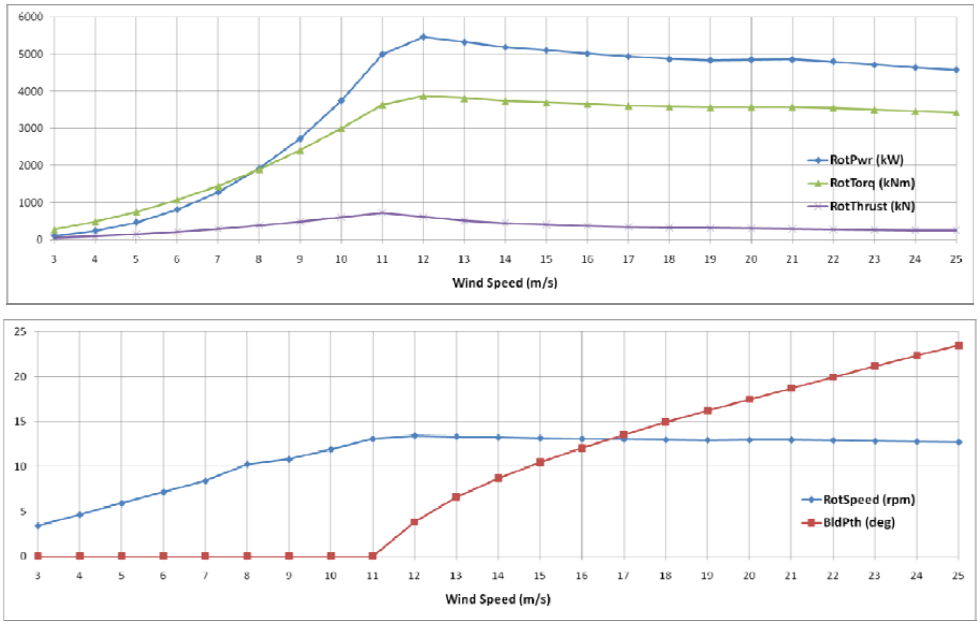

Figure 6: Results at Steady State Conditions

4 CONCLUSIONS

In this paper, the bond graph method is applied to the modelling of a wind turbine rotor. The method is intuitive, systematic and easy to use. The feature of automatic system equations generation allows one to focus more on modelling of the system of interest. Therefore, the bond graph method is useful and effective for use as a modelling tool for large complex systems such as the wind turbine.

BIBLIOGRAPHY

[1] Hansen, O.L. *Aerodynamics of Wind Turbines 2nd Edition.* UK : Earthscan, 2009. ISBN 978-1-84407-438-9.

[2] Jonkman, J., et al. *Definition of a 5-MW Reference Wind Turbine for Offshore System Development, Technical Report.* s.l. : NREL/TP-500-38060, 2009.

[3] Karnopp, D.C., Margolis, D.L. and Rosenberg, R.C. *System Dyanmics: Modeling and Simulation of Mechatronic Systems.* New Jersey : John Wiley & Sons Inc., 2006. ISBN 0-471-70965-4.

Modelling the Aerodynamics of Vertical-Axis Wind Turbines in Urban Wind Conditions

Frank Scheurich [1)]

[1)] University of Glasgow, Glasgow, United Kingdom

1 INTRODUCTION

In contrast to current on- and offshore wind farms where mostly large-scale horizontal-axis wind turbines are deployed, one of the strategies of harvesting wind energy in the urban environment is based on small-scale vertical-axis wind turbines with rotor diameters of only several metres. The aerodynamics of the urban environment are characterised by unsteady winds and frequent changes of wind direction. In addition, the presence of buildings might cause urban wind turbines to operate in oblique flow, in other words in conditions in which the wind vector is non-parallel to the horizon. The application of vertical-axis wind turbines in cities (Fig. 1) is mainly due to their inherent advantages over horizontal-axis wind turbines in urban wind conditions. Particularly, vertical-axis wind turbines are, by design, insensitive to the wind direction, whereas horizontal-axis wind turbines have to be rotated into the wind each time the wind direction changes.

In the present paper, results of a numerical study will be presented that show the effect of unsteady and oblique flow on the performance of several different vertical-axis wind turbine configurations.

(a) Arena at Kings Dock, Liverpool, UK **(b) Cleveleys Promenade Café, Cumbria, UK**

Figure 1: Current examples of arrangements of urban vertical-axis wind turbines. (Courtesy of Quiet Revolution Ltd.)

2 COMPUTATIONAL AERODYNAMICS

The aerodynamic performances of three different vertical-axis wind turbines have been simulated using a Computational Fluid Dynamics (CFD) method that is called the Vorticity Transport Model (VTM), developed by Brown [1]. In contrast to more conventional CFD techniques in which the flow variables are pressure, velocity and density, the VTM is based on the vorticity-velocity form of the unsteady incompressible Navier-Stokes equation

$$\frac{\partial}{\partial t}\omega + u \cdot \nabla \omega - \omega \cdot \nabla u = S + \nu \nabla^2 \omega \ , \qquad (1)$$

where ω is vorticity, u is flow velocity, S is the vorticity source and ν is the kinematic viscosity.

3 TURBINE MODEL

Three vertical-axis wind turbines, one with straight blades, another with curved blades and another with a helically twisted blade configuration (Fig. 2) have been investigated. The configurations are described in more detail in Ref. [2]. The orientation of the blades and specification of the azimuth angle of the turbine with respect to the mid-span of blade 1 is shown in Fig. 3.

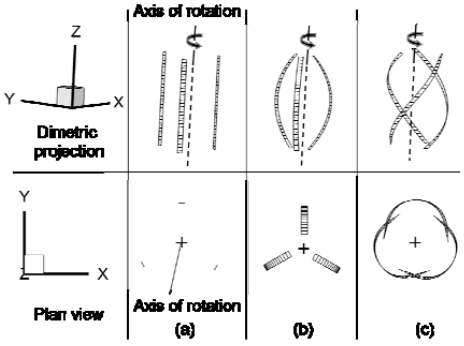

Figure 2: Vertical-axis wind turbines with (a) straight, (b) curved, and (c) helically twisted blades.

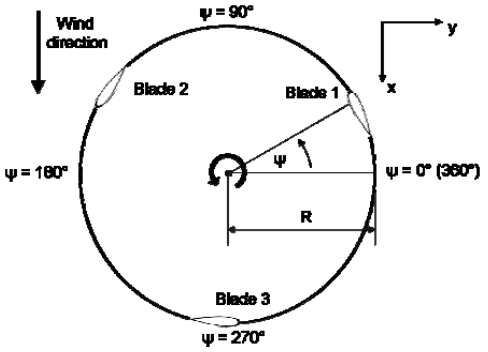

Figure 3: Definition of rotor azimuth

4 PREDICTION OF TURBINE PERFORMANCE AND WAKE DYNAMICS

4.1 Normal and Oblique Flow Conditions

Each configuration was operated in normal flow, in other words, in conditions in which the wind vector is normal to the axis of rotation, and in oblique flow, in other words, in conditions in which the wind vector was non-perpendicular to the axis of rotation of the turbine. The

straight- and curved-bladed configurations develop a torque coefficient that oscillates considerably during each rotor revolution, as shown in Fig. 4. The helically twisted configuration produces a relatively steady torque, in comparison, in both normal and oblique flow. The vorticity field in the rotor wake, as it intersects a plane that is immersed in the flow and contains the axis of rotation, is depicted in Fig. 5.

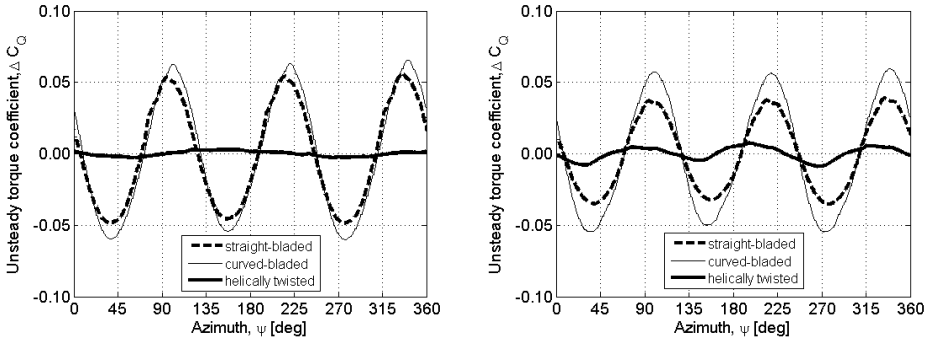

(a) normal flow (flow angle: β=0°) **(b) oblique flow (flow angle: β=20°)**

Figure 4: VTM-predicted variation of the unsteady component of the torque coefficient developed by different wind turbine configurations in (a) normal and (b) oblique flow.

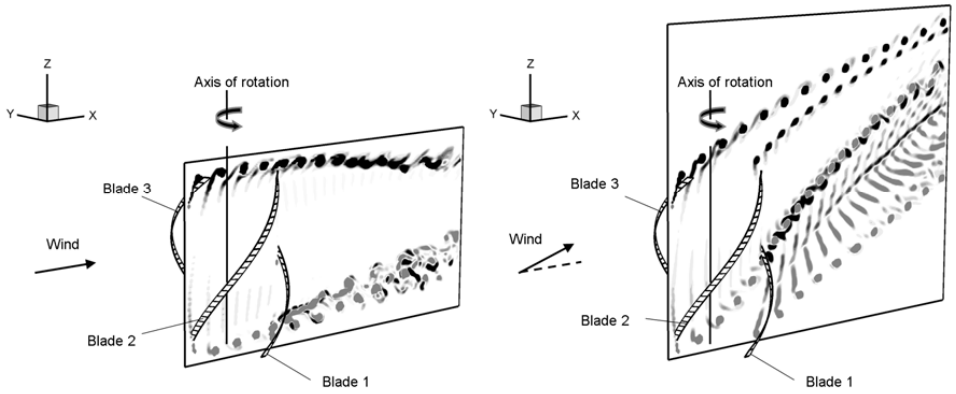

(a) normal flow (flow angle: β=0°) **(b) oblique flow (flow angle: β=20°)**

Figure 5: Computed vorticity field surrounding a vertical-axis wind turbine with helically twisted blades in (a) normal and (b) oblique flow.

4.2 Unsteady Wind Conditions

The VTM-predicted variation of the torque coefficient for each turbine configuration during one rotor revolution is presented in Fig. 6(b) for when the turbines were operated in a free stream velocity that varied with time according to the profile shown in Fig. 6(a). Each of the three configurations that were investigated develops a torque coefficient that oscillates significantly over the period of a single rotor revolution. Both straight- and curved-bladed

turbines produce a torque that features considerable high-frequency content, whereas the helically twisted configuration develops a torque that varies sinusoidally but lags the unsteady free stream by approximately one half of a revolution.

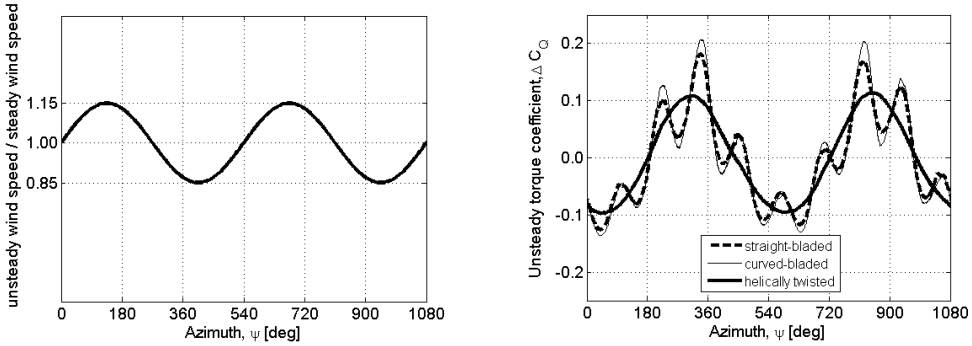

(a) unsteady wind **(b) torque**

Figure 6: VTM-predicted variation of the unsteady component of the torque coefficient developed by different wind turbine configurations in unsteady wind conditions.

5 CONCLUSIONS

The VTM simulation results indicate that a turbine with helically twisted blade configuration produces steadier torque within one rotor revolution, both in normal and oblique flow, when compared to either straight- or curved-bladed turbines. Significant oscillations in torque are developed by each turbine when it is operated in unsteady wind conditions. In an unsteady wind, both the straight- and the curved-bladed turbine produce a significant high-frequency component to their torque, whereas the variation in torque of the helically-twisted configuration is very much smoother and follows the sinusoidal variation of the unsteady free stream. The results suggest that vertical-axis wind turbines with helically twisted blades might be more suited to the urban environment since they develop a steadier torque, by comparison, and thus reduced noise and vibration – important characteristics for both the public acceptance of wind turbines within cities and the design life of the system. The research also reveals that the consideration of off-design operating conditions is essential in any study that aims to evaluate the performance of an urban wind turbine.

REFERENCES

[1] Brown, R.E. Rotor Wake Modelling for Flight Dynamic Simulation of Helicopters. *AIAA Journal*, Vol. 38, No. 1, pp. 57-63, 2000.

[2] Scheurich, F., Fletcher, T.M., and Brown, R.E. The Influence of Blade Curvature and Helical Blade Twist on the Performance of a Vertical-Axis Wind Turbine. AIAA-2010-1579. 48th AIAA Aerospace Sciences Meeting, Orlando, FL, USA, 4-7 January 2010.

Comparative Study of Distributed Active Load Control Concepts for Wind Turbine Blades

Peter Bæk[1,2], Mac Gaunaa[2], Peter Fuglsang[1], Niels Sørensen[2]

[1] LM Wind Power, Denmark, [2] Risø-DTU, Denmark

ABSTRACT

The objective of this study has been to compare two promising concepts for load control on one modern wind turbine airfoil. The two concepts, a trailing edge flap, and a microtab, have been modeled using 2D CFD to compare their steady and unsteady characteristics. The steady state results for the microtab have been compared with wind tunnel measurements, and found to agree very well at moderate angles of attack. A flap was designed to have the same steady state lift response as the microtab, and the unsteady responses were compared. It was found that the microtab exhibits an initial reverse lift response, not seen in the flap response. This gives the microtab a disadvantage compared to the flap also in terms of control delay. In general the microtab was found to have a higher drag than the flap for the same lift increment.

KEYWORDS

Flap, Microtab, Flow Control, Wind Turbine, Unsteady CFD

INTRODUCTION

The scope of this study has been to compare the performance of two promising distributed active load control (DALC) concepts for wind turbine blades. The first concept known as the deformable trailing edge flap, has been investigated by Risø-DTU for several years [1][9][9]. A second concept, namely the microtab, has been proposed and investigated by UC Davis largely by the means of CFD [2]. In this study the 2D characteristics, both steady and unsteady, of the two concepts applied to a typical wind turbine airfoil have been computed by using Ellipsys2D, a Navier Stokes equation solver developed at Risø-DTU [3][4][5]. The computations were validated by wind tunnel tests performed in the Low Speed Wind Tunnel (LSWT) of LM Glasfiber. By using the same tools and the same airfoil at similar flow conditions a direct comparison of the two DALC concepts was possible. This study contributes to a basis for selecting the most suitable concept for implementation on future multi MW wind turbines with distributed active load control.

The microtab (MT) is a small tab or plate emerging from the surface of the airfoil near the trailing edge. It is similar to a Gurney flap, except that it is retractable. A MT deployed on the

pbk@lmwindpower.com

pressure side of the airfoil will increase lift, while a MT deployed on the suction side will decrease lift. The effect of the MT can be thought of as changing the effective camber of the airfoil. An earlier parameter study of MT's performed by UC Davis [2] was used for selecting the baseline case, which is a tab with a height of 1% of the chord-length (*c*) high, placed 5% of the chord-length from the trailing edge. Studies at Risø-DTU have shown that a trailing edge flap of 10% of the chord length is a good baseline case for DALC purposes [9].In this study the DU-96-W-180 airfoil was investigated. This airfoil is typically found on the outer part of modern wind turbine blades. The airfoil is lightly loaded at the trailing edge and was considered good for applying load control devices. A baseline flap was found by deflecting a rigid trailing edge flap hinged at 90% of the chord-length until the lift increment matched that of the microtab. At the operational point of the chosen airfoil (aoa=6°) a 8° deflection downwards of the flap corresponded to a 1%chord MT deployed on the pressure side at flow conditions.

NUMMERICAL STUDY

Ellipsys2D has been used throughout this study, both for steady and unsteady calculations. Ellipsys2D is a Navier Stokes equation solver developed at Risø-DTU [3][4][5]. The γ-Re_θ correlation based transition model by Menter [12] was used during all computations, unless otherwise stated, in the present investigation, in the version implemented by Sørensen [6] with a k-ω SST turbulence model. The grids were generated using Hypgrid2D [13] on a 512 cell (along the airfoil) by 256 cell (perpendicular to surface) mesh. The y+ of the first cell was kept below ~2. In Figure 1 the meshes are shown.

For the steady state calculations a QUICK difference scheme and SIMPLE pressure correction were used. For the unsteady unsteady calculations the second order upwind scheme, and PISO pressure correction were used. For each time step 6 sub-iterations were performed.

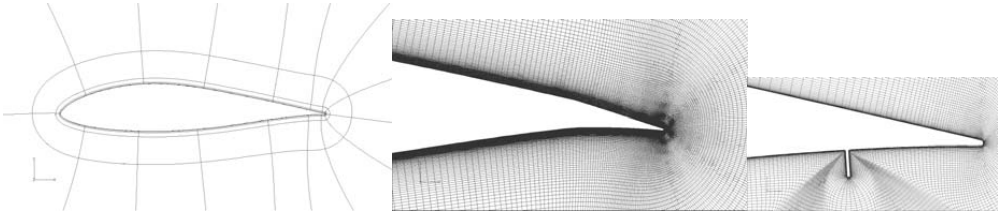

Figure 1: CFD Mesh. Left, block layout. Middle, flap deflected 5 deg down. Right, microtab deployed with height 1% chord.

Steady State Results

Figure 2 shows a comparison of the steady state CFD results. It is seen that there is an excellent correspondence between the experiments and the CFD results for the linear part of the lift slope. Above 7° angle of attack the CFD and the experimental results do not agree. This is not surprising, since the onset of separation is highly dependent on the setup, both in experiments and in CFD, and it is very difficult to obtain a reference. On wind turbines the blades are operated close to the maximum lift over drag ratio, which is at 7° angle of attack for this profile. This study has been limited to only investigate close to operating conditions, and therefore the stall characteristics were not in focus. At the same lift increment, the drag of the microtab is generally higher than that of the flap. The lift enhancement of the microtab diminishes towards lower angles of attack. This is believed to be caused by the increasing boundary layer size on the pressure side.

Unsteady Calculations

In order to assess the time response of the two DALC concepts the grid morphing capability of Ellipsys2D was utilized. The grid morphing was performed by specifying the grids at the extreme positions of the actuators (MT or flap). A time dependent mixing ratio of the grids was used to obtain intermediate positions of the device by interpolation. For modeling the microtab it was necessary to introduce intermediate grids in order to avoid highly skewed cells due to the stretching of the cells in the grid. Intermediate meshes were made at h=0.1, 0.25, and 0.5%c.

A series of step responses were calculated for both the microtab and flap. The step had form of a sinusoidal ramp from 0 to 1:

The nondimensional frequency was varied from f=1 U/c, which gives a ramp time of T=0.5 c/U to f=0.166 U/c, which gives a ramp time of T=3 c/U.

The time step of the CFD computation were limited by the requirement that the surface of the microtab traveled less than one normal cell hight during one time step. For a deployment time of T=1 c/U the time step was 10^{-4} c/U, and this was inversely scaled with the deployment time. For all cases, the initial condition was a converged steady state solution. The simulation was then run for one non-dimensional time unit c/U, after which the device action commenced.

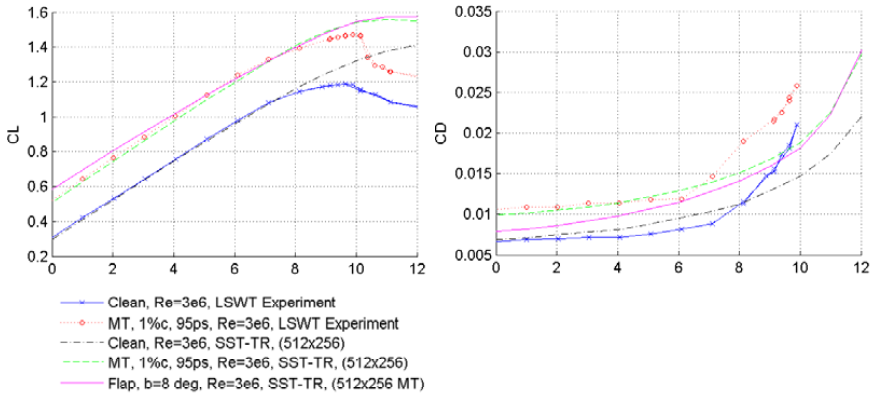

Figure 2: Steady state CFD results (full lines) for the two concepts. Upper: lift coefficient, lower: drag coefficient. Re=3*10^6. Experimental results for the microtab (squares) and the clean airfoil (circles) are shown.

In Figure 3 the responses of the deployment of flap and microtab are shown. There is a remarkable difference in the initial phase. Whereas the flap lift increases monotonously, the microtab features an initial reverse lift peak. This means that the lift of the flap reaches its steady state faster that the microtab. The flap response features a very small discontinuity of the lift at the beginning and end of the deflection ramp. This is caused by the discontinuity in the acceleration of the flap, which is unphysical. However, the simple ramp function was favoured over a more physical behavior, due to the lack of information about the actual transient.

The initial reverse control is also found in the studies of Baker et al. [2]. Depending primarily on the speed of the deployment a region of suction develops just downstream of the microtab. This region of suction will then grow with some convection velocity which is considerably slower than the free stream velocity. The effect on the global circulation of the airfoil, and hence lift, is seen when the suction region has been convected all the way to the trailing edge. Until then the suction region on the microtab surface creates a force opposite of that of the steady state deployed microtab. Once the suction region has merged with the suction side of the airfoil, the circulation of the airfoil increases and vorticity is shed into the wake. This effect can be modeled by the Jones approximation.

It was found that for the 5MW UPWIND Reference Turbine, a delay of 50ms would reduce the load reduction potential of an active control device by 50% [11]. A delay corresponding to that of the step response with a non-dimensional time of T=1 c/U, is in the order of

magnitude of 50 ms, which might indicate that the load reduction potential of the microtab is only 50% of that of the flap.

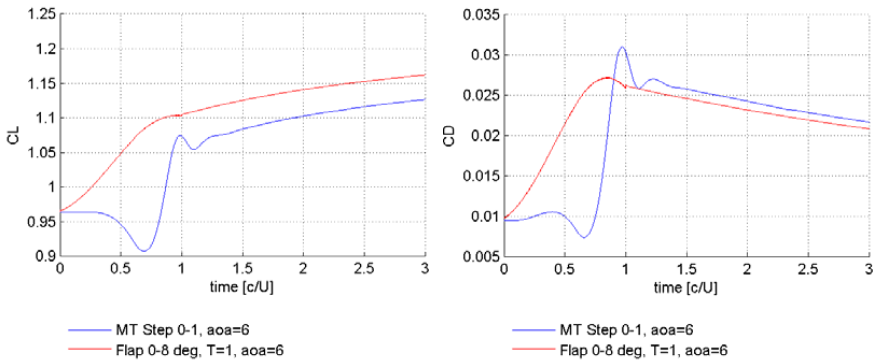

Figure 3: Lift and drag coefficient response to a deployment of a microtab and a flap.

CONCLUSIONS

A 10% c rigid flap deflected 8deg was found to be equivivalent, with respect to the obtained change in lift, to the fully deployed microtab with a height of 1%*c* placed at 95%*c.*

With respect to dynamic response, the flap concept is more well behaved, as the microtap suffers from a reversed lift response during the intial phase of the movement. Compared to the flap concept, the microtap thus experiences longer time delays for obtaining the desired load changes, which might be critical for obtaining maximum load aleviation.

REFERENCES

[1] Basualdo, S. *Load Alleviation on Wind Turbines using Variable Airfoil Geometry*, M.Sc. Thesis Project, Technical University of Denmark, 2004.

[2] Baker, J. P., Standish, K. J. and van Dam C. P.*, Two-Dimensional Wind Tunnel and Computational Investigation of a Microtab Modified S809 Airfoil*, AIAA 2005-1186, 2005.

[3] Michelsen, J.A. *Block structured Multigrid solution of 2D and 3D elliptic PDEs*, Technical Report AFM 94-06, Technical University of Denmark, 1994.

[4] Michelsen, J. A. Basis3D - a Platform for Development of Multiblock PDE Solvers. Technical Report AFM 92-05, Technical University of Denmark, 1992.

[5] Sørensen, N. N. General Purpose Flow Solver Applied to Flow over Hills. Risø-R-827-(EN), Risø National Laboratory, Roskilde, Denmark, June 1995.

[6] Sørensen, N. N., *CFD modelling of laminar-turbulent transition for airfoils and rotors using the gamma-(Re)over-tilde (theta) model*, in journal: Wind Energy (ISSN: 1095-4244) (DOI: 10.1002/we.325) , vol: 12, issue: 8, pages: 715-733, 2009

[7] Gaunaa, M. Unsteady *2D Potential-flow Forces on a Thin Variable Geometry Airfoil Undergoing Arbitrary Motion*, Risø–R–1478(EN), 2006.

[8] Fuglsang, P and Bove, S. *Wind tunnel testing of airfoils involves more than just wall corrections*. In EWEC 2008, Brussel, 2008

[9] Troldborg, N. *Computational study of the Risø-B1-18 airfoil with a hinged flap providing variable trailing edge geometry*. Wind Engineering, vol. 29, no. 2, 2005

[10] Buhl, T.; Gaunaa, M.; Bak, C.; *Potential Load Reduction Using Airfoils with Variable Trailing Edge Geometry*. Journal of Solar Energy Engineering. November 2005, Vol. 127, p. 503-516

[11] Andersen P. B et al. *Deformable trailing edge flaps for modern megawatt wind turbine controllers using strain gauge sensors*. Wind Energy. 2009. Published online. DOI: 10.1002/we.371

[12] Menter F. R. et. al. *A Correlation-Based Transition Model Using Local Variables, Part I - Model Formulation*. In Proceedings of ASME Turbo Expo 2004, Power for Land, Sea, and Air , Vienna, Austria, June 14-17 2004. ASME. GT2004-53452.

[13] Sørensen N. N. *HypGrid2D a 2-D Mesh Generator*. Risø-R-1035 (EN), Risø National Laboratory, Roskilde, Denmark, Feb 1998.

Root Flow Aerodynamic Investigation of a HAWT

B. Akay[1)], C.S. Ferreira[2)], G.J.W. van Bussel[3)]
N.A. Olesen[4)], D. Veldkamp[5)]
[1, 2, 3)] Delft University of Technology, The Netherlands.
[3, 4)] Vestas Technology R&D, Denmark.

ABSTRACT

The objective of the present work is to identify and explain the different physical phenomena that play role at the inboard region of a horizontal axis wind turbine-HAWT. The present research aims also to find out the most convenient experimental set-up to measure root region in the Open Jet Facility of TU Delft, the parameters to compare CFD and PIV data, to extrapolate the results obtained with the experimental model to full scale aerodynamic systems. CFD as a numerical tool, Particle Image Velocimetry-PIV as an experimental tool are used for this investigation.

KEYWORDS

Root flow aerodynamics, PIV, CFD.

1 INTRODUCTION

Without having knowledge of the aerodynamic characteristics of a rotor and its most important parameters, accomplishing a general understanding of the operation of a wind turbine would be impossible [1]. However, rotor aerodynamics presents several aspects which are not entirely known and/or currently in the field of research. The physical mechanisms that play role at the root region of a HAWT blade are one of the less understood topics.

One of the most important issues at the inboard region is 3D rotational effects. Rotation has two main effects on the behavior of the flow. First, rotation causes a dynamic pressure which increases towards the tip. Second, it causes two external forces namely Centrifugal and Coriolis forces [2]. At the root area of the blade, the effect of these forces is strong [3]-[5]. While 3D effects do not influence the aerodynamic performance in the attached flow regime significantly, there are visible changes in the separated flow regions. In the regions where the boundary layer flow is 2D and generally moves along the chordwise direction, there is little or no rotational augmentation, but the region where the boundary layer flow directed outboard

and forward towards the leading edge tend to undergo the greatest degree of rotational augmentation. It is also observed that rotation amplifies the aerodynamic forces dramatically and alter the surface pressure distribution [6]-[7]. Although it is well known that the flow is 3D: the angle of attack is high and the flow is highly separated at the root region, still some aerodynamic models use pure 2D airfoil data which may lead clear discrepancies between measured and computed power and load distributions. Therefore, 3D correction for stall which is a correction to the 2D wind tunnel determined aerofoil characteristics data to account for the effects that radial flow has in a rotating system is needed. There are some correction models [8]-[10], intended to correct for stall delay effects.

The present research aims to bring a clear explanation of the rotational effects; the behavior of spanwise flow, the role of Coriolis and centrifugal forces, and root vortex. And it also aims to result in a broad flow visualization of the structures at the root region. To do these, CFD simulations and PIV measurements are performed and compared.

2 EXPERIMENTS

Two sets of PIV experiments were performed; one was in August 2009 and the second one was April 2010. The experiments are performed in the Open Jet Facility (OJF) at the Faculty of Aerospace Engineering at Technical University of Delft (see Figure 1). A 1m radius two-bladed rotor is used in the experiments. The blades are mounted into a new designed model rotor test bench. The Stereo PIV technique is applied to obtain the three components of velocity on the 2D planar fields of view around the blade. Two different measurement setups are designed in the OJF to scan the flow field around the blade by stereo PIV (see Figure 2). The idea behind having two measurement sets in two directions (spanwise and chordwise) is to combine the results to have a solid structure of the flow field around the blade. One can find the results of experiments in Ref. [11].

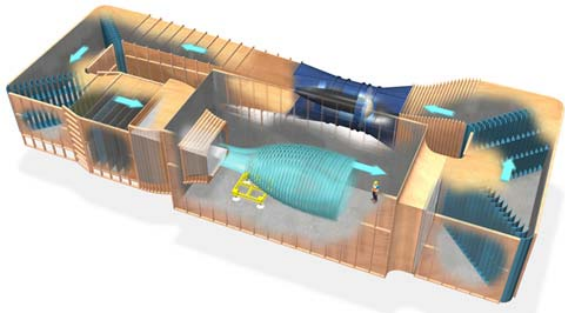

Figure 1: Schematic representation of OJF.

Figure 2: Chordwise (left) and spanwise (right) measurement setups.

3 CFD

3.1 Actuator Disc Simulations

A CFD analysis was carried out to see if the measurements are independent from the geometry of the open jet facility. A numerical solution to the axisymmetric actuator disk-AD problem was performed. Computations were done with the incompressible version of the Reynolds Averaged Navier-Stokes (RANS) equations and the SST k-ω turbulence model. The AD model corresponds to the size of the test rotor which has 1 m radius. Computations were performed for different thrust coefficients, C_T. The results of this study can be found in Ref. [12].

3.2 3D Simulations

There is an on-going study to be able to see the computational requirements such as fine enough grid domain but not computationally expensive etc. One test have been performed by revolving the 2D AD computational domain to a 3D domain. The 3D AD simulations gave the same result with 2D AD simulations.

4 CONCLUSIONS

This study aims to understand the physical phenomena play role at the root flow of a HAWT. The investigations are performed experimentally and numerically by means of PIV and CFD. Two experiments have already been done and AD, 3D freestream CFD simulations have been performed. Besides building the best experimental set-up at OJF to measure root flow, the present research intends to find out some parameters to compare CFD and PIV data, to extrapolate the results obtained with the experimental model to full scale aerodynamic systems.

BIBLIOGRAPHY

[1] E. Hau and H. von Renouard, Wind Turbines, ch. 5 Rotor Aerodynamics, pp. 91–160. Springer Berlin Heidelberg, 2005.

[2] S. Breton, Study of the stall delay phenomenon and of wind turbine blade dynamics using numerical approaches and NRELs wind tunnel tests. PhD thesis, Norwegian University of Science and Technology, 2008.

[3] D. Hu, O. Hua, and Z. Du, "A study on stall-delay for horizontal axis wind turbine," Renewable Energy, vol. 31, pp. 821–836, 2006.

[4] Z. Du and M. Selig, "The effect of rotation on the boundary layer of a wind turbine blade," Renewable Energy, vol. 20, pp. 167–181, 2000.

[5] H. Dumitrescu and V. Cardos, "Rotational effects on the boundary-layer flow in wind turbines," tech. rep., AIAA Journal-Technical Notes, 2003.

[6] S. Schreck and M. Robinson, "Rotational augmentation of horizontal axis wind turbine blade aerodynamic response," AIAA, vol. 0029, pp. 70–82, 2002.

[7] S. Schreck, N. Srensen, and M. Robinson, "Aerodynamic structures and processes in rotationally augmented flow fields," Wind Energy, vol. 10, pp. 159–178, 2007.

[8] H. Snel, R. Houwink, G. van Bussel, and A. Bruining, "Sectional prediction of 3d effects for stalled flow on rotating blades and comparison with measurements," in 1993 European Community WindEnergy Conference Proceedings, Lubeck-Travemunde, Germany, 1993.

[9] J. Corrigan and J. Schillings, "Empirical models for stall delay due to rotation," in American Helicopter Society Aeromechanics Specialists Conference Proceedings, San Francisco, 1994.

[10] P.K. Chaviaropoulos and M. O. L. Hansen, "Investigating three-dimensional and rotational effects on wind turbine blades by means of a quasi-3d navier-stokes solver," Transactions of the ASME, vol. 122, pp. 330–336, JUNE 2000.

[11] B. Akay, G. Tescione, C.S. Ferreira, G.W.J. van Bussel, "Experimental Investigation of the Wind Turbine Blade Root Flow," 48th AIAA Aerospace Sciences Meeting Including the New Horizons Forum and Aerospace Exposition, Orlando, Florida, AIAA 2010-641.

[12] B. Akay, G. Tescione, C.S. Ferreira, G.W.J. van Bussel, "Experimental and Numerical Investigation of the Effect of Rotor Blockage on Wake Expansion," The Science of making torque from wind Conference, Crete, Greece, 2010.

Part 4

Session 3B - Dynamic Loading of Support Structure, Blades and Drive Train

- Effect of Foundation Modeling Methodology on the Dynamic Response of Offshore Wind Turbine Support Structures
  Eric Van Buren, NTNU
- Sizing Process of a Semi-Submersible for Offshore Wind Generation
  Rafael Arias, Universidad Politécnica de Madrid
- Evaluation of Dual Axis Resonant Testing of Wind Turbine Blades
  Peter Greaves, Durham University
- Simulation and verification of the interaction of the dynamics of the all system with the loading of the main components of wind turbines
  Thomas Hecquet, Endowed Chair of Wind Energy

Effect of Foundation Modeling Methodology on the Dynamic Response of Offshore Wind Turbine Support Structures

Eric Van Buren[1)]
[1)] NTNU, Norway

ABSTRACT

Two offshore wind turbine support structures are modeled in the dynamic wind turbine analysis program HAWC2©; a four-legged, full height lattice tower with piled foundations, and a traditional monotower with a monopile foundation. Dynamic time series analyses under operating conditions have been carried out for both structures, each with several different foundation models, including both sand and clay soils. The results are compared based on the modal properties of the structures and the dynamic performance of the tower and turbine.

KEYWORDS

Offshore lattice tower, foundation modeling, piled foundation

1 INTRODUCTION

The in-service performance of an offshore wind turbine foundation can have significant impacts on the operation of the entire system, particularly the dynamic response. Offshore wind turbines are highly dynamic systems and experience significant loading in a wide range of excitation frequencies, including wave loads, wind loads, and vibrations from the rotor and blades [1]. It is therefore rather important to have a relatively accurate prediction of the dynamic properties of the full wind turbine structure, including the foundation and the interaction between it and the soil. In order to achieve this, the structural model of the system must include provisions for the characteristics of the foundation in some form or fashion. The modeling of offshore foundations can be done in a number of ways ranging from extremely simple and generic, to complex and site specific finite element models. The additional complexity and detail can come at a significant cost, however, with greater expenditures in the testing, design, and analysis phases of the project.

2 FOUNDATION MODEL CONCEPTS

2.1 Fully simplified analysis

In the absolute simplest case, wind turbine structures can be preliminarily designed with no foundation model whatsoever; simply a fixed boundary condition is assumed at the base of

the support structure. While this is clearly incorrect and assumes a much higher stiffness than the actual system, it may nevertheless allow for a decent first pass estimation of the structural performance of a wind turbine support tower to be made. The dynamic response using this method may be significantly incorrect, but the modeling procedure and analysis computations will take much less time than for a model with foundation elements included.

2.2 Design standard based analysis

When certifying offshore structures, certain design standards must be followed which include provisions for the design and performance of the foundations [2]. These design standards contain rather simple, and largely empirical methods of estimating the resistive forces and associated movements of a wind turbine foundation for both sand and clay soils. These methods are much quicker and cheaper than full finite element analysis techniques, and require far fewer soil samples and geotechnical tests. The result is far less human and computational effort, as well as capital expenditures on testing, required for modeling and analysis. On the downside, however, these methods are much cruder than a full geotechnical investigation and finite element analysis, and can lead to a great degree of uncertainty. Due to this high uncertainty, many of the wind turbine foundations designed by this method are likely to be highly overdesigned, leading to larger material and installation costs.

2.3 Finite element analysis

To perform a fully detailed, and as closely as possible, accurate foundation design for every turbine in an offshore wind farm requires a significant investment of both time and money. Soil samples must be taken at every turbine location within the wind farm, a wide range of geotechnical tests must be performed, and substantial efforts must be put into computer modeling and analysis. A wide range of considerably complex non-linear finite element analysis tools have been developed for the design and analysis of offshore foundations for the oil and gas industry, tools which could allow for an efficiently and optimally designed foundation to be created for each wind turbine in a wind farm [3]. This would result in lower material use and faster installation periods, but this optimization comes at quite a substantial cost when all of the additional testing, computing power and man-hours are considered.

2.4 Method Comparison

Two important questions regarding offshore turbine foundation modeling may then be asked:

1) Does assuming a fixed boundary condition for the foundation of an offshore wind turbine tower provide an accurate enough estimation of the dynamic characteristics of the tower to warrant its use for preliminary design practices?

2) Does the additional certainty and accuracy in the foundation design of an offshore turbine when utilizing purpose built finite element analysis tools reduce the total costs enough to warrant their use in place of the simple methods in the design codes?

The first of these two important questions will be investigated in this paper, with the second question currently being investigated as the topic of a future paper.

3 HAWC2 MODEL DEVELOPMENT

3.1 Turbine and support structure layout

The layout and design of the components of each tower and of the foundations were chosen to create simple models which are quickly comparable and easily analyzed, thus the NREL 5MW reference turbine and controller were used in all of the analyses [4]. The monotower and piles for each structure were not specifically engineered in any manner, but were rather chosen as representative models for potential offshore wind turbine support structure components. While the designs considered here may not present the most ideal design solution for the cases considered, they nevertheless provide a decent basis for comparing the differences in foundation modeling techniques in line with the scope of this project. The soil parameters used are representative of soils commonly found in the North Sea.

3.2 Soil-structure interaction model

A HAWC2 soil module input file was created which contains the foundation-soil reaction forces based on the equations provided in section 17.7 of the ISO 19902 design standard. The standard treats offshore soils in two main categories, cohesionless and cohesive, and outlines methods for the development of force-displacement curves for each of these soils, so called p-y curves. The soil module also allows for rotational springs which model the resistance of the soil to overturning moments. Because no methods for determining the reaction to this motion are mentioned in the design codes, a method proposed by Randolph, et.al was used [5]. The soil module in HAWC2 consists of tabular values representative of these nonlinear spring forces which are placed on the foundation as seen below in Figure 1.

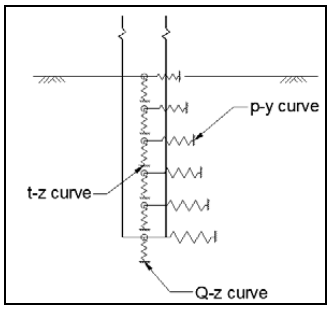

Figure 1: Soil Spring Layout

3.3 Analysis Parameters

All of the analyses were run for time series of 100 seconds using an asymmetric Newmark type solver. The average wind velocity was set to 12 meters per second, a velocity one can reasonably expect to find at an offshore wind farm site. The wind profile also included vertical shear and turbulence developed using a Mann type turbulence generator. The HAWC2 program also computes the aerodynamic drag forces applied to the structural components of the tower using a representative radius and drag coefficient for each body. Only the main legs and the nacelle were included in aerodynamic drag calculations for the lattice tower; a very crude approximation but necessary to keep computation times at a reasonable length. In total there were 11 HAWC2 files to be run, 4 for the monotower and 7 for the lattice tower. Both towers were analyzed with fixed conditions, a sand model with rotational springs, a static clay model with rotational springs, and a cyclic clay model with rotational springs. Each soil model for the lattice tower was also run without rotational springs.

4 RESULTS

4.1 Monotower

The outcomes of the analyses on the monotower structure did not differ greatly apart from the displacements of the nacelle. The moments and forces experienced at the base of the tower showed little variation, with the reactions of the three models including soil modules nearly identical, although the maximum horizontal force for the sand model was somewhat higher. The two clay models showed no difference whatsoever in any of the comparison criteria. This stems from the fact that the extremely large diameter of the monopile significantly limits the lateral deflections and thus never displaced greatly enough to enter the region of the p-y curve where the cyclic effects come into effect.

It is interesting to note that the base bending moments were higher in the models with soil modules which are actually less stiff at the base than the fixed model. This fact shows that the increase in bending moments must be due to dynamic amplification. The largest discrepancy arose in the comparison of the displacements of the nacelle. Surprisingly, the tower with the fixed foundation condition experienced significantly higher displacements than the three models with soil inputs. This is likely due to dynamic amplification factors arising from the fact that the fixed tower is much stiffer horizontally than the towers founded on soil giving it a natural frequency much closer to the excitation frequencies of the loads.

4.2 Lattice tower

The moments present in the base of the leg of the lattice tower were almost negligible as compared to the base moment in the monotower. This is to be expected, as the purpose of the lattice tower is to spread the base of the tower over a wider area in order to reduce the bending in the structural members. The horizontal forces did not vary significantly between foundation concepts, although the soil based foundations did provide some slight relief in the shear and normal forces experienced. There was again quite a large difference in the displacements of the nacelle experienced between the different models, although the discrepancy was not nearly as great as with the monotower. Opposite to the monotower, the lattice tower experienced the larger displacements for the towers founded on soils. This is due to the fact that the lattice tower is much, much stiffer than the monotower, and the added flexibility of the soil foundations moves the natural period of the structure towards the excitation frequencies from the rotor loads.

5 CONCLUSIONS

After examining the data, it can be seen that including a representation of the foundation with non-linear soil springs can provide significant difference in the results of a dynamic analysis of a wind turbine. While it cannot be directly said that this result is more *accurate,* per se, the difference still exists and is worth reporting. It would be very worthwhile to compare the various models of a wind turbine, with and without foundation models, to the data of an actual turbine in operation to determine the accuracy of each model.

It can also be seen from the data that significant differences exist between the monotower structure and a lattice tower. The monotower experiences much higher forces and moments which requires thicker and cross sections and more robust foundations. While the monotower is an elegant and simple solution, the lattice tower is a better solution for deeper waters.

BIBLIOGRAPHY

[1] Manwell JF, McGowan JG, and Rogers AL. “Wind Turbine Siting, System Design and Integration: Offshore Wind Farms.” *Wind Energy Explained: Theory, Design and Application*. Wiley and Sons: West Sussex, 2002. 403-409. Print.www.enercon.de.

[2] International Standards Organization. *ISO 19902:2007(E) - Petroleum and natural gas industries. Fixed steel offshore structures.* First Edition. 2007.

[3] Chen L and HG Poulos. *Analysis of pile-soil interaction under lateral loading using infinite and finite elements.* Computers and Geotechnics, Vol. 15: 1993. 189-220.

[4] Jonkman, Butterfield, Musial, and Scott. “Definition of a 5-MW Reference Wind Turbine for Offshore System Development.” Tech. Rep. NREL/TP-500-38060, 2009.

[5] Guo WD and MF Randolph. “Torsional piles in non-homogeneous media.” Computers and Geotechnics, Vol. 19: 1996. 265-287.

Sizing Process of a Semi-Submersible for Offshore Wind Generation

Rafael Arias,
ETSIN, Universidad Politécnica de Madrid, Spain

ABSTRACT

Although there is huge experience in the design and exploitation of floating platforms for the offshore oil & gas industry, the unique technical features of offshore wind farms together with the requirement of high levels of cost-effectiveness in order to reach the project viable, make the design of the floating solutions for wind power generation significantly different from those applied in the traditional offshore industry.

This document deals with the Naval Architecture of a semi-submersible for offshore wind generation. The objective of this work is to highlight the key sizing parameters and to propose a methodology for the sizing process of a semi, based on the intact stability of the structure.

A case study of a semi-submersible for the north coast of Spain will prove the effectiveness of this proposed methodology in the decision-making process during the early stages of the design and it provides relevant practical information for the actual paper.

KEYWORDS

Naval Architecture, sizing process, semi-submersible design, floating offshore wind.

1 INTRODUCTION

The sizing process is the basis of the design of a floating structure as its configuration and main dimensions will not only govern the behaviour of the platform, but also the cost-effectiveness of the project. A good sizing of the structure can definitively improve and speed up the overall project.

The aim of the sizing of a semi-submersible is to select its configuration and set its main dimensions –overall length, draft and freeboard, and distances among the columns- and the dimensions and shape of its components –i.e. columns, pontoons, deck and bracing.

The sizing method proposed in this paper is based on intact stability considerations and take into account its influence in all the project phases, i.e. construction, installation, operation and maintenance, and removal.

2 BASIC CONSIDERATIONS AND ASSUMPTIONS

An efficient sizing method must rely on basic Naval Architect principles. This process only requires the use of CAD software and simple spreadsheets.

Following the sizing of the structure, detailed analysis will be carried out regarding its structural resistance and dynamics –dynamic stability, mooring design, sea-keeping and dynamic behaviour of the moorings-platform-wind turbine system. These analyses do need to be performed with FE methods and specialized software. The results of these thorough studies will feed back the first sizing attempt, correcting or optimizing the configuration, dimensions and shapes estimated.

The proposed method of sizing is divided into the following steps:

STEP 1 Preliminary studies

STEP 2 Selection of the basic configuration

STEP 3 Sizing process

Each step is to be analyzed from the point of view of the following four project phases: a) construction; b) installation; c) operation and maintenance –O&M; d) removal.

The main assumptions accepted in this paper, as a result of the analysis of the offshore wind technology state of the art, are:

- ✓ The semi is required to stay on position during its lifetime
- ✓ A reliable active ballast system will be implemented for stability purposes.
- ✓ The positive mooring effects will not be taken into in the stability calculations

3 SIZING PROCESS

3.1 STEP 1: Preliminary studies

In this step, all the main issues of the project must be envisaged focusing in their influence in the configuration and dimensions of the structure. This step can be split into three tasks:

TASK 1: research of the following points:

- Project specifications (number of turbines, turbine specifications, S.C., etc)
- Physics of the site (weather windows, wave heights, wind speeds...)
- Harbor facilities
- Possible shipyards for the construction of the semis (construction means and methods)

- Possible installation and removal operations (available supply vessels, tugs, etc.)
- O&M of the offshore wind farm (hotel vessel or a semi, accesses to the platforms, etc)

TASK 2: review of the whole table of contents of a floating structure project must be carefully carried out, again, focusing on their influence in the stability of the structure.

TASK 3: estimate a first rough draft of the general arrangement and a preliminary estimation of all the semi-submersible weights (wind turbine, components and equipment onboard, structural steel and ballast). A symmetrical distribution is to be attained.

Throughout this intensive study, the information must be gathered and structured in tables (spreadsheets) which clearly show, for each of the four phases, the main factors to take into account, possible measures or decisions to take, regarding the sizing process.

In this step, it will be very useful to get in touch with the possible actors in the project, for instance, with the possible shipyards, whose experience and local industry and supplier`s contacts can be very useful to the designer.

3.2 Selection of the basic configuration

Once the first step has been finished, one can start to decide the basic configuration of the semi. In this step, only simple configurations must be considered, and later on, after the first sizing attempt, a more refined configuration will be approached.

The basic configuration of the semi-submersible consists on establish:

- The number of columns
- Pontoons configuration
- Shape of the column cross section
- Shape of the deck plant view
- Bracing

Based on the case study works, a three-column and close ring pontoons configuration is recommended. Depending on the construction facilities and methods, both circular and triangular cross sections can be applied to the columns. And it is desirable to eliminate, if possible, the bracing, due to the fatigue problems and regular weld inspections. The deck must be sized with the minimum steel weight enough to support and transmit to the columns the tower loads.

A number of possible configurations (scenarios) can be selected, and the following third step is to be applied for each scenario in order to make a comparison.

3.3 Sizing process

Semi-submersibles for offshore wind generation do not deal with the typical oil&gas heavy payloads, but the functional weights are in the order of 1.000-1.500 tonnes. Therefore, the size of the structure is not driven by the buoyancy required to support the gravity loads.

On the other hand, the stability of the structure is the key point, due to the big heeling moment from the maximum wind turbine load at the rotor height. Therefore, the approach of this sizing method is to use as a start point the formula of the maximum heeling angle to estimate a displacement:

$$P_{max} = \Delta \cdot GM \cdot Sin(\theta_{max}) = F_{max} \cdot d$$

It can be set

F_{max} = this force is given by the wind turbine manufacturer

θ_{max} = this maximum heeling angle can be estimated with wind turbine manufacturer

Now, an optimistic target for the GM value can be proposed

GM = 6 m (estimated from the case study works)

Finally, it is necessary to evaluate the *d* value. This value is the distance between the rotor height and the fairleads, so that we need to propose a draft and a depth for the structure. From the preliminary studies and the collaboration with the shipyard and other actors, a maximum depth can be proposed, based on construction and installation constraints. In general, it seems that semis for offshore wind will trend to have significant drafts.

On the other hand, from the site environmental data, it is possible to obtain the maximum significant wave height, which together with an additional airgap will give the freeboard. Here it must be underline the importance of the study of the tolerable *wetness* and *green water* effects.

The draft is, then, derived from difference between the depth and the freeboard. Each of the various possible depth values considered will imply a different scenario.

In this way, the main vertical dimensions –the draft or the depth- are set as a fixed parameter, mainly dependent on the location –site environment and construction and harbor facilities.

Once the operational displacement is estimated, a set of variables that represent the basic configuration of the actual semi are combined, forced to sum up the displaced volume

estimated. It is also recommended, as an error margin, that the alternatives which sum up until 1000 tons more of that displacement value, are considered.

Typical variables are the overall length, *L,* –assuming a symmetrical configuration-, the pontoon height, H_p, and the transverse dimension of the column, *a*, but it can be necessary more variables depending on the basic configuration.

For each set of values of these variables –item- it is calculated by means of a spreadsheet the steel weight, the weight of operational ballast, the different gravity centers, moment of inertia, etc., and finally, a value for the GM is obtained. See the scheme below:

$$GM_{proposed} \rightarrow \Delta \rightarrow [L, H_p, a] \rightarrow W_{steel} \rightarrow [KG, KB, BM] \rightarrow GM$$

If the GM value is lower than the proposed, firstly the configuration must be tried to be changed in some way –just some geometrical changes in some components of the structure, not the basic configuration selected in the step 2- without altering the vertical parameter. Creativity and technical knowledge must give more alternatives.

For each scenario, step 3 is repeated, and it will be decided which alternative is the best solution based on the preliminary studies.

4 CONCLUSIONS

Basic principles of the Naval Architecture and simple calculations can be enough for the sizing process in the early stages of the project. It is important to underline that, as a first attempt, no structural or dynamic analysis software is required.

In general, the structure of the process is to set some parameters and variables (different dimensions) and establish some objective functions related to intact stability requirements. The configuration choices and the assessment of the results must take into account all the project phases, not only the dynamic performance of the platform.

The mentioned case study of a semi in the north coast of Spain is being carried out and showing good results for this sizing approach.

BASIC BIBLIOGRAPHY

[1] Principles of Naval Architecture, Society of Naval Architects and Marine Engineers

[2] Guideline for offshore floating wind turbine structures, DNV

[3] Handbook of Offshore Engineering, Subrata K. Chakrabarti

European Academy of Wind Energy

Norwegian University of Science and Technology

Evaluation of Dual Axis Resonant Testing of Wind Turbine Blades

Peter Greaves[1)], Rob Dominy[1)], Grant Ingram[1)], Richard Court[2)]

[1)] Durham University, UK [2)] Narec, UK

ABSTRACT

A new method for the resonant fatigue testing of large wind turbine blades has been investigated. The method tests the blade in the flapwise and edgewise directions simultaneously, and it has been evaluated by comparing the Miner's damage sum around the blade root after simulated testing and service life. Bending moments at the blade root were generated using wind turbine simulation software and the test loads were designed to cause the same amount of damage as the service life. The loads were converted to strain time histories using simple stress analysis techniques and then fatigue analysis was performed. The results show that dual axis resonant testing is an improvement over single axis testing.

KEYWORDS

Wind Turbine Blades, Fatigue, Full Scale Testing, Resonant, Dual Axis

1 INTRODUCTION

As part of the certification process, all new designs of wind turbine blade must be fatigue tested. Large wind turbines will typically rotate 10^8 times during their 25 year design life. It is not practical to put the blades through this many cycles during the test so the loads on the blade are increased so that an equivalent amount of damage accumulates after around 10^6 cycles.

The blades are tested by mounting them on a concrete hub. Load cycles are then applied either by using hydraulic cylinders attached to the blade or by resonating the blade using masses mounted to the blade that are moved at the natural frequency of the system. These two methods are shown on the left and right respectively in figure 1. Resonant testing is a better option for large blades as the large tip displacements involved mean that it is difficult to scale forced displacement testing. Dual axis resonant testing, in which the flapwise and edgewise loads are applied simultaneously, is currently not well understood.

p.r.greaves@dur.ac.uk

Both the flapwise loads (which are predominantly aerodynamic) and the edgewise loads (which are mainly due to the blades self weight) have periodic components. The interaction between the two is very important, and it has been shown that blades will fail an order of magnitude sooner if the loads are in phase compared to 90° out of phase [1]. A test method which takes account of this is desirable [2].

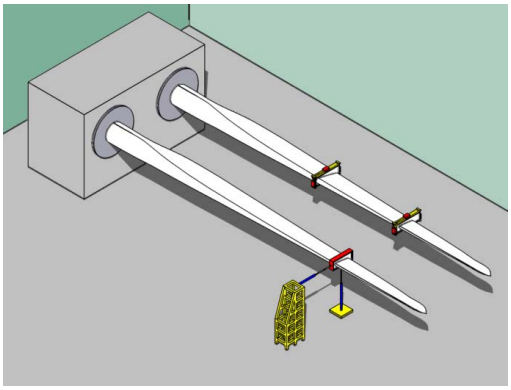

Figure 1 - Blade fatigue testing methods

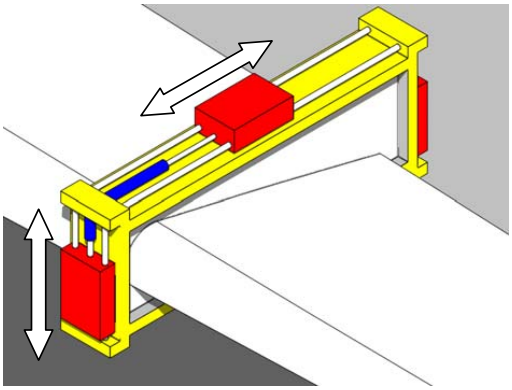

Figure 2 - Dual axis resonant masses

2 FATIGUE ANALYSIS METHODOLOGY

2.1 Wind Turbine Load Cases

GH Bladed was used to perform the load case simulations. The service life loads were obtained at the blade root of a Class Ia 2MW variable pitch - variable speed turbine model that is included for demonstration purposes with the software package.

Wind turbine design standards [3] were used to obtain the design wind speed distribution for a class Ia turbine, as well as the turbulence characteristics at each wind speed. The standards also define which load cases to simulate for fatigue analysis.

The output from GH Bladed is time histories of the root bending moment in the flapwise and edgewise directions.

2.2 Strain Analysis

Strain Analysis was performed using simple classical techniques. As GH Bladed is an aero-elastic code, it requires information about the stiffness distribution along the blade. This information along with the blade's geometry can be used to perform strain analysis. Sixty points around the circumference of the blade root were analysed using equation 1, where ε is

the total strain, M_{flap} is the bending moment in the flap direction, y is the distance from the neutral axis to the skin for the flap direction and EI_{flap} is the stiffness in the flap direction. The same nomenclature applies for the edgewise direction.

$$\varepsilon = \frac{M_{flap}y}{EI_{flap}} + \frac{M_{edge}x}{EI_{edge}} \quad (1)$$

2.3 Fatigue Analysis

The strain time histories were rainflow counted so that the variable amplitude loading was reduced to a series of constant amplitude strain cycles defined by their range and mean.

The amount of damage done to the blade by each series of constant amplitude cycles was calculated using a Goodman diagram for a typical composite lay-up for which much fatigue data is available (Material DD16 from the Montana State University composite database [4]).

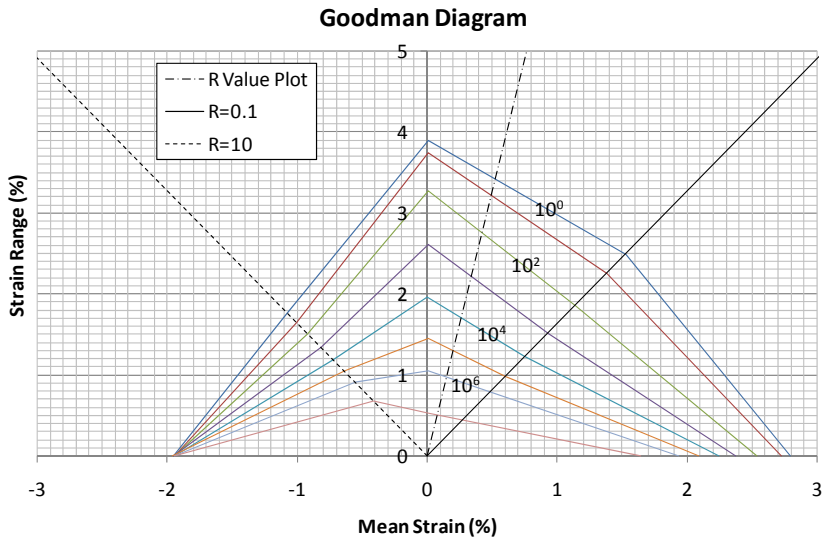

Figure 3 - Goodman Diagram for Material DD16

A Wöhler curve was generated from the Goodman diagram for each cycle, and Miner's rule was used to calculate the damage that each cycle caused. The wind speed distribution was used to estimate how many times the cycle would occur.

2.4 Simulated Fatigue Tests

Once the amount of damage caused by the service life is known, it is possible to calculate a bending moment that will cause the same amount of damage at any one point on the blade

using the Goodman diagram. For the edgewise loads the damage was matched on the flap neutral axis and vice versa, so that the two loads did not influence one another.

3 RESULTS AND CONCLUSION

The graph below compares the damage sum around the circumference of the blade root for the service life and various tests (safety factors have been added to the test loads as defined in the draft blade test standards [2]).

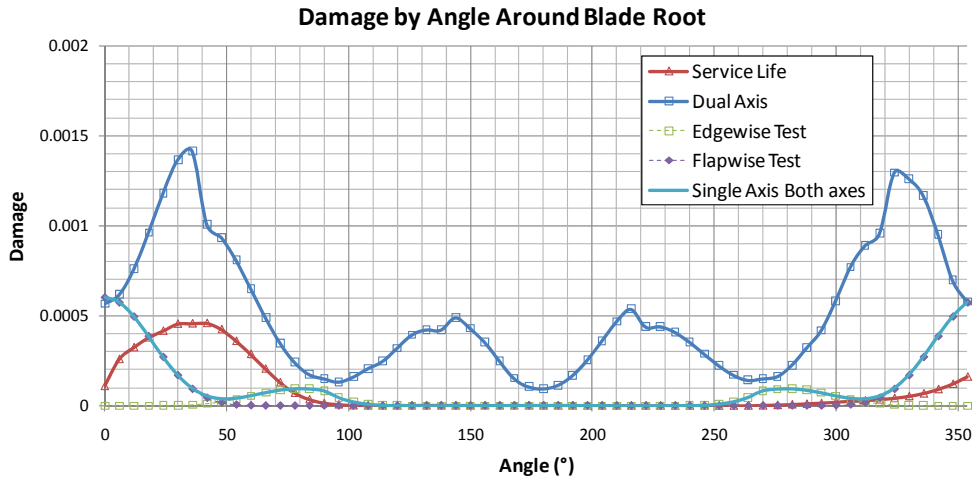

Figure 4 - Comparison of damage done to the blade root by a service life and various test methods

Note that even with the safety factors applied, there are significant portions of the blade that are not accumulating as much damage as the service life causes when the blade is tested in the flap and edge directions sequentially. For this reason it is believed that dual axis testing is superior to sequential single axis tests, and further work will focus on improving the understanding of this test method.

4 BIBLIOGRAPHY

[1] White, D.; New Method for Dual-Axis Fatigue Testing of Large Wind Turbine Blades Using Resonance Excitation and Spectral Loading. 2004, University of Boulder, Colorado.

[2] BSI; BS EN61400 Wind Turbine Generator Systems, in BS EN61400-23: Full Scale Structural Testing of Rotor Blades. 2005.

[3] BSI; BS EN 61400 Wind Turbines, in BS EN 61400-1: Design Requirements. 2005.

[4] http://www.coe.montana.edu/composites/

Simulation and verification of the interaction of the dynamics of the all system with the loading of the main components of wind turbines

Thomas Hecquet
Endowed Chair of Wind Energy (SWE), University of Stuttgart, Germany
thomas.hecquet@ifb.uni-stuttgart.de

ABSTRACT

New manufacturers and a number of machines continuously emerge on the growing market for wind turbines. In addition, as the size of the turbines is still increasing, their components become bigger and more flexible. This is why the influence of the dynamics on the strength of components becomes more critical. Studies showed ([1],[2],[3]) that even though the breakdowns of electrical components or control systems occur more often, the financial impact of the failure of mechanical parts is still dominating the O&M costs and downtime. Whereas the computation of loads acting on and inside a wind turbine is still widely realized with codes solely developed for that purpose (e.g. Flex5, Bladed, Focus), their limitation, (for example a fixed number of degrees of freedom) motivates the implementation of more flexible and extendable methods such as multi-body simulation.

However, as advanced detailing of models leads to longer computation times, their implementation for a full load simulation set (e.g. according to IEC61400-1[4] or GL-2003[5]) is not probable in the nearest future.

A wind turbine designer trying to improve the simulation of turbine loads faces the challenges of accessing the required input parameters, creating new models, and of estimating the sensitivity of the model to these parameters (or to their uncertainty). Moreover, the model should be validated as exactly as possible, using measurement results.

The aim of this Phd thesis is to develop methods to overcome these challenges by focusing on the influence of the components dynamics on the behaviour of global loads.

KEYWORDS

Modelling, Simulation, Validation, Measurement, Procedures, Multi Body System, Drive Train, Pitch System

1 INTRODUCTION

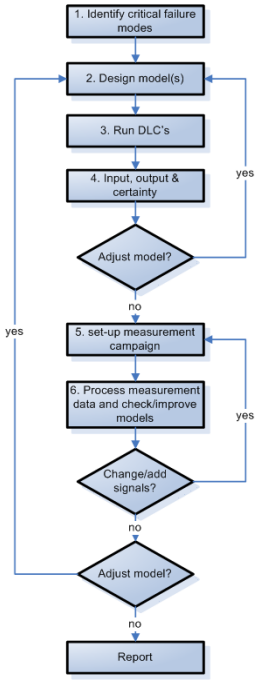

Figure 1: 6 steps approach for designing model (Protest Project)

Up to now, wind turbine design has mostly been based on the IEC-61400 standards (see [4] and [6]) or GL-Guidelines (see [5]). The designer is expected to find the worst case scenario within the design envelope of the turbine model and design load cases and use it as the governing condition to determine the design loads. Measurements are so far used to support the design process, certify a new prototype or determine the structural loads in specific conditions.

Relative to a given failure mode, or to a set of failure modes (step 1), a first model should be developed (step 2), tested by running relevant design load cases (step 3 and 4) and a corresponding measurement campaign set up (step 5) whose results are then processed to eventually tune the obtained model to finally simulate the load set. In the coming chapters, it will be illustrated how such a model could be designed and validated.

2 MODELLING OF WIND TURBINE WITH A MULTIBODY SOFTWARE (SIMPACK)

2.1 Increasing the number of DOF

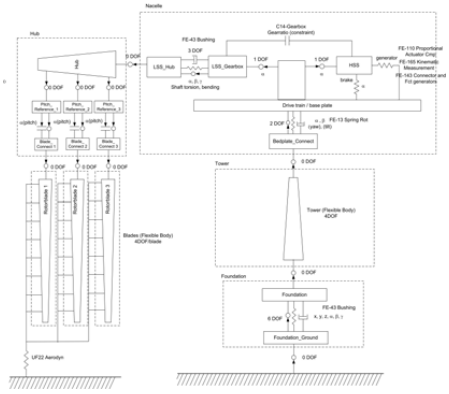

Figure 2, stage 1, topology of basic mode (similar Flex 5) unter SIMPACK

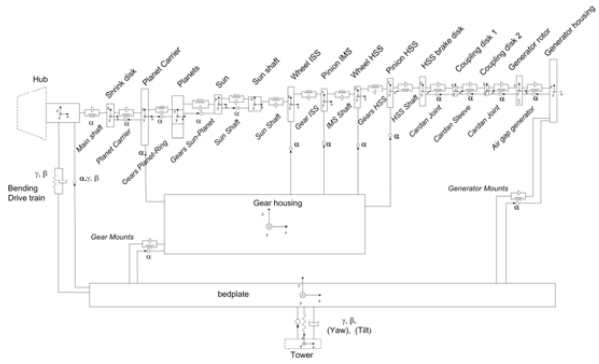

Figure 3: Stage 2: advanced torsional model of the drive train

In a first step, the model of the complete wind turbine has been reproduced under SIMPACK, based on the Flex 5 topology, with a total of 28 degrees of freedom.
Aiming at reproducing the dynamic behaviour of the whole turbine and in particular of the drive train, the stage 1 of the model has been extended with a multiple torsional model of the gearbox. In this more detailed approach, inertias and stiffnesses of gears and shafts are represented, as well as the stiffnesses of the gear teeth, with a total of 14 supplementary DOFs. Modal analyses and time simulations have been run to validate the models with Flex 5 as benchmark and to estimate the additional value of the new model (see figures 5 and 6).

2.2 Integration of Flexible bodies as a further step

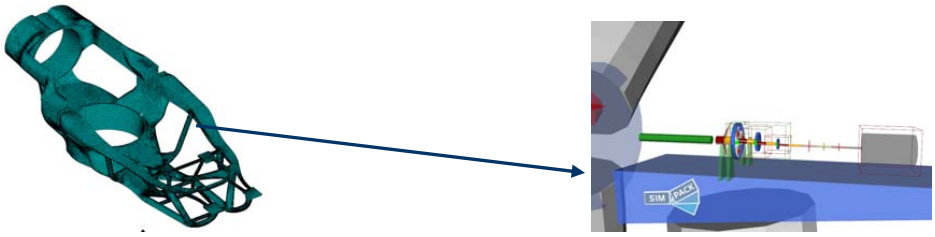

Figure 4: illustration of the integration of a bedplate as a flexible body into the MBS model

The abilities of MBS softwares have fewer limitations; indeed they can consider non-linearities, teeth contacts, bearings or bushings. Furthermore, flexible bodies modelled with FEM can be integrated into the model (see figure 4) after modal reduction; however, the extension of the model always involves longer computation times, which has to be considered by the designer.

3 DEVELOPMENT OF PROCEDURES TO DETERMINE THE OPTIMAL DETAILS OF MODELLING

3.1 Comparison of models using simulations

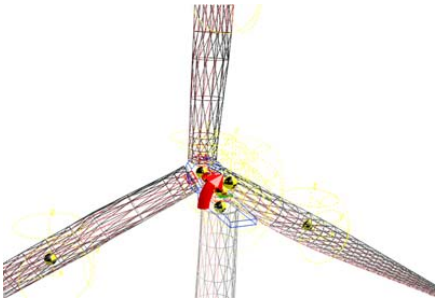

Figure 5: first torsional eigenmode at the SUZLON S82 Wind turbine (SIMPACK)

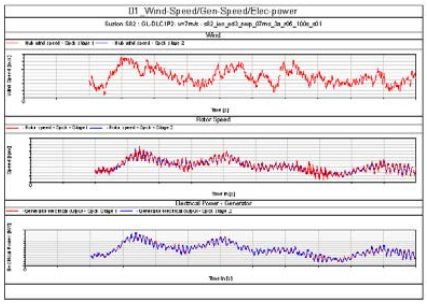

Figure 6: comparison of time simulations between stage 1 and 2 (production load case)

Models can be compared using modal analyses (eigenfrequencies and eigenmodes) or time simulations (time signals, min-max values, frequency spectra, rain flow counts).

3.2 Validation of models using measurements

Beyond all the simplifications which tend to separate the world of simulations and the one of measurements, the use of test field data is highly recommended to verify a new model. Currently, the measurement campaigns on wind turbines are typically carried out following the IEC-61400-13 (see [6]), even though in the current standards there are no procedures for validating and tuning models on the basis of measurement data. Comprehensive investigations in that direction should be perceived as prenormative works.

4 CONCLUSIONS

The Phd thesis will define methods to validate and tune new models (e.g. what simulations are to be run, what signals and what statistical values are to be compared). These methods will be implemented in several case studies which should permit to gain experience values and to investigate to what extent detailed modeling of the wind turbine components, in particular the drive train and the pitch system, can improve the computation of global loads.

BIBLIOGRAPHY

[1] M. Durstewitz et. Al. .” Wind Energy Report Germany 2001; Annual Evaluation of WMEP”; ISET, Germany 2002

[2] Energy- og Miljodata (EMD), database with energy production figures, incidents and accidents

[3] BTM Consult: « International Wind Energy Development ; World Market Update 2005 » ; Denmark, March 2006

[4] IEC-61400-1, “Wind turbines – part1: Design requirements”, third edition 2005-08

[5] GL-Wind - Guideline for the Certification of Wind Turbine, Edition 2003

[6] IEC/TS 61400-13: 2001, Wind Turbine Generator Systems – Part 13: Measurement of Mechanical Loads

Part 5

Session 4A - Rotor Design II

- Multidisciplinary Optimization of Flatback Airfoils for Large Wind Turbine Blades
  Mehdi Doosttalab, University of Applied Sciences Bremen
- Unsteady Quasi 3D Aerodynamic Code for Analyzing Dynamic Flap and Sensor Response
  Néstor Ramos García, DTU
- Stochastic modelling of lift dynamics in turbulent inflows
  Muhammad Ramzan Luhur, University of Oldenburg
- Conceptual Design of a Stall-Regulated Rotor for a Deepwater Offshore Wind Turbine
  Karl O. Merz, NTNU

European Academy of Wind Energy

Norwegian University of Science and Technology

Multidisciplinary Optimization of Flatback Airfoils for Large Wind Turbine Blades

Mehdi Doosttalab[1)], and Olaf Frommann[2)]

[1,2)] University of Applied Sciences Bremen, 28199, Germany

ABSTRACT

According to the recent researches in the field of the design and optimization of the large wind turbine blades, using blunt or flatback airfoils at the inboard section of blade has several structural and aerodynamical benefits. In the present research, two optimized flatback airfoil sections (HB-FB airfoil families) with 35% relative thickness and trailing edge gap of 10% and 12.5% were designed, and then they were compared with a conventional flatback airfoil section, which is based on the sharp trailing edge DU-97-W-300 airfoil. The design Reynolds number was 6×10^6, and The Simulated Annealing (SA) algorithm was used to design the optimized shape of the flatback airfoil sections concerning several desirable parameters. The results for these new optimized flatback airfoils are mainly a higher lift coefficient and high sectional moment of inertia compared to the current flatback airfoils.

KEYWORDS

Large Wind Turbine, Flatback Airfoil, Multidisciplinary Optimization.

1 INTRODUCTION

In 2002, the Wind Energy Technology Department of Sandia National Laboratories (SNL) started a research programme to investigate new design solutions for the large scale wind turbine blades in the size range of 1 to 10 megawatts, known as the BSDS [1]. The result of this investigation showed that, increasing airfoil section thickness at the inboard section of blades, and utilizing flatback airfoils at the inboard section up to 40 % of the blade span has several structural and aerodynamical benefits [1,2]. These so-called flatback airfoils are generated by adding thickness over the camber line at the aft portion of the sharp trailing edge airfoils. A flatback airfoil has a higher lift coefficient, higher lift curve slope, lower sensitivity of the lift coefficient to the leading edge soiling, higher sectional area, and higher sectional moment of inertia compared to the sharp trailing edge airfoil with the same thickness. Therefore, the blade with the flatback airfoil is lighter and has a smaller chord at

Mehdi.Doostalab@hs-bremen.de

Olaf.Frommann@hs-bremen.de

the root, thus it is cheaper and also easier to transport. However, theses airfoils generate more noise and they have a higher base drag compared to the sharp trailing edge airfoils [3]. Since the previously flatback airfoils were based on sharp trailing edge airfoils, the motivation to do research in this field is to design optimized flatback airfoils, concerning both aerodynamical and structural aspects simultaneously.

2 DESIGN STRATEGY

The desirable structural and aerodynamical characteristics of wind turbine airfoils have been discussed in several publications [4,5,6]. The desirable structural goals in the current design process were high sectional moment of inertia, and compatibility with modern thin airfoils like RISØ-B1 or DU-9X-W airfoil families [5,6]. The latter is achieved by setting the maximum thickness location at 28% of chord position. The most important aerodynamical goal for flatback airfoils is high lift coefficient [6]. This goal and the other aerodynamical goals like high lift/drag ratio, low pitching moment coefficient, low sensitivity to the leading edge roughness [7] are considered at design angle of attack. To compare the resulted optimized airfoils, the flatback variant of the Delft DU-97-W-300 airfoil was selected as a reference.

3 DESIGN TOOLS

The optimization software framework CAOne [8], which offers several optimization algorithms, was used to control several desirable goals simultaneously in the design process. SynapsAirfoil1 [9] was used to generate the shape of the airfoil using B-spline curve, and another code determined the maximum thickness location. Fluent was used as a flow solver, using k-ω turbulence model (SST version), GAMBIT employed as a mesh generator, and finally XFOIL code was utilized to determine transition location on the airfoil in the optimization process. All codes were easily linked together into a single process chain within the framework CAOne. Note that the design variables were 16 control points which formed the B-Spline curve.

4 RESULTS

Figure 1 shows the optimized airfoil profiles compared to the modified DU-97-W-300 airfoil. Figure 2 shows the calculated lift coefficients at a wide range of angles of attack for both airfoil families. It is visible that in comparison to the old flatback airfoils, the optimized airfoils have a higher Cl. In general, the lift coefficient was

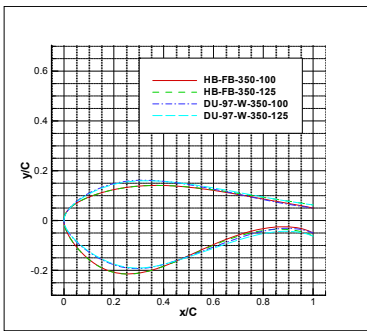

Figure 1: Optimized flatback airfoil section, HB-FB-350-XXX & DU-97-W-350-XXX profiles.

Mehdi.Doostalab@hs-bremen.de
Olaf.Frommann@hs-bremen.de

increased by 7.9% and 7.1% for the optimized airfoils with 10% and 12.5% trailing edge gap respectively.

The simulation results showed that, although the optimized airfoils have higher Cl, but the lift to drag ratio is rather the same for both airfoil families and the maximum lift to drag ratio angle of attack in optimized flatback airfoils is higher than the older ones, which is a favourable characteristic for the inboard airfoil sections, because it decreases the twist angle of the blade.

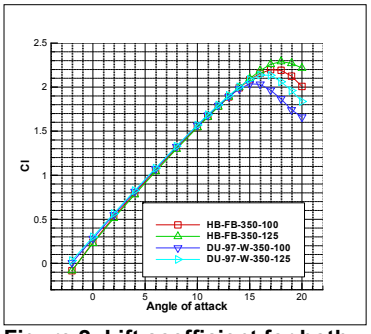

Figure 2: Lift coefficient for both airfoil families at Re=6×10^6.

Figure 3 depicts the calculated pitching moment coefficient for both airfoil families at Re=6×10^6 about quarter-chord position. Because of the higher lift coefficient of the optimized airfoils, higher moment coefficient would be expected. Generally, flatback airfoils produce a larger nose-down pitching moment than airfoils with sharp trailing edge, and the amount of the pitching moment decreases with some modifications at trailing edge like a splitter plate [10], but usually, a high pitching moment is not an important factor at the inboard span of the blade.

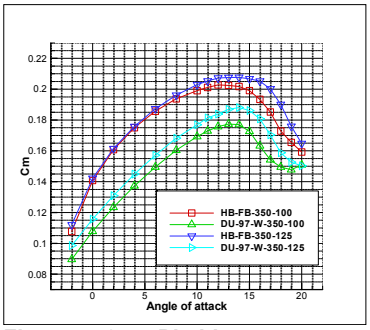

Figure 3: Pitching moment coefficient for both airfoil families at Re=6×10^6.

The XFOIL code was used to determine the sensitivity of airfoils to leading edge roughness, and the results showed 1.0%, 0.8%, 3.4%, and 1.7% drop in lift coefficient with simulated leading edge roughness at Re=6×10^6, and at maximum L/D angle of attack, for the HB-FB-350-100, HB-FB-350-125, DU-97-W-350-100, and DU-97-W-350-125 airfoils respectively. Table 1 shows the most important characteristics of both airfoil families.

Table 1: Characteristics of the DU-97-W-350-XXX and the HB-FB-350-XXX flatback airfoils at Re=6×10^6.

Airfoil	Location of Maximum Thickness (x/C)	Trailing edge Thickness (t/C)	Maximum Cl (α)	Maximum L/D(α)	Solid Ixx (m^4)	Skin Ixx/t (m^3)
DU-97-W-350-100	0.3	0.1	2.03 (15º)	33.4 (13º)	1.49e-3	3.17e-2
DU-97-W-350-125	0.3	0.125	2.13 (16º)	31.6 (14º)	1.51e-3	3.24e-2
HB-FB-350-100	0.28	0.1	2.19 (17º)	33.6 (15º)	1.52e-3	3.20e-2
HB-FB-350-125	0.28	0.125	2.29 (18º)	30.9 (16º)	1.55e-3	3.27e-2

Mehdi.Doostalab@hs-bremen.de
Olaf.Frommann@hs-bremen.de

5 CONCLUSIONS

From the above results, it can be concluded that the optimized airfoils have more desirable characteristics than the normal flatback airfoils with sharp trailing edge base, especially more lift and more sectional moment of inertia which are most demanded for the inboard section of large wind turbine airfoils.

6 ACKNOWLEDGEMENT

The authors wish to thank the German Ministry of Education and Research (BMBF FKZ: 17N2107) for supporting this project.

BIBLIOGRAPHY

[1] TPI Composites Inc., "Innovative Design Approaches for Large Wind Turbine Blades–Final Report," SAND2004-0074, 2004.

[2] TPI Composites., "Parametric Study for Large Wind Turbine Blades," SAND2002-2519, Sandia National Laboratories, Albuquerque, NM, August 2002.

[3] Berg, D.E., and Barone, M., "Aerodynamic and Aeroacoustic Properties of a Flatback Airfoil," Windpower 2008 Houston, TX, June 2008.

[4] Fuglsag, P., Bak, C., Gaunaa, M., and Antoniou, I., "Design and Verification of the Riso-B1 Airfoil Family for Wind Turbines," J. Solar Energy Engineering, Vol. 126, Nov. 2004, pp. 1002-1010.

[5] Timmer, W.A., and van Rooij, R.P.J.O.M., "Summary of the Delft University Wind Turbine Dedicated Airfoils," J. Solar Energy Engineering, Vol. 125, Nov. 2003.

[6] Björck A., "Airfoil Design for Variable RPM Horizontal Axis Wind Turbines," FFA TN 1990-02; FFA: Stockholm, 1990.

[7] Larsen, G.C., Hansen, K.S., Larsen, T.J., and Mann, J., "Research in aeroelasticity EFP-2005," Risø National Laboratory (DK), Wind Energy Department, Risø-R-1559(EN).

[8] CAOone, CAOtec Software GmbH, www.caotec.com, Ver. 3.1.4.

[9] SynapsAirfoil1, Synaps Ingenieur-GmbH, www.synaps.de.

[10] Matthew, F. Barone., Dale, E. Berg., William, J. Devenport., and Ricardo, Burdisso., "Aerodynamic and Aeroacoustic Tests of a Flatback Version of the DU97-W-300 Airfoil," SAND2009-4185.

Mehdi.Doostalab@hs-bremen.de
Olaf.Frommann@hs-bremen.de

Unsteady Quasi 3D Aerodynamic Code for Analyzing Dynamic Flap and Sensor Response

Néstor Ramos García

Danmark Tekniske Universitet, Lyngby, DK-2800, Denmark

ABSTRACT

In the paper a 2D unsteady and a Quasi 3D steady version of the code will be presented. The code is developed to analyze the local aerodynamic behaviour of an airfoil section of a wind turbine with a moving trailing edge flap. The code is based on viscous-inviscid interaction using strong coupling between the viscous and the inviscid parts. The inviscid part is modelled using a panel method and the viscous part is represented by the boundary layer equations put into integral form and with extensions for 3D rotational effects. Laminar-turbulent transition is predicted using spatial-amplification theory based on the Orr-Sommerfeld equation, commonly known as the n^9 method. Unsteady effects are taken into account via unsteady terms in the momentum and the kinetic energy equations. For unsteady computations a single wake model has been implemented, in which a point vortex leaves the airfoil trailing edge at every time step and after which it is convected downstream. A double wake model will also be presented in the paper, with capability for reaching deep stall conditions.

Stochastic modelling of lift dynamics in turbulent inflows

Muhammad Ramzan Luhur, Jörge Schneemann, Patrick Milan and Joachim Peinke

ForWind, Center for Wind Energy Research, University of Oldenburg, D-26111, Germany.

ABSTRACT

This paper presents lift measurements on an airfoil FX 79-W-151A in a closed wind tunnel. The measurements were performed using two force sensors mounted on the airfoil as well as wind tunnel wall pressure measurements. Various turbulent inflows were generated using various grids including a fractal grid. The analysis of the measured data is done following the classic averaging procedure as well as a novel stochastic approach. The stochastic analysis brings further insight on the high-frequency lift dynamics of the airfoil. This suggests the integration of a stochastic lift model into a general wind energy converter model.

KEYWORDS

Wind tunnel measurements, lift dynamics, turbulent inflows, fractal grid, stochastic model.

1 INTRODUCTION

The fluctuating nature of the wind in terms of speed and direction contributes to the complex operation of wind turbines. Integrating all these variations and/or physical effects into a wind turbine design to operate it in an optimised mode is a challenging task. The models taken so far are mostly based on static lift and drag curves for an airfoil in a laminar inflow at constant angles of attack. However, wind turbines are mostly exposed to highly volatile wind leading to high and rapidly changing loads. Our goal is to provide a better understanding of the high-frequency dynamics of the lift effects under turbulent inflows. A stochastic lift model is being developed, that could be integrated into a general wind energy converter model in the future.

2 METHODOLOGY

2.1 Experimental setup

All measurements were taken in the wind tunnel (closed test section of 2mx1mx0.8m) of University of Oldenburg. A FX 79-W-151A airfoil with a chord length of 0.2 m was installed in vertical position in the closed test section. The mean velocity of the wind tunnel was v≈50 m/s with Re≈700,000. The turbulent inflows were generated using a 5 cm mesh grid; a 10 cm mesh grid and a fractal grid with turbulence intensity of 3.6%, 6.7% and 4.6% respectively.

2.2 Lift coefficient

The lift and drag forces were measured directly using two strain gauge based force sensors installed at the end points of the airfoil in span-wise direction. The sampling frequency of the measurement was 1 KHz. The equation used to calculate the lift coefficient C_L [1] is

$$C_L = \frac{F_L}{q \cdot A} \ , \tag{1}$$

where q is the inflow dynamic pressure, F_L the lift force and A the area of the airfoil. In parallel, wall pressure measurements were also performed, as discussed in [1, 2].

2.3 Stochastic approach

In order to understand the high-frequency dynamics of the system beyond the averaging procedure usually performed, a stochastic approach is introduced. For the purpose, a Langevin process is used to model the airfoil lift coefficient. The Langevin equation, i.e. a first order stochastic differential equation is applied on the time series $C_L(t)$, as defined by [1, 3]

$$\frac{dC_L(t)}{dt} = D^{(1)}(C_L(t)) + \sqrt{D^{(2)}(C_L(t))} \cdot \Gamma(t) . \tag{2}$$

$\Gamma(t)$ is called the Langevin force [3], it is a Gaussian white noise with mean value $\langle \Gamma(t) \rangle = 0$ and variance $\langle \Gamma^2(t) \rangle = 2$. The functions $D^{(n)}(C_L)$ are obtained from measurement data using

$$D^{(n)}(C_L;\alpha)_{(n=1,2)} = \frac{1}{n!} \lim_{\tau \to o} \frac{\langle (C_L(t+\tau) - C_L(t))^n \rangle}{\tau} \Big|_{C_L(t)=C_L;\alpha} \ , \tag{3}$$

where α is the fixed angle of attack (AOA) of the airfoil. For n *=1,* equation (3) gives the drift function $D^{(1)}(C_L)$ reflecting the deterministic part of the system. For n *=2,* it gives the diffusion function $D^{(2)}(C_L)$, which quantifies the amplitude of the stochastic fluctuations. The drift and diffusion functions are the first order two Kramers-Moyal coefficients for $C_L(t)$.

3 RESULTS AND DISCUSSION

3.1 Static lift curves

An airfoil lift curve is defined as the mean of the lift coefficient $\langle C_L(t) \,|\, \alpha(t) = \alpha \rangle$ as a function of the AOA. A static lift curve was determined for various fixed (static) AOAs. The results presented in Figure 1 were obtained using the fractal grid, following equations (1) and (3). The standard deviation σ_{C_L} is provided to indicate the magnitude of the fluctuations around the mean. Both the force and wall pressure measurement methods yield similar mean lift curves. However, the force measurement method gives better results as it directly measures

the force on the airfoil, while the pressure measurement is spoiled by the wind inflow that contributes negatively to the measurement. The local dynamics (i.e. local in the values of C_L) modelled in the form of the drift field for each AOA gives better insight on the acting loads on short time scales. The stable fixed points illustrate the attractive regions of the dynamics and match with the mean lift curve. The value of drift function at these attractive regions is zero. Below the mean lift curve, the drift is positive, indicating that the airfoil tries to increase $C_L(t)$, as can be seen in equation (3). While above the mean lift curve, the case is opposite to this.

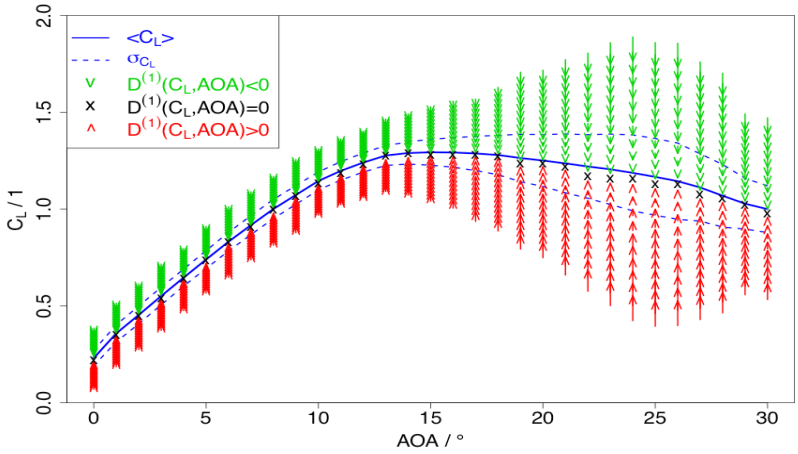

Figure 1: Static lift curve for a turbulent inflow generated by a fractal grid. The solid line represents the mean $\langle C_L \rangle$ and the dotted lines standard deviation σ_{C_L}. The arrows represent the drift function in terms of color (sign of $D^{(1)}(C_L)$) and length (amplitude of $D^{(1)}(C_L)$). The black crosses represent the stable points of attraction where the drift function becomes zero.

3.2 Stochastic lift model

Here a stochastic lift model based on the Langevin equation (2) is developed for each AOA for each turbulent inflow. The model is based on a measurement time series $C_{L,measure}(t)$. From this time series, the $D^{(n)}(C_L, AOA)$ functions can be estimated using equation (3), which can then be inserted into the Langevin equation (2). When solved in time, the Langevin equation can model time series $C_{L,measure}(t)$. Figure 2 shows the results for AOA=23° using the fractal grid. The modelled time series shows some similarity with the actual measured time series. Their probability distributions suggest acceptable agreement. The results presented here were optimised using a chi-square test [4] on the probability distribution functions. This optimisation consists in a quadratic modification of $D^{(2)}(C_L, AOA)$, as its estimation following equation (3) suffers finite-sampling deviations [3]. The model in the

present state is the initial step towards the goal; thus needs further optimisations and that work is in progress.

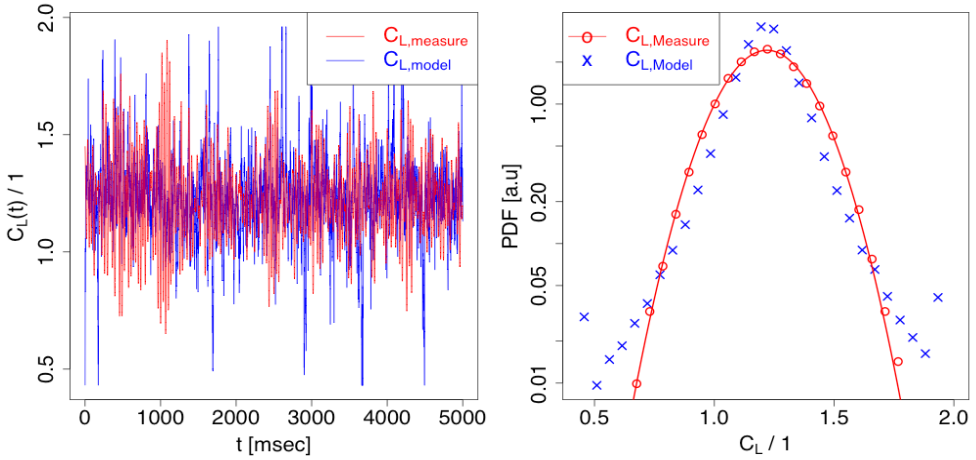

Figure 2: (a) Excerpt of time series of $C_{L,Measure}(t)$ (red) and $C_{L,Model}(t)$ (blue). (b) Probability density functions of $C_{L,Measure}$ (red circles and Gaussian fit) and $C_{L,Model}$ (blue crosses).

4 CONCLUSION

Lift measurements on an airfoil FX 79-W-151A were performed in a wind tunnel. Static lift curves were determined using the usual averaging procedure as well as a new stochastic approach. The stochastic approach, based on the Langevin formalism, brings further insight on the lift dynamics. The drift function displays the local high-frequency behaviour of the lift coefficient, and its stable fixed points match the usual mean lift curve. Thereafter, the drift and diffusion functions estimated; can be inserted into the Langevin equation, which becomes a lift model. The initial results presented for the lift model seem encouraging, and further optimisations are in progress, towards a general wind energy converter lift model.

BIBLIOGRAPHY

[1] Schneemann, J., Knebel, P., Milan, P. and Peinke, J.: Lift measurements in unsteady flow conditions. EWEC 2010, Warsaw Poland.

[2] Althaus, D.: Measurement of lift and drag in the laminar wind tunnel. http://www.iag.uni-stuttgart.de/laminarwindkanal/pdf-dateien/liftdrag2.pdf

[3] Gottschall, J. and Peinke, J.: On the definition and handling of different drift and diffusion estimates. New Journal of Physics 10 (2008) 083034 (20pp).

[4] Numerical Recipes in C. The art of scientific computing, second edition published by Cambridge University Press 1988, 1992.

Conceptual Design of a Stall-Regulated Rotor for a Deepwater Offshore Wind Turbine

Karl O. Merz[1)]
[1)] NTNU, Norway

ABSTRACT

The optimum rotor design for a floating offshore wind turbine is being investigated, and compared with that of a land-based turbine. Preliminary results indicate that from a purely cost-based perspective (not considering aesthetics and noise), and for a given wind climate, the optimum design of the rotor is similar between a floating and land-based turbine. For either type of turbine, there may be a region of design space worth investigating in more detail: a long, skinny blade with a high thickness-to-chord ratio, and relatively low maximum power coefficient.

KEYWORDS

Blade design, offshore, floating, stall regulated

1 INTRODUCTION

A downwind, direct-drive, stall-regulated turbine can be designed to be almost mechanically passive, with one primary moving part (the aerodynamic rotor / hub / shaft / generator rotor), together with an intermittently-active yaw bearing and emergency brake. Power and speed regulation is obtained by the aerodynamic design of the rotor, and active control of the generator torque. Such a simplified design could be suitable for installation far offshore, where maintenance costs are high. [1]

But what would the rotor of such a turbine look like? Would it be similar to those found on current commercial, land-based turbines? Or does the unique relationship between the rotor loads and support structure costs of a deepwater turbine change the optimal rotor design?

Preliminary results so far indicate that there is not a large difference in the optimal rotor design between land-based and floating turbines. In either case, the optimal design may lie farther from the aerodynamic optimum than is common in existing designs, according to the cost model used in this study. But the uncertainty in the cost model is likely greater than the difference in the cost function.

2 METHODS

2.1 Frequency-Domain Analysis

Analysis in the frequency domain is orders of magnitude faster than analysis in the time domain, which allows more of design space to be explored during the conceptual phase, albeit at a reduced accuracy.

A frequency-domain analysis method was developed to account for dynamic stall. This method provides fairly accurate estimates of damping and excitation of the blade (Figure 1). A description of this method has been submitted for publication. [2]

2.2 Optimization

A combination of sequential linear programming and the method of feasible directions is used, after Fuglsang and Thomsen. [3] This approach is potentially problematic, because near the optimum there could be an interaction between material thickness and aerodynamic profiles that results in local minima. This problem has been identified by Hjort et al. [4] However, the recommended solution -- optimize material thickness as a sub-optimization every time the geometry is perturbed -- takes too long, unless compromises are made on the way in which the thickness is optimized. (For example, Fuglsang et al. [5])

The analyses that have been run so far as part of this study show a good decrease in the cost function from a non-optimal starting configuration, and consistent geometry in the near-optimal configurations. Calculated blade mass compares well with commercial designs. However, final convergence of the linear method is slow, and it has not yet been established that the true, global optimum has been found. (Note that useful information can be obtained without necessarily finding the true optimum.)

2.3 Cost Function

A cost function similar to that of Fuglsang and Thomsen [3] is used. This gives rough trends in the costs of various components, using the assumption that component cost is proportional to mass, and calculating mass based upon (what are assumed to be) governing loads. A similar cost function was developed for a floating platform.

3 RESULTS

Figure 2 shows an example of the type of chord, airfoil *t/c*, and twist (ξ) distributions that are obtained from the optimization. The results (which should be considered preliminary) indicate that there may be something to be gained from going a bit farther than usual in trading off reduced aerodynamic performance for better structural efficiency. Modern, high-

t/c (around 0.3) airfoil designs perform quite well, [6] and holding *t/c* = 0.3 over most of the blade span allows the chord to be very small. This results in a blade which is light and whose extreme loads are low, but which has a low maximum C_P of 0.40 (in other words, a slightly longer-than-usual blade length, for a given power). This applies to both land-based and offshore turbines. (Note that noise was not considered, in the context of land-based turbines. The tip speed is quite high, around 80 m/s.)

Preliminary results also indicate that a two-bladed rotor may be slightly preferable on land (aesthetics aside), but that a three-bladed rotor is preferable on a floating platform. This is because the reduced diameter of a three-bladed rotor allows the nacelle height, to which the platform cost is sensitive, to be marginally lower, while maintaining a minimum clearance over the mean water level.

The optimum of the cost function is very flat. On a stall-regulated turbine, there is a tradeoff between aerodynamic efficiency at low windspeeds, and maximum generator power. There is also a tradeoff between chord length (hence maximum loads), rotational speed, and aerodynamic efficiency (diameter, really). The cost function depends weakly upon these tradeoffs, so that, for example, a 20% change in the chord distribution may change the cost function by just a couple percent, once the rotational speed schedule, diameter, and material thickness have been updated. The difference between two and three blades is only a couple percent, too.

The cost function provides only a rough estimate of actual cost trends, so it is perhaps misleading to talk about a single “optimum” design. Rather, optimization analyses such as this are useful for identifying regions of design space that are worthy of further study.

4 FUTURE WORK

So far, the analyses have been limited to turbines producing 1.42×10^{13} J/year (roughly 1.25 MW nominal rated power), in a climate with an average annual windspeed of 7 m/s. It is planned to investigate different levels of annual energy (different turbine sizes) and different wind climates.

BIBLIOGRAPHY

[1] Bulder, B.H., et al. ; The ICORASS Feasibility Study ; Report ECN-E—07-010, Energy Research Centre of the Netherlands

[2] Merz, K.O., et al. ; A simple frequency-domain method for stress analysis of stall-regulated wind turbines ; [Submitted to Wind Energy]

[3] Fuglsang, P.; Thomsen, K.; Cost Optimization of Wind Turbines for Large-Scale Off-Shore Wind Farms; Report Risø-R-1000(EN), Risø National Laboratory, Roskilde, Denmark, 1998

[4] Hjort, S., et al.; Fast Prototype Blade Design; Wind Engineering 33 (2009) 321-334

[5] Fuglsang, P., et al.; Site-Specific Design Optimization of Wind Turbines; Wind Energy 5 (2002) 261-279

[6] Timmer, W.A.; van Rooij, R.P.J.O.M.; Summary of the Delft University Wind Turbine Dedicated Airfoils; Journal of Solar Energy Engineering 125 (2003) 488-496

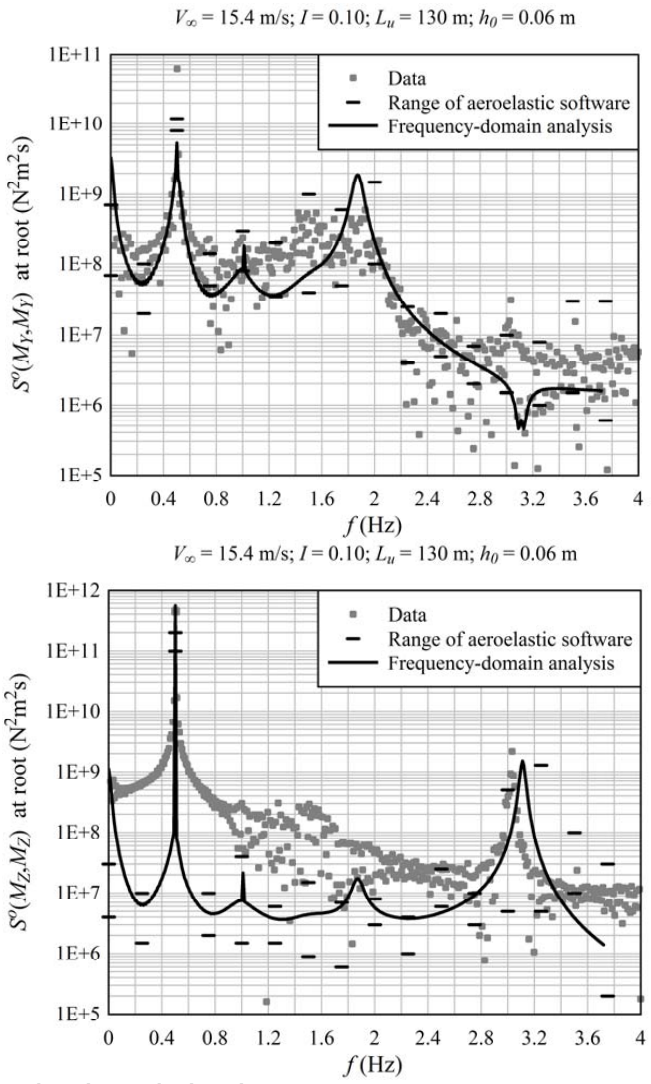

Figure 1: Flapwise and edgewise root moment spectra – VEWTDC, NTK500 turbine

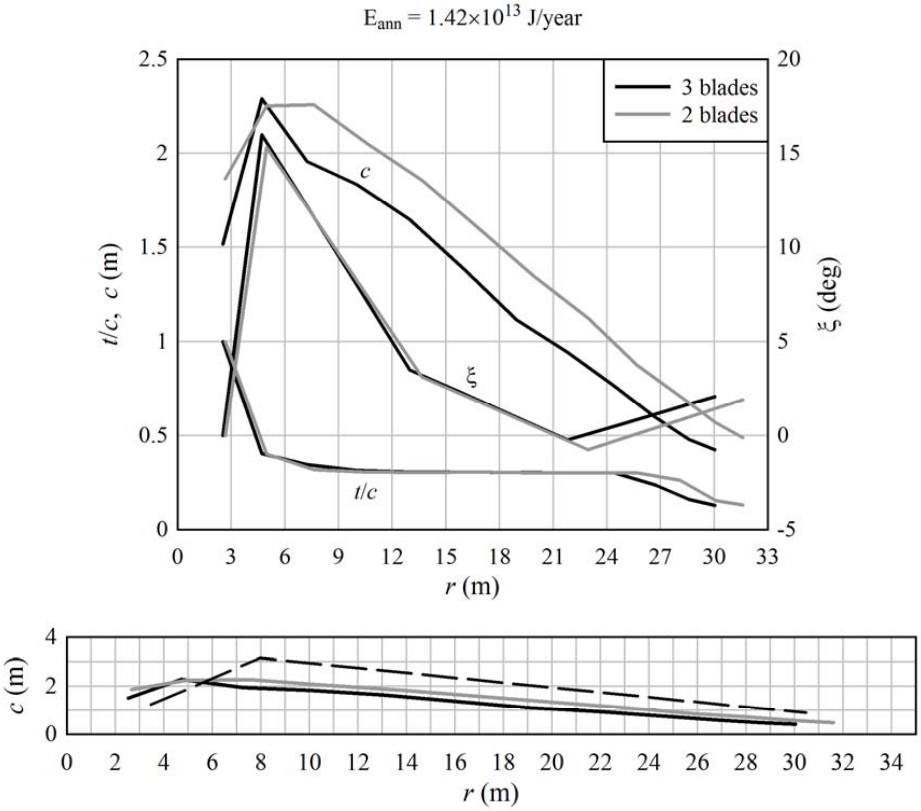

Figure 2: Optimal blade geometry; for reference, the dashed line in the lower plot is the Tjæreborg 2MW blade

Part 6

Session 4B - Maintenance of Offshore Wind Turbines

- Analysis framework for the reliability and maintainability of offshore wind Turbines
  Zafar Hameed, NTNU
- Risk based maintenance of offshore wind turbines using Bayesian networks
  Jannie Jessen Nielsen, Aalborg University
- Remote Presence, Cost-Effective Robotic Inspection and Maintenance of Offshore Wind Turbines
  Øyvind Netland, NTNU
- Condition monitoring methods for offshore wind turbines
  Mahmoud Valibeiglou, NTNU

Analysis framework for the reliability and maintainability of offshore wind Turbines

Zafar Hameed, **Jørn Vatn**

Norwegian University of Science and Technology, Production and Quality Engineering N-7491 Trondheim, Norway

ABSTRACT

Reliability and maintainability of offshore wind turbines (OWT) is full of new challenges due to accessibility, logistics, transportation, and safety of the personnel. In this paper we present general framework based on so-called influence diagram to structure the various elements influencing reliability and maintainability. The approach is flexible and it can be carried out at various levels of detail like adaptation to available resources and catering of any untoward incident during the operation of wind farms. Experience has shown that influence diagrams have strong communication advantages. The various type of knowledge among experts may be structured in order to elaborate the optimization model with respect to the most dominant factors to include. An influence diagram is primarily a qualitative description, but will also serve as a basis for quantification in a later state in the analysis. The paper presents the overall influence model, and discusses some aspects to be included in the optimization.

KEYWORDS: Reliability, Maintainability, OWT, Analysis, Framework.

1 INTRODUCTION

The wind energy is the emerging source of power now a days and its share in the energy production is increasing on a very rapid scale. Currently the installations of wind turbines are on their peak and focus is shifting from onshore to offshore locations. The projection of wind energy growth worldwide is expected to be 50,000MW till 2020 and key players will be from Europe, US, and Asia Pacific [1]. Moreover it is estimated that the share of offshore wind energy will increase too many folds in coming decades as compared to previous years.

It is highly expected that the share of offshore wind energy will increase with a rapid speed as the time passes and possibility is there that it may surpass other traditional and renewable energy sources. One such scenario for the growth of offshore wind energy is shown in Table 1.

From Table 1, total offshore wind power production is calculated to 2,559 TWh in 2050, offshore wind power supplying a little more than 6% of global final electricity consumption and constituting approximately 18.4% of total wind power capacity. The assumed growth

implies that the accumulated global offshore wind power capacity will double each 2nd to 3rd year until 2015 , each 3th year from 2015-20 and, finally 5th year from 2020-30 [1].

Table 1: Scenario for global offshore wind power development

Year	Offshore wind GW	Yearly growth offshore wind /%	Offshore of total wind power/ %	Production from offshore wind/ TWh/y	Expected global electricity consumption /TWh/y	Penetration of offshore wind, %
2006	0.9		1.2	3	15500	0.0
2015	12.8	34	2.6	42	21300	0.2
2020	42.4	27	4.0	140	23800	0.6
2030	251.1	19.5	9.5	829	29750	2.8
2050	773.8	5.5	18.4	2559	40100	6.4

The rapid growth of OWT has posed new managerial and technical challenges for having a reliable and efficient running offshore wind farms. These both challenges are heavily intertwined with each other which necessitate the employment of common tool which will address them holistically and in an integrated fashion. To accomplish this task, the so-called influence diagram is used for establishing the key link among the different components of OWT both from the managerial and technical point of view. The proposed influence diagram could be beneficial for the management to see a broader picture of the whole system and then making key decisions accordingly. Moreover, it could be a tool for technical managers to build detailed and structured sub-models based on this broader over all model.

2 ANALYSIS FRAMEWORK

Influence diagrams are used to visualize the overall analysis framework. An influence diagram demonstrates the relations between the decisions to be taken e.g. regarding type (and frequency) of maintenance and the various measures of system performance. Formally an influence diagram is a directed graph, G= (N, A) where N is the set of nodes, and A is a set of arcs connecting the nodes [2].

The relationship among three different types of nodes is shown in figure 1. The OWT farms are evaluated by different decision phases and then the effect of these choices on the overall cost of the system is established based on this diagram.

1. **Decision nodes**
   It represents the decisions at a management level which will have an impact on performance and value nodes. It is more relevant to decision makers regarding what type of yardstick they will use to opt for a certain type of design, site, layout, and O&M strategies for OWT. However, it is expected that the management will not decide in isolation and based on this influence diagram, they may be able to comprehend the implications of their possible choices and their possible effect on the reliability and maintainability of OWT as a whole.

Different parameters shown in the decision nodes could be briefly described as under:

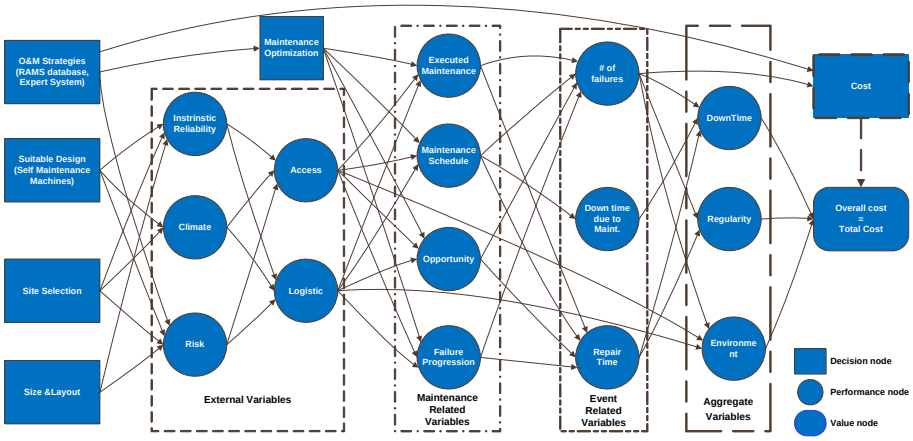

Figure 1: Influence diagram with special focus on the reliability and maintainability of OWT

- *Suitable Design*
  - i. Evaluation of available design option
  - ii. Performance of available design choice in different atmospheric conditions especially with respect to wake losses
  - iii. Selection of suitable design
  - iv. Implication of each design option on the performance and value nodes
  - v. Choice for having a design with redundancies like self-maintenance machines(SMM) to lower the O & M cost
- *Site Selection*
  - **i.** Continuous availability of wind
  - **ii.** Less harsh weather to ensure efficient logistics, access, and transportation
  - **iii.** Closeness to grid connection
- *Size and Layout*
  - **i.** Optimized size and layout
  - **ii.** Moderated wake effect to have less damage on the structure
  - **iii.** Efficient accessibility from one turbine another within one wind farm
- *O & M Strategies*
  - **i.** Choice for the employment of expert , Monte Carlo based or other existing system
  - **ii.** Higher level of availability
- *Maintenance Optimization*
  - **i.** Undertaking preventive, corrective, condition based, risk based, or opportunity based maintenance strategy
  - **ii.** Optimizing maintenance interval

2. **Performance nodes**
   - *External Variables*
     - i. Built-in reliability of the different components and sub-systems of OWT

ii. Climate conditions of the selected site like frequency and probability of hurricane or gust of winds

- *Maintenance Related Variables*
  i. Optimized maintenance system based on maintenance techniques as well as keeping in view the accessibility and logistic issues
  ii. Continuous monitoring of failure progression and adopting means to control its speed
- *Event Related Variables*
  i. Number of failure of components
  ii. Down time due to delay in carrying out maintenance activities due to sub optimal maintenance schedule
- *Aggregate Variables*
  i. Total system down time due to higher frequency of the number of failures and poor planning in having an optimized maintenance schedule
  ii. More repair time than expected due to number of factors like weather conditions, safety concerns for maintenance personnel

3. **Value node**
   It represents the choices regarding what type of factors are mostly affecting the overall performance of the system and then contributing in the overall costs. All parameters mentioned in figure 1 contribute directly and indirectly in the value node.

3 CONCLUSIONS

The introduction of the influence diagram has given the preliminary and overall understanding of the effect of different parameters on each other and their contributions on the cost.

A general framework has been presented on a macro scale and it could be constructed on the detail level for conducting the analysis.

BIBLIOGRAPHY

[1] Twidell, J., Gaudiosi ,G., Offshore Wind Power, ISBN 978-0906522-639

[2] Vatn, J., P. Hokstad, et al. (1996). "An overall model for maintenance optimization." Reliability Engineering & System Safety **51**(3): 241-257.

European Academy of Wind Energy

Norwegian University of Science and Technology

Risk based maintenance of offshore wind turbines using Bayesian networks

Jannie Jessen Nielsen[1)], John Dalsgaard Sørensen[1,2)]

[1)] Aalborg University, Denmark, [2)] Risø-DTU, Denmark

ABSTRACT

This paper presents how Bayesian networks can be used to make optimal decisions for repairs of offshore wind turbines. The Bayesian network is an efficient tool for updating a deterioration model whenever new information becomes available from inspections/monitoring. The optimal decision is found such that the preventive maintenance effort is balanced against the costs to corrective maintenance including indirect costs to reduced production. The basis for the optimization is the risk based Bayesian decision theory. The method is demonstrated through an application example.

KEYWORDS

Wind turbines, Maintenance, Bayesian networks, Risk based optimization

1 INTRODUCTION

Operation and maintenance is an important issue for offshore wind turbines, as the costs are large, up to 25-30% of the cost of energy. Especially a large number of component failures lead to reduced power production and a need for corrective maintenance. These costs can be reduced by applying preventive maintenance strategies, such as condition based maintenance. Here decisions on repairs are made based on information gained using condition monitoring. Condition monitoring methods are subject to uncertainties, and more optimal decisions can be made if the monitoring results are combined with all available knowledge from past experience and theoretical models using Bayesian updating. Risk based methods can then be applied to find the optimal maintenance strategy, and make optimal decisions on preventive repairs, see the framework in [1]. Bayesian networks and influence diagrams can be used for updating a damage model, whenever new information becomes available, and to find the optimal decisions.

2 BAYESIAN NETWORKS

A Bayesian network is a graphical model that consists of nodes, representing stochastic variables, and links, representing conditional dependencies among them. A link from A to B

means that B is caused by A, and A is called the parent of B, and B the child of A. For each node in the Bayesian network the conditional probability distribution should be specified conditional of the parents, thus for nodes without parents the marginal distribution should be specified. The network can then be used to find the posterior distributions using Bayesian updating based on Bayes formula. See [2] for an introduction to Bayesian networks, and [3] for a framework for deterioration modelling using Bayesian networks.

2.1 Deterioration modelling

In the present application it is assumed that the overall health of a component can be described by a damage model. Inspections are performed on a regular interval, and there it is possible to measure the health of the component, but with some uncertainty. The Bayesian network for this model consists of a number of equal time slices, one for each time step, and a first time slice with the initial values. The first part of the Bayesian network with two time slices is shown in Figure 1. The health of the component is represented by the damage size, D, that increases with time. In the damage model two parameters are modelled by random variables, Mu and A, which are time invariant and variant parameters respectively. The inspection result is included in the node Ins.

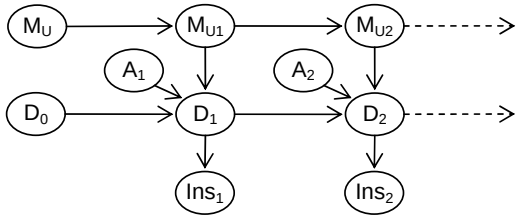

Figure 1: Bayesian network for updating of the damage size. D: damage size, Ins: inspection, A, M_U: damage parameters.

2.2 Influence diagram

The network presented above can be used for updating the probability distribution of the damage size, and if a failure criterion is formulated, the probability of failure can be found. The Bayesian network can be extended to an influence diagram, which can be used for finding optimal decisions. An influence diagram consists of nodes and links, like the Bayesian network, but there are two additional types of nodes, utility nodes and decision nodes, shown with diamonds and rectangles respectively. The utility nodes are used to include the costs in the model, in this case the cost of failure (including lost production and cost of corrective repair), and the cost of preventive repairs. Decision nodes are used to include decisions in the model, here the decision of making a preventive repair.

The optimal decisions for the repair times are the ones that give the smallest expected costs through the lifetime. These can be found using a Bayesian pre-posterior decision analysis, where decision policies are included for all future decisions, see theory in [4]. In this paper a LIMID (Limited Memory Influence Diagram) has been used for the optimization, see [5].

3 APPLICATION EXAMPLE

It is assumed that an inspection is performed every year, and after each inspection it can be decided to make a preventive repair. The component has a mean time between failures of 8 years, and the damage development is described by Paris law. The wind turbine is assumed to have a lifetime of 20 years, and the first part of the LIMID is shown in Figure 2.

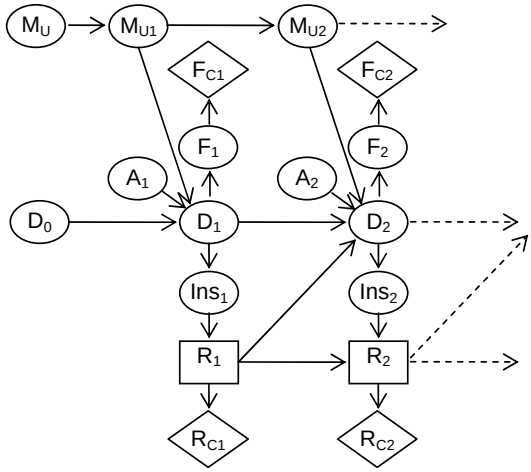

Figure 2: Influence diagram for finding optimal repair decisions. D: damage size, F: failure, R: repair, Ins: inspection, A, M_U: damage parameters,

Failure occurs at the damage size 1, and at the inspections there is assumed to be an additive measurement error that is normal distributed with mean zero and standard deviation 0.05. In general the variables used in the model are continuous, but for a LIMID it is necessary to discretize all variables. The variable representing the damage size, D, is discretized in 30 states, where the last state is failure. The other states have exponentially increasing size, and are numbered 1 to 29. For details about the damage model and discretisation of variables, see [6]. The observations used for the case study is shown in Table 1.

Table 1: Observations for the case study. Numbers refer to states.

Year	1	2	3	4	5	6	7	8	9	10
Observation	14	15	21	17	19	23	27	28	29	Failure

3.1 Results

The probability of failure calculated based on the information available on the last time step, and the expected utility for the decisions repair and no repair is shown in Figure 3. In year 7 the utility of repairing is larger than the utility of not repairing, and thus a repair should be performed.

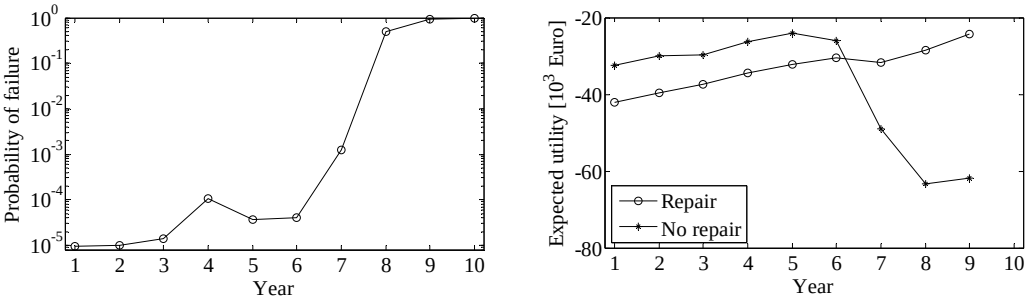

Figure 3: Probability of failure and expected utility for case study.

4 CONCLUSIONS

This paper demonstrates how Bayesian graphical models can be used to assist in optimal decision making for preventive repairs of offshore wind turbines. The method can be applied to components where a damage model can be formulated.

5 ACKNOWLEDGEMENTS

The work presented in this paper is part of the project “Reliability-based analysis applied for reduction of cost of energy for offshore wind turbines” supported by the Danish Council for Strategic Research, grant no. 2104-08-0014. The financial support is greatly appreciated.

BIBLIOGRAPHY

[1] Sørensen JD, 2009 ‘Framework for risk-based planning of operation and maintenance for offshore wind turbines,’ Wind Energy, vol. 12(5), pp. 493-506.

[2] Jensen FV, Nielsen TD, 2007 ‘Bayesian Networks and Decision Graphs’, Information Science and Statistics, Springer.

[3] Straub D, 2009 ‘Stochastic modeling of deterioration processes through dynamic bayesian networks,’ J.Eng.Mech., vol. 135(10), pp. 1089-1099.

[4] Raiffa H, Schlaifer R, 1961 ‘Applied statistical decision theory’, Harvard University.

[5] Lauritzen SL, Nilsson D, 2001 ‘Representing and solving decision problems with limited information,’ Management Science, vol. 47(9), pp. 1235-1251.

[6] Nielsen JJ, Sørensen JD, 2010 ‘Bayesian networks as a decision tool for O&M of offshore wind turbines,’ Proceedings of the 5th international ASRANet Conference.

Remote Presence, Cost-Effective Robotic Inspection and Maintenance of Offshore Wind Turbines

Øyvind Netland, Amund Skavhaug
Norwegian University of Science and Technology
Department of Engineering Cybernetics

ABSTRACT

The operation and maintenance costs for offshore wind turbines can be significantly higher than for their land-based siblings, caused by reduced accessibility, mainly due to harsh weather conditions. This paper discusses a new concept of O&M optimization for offshore wind farms, based on remote presence, i.e. robotic inspection and maintenance controlled remotely from onshore. Hopefully, the remote presence can reduce the need human visits from months to years. Inspections can for example confirm/reject a fault diagnosed by a condition monitoring system, where remotely controlled robotic maintenance might be able to handle a number of minor tasks, before they become serious issues. The proposed technologies have the potential of reducing the number of necessary maintenance visits, maintenance cost and downtime, as well as improve worker safety.

1 KEYWORDS

Offshore wind energy, O&M, Remote presence, Remote inspection, Robotic maintenance,

2 INTRODUCTION

In the last decade, offshore wind turbines have become a reality and an emerging industry [1]. It offers higher average wind conditions than on land, which gives a cubic increase, and does not have the same limitations for transporting large machinery and with proximity to inhabited areas. Constructing and operating offshore wind turbines are unfortunately expensive, and the focus of this paper is to reduce the operation and maintenance (O&M) costs, which are higher than for onshore wind turbines. Reasons for this are:

- Offshore transport is more expensive and takes longer than transport on land.
- Offshore wind turbines are often inaccessible due to weather conditions.
- Equipment for heavy lifting is less available and more expensive.

The due to low accessibility to an offshore wind turbine, the frequency of maintenance visits is an important factor for the O&M cost, and should be decreased. Building more reliable

wind turbines will help, but we believe that the ability to perform maintenance without having to travel to the wind turbine have a higher potential. This can be achieved with an inspection and maintenance system that can be controlled remotely from onshore, and give an onshore operator a *remote presence* on the turbine. Cameras and sensors can be used for *remote inspection*, and by adding tools needed for performing maintenance and repairs, the system can also be used for *remote maintenance.*

Remotely operated O&M robots are traditionally seen in locations where human workers are not an option, like inside nuclear reactors and in space. It is predicted in [2] that offshore oil and gas installations of the future will be highly robotized, especially the ones that are located in extreme weather conditions.

3 CONDITION MONITORING

A condition monitoring (CM) system continuously monitors the health of a system by analysing sensor information, and informs operators of any noteworthy situations. Over the last 10 years, several research projects have focused on condition monitoring of wind turbines, which is especially important for offshore wind turbines, due to the high cost of maintenance and transport. CONMOV [3] and CleverFarm [4] are two examples projects that have implemented and tested CM system onboard wind turbines.

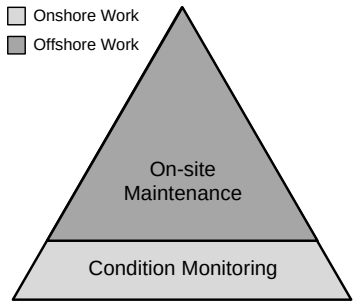

Figure 1: O&M tasks with CM

Figure 1 describes the O&M tasks in a system where continuous CM of the wind turbine is represented as the widest, lower part of the pyramid. The rest of the pyramid represents inspections and maintenance tasks that must be done offshore.

4 REMOTE PRESENCE

4.1 Purpose

Remote presence is intended to work together with a CM system, and it can perform tasks that would normally require visiting the wind turbine.

This is represented in Figure 2, where some of the on-site maintenance has been replaced by remote inspection and maintenance. Some maintenance tasks will be impossible to do remotely, so the top of the pyramid will always be

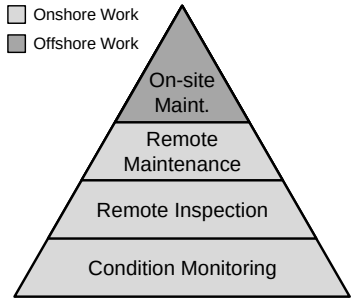

Figure 2: O&M tasks with remote presence

dark grey, but reducing its size will lower the total O&M cost.

4.2 Remote Inspection

Remote inspection allows an operator to study a part of a turbine in detail, by taking pictures, recording video and performing measurements from a mobile remote inspection device. Confirming CM diagnosis, plan for future maintenance visits and performing routine inspections are examples of applications of such a system.

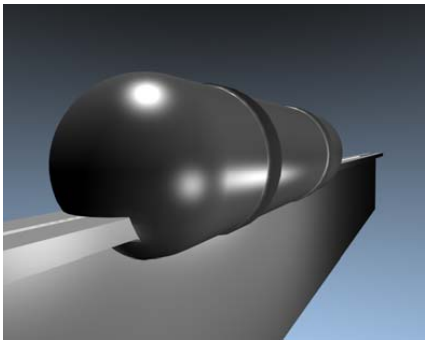

Figure 3: Concept drawing of mobile remote inspection device

Our first remote inspection prototype will consist of a remote inspection device that are able to move on a rail installed in the roof and walls of the nacelle of a turbine. We hope to install and test this inside a wind turbine, to learn more about how it can interact with the turbine.

4.3 Remote Maintenance

Remote inspection can observe a problem, but will be unable to do anything about it. A remote maintenance system that can perform preventive maintenance and repairs controlled from onshore is needed. A robot equipped with necessary tools that can move on and around the drive train is a possible solution. To access the necessary maintenance locations, a robot with similar mobility to the one described in [5] will be necessary.

It will not be possible to create a robot that is able to do all maintenance tasks to a reasonable price. The best compromise between abilities and cost must be found, but reliability must be the first priority. If a maintenance robot fails before the wind turbine, it will be part of the problem, not the solution.

4.4 Networking

Most offshore wind farms have high speed Internet connection, that can be used for control and data transfer between the remote presence system and an onshore computer. It is important that the communication interface is secure, either that the network link is not exposed to the open Internet, or that state of the art encryption is used. Unauthorized access to the remote presence system can be used for industrial espionage and possible even damage the wind turbine.

The concept of controlling robots over Internet has existed since the Mercury project [6] in 1994. One of the challenges of controlling a robot over a computer network is the variable

capacity, lag and traffic. In 2001, the first remote surgery was performed [7], where surgeons in New York removed a gallbladder from a patient in France. This is in many ways a similar task as remote maintenance of a wind turbine, and shows that such an operation over a great distance is technically possible. In [8], an experimental setup for testing real-time control data exchange over Internet connections is described.

5 CONCLUSIONS AND FURTHER WORK

Due to the remote location of offshore wind turbines, often with harsh weather condition, the O&M costs are much higher than for onshore wind turbines. To reduce this cost, we propose to install remotely operated systems onboard the turbines, giving onshore operators a *remote presence* onboard the wind turbine. This can be used to perform O&M tasks that traditionally would require expensive and time consuming transport offshore.

We plan to continue this research, with focus on the following:

- Create an overview of the maintenance tasks performed onboard a wind turbine, and what will be required of a remote system to perform these.
- Find a good method of movement for a maintenance robot.
- Reduce problems with variable network delays with semi-autonomous control.
- Implement and test system onboard a wind turbine.

6 BIBLIOGRAPHY

[1] Peter Musgrove : Wind Power, Cambridge University Press, 2010

[2] Skourup et al : The robotized field operator, ABB review 1, 2009

[3] Energy research Centre of the Netherlands (ECN) – Condition Monitoring for Offshore Wind Farms CONMOW. Final Report, June 2007.

[4] Risø DTU, National Laboratory for Sustainable Energy - CleverFarm® - A SuperSCADA system for wind farms. Final Report, August 2004

[5] Tâche et al : Magnebike: A magnetic wheeled robot with high mobility for inspecting complex-shaped structures, Journal of Field Robotics, Vol 26, No 5, 2009

[6] Goldberg et al : The Mercury Project : a feasibility study for Internet robots, IEEE Robotics and Automation Magazine, Vol 7, No. 1, March 2000.

[7] Larkin : Transatlantic, robot-assisted telesurgery deemed a success, The Lancet, Vol 358, No 9287, 2001

[8] Lunheim et al : An experimental setup for vertical integration in network systems for industrial use, 2nd Intl Workshop on Real-Time LANS in the Internet Age, 2003

European Academy of Wind Energy

Norwegian University of Science and Technology

Condition monitoring methods for offshore wind turbines

Mahmoud Valibeiglou

NTNU, Norway

ABSTRACT

Condition monitoring methods, like vibration analysis, oil analysis, and crack measurement are very useful in order to prevent failures in offshore wind turbines. With these methods we can monitor and predictive the condition of equipments and make decision to perform proper maintenance task. In this paper we discuss condition monitoring methods and their applicability for wind offshore turbines. Advantages and disadvantages of the various methods are discussed.

Part 7

Session 5A - Wind Field Measurements and Simulations I

- Multifractal Analysis and Simulation of Wind Energy Fluctuations
  George Fitton, Université Paris Est
- Intermittent Structures in Atmospheric Wind Fields
  Örsan Yüksek, University of Oldenburg
- Turbulent Flow over Hills and a Call for Guidelines in Wind Tunnel Simulation
  Graciana Petersen, University of Hamburg
- Physical Modelling of a Wind Turbine
  Francesco Cuzzola, Meteorologisches Institut Hamburg

Multifractal Analysis and Simulation of Wind Energy Fluctuations

G.F.Fitton

Université Paris Est, Ecoledes Ponts Paris Tech, LEE, SU 6-8Av.BlaisePascal-Cité
Descartes Champs sur Marne, 77455 Marnela Vallée Cedex 2, France
George_Fitton@Yahoo.co.uk

ABSTRACT

One of the key thematic areas for the development of future research in wind energy is wind conditions. To better understand this topic requires the development of new numerical methods and measuring techniques capable of reaching micro scale effects. My PhD thesis will focus on advanced characterisation of micro-scale wind turbulence with respect to non-Gaussian heavy tailed statistics and short term extreme events (gusts) on the scales of 1 to 1000 m and/or 1 to 100 sec. Based on experimental data, multifractal wind field models with high frequency turbulent dynamics will be developed. Such models are promising candidates for providing initial flow conditions for turbulent dynamic CFD calculations. A combination of multifractals with other more classical models can open new perspectives for many industrial applications.

1 INTRODUCTION

Over the last twelve months I have studied mathematical and numerical methods for modelling atmospheres and oceans; specifically fluid dynamics, atmospheric physics, conservation laws and numerical techniques. The outcome, an ability to model fluid and gas flow based on an understanding of governing equations and their physical properties. I am now looking to apply this knowledge to a new and exciting area of research, multifractals.

Traditional numerical approaches are forced to transform partial differential equations (PDE's) into ordinary differential equations (ODE's) by implicitly imposing the regularity and homogeneity assumptions. The problem encountered with these assumptions is a violation of the fundamental symmetry of the nonlinear PDE's which can lead to a reduction in variability. This then questions the relevance of the resulting numerical codes because their scales are different from those of the observations. Using multifractals on the other hand allows us to understand and to model extremely variable space-time fields thus accounting for extreme events (gusts). If properly applied, I believe a multifractal wind analysis and model will be a greatly beneficial contribution to weather/wind prediction.

2 ATMOSPHERIC DYNAMICS AND THE CASCADE PARADIGM

In 1922, the meteorologist Lewis Richardson in his book “Weather Prediction by Numerical Processes" expressed the idea of atmospheric dynamics. In poetic form, he suggested that the turbulence in the atmosphere produced by an outer force, giving rise to kinetic energy at big scales, is transferred to smaller scales without dissipation until the terms of viscosity can not be neglected anymore. The theory of turbulence went on with the work of [3] about homogeneous turbulence. With the help of the so-called refined self-similar hypothesis [4], the velocity increment singularities were linearly related to the singularities of the energy flux whose energy spectrum obeys the famous -5/3 law over the scaling range (Fig.1). However, it required some time and various developments before providing well-defined cascade models ([8]; [5]; [2]).

Simple cascade models were developed to explain how geophysical variability occurs over a very large range of scales supposing that the same elementary process act at each scale. In the pedagogical case of “discrete" in scale cascade models “eddies" are defined by the hierarchical and iterative division of a D-dimensional cube into smaller sub-cubes (see Fig. 2), with a constant ratio of scales λ = L/l, where l is the scale of observation, L the outer scale. The energy flux is modulated in a multiplicative way from one scale to the next smaller scale. Thus, after a big number of cascade steps, the energy is concentrated in small areas. Since we simply follow how the turbulent energy flux becomes more and more inhomogeneous as large structures break up into smaller and smaller scales, cascades are a very general paradigm. After 1983 multiplicative cascades evolved to a multifractal theory [6], allowing a statistic evaluation of the variability for all scales.

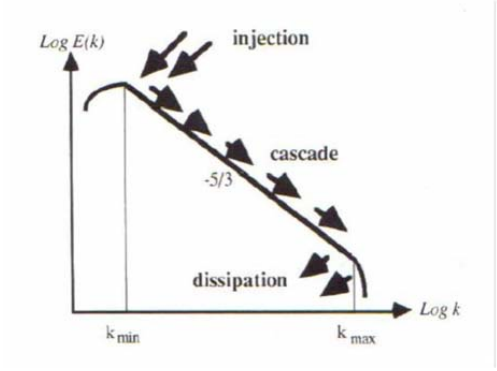

Figure 1: Schematic illustration of the Kolmogorov-Obukhov spectrum that follows the power law with the exponent -5/3, developing Richardson’s idea

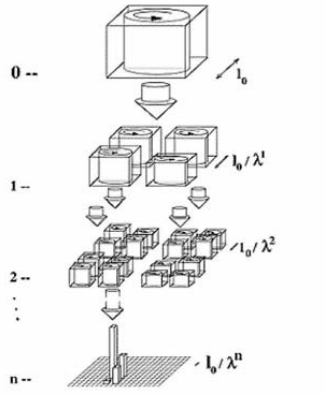

Figure 2: Schematic illustration of “discrete” in scale cascade model. The energy is concentrated in small areas after a big number of cascade steps

In a very general manner, multifractals are space or space-time fields that have structures at all scales. The wind velocity field is strongly turbulent and variable over a wide range of scales in space and time. Figures 3 and 4 display examples of numerical simulations for the city of Marseille (France) performed with the mesoscale model MESO-NH (developed by Meteo-France and the Laboratoire d'aérologie) to illustrate such a variability. Multifractal analyses of simulations can be used to get better incite on a performance of numerical models. For instance, [7] analysed a variability of these data by estimating statistical moments at various scales. He concluded that for the horizontal wind velocity field the results agree with earlier empirical and theoretical results within the realms of statistical variability. On the contrary, the vertical wind velocity field does not coincide with a scaling theory.

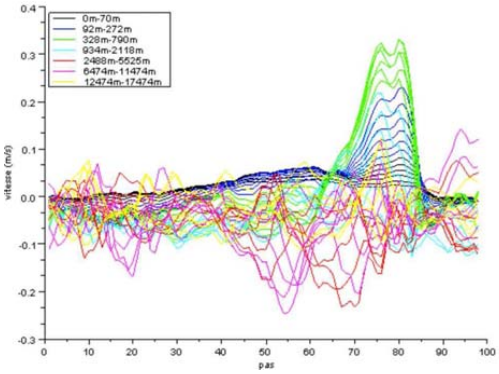

Figure 3: Time fluctuations of a vertical component of wind velocity at city of Marseille (France) simulated by the MESO-NH model.

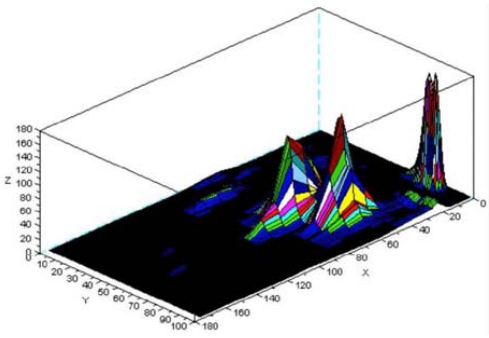

Figure 4: Space-time intermittency of the energy fluxes (z-axis) simulated during 100 time steps of MESO-NH model with Buoyancy forces.

3 INTERMITTENCY AND MULTIFRACTAL WIND GUSTS

Multiplicative models produce hierarchies of self-organised random structures that yield not so trivial consequence. As already mentioned, higher and higher levels of 'activity' of the field are concentrated on smaller and smaller fractions of space. That is the intermittency, also referred to as micro scale effects that appear in the range of 1 to 1000m or 1 to 100sec. Fluctuations on these scales are known to show extremely non-Gaussian statistics, i.e. with probabilities of extreme events (wind gusts) much higher than for quasi-Gaussian fields. These more frequent intermittent bursts may cause additional mechanical loads, deviations in the expected power production and large short time power fluctuations. Our current understanding of multifractal extremes points out the necessity – as well as the possibility – of developing a new extreme value theory that could deal with processes having long-range dependences. At the same time, there remains the fundamental question of establishing a

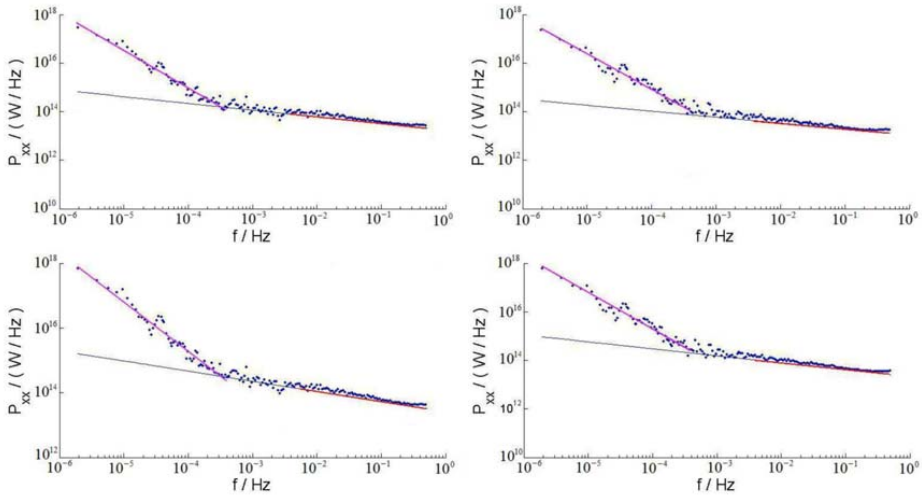

Figure 5: (from Fuchs (2008): The spectra calculated from the energy fluxes of the wind data measured at the altitude of 23m (left) and 43m (right). Thespectra correspond to a horizontal component of the wind measurements (top) and to three dimensional wind data (bottom).

more direct connection between multifractals and the deterministic-like nonlinear equations that are supposed to generate them, in particular the Navier-Stokes equations. This would have many fundamental consequences such as opening the road to new renormalisation techniques able to grasp intermittency as well as to a better knowledge of the mathematical properties of the solutions of these equations.

ACKNOWLEDGMENTS

The organisers of the EAWE 6th PhD Seminar on Wind Energy for allowing me to take part. The European Wind Energy Academy (EAWE) for the training opportunity. Marie Curie Initial Training Network (EU-FP7-ITN-WAUDIT) for financial support during my PhD.

REFERENCES

[1] Fuchs K. 2008, Multifractal Analysis of the wind in the wind park ERSA, Mémoire de Projet de fin d'Etude, Ecole des Ponts Paris Tech, 74p

[2] Frisch, U., P.L.Sulem, etal. (1978). "A simple dynamical model of intermittency in fully develop turbulence." Journal of Fluid Mechanics 87: 719-724.

[3] Kolmogorov A. N., 1941, A local structure of turbulence in an incompressible viscous fluid for very large Raynolds numbers. Proc. Acad. Sci. URSS., Geochem. Sect.30,

299-303

[4] Kolmogorov A.N., 1962, A refinement of previous hypotheses concerning the local structure of turbulence in a viscous incompressible fluid at high Raynolds number. J. Fluid Mech. 83, 349

[5] Mandelbrot, B.B. (1974). "Intermittent turbulence in self-similar cascades: divergence of high moments and dimension of the carrier." Journal of Fluid Mechanics 62: 331-350.

[6] Menyah K. 2009, Dynamique dans le modéle MESO-NH, une analyse multifractale, Mémoirede Projet de fin d'Etude, Ecole des Ponts Paris Tech, 44p.

[7] Schertzer, D. and S. Lovejoy (1983). On the dimension of atmospheric motions. Turbulence and Chaotic phenomenain Fluids, IUTAM, Kyoto, IUTAM.

[8] Yaglom A.M., The influence on fluctuaion in energy dissipation on the shape of turbulent characteristics in the inertial interval. Sov. Phys. Dokl. 2, 26

Intermittent Structures in Atmospheric Wind Fields

Örsan Yüksek, Tanja Mücke, Joachim Peinke

ForWind-Center for Wind Energy Research, Institute of Physics, University of Oldenburg, 26111 Oldenburg, Germany

E-mail: oersan.yueksek@uni-oldenburg.de, tanja.muecke@forwind.de, peinke@uni-oldenburg.de

ABSTRACT

For design processes and load calculations realistic synthetic wind fields are needed. The widely used norm is the standard of the International Electrotechnical Commission (IEC). The IEC standard considers different simulation methods which are based on Gaussian statistics. However, the analysis of the measured wind fields by means of velocity increment statistics yields that the turbulence of the wind field does not obey Gaussian statistics but are quite intermittent. Recently, a new approach based on continuous time random walks (CTRW) to generate intermittent synthetic wind fields was proposed. The new-model adequately reproduces the intermittency of turbulent atmospheric velocity increments on small time scales and provides wind fields with the desired high order two point statistics. In this work, we analyse highly time-resolved data sets measured in an extensive grid over the whole rotor plane between 50m and 150m height. The atmospheric wind fields are characterized statistically and the dependency of the higher order two point statistics on turbulence intensity, mean wind speed and height is searched. With this knowledge we are able to generate synthetic CTRW wind fields with the right small scale structure.

The aim of this work is to verify if there are universal intermittent structures in the probability density functions (pdfs) of atmospheric wind fields. This would allow simplified approaches to model synthetic wind fields.

KEYWORDS

Wind turbines, intermittency, synthetic field generation

1 INTRODUCTION

For design processes and load calculations realistic synthetic wind fields are needed. The widely used norm worldwide is the standard of the International Electrotechnical Commission (IEC). The IEC standard considers different simulation methods which are based on Gaussian statistics. However, the analysis of the measured wind fields by means of velocity

increment statistics yields that the turbulence of the wind field does not obey Gaussian statistics but are quite intermittent [1]. The intermittent - gusty nature of atmospheric wind affects the whole *chain of the wind energy conversion process and is assumed to be a major effect for additional loads and fatigue [2]. Therefore, it is very crucial to consider also the small scale structure of atmospheric turbulence in synthetic wind field modelling.*

Recently, David Kleinhans et al. proposed a new approach based on continuous time random walks (CTRW) to generate intermittent synthetic wind fields [3]. The CTRW-model adequately reproduces the intermittency of turbulent atmospheric velocity increments on small time scales and provides wind fields with the desired high order two point statistics.

In this work, we analyse highly time-resolved data sets measured in an extensive grid over the whole rotor plane be-tween 50m and 150m height [4]. The atmospheric wind fields are characterized statistically and the dependency of the higher order two point statistics on turbulence intensity, mean wind speed and height is proven. With this knowledge we are able to generate synthetic CTRW wind fields with the right small scale structure.

The aim of this work is to verify if there are universal intermittent structures in the probability density functions (pdfs) of atmospheric wind fields. This would allow simplified approaches to model synthetic wind fields.

2 DESCRIPTION OF WIND FIELDS

2.1 Measurement Setup of the Atmospheric Data

The measurement data used in this work are taken from the 3-MW GROWIAN wind turbine which is in Kaiser- Wilhelm-Koog, by the German coastline of the North Sea. The data which consists of 334 data sets were recorded for a time length of 10 minutes. The horizontal wind speed was measured by totally 16 anemometers which were placed at two met masts having a separation of 52 m in between. Each met mast has an arm having a length of 12 m at the heights of 50 m, 75 m, 100 m, 125 m and 150 m and each arm has two anemometers expect the ones at the heights of 50 m and 150 m which have 2 anemometers.

2.2 Characterization of the Wind Fields

Having the wind speed time series taken from the GROWIAN site, the initial step is to characterize the wind fields by means of their mean velocity $\langle u \rangle$ and the turbulence intensity I for each data set. The mean velocity and the turbulence intensity are related by

$$I = \sigma / \langle u \rangle$$

where σ is the standard deviation of the mean wind speed. Figure 1 shows a plot of mean wind speed vs. turbulence intensity for a measurement of 100 m weight.

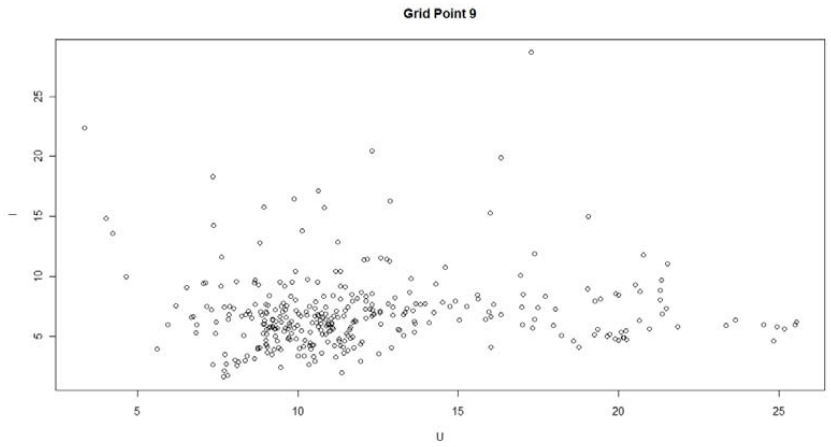

Figure 1. Mean velocity vs. turbulence intensity for all data sets having a height of 100 m.

The data points between 5 and 25 m / s wind speed and 0 and 20 % turbulence intensity are divided into 3 regions and the corresponding probability density functions (PDF) of each region is determined. Figure 2 shows the PDF of one of those regions for the mean wind speed between 0 and 25 m / s mean wind speed and 0 and 5 % turbulence intensity. The intermittent structure of the PDF is clearly seen when compared with the corresponding Gaussian curve.

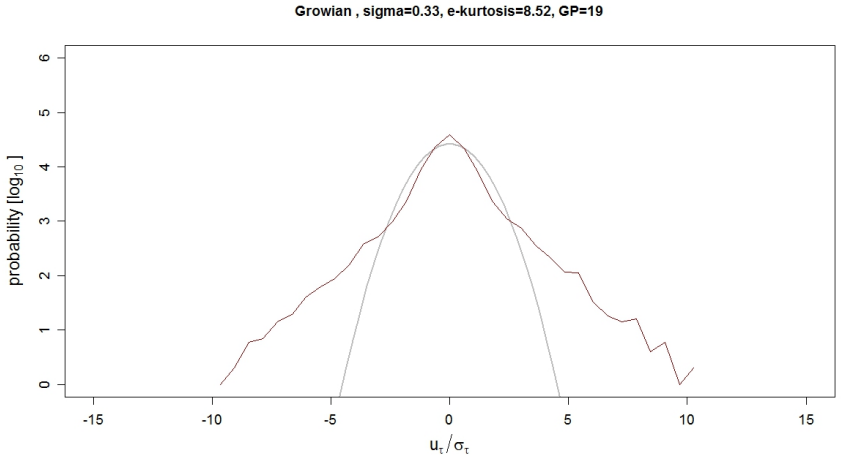

Figure 2. Probability density function of velocity increment at the height of 100 m for a time lag of 1.2 s normalized to σ = 1. The gray line is the corresponding Gaussian distribution.

2.3 Generating Synthetic Wind Fields

After characterising the wind fields by means of the mean wind speed, turbulence intensity and other higher-order moments, the corresponding synthetic wind fields are generated by means of a program called FAST. It is shown that the generated wind fields with the CTRW model do fit with the measured atmospheric wind fields much more accurately than the IEC-Kaimal Model. At the time of writing this paper the generated wind fields are not yet prepared and therefore cannot be shown. Establishing a form parameter for different mean wind speeds and turbulence intensity to optimise the simulation results will be the ultimate goal of the work.

3 CONCLUSION

As already mentioned, design processes and load calculations need realistic synthetic wind fields for many reasons- Fatigue loads or extreme loads are among them. The proposed CTRW-Model generates much better synthetic fields compared to the standard model which is based on the one-point statistics up to the second order. Other than better fittings with the measured data, this work also tries to define a parameter for different means wind speed and turbulence intensity for optimising the generated synthetic wind fields.

BIBLIOGRAPHY

[1] Böttcher, F.; Barth, S. and Peinke, J. Small and large scale fluctuations in atmospheric wind speeds, Stochastic Environmental Research and Risk Assessment (SERRA), 2007, 21, 299-308

[2] T. Mücke, D. Kleinhans and J. Peinke, Atmospheric turbulence and its influence on the alternating loads on wind turbines. Submitted for publication 2010.

[3] David Kleinhans and R. Friedrich, Simulation of intermittent wind fields: A new approach. In DEWEK 2006 - Proceedings, Bremen (Germany), 2006.

[4] H. Günther, B. Hennemuth, Erste Aufbereitung von flächenhaften Windmessdaten in Höhen bis 150 m, DWD BMBF-Projekt 0329372A, 1998.

European Academy of Wind Energy

Norwegian University of Science and Technology

Turbulent Flow over Hills and a Call for Guidelines in Wind Tunnel Simulation

Graciana Petersen[1)]

[1)] Meteorological Institute KlimaCampus, University of Hamburg, Germany

ABSTRACT

Atmospheric boundary layer (ABL) flow over complex terrain is very important with regard to siting of wind energy converting systems (WECS). Firstly, wind speed up over hill crest is an important feature in order to predict energy gain. Secondly, turbulence effects due to hills can cause failure and damage of wind turbines. That is why the development of computational wind prediction tools that properly treat topography effects is very important for nowadays wind energy assessment. In this paper, a short summary of theory and wind tunnel simulation of ABL flow over hills is given and it is called for a guideline of wind tunnel experiments concerning turbulent flow over complex terrain.

KEYWORDS

Wind energy assessment, siting of wind energy conversion systems (WECS), atmospheric boundary layer (ABL) flow over hills, turbulent flow in complex terrain, wind tunnel simulation

1 INTRODUCTION

Flow over complex terrain and hills is an ongoing research area. It has been focused on in a number of areas such as determination of air pollution zones, predictions of smoke movement from forest fires, wind energy assessment and siting of wind energy converting systems (WECS). Such problems ask for models of atmospheric boundary layer (ABL) flow over real terrain. Considering computer simulation, one of today's problems of flow over non-flat topography is scaling up the unresolved effects of flow interactions with the fine-scale topography and combine it with the resolution of regional or global scale models. Focusing on the area of wind energy, a very interesting question is how to calculate properly wind energy assessment in conjunction with complex terrain, for example wind speed-up of flow over hills, and to decide where WECS are best positioned. In addition to wind speed-up over hill crest, another important feature are turbulence effects due to topography and flow separation. Turbulence effects such as wind shear can cause in- or decrease of wind energy profit but can also exceed design basis with respect to for example wind shear. Actually, in the worst case, this can lead to failure or damage of the WECS. Thus, turbulence effects of

graciana.petersen@zmaw.de

ABL flow over hills is very important with regard to construction guidelines and safety questions.

2 THEORY ON FLOW OVER HILLS

2.1 Historical overview

Examination of ABL flow over hills exists since the 1930s, on phenomenological explanation of lee waves. By the end of the 1960s there is a good understanding of inviscid flow dynamics over hills in stable stratification, mainly with regard to streamline curvature. Attention should be drawn to the fact that no turbulent atmospheric boundary layer flow is considered at that time! In 1975, Jackson and Hunt develop an innovative theoretical ansatz for turbulent flow over a low hill in neutral stratification. Their paper can be seen as response to the need for a simple analytical theory which is able to predict the general features of a small hump on a turbulent boundary layer, [1]. The main underlying effect is the Bernoulli effect and the main idea of the paper is to use a first order perturbation formula for perturbed vertical and horizontal velocity components in order to treat the 2dimensional equation of motion. The assumptions have to be considered carefully since the theory is, strictly speaking, only valid for infinitely low hills. Despite of that, Jackson's and Hunt's Linear Theory is a stepping stone in research on ABL flow over hills. Since 1975, due to increase of computational capacities numerical modeling has become more and more important in contrast to pure analytical theory. The interested reader is referred to [14], [16] and [17].

2.2 Summary of achievements

In brief, it is important to know: Due to the Bernoulli effect wind speed up over hill crest occurs and can double the wind speed of upstream flow. Furthermore, in stable stratification lee wave phenomena can be observed, which are gravity waves depending on Froude number. This idea is linked to the dividing streamline concept for 3dimensional hills in stable stratification which determines the dividing height in which the upper part of the flow has enough kinetic energy to rise over hill top whereas the lower part flows around the hill.
Maximum wind speed up in stable stratification is assumed to occur behind hill top. See also [3], [4], [7], [16]. In neutral stratification, maximum wind speed up usually occurs at hill crest close to the ground, but there is no absolute clearness in which height, i.e. there are different observations in field studies, wind tunnel simulation and theoretical models. However, the maximum speed up height depends on hill shape, hill roughness length and inflow conditions. In addition to lee waves and wind speed up, flow separation is a very important point for ABL flow over hills. For 2dimensional hills, 0.31 can be assumed to be the critical

slope for which flow separation occurs, and 0.63 in 3dimensional case [15]. For unstable stratification, no detailed examination for ABL flow over hills exists so far, but due to field measurements wind speed up is found to be lower than in the neutral case.

3 WIND TUNNEL SIMULATION

Briefly, Abe, Putnam, Field and Warden were the pioneers in wind tunnel modelling. For example neutral flow over the Rock of Gibraltar was modelled by Field and Warden in 1929. Important work has been done by Britter, Hunt and Richards (Bernoulli hill effect of 2-dimensional hills and turbulence and the impact of roughness) or experiments in relation with the Askervein Hill Project [10], [11], [12], or other field measurements in the 1980s, such as Kettles Hill, [13]. Meroney's literature review, [14], is highly recommended to the reader. Experimental set up of wind tunnel simulation of ABL flow over complex terrain depends on the aim of investigation and field data that are possibly used as initial data. To obtain general information about structure of ABL flow over hills emphasis is put on the hill-model shape and experimental set-up promising new insights. On the other hand, if real existing terrain is to be modeled questions are amongst others how to choose the full-scale detail to ensure an expedient scaling rate in conjunction with matching flow characteristics of a given full-scale atmospheric boundary layer flow. This problem is analogous to the computer modelers' problem of matching small-scale models to boundary conditions. Regarding wind tunnel simulations of the last 20 years, unfortunately, it has to be pointed out that experimental set ups often are not well documented. But without an accurate documentation of the experimental set-up, for example inflow conditions and measurement details, reproducibility is not warranted. Furthermore, in many cases, experiments were not Reynolds independent, a basic requirement for proper wind tunnel simulation. This leads to severe problems since the interpretation and validity of wind tunnel experiments with insufficient Reynolds number is not clear.

4 CONCLUSION

Wind speed up effects of ABL flow over complex terrain and turbulence effects are very important for siting of wind turbines. Since theory can, so far, not explain turbulent flow over hills sufficiently, advanced computer models are needed for wind predictions. In order to validate computer models properly or gain more structural insight of ABL flow in complex terrain, wind tunnel simulations have to be conducted carefully. But in fact, no uniform practice in documentation and conduction of wind tunnel experiments concerning ABL flow over hills exists so far. Thus, we call for guidelines concerning the proper modeling and documentary praxis of wind tunnel simulation concerning ABL flow over hills.

BIBLIOGRAPHY

[1] Jackson, P. & Hunt, J.: Turbulent wind flow over a low hill Quart. J. R. Met. Soc., 1975, 101, 929-955

[2] Meroney, R.N., et al: Physical modeling of flow over complex terrain, Fifth international conference on wind engineering, 1979

[3] Bradley, E. F. : An Experimental Study of the Profiles of Wind Speed, Shearing Stress and Turbulence at the Crest of a Large Hill, Quart. J. Roy. Meteorol. Soc., 1980, 106, 101-124

[4] Snyder, W. H.: Guideline for Fluid Modeling of Atmospheric Diffusion United States Environmental Protection Agency, 1981

[5] Cermak, J. E.: Physical modelling of flow and dispersion over complex terrain Boundary Layer Meteorology, 1984, 30, 261-292

[6] P.J. Mason, J. K.: Measurements and predictions of flow and turbulence over an isolated hill of moderate slope, Quart. J. R. Met. Soc., 1985, 111, 617-640

[7] Snyder, W.H., et al. : The strucure of strongly stratified flow over hills: dividing-streamline concept, J. Fluid. Mech., 1985, 152, 249-288

[8] Mason, P. : Flow over the summit of an isolated hill, Boundary Layer Meteorology, 1986, 37, 385-405

[9] Taylor. P.A., et al. : Boundary Layer Flow over Low Hills (A Review) Boundary Layer Meteorology, 1987, 39, 107-132

[10] Teunissen, H.W., et al. : The Askervein Hill Project: Wind-Tunnel Simulations at three length scales, Boundary Layer Meteorology, 1987, 40, 1-29

[11] Taylor, P. & Teunissen, H. : The Askervein Hill Project: Overview and background data, Boundary Layer Meteorology, 1987, 39, 15-39

[12] Mickle, R. E., et al : The Askervein Hill Project: Vertical profiles of wind and turbulence Boundary Layer Meteorology, 1988, 43, 143-169

[13] Salmon, J. R., et al. : The Kettles Hill Project: Field observations, wind-tunnel simulations and numerical model predictions for flow over a low hill Boundary Layer Meteorology, 1988, 43, 309-343

[14] Meroney, R. N. : Wind-Tunnel Modelling Of Hill And Vegetation Influence On Wind Power Availability Task1: Literature Review, Meteorological Services U.S. Windpower, 1993

[15] Wood, N. : The onset of separation in neutral, turbulent flow over hills Boundary Layer Meteorology, 1995, 76, 137-164

[16] Miller, C. & Davenport, A. : Guidelines for the calculation of wind speed-ups in complex terrain, Journal of Wind Engineering and Industrial Aerodynamics, 1998, 74-76, 189-197

[17] Wood, N. : Wind Flow over Complex Terrain: A Historical Overview and the Prospect for Large-Eddy Modelling, Boundary Layer Meteorology, 2000, 96, 11-32

[18] Athanassiadou, M. & Castro, I. P. : Neutral flow over a series of rough hills: A laboratory experiment, Boundary Layer Meteorology, 2001, 101, 1-30

[19] Ayotte, K. W. & Hughes, D. E. : Observations of boundary-layer wind-tunnel flow over isolated ridges of varying steepness and roughness, Boundary-Layer Meteorology, 2004, 112, 525-556

European Academy of Wind Energy

Norwegian University of Science and Technology

Physical Modelling of a Wind Turbine

Francesco Cuzzola[1)], Bernd Leitl[1)], Michael Schatzmann[1)]

[1)] Meteorologisches Institut Hamburg, Germany

ABSTRACT

Wind tunnel simulation of the flow field around a wind turbine is still a tool of great value to deliver data that can be used to assess wind resource, to improve blade aerodynamics and to validate related numerical codes. With this paper we aim to describe pro and cons of the two approaches used for the simulation of wind turbines: porous discs (according to the actuator disc theory) and scaled models (reflecting full scale aerodynamics characteristics).

KEYWORDS

Wind Tunnel Turbine Scaling Actuator Disc Blade Design

1 INTRODUCTION

Wind energy research through wind tunnel testing of model wind turbine started in the late seventies in Europe.

The modeling of these wind turbines is done with the objective of either achieving geometrical similarity or trying to achieve dynamic similarity within certain ranges. In the next sections we will review some of the previous work and classify them with respect to the concept used in the scaling procedure.

2 ACTUATOR DISC CONCEPT (ADC) MODELS

This approach was first used by Vermeulen and Builtjes [1] at the Energy research Centre of the Netherlands (ECN) and the authors claim that after several diameters not only the velocity structure of the wake was correctly simulated by the so-called “Tea Strainer”. Also the turbulence structure compared fairly well with that of a rotor model.

Nowadays this approach is being used by S. Aubrun [2],[3] who is using discs of 100mm, 200mm and 300mm in diameter, built with metallic mesh. In [2] these simulators were tested in the “Malavard” wind tunnel at the Laboratoire de Mecanique et d´Energetique in Orleans with homogeneous freestream conditions and with a simulated offshore atmospheric boundary layer at 1:400 scale. The interesting result is that, changing the porosity level of the mesh, any velocity deficit can be reproduced, and varying the homogeneity of the porous material it is possible to reproduce non-uniform velocity deficit as well.

francesco.cuzzola@zmaw.de

The great advantage of this approach lies in the reliability of the mesh models and in the direct easiness of constructing them. Furthermore many numerical models are based on ADC and this means that comparisons can be made. The drawback of this approach is that one needs to know the desired wake characteristic of the wind turbine which is not properly known before it has been built. In addition, effects of rotation on the wake flow can not be investigated.

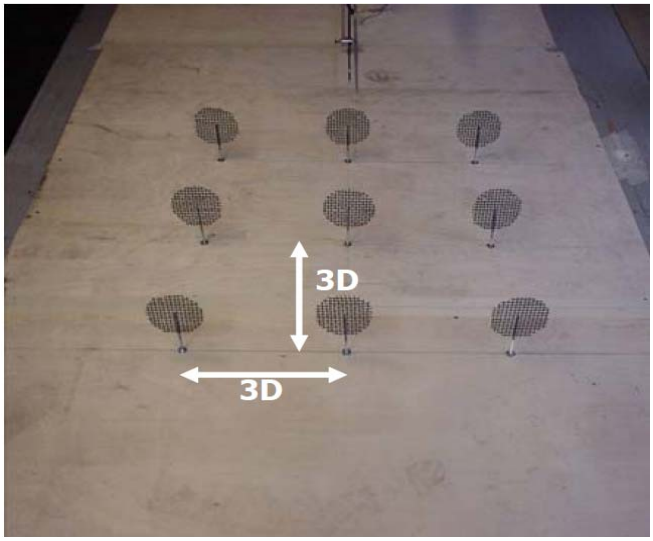

Figure 1: Wind farm simulated through ADC [3]

3 ROTOR MODELS

Many researchers tried to investigate the behaviour of wind turbines reproducing them at small scales in wind tunnels. The Aeronautical Research Institute of Sweden is one of the most active institutions in this field starting the research work already in 1979 [4]. More recently a model wind turbine was used to investigate the phenomenon of meandering [5].

Another important work came in 1988 from Colorado State University [6] suggesting that since wake characteristics are strongly dependent upon the thrust perceived by the rotor disc a wind turbine model has to be designed in order to produce an equivalent magnitude thrust coefficient.

In 2003 at ECN Corten et al. [7] designed model wind turbines of 25cm diameter. These were tested in a boundary layer wind tunnel assembled as a wind farm. It is important to note that much care was paid to the aerodynamical characteristics at lower Reynolds numbers and that the chord of the blade was extended in order to increase lift and efficiency. They

report that the simulated wake resembled the full scale behaviour in good approximation and claim that results in terms of performances are comparable with full scale wind turbine characteristics.

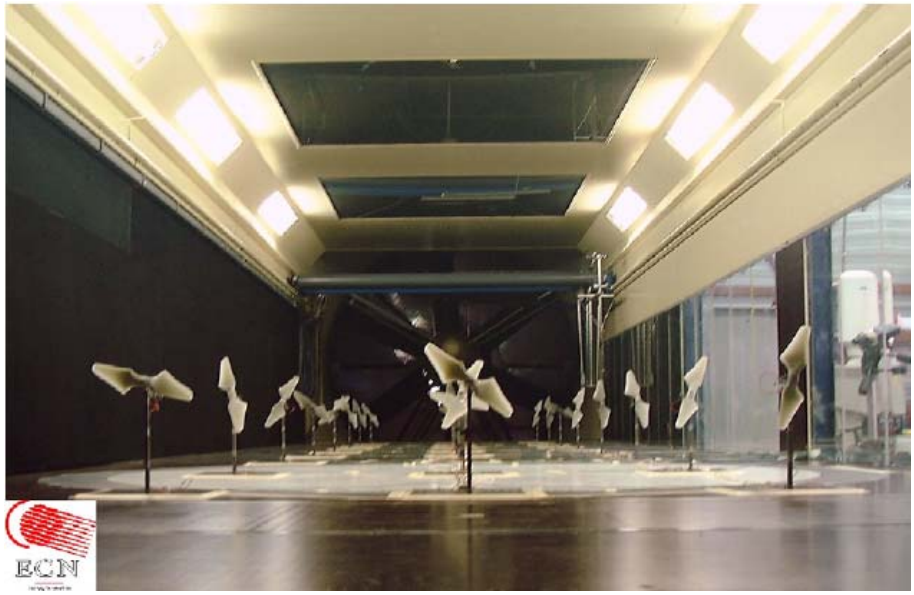

Figure 2: Model Wind Farm from [7]

4 OUTLINE OF WP6

In order to develop a quality assurance procedure within WAUDIT it is necessary to be sure of the high quality of the data. Learning from previous works we are of the opinion that using Blade Element Momentum theory it will be possible to design and build 3-bladed rotors that can resemble the wake characteristics of a full scale wind turbine.

Preliminary tests are planned to investigate performances and wake behaviour of a single rotor in order to make necessary adjustments, if needed. Once the model is tested experiments with presence of a simulated atmospheric boundary layer are also planned.

Complementary work in Hamburg will focus on the physical modelling of wind farms in complex terrain.

BIBLIOGRAPHY

[1] Vermeulen P.E.J., Builtjes P.J.H., Turbulence Measurements in Simulated Wind-Turbine Clusters, TNO report nr. 82-03003, 1982.

[2] Aubrun S., Modelling wind turbine wakes with porosity concept, proceedings of the Euromech colloquium 464b. Wind Energy pp265-270. J Peinke, P. Schaumann, S. Barth (eds), 2005.

[3] Aubrun S., Devinant Ph., Espana G., Physical modelling of the far wake from wind turbines. Application to wind turbine interactions, proceedings of EWEC 2007, Milan, Italy.

[4] Alfredsson PH, Dahlbeg J, A preliminary wind tunnel study of windmill wake dispersion in various flow conditions, FFA TN AU-1499, Part 7, Stockholm, September, 1979.

[5] Medici D., Alfredsson PH, Measurements on a wind turbine wake: 3D effects and bluff body vortex shedding, Wind Energy 9:219-236, 2006.

[6] Neff D.E., Meroney R.N., McCarthy E., Davis E., Upstream and lateral wake effects on wind turbine performances, Journal of Wind Engineering and Industrial Aerodynamics 36, pp 1405-1414, 1990

[7] Corten G.P., Schaak P., Hegberg T., Turbine interactions in large offshore wind farms-wind tunnel measurements, ECN report ECN-C—04-048, 2004.

Part 8

Session 5B - Grid Integration of Wind Farms

- A North Sea Super Grid for Offshore Wind Integration
  Til Kristian Vrana, NTNU
- Simulation of the Impact of Larger Offshore Wind Farm on System Stability
  Hui Guo, Otto-von-Guericke-University
- Dynamic Modelling of Wind Turbine and Power System for Fault Ride-through Analysis
  Fan Zhang, University of Strathclyde
- Large Scale energy storage for a 100% renewable electricity system in Germany
  Amany von Oehsen, Fraunhofer Institute for Wind Energy and Energy Systems Technology

A North Sea Super Grid for Offshore Wind Integration

T.K. Vrana, R.E. Torres-Olguin, B. Liu, T.M. Haileselassie

Norwegian University of Science and Technology, Trondheim, Norway

ABSTRACT

The North Sea Super Grid (NSSG) will interconnect several independently planned wind farms, comprising a variety of different AC and DC technologies. The internal wind farm collection grids will most likely be AC based. Long distance transmission will be HVDC and nowadays Voltage Source Converter (VSC) technology is applied for offshore projects. However in the future, Line Commutated Converter (LCC) technology could become an interesting option. Hybrid HVDC systems that combine VSC and LCC technology, Multiterminal HVDC systems (MTDC) and parallel HVDC links will gain importance for the development of the NSSG. In this paper an overview over possible technologies is given and it is discussed how these can be utilised to realise the North Sea Super Grid.

KEYWORDS

North Sea Super Grid, Multi Terminal, High Voltage Direct Current, Voltage Source Converter, Line Commutated Converter, Offshore Wind.

1 INTRODUCTION

Several far offshore wind farms are planned and considered in the North Sea for the next decades. Considering the number and scale of the planned offshore wind parks, integration via the NSSG has many advantages. An existing grid will also improve the possibility of adding smaller wind parks later, which would not have been feasible, if they needed a long separate cable connection to shore.

The current focus on the electrification of oil and gas rigs also gives positive impulses towards the establishment of a NSSG. These platforms could also be supplied by nearby wind parks, avoiding long transmission distances and carbon dioxide emissions.

The pan-European electricity market would also highly benefit from an electricity grid in the North Sea [13]. The increasing share of wind power in Europe demands stronger interconnections, to balance regional wind fluctuations, because the cross correlation of wind speeds all over Europe is much lower than within a region or a country.

Furthermore, the tremendous value of the storage capacity and flexibility of Norwegian hydro power can only be utilized, if the interconnections between Norway and the rest of Europe are sufficient.

Since this grid cannot be planned and built in one step, a modular approach is suitable, just like for onshore grids. To justify the tremendous investments, reliability, redundancy, robustness and flexibility will be of major importance. The NSSG will be built by several countries, involving many different TSOs and companies, combining projects with different goals and time horizons.

The technology to realise the NSSG is not fully developed yet. Pure HVAC transmission is not possible, due to the long distances involved. HVDC has not been proven in multi-terminal arrangements, and for MTDC a full grid might be a too advanced project to gather practical experience. If AC is used within offshore clusters and DC for long distance transmission, the benefits of both technologies can be combined. A possible NSSG topology is shown in Figure 1.

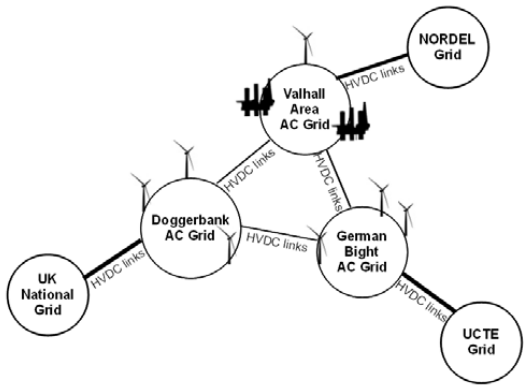

Figure 1: Possible NSSG topology

2 HVDC CONVERTER TECHNOLOGY

The two major converter types for HVDC systems are the VSC using IGBTs and the LCC using thyristors. An overview over the most important characteristics is given in Table 1.

Converter	Cost	Losses	Power	Flexibility
VSC	High	High	Low	Yes
LCC	Low	Low	High	No

Table 1: Comparison of converter technologies

2.1 Voltage Source Converter

VSC HVDC is the latest development in the field of HVDC technology and has gained more and more attention. The voltage polarity on the DC side is fixed, which makes it possible to connect several converters to the same DC bus.

VSC stations are able to form their own AC voltage waveform and act as a true voltage source. This makes it possible to connect to weak grids or even passive networks. Therefore, without any auxiliary equipment, the VSC HVDC can be connected to electrical islands such as offshore wind farms or oil & gas installations. Furthermore, when the offshore AC network suffers a blackout, the connected VSC HVDC link is able to support grid restoration. A VSC has the capability to control active and reactive power independently. Power flow direction can easily be reversed by reversing the DC current.

The features mentioned above and the compact design (it is about 60% of the size of a LCC station) make VSC technology ideal for offshore stations [1].

2.2 Line Commutated Converter

LCC HVDC is a mature and established technology. Typically, the reactive power consumption of a classic HVDC converter station is 50% of the active power transfer [7].

The applied thyristors have lower conduction losses than active devices like IGBTs and the switching frequency is as low as line frequency, leading also to low switching losses.

LCC HVDC is preferred for bulk power transmission, in excess of 1000 MW, due to its lower losses, lower investment costs and its proven reliability and service life [1].

LCC HVDC technology is best suited for transmissions between relatively strong AC networks [7,15].

3 HVDC LINKS

Considering point to point HVDC links and two possible converter technologies results into three options for HVDC links: VSC, LCC and hybrid HVDC systems. An overview over the most important characteristics is given in Table 2.

Link	Bidirectionality	Losses	Power
VSC	Yes	High	Low
LCC	Depends	Low	High
Hybrid	No	Medium	Medium

Table 2: Comparison of HVDC links

3.1 VSC HVDC links

In 1997, the first VSC HVDC system was installed by ABB for Hällsjön project in Sweden. Since then, more and more VSC HVDC systems have been installed worldwide. The Bard offshore 1 wind farm can be seen as a pioneer project, since it is the first HVDC connected wind farm, via the BorWin link (2009, 400MW) which is using 2 x 120km submarine cable [17]. 800MW Projects are right now being planned and a maximal power rating of approximate 1200MW has been proposed [17].

Due to these characteristics, VSC-HVDCs can offer a competitive mean to integrate offshore wind energy and oil rigs.

3.2 LCC HVDC links

LCC based HVDC links can operate at high voltages and have therefore low transmission losses. In addition to the earlier mentioned low losses of the converter, the total efficiency of a LCC based system is superior.

The power ratings achieved with LCC technology are larger than with VSC technology. A 1400MW HVDC cable connection is in operation in Japan, while a 3000MW connection between Java and Sumatra, which partly will be a HVDC cable, is under construction.

LCC HVDC is less vulnerable towards DC faults (because of the absence of anti-parallel diodes, which operate as rectifier feeding power directly into the fault). The DC inductor also limits the fault current. DC faults can be cleared by operating both converters as inverter [16].

3.3 Hybrid HVDC links

Hybrid HVDC is composed by a VSC on one side and a LCC on the other side connected to the same DC link, as it was proposed in [16]. Hybrid HVDC has some advantages for the connection of offshore power systems. The compact VSC terminal fits on an offshore platform and can be connected to a weak offshore AC system. The large LCC terminal is placed onshore and has lower cost and losses.

In spite of the above mentioned advantages, the Hybrid HVDC cannot reverse the power flow easily. Power flow reversal in a hybrid system, requires to discharge the DC link and to reconnect with changed polarity at one terminal.

For connection of wind farms, where power flow usually goes from wind farm to shore, this problem should not be of major importance. To avoid the complicated power inversion procedures, the hybrid link could be planned for unidirectional power flow. The development of this technology is still at an early stage and it has so far not been tested [12,16].

4 ARRANGEMENTS OF MULTIPLE HVDC LINKS

The NSSG will include many HVDC cables to integrate all offshore power systems and to cope with the large amounts of planned offshore generation.

4.1 Multiterminal HVDC

MTDC consists of several HVDC converters which are connected by a DC network [8]. The increasing number of electrical systems in the North Sea indicates that multiterminal HVDC might be a potential attractive solution for the grid integration problem in the near future [2].
VSC, LCC and hybrid MTDC have been suggested and studied in literature [4,5,10,11]. VSC based MTDC has been investigated most, due to the earlier mentioned advantages. Hybrid MTDC has gained little attention, but it will become important for the integration of already existing point to point HVDC connections of both types into the MTDC. A few strong LCC onshore terminals could be connected to several weaker offshore VSC terminals.
The Quebec-New England connection and the Shin-Shinano connection in Japan [10,17] are operational systems that indicate the possibility of establishing MTDC, but they do not fully reflect the technical capabilities, because converter construction and control technology have improved since then. With all the new opportunities it provides, MTDC is still a technology under development, especially when it comes to system protection and fault handling.

4.2 Multiple Converter Control

Due to the large amounts of power that need to be transferred from the offshore wind clusters towards shore, parallel HVDC links might be the only realistic solution. Two or more converter stations at the same busbar give possibility for new operational concepts. VSC based terminals could be built with increased power ratings, to be able to supply also reactive power to the nearby LCC terminals. Due to the independence of active and reactive power, a slightly overrated VSC could supply significant amounts of reactive power.
Reducing the requirements for capacitor banks and filters, the LCCs could possibly shrink significantly, making it more attractive for offshore applications. VSCs provide bidirectional and flexible operation with black start capability and power transfer to the offshore cluster, while the LCCs provide bulk power transmission at low cost and losses unidirectional to shore. The main draw backs of both technologies could be compensated.
The amount of literature on parallel HVDC links is limited. Studies like [6] have proposed parallel HVDC links for increased power transfer capability, but the matter was rather treated from an economic point of view, than in technical detail.

5 OFFSHORE AC CLUSTERS

In regular onshore AC grids, the generation is mostly based on synchronous generators, and a significant share of the load is induction motors. All of those rotating machines have some inertia and add to the total system inertia, which usually is large resulting in a system time constant of several seconds. This rotating energy storage makes the entire system less vulnerable to power imbalances. The applied frequency control mechanisms can therefore be rather slow [8].

The operation of an offshore AC grid is challenging, since no classical rotating machines might be connected directly to the grid. The load of an offshore grid is most likely based on inertialess HVDC converters, which transfer the generated power to shore. The generation of the offshore AC grid will be based on wind turbines, where two different concepts, which today are applied to large wind turbines (5MW+), are likely to dominate in the future. Wind turbines with doubly fed induction generator (Repower, Bard) have the grid frequency and rotational speed decoupled. Wind turbines with a permanent magnet synchronous generator and a full back-to-back converter (Multibrid, Enercon) have no direct coupling of the rotating machine to the grid at all.

Neither the generation nor the load contributes in this case to the system inertia. Due to this lack of energy storage, power production, losses and consumption have to be balanced in real time. The problem caused by the absence of electrical machines can partly be overcome, if power converters are controlled as virtual synchronous machines. This control strategy can help to balance power in AC systems with a large number of power converters [14].

The grid frequency is not linked to the rotational speed of electrical machines. It is only determined by the controllers of the power converters and it could change instantaneously. If the frequency is set by the largest converter, control is easier but vulnerable if that unit has a failure. If frequency is determined by all units (like in a regular AC grid) synchronism problems could arise.

6 IMPLEMENTATION OF THE NSSG

The starting point from where the NSSG could grow to finally connect all countries around the North Sea is the German Bight. There, the first far offshore wind park (Bard Offshore 1) is under construction, which is connected via HVDC (400MW). Several other wind farms are planned in that region, which makes interconnections between the wind farms feasible.

The Norwegian Valhall gas field will be connected via HVDC (78MW) [17], which also could be seen as a step towards the electrification of the North Sea. England has huge long term

plans for the Doggerbank, where several GW of wind farms are to be constructed there, but the projects are still in an early stage.

The most realistic option might be a modular system that comprises all available technologies and utilises their advantages. Within offshore fields, AC could be used to link wind parks and offshore loads together to a grid. The feasibility of DC collection grids has been studied in literature and might gain importance in the future [9].

These offshore AC grids could be connected to each other or to shore via VSC HVDC links in the near future. With increasing size of the offshore clusters, LCC technology might offer good solutions either as a regular LCC link or as a hybrid link. With an increasing number of separate offshore AC clusters, MTDC will gain importance. MTDC systems could be operated in parallel with regular point to point HVDC links.

The maximum power rating of the applied HVDC links is not only limited by the technical possibilities, but also by the primary reserves of the connected systems. While the primary control reserve of the UK national grid is about 1,5GW, HVDC links up to 10GW have been proposed in literature [3]. A failure of such an HVDC link would have unacceptable impact on the entire system and therefore the feasibility of such a link has to be questioned. Parallel HVDC connections could therefore be the only realistic option to connect several GW of offshore wind farms.

7 CONCLUSIONS

The North Sea Super Grid can probably not be built as a planned and optimised structure. Independently planned projects can be coupled together, leading to a rather grown grid, comprising several DC and AC voltage levels and maybe even different AC frequencies.

Due to a lack of operational experience with DC systems, AC will play a major role in the internal wind farm collection grids at medium voltage, as well as for high voltage wind farm cluster grids. Power frequency control might become a challenge for offshore AC grids, due to the absence of directly connected electrical machines, which add to the system inertia.

Long distance subsea transmission will be HVDC, where several technical options are possible. VSC technology will be the most promising option in the near future, but LCC technology is also interesting, because of its lower cost, lower loss, and higher transmission capability. Furthermore, some cutting edge technologies such as the hybrid HVDC, Multiterminal HVDC and parallel HVDC links will be interesting options for the development of the North Sea Super Grid, if certain technical challenges can be solved.

BIBLIOGRAPHY

[1] C.D. Barker, N.M. Kirby, N.M. Macleod, R.S. Whitehouse. “Renewable Generation: Connecting the generation to a HVDC Transmission Scheme”, CIGRE Canada Conference on Power Systems, Toronto October 4-6, (2009)

[2] N. Fichaux, J. Wilkes. “Oceans of Opportunity”, European Wind Energy Association, page 34, September (2009)

[3] F. Groeman, N. Moldovan, P. Vaessen. ”Ocean grids around Europe”, KEMA Briefing Paper, Novmber (2008)

[4] T. Haileselassie, M. Molinas, T. Undeland. “Multi-Terminal VSC-HVDC System for Integration of Offshore Wind Farms and Green Electrification of Platforms in the North Sea”, Nordic Workshop on Power and Industrial Electronics, June 9-11, (2008)

[5] R.L. Hendriks, G.C. Paap, W.L. Kling. ”Control of a multi-terminal VSC transmission scheme for connecting offshore wind farms”, European Wind Energy Conference (2007)

[6] F. VanHulle. “Integrating Wind”, TradeWind project report, (2009)

[7] T. Jonsson, P. Holmberg, T. Tulkiewicz. “Evaluation of Classical, CCC and TCSC Converter Schemes for Long Cable Projects”, EPE 09, Lausanne, Switzerland, (1999)

[8] P. Kundur. “Power System Stability and Control”, McGraw-Hill, (1994)

[9] L. Max. “Design and Control of a DC Collection Grid for a Wind Farm”, Doctoral thesis, Chalmers University, (2009)

[10] T. Nakajima, S. Irokawa. “A control System for HVDC Transmission by Voltage Source Converters”, IEEE Power Engineering Society Summer Meeting, pp. 1113-1119, (1999)

[11] W. Pan, Y. Chang, H. Chen. “Hybrid Multi-terminal HVDC System for Large Scale Wind Power”, PSCE Proceedings pp. 755-759, (2006)

[12] R.E. Torres-Olguin, M. Molinas, T.M. Undeland. ”A model-based controller in rotating reference frame for Hybrid HVDC”, ECCE, (2010)

[13] T. Trötscher, M. Korpås, J.O. Tande. “Optimal design of subsea grid for offshore wind farms and transnational power exchange”, Sintef Energy Research, (2009)

[14] T.K. Vrana. “Analysis and Definition of Technical Specifications of Dispersed Inverter-Based Energy Conversion Units in Distribution Grids“, RWTH-Aachen University, Diploma thesis, (2008).

[15] L. Xu, B.R. Andersen. “Grid Connection of Large Offshore Wind Farms Using HVDC”, Wind Energy. 9:371–382, (2006)

[16] Z. Zhao, M.R. Iravani. “Application of GTO voltage source inverter in a hybrid HVDC link”, IEEE Transactions on Power Delivery, 9(1):369–377, 1994.

[17] www.abb.com/hvdc accessed on July 5, (2010)

Simulation of the Impact of Larger Offshore Wind Farm on System Stability

H. Guo, K. Rudion

Otto-von-Guericke-University Magdeburg, Germany

ABSTRACT

Currently, most offshore wind farms are connected to the onshore grid by an HVAC transmission system. Compared with the HVDC technology, the HVAC has advantages in its lower investment costs and long term practical experience. However, there are several technical problems that still need to be solved. These problems are usually related to the high charging current, which may cause system overvoltage. This paper deals with the modeling and dynamic simulation of an HVAC grid-connected offshore wind farm, which was developed based on the Alpha Ventus offshore wind farm in Germany. The impact of the offshore wind farm on system voltage stability will be analyzed taking into consideration the grid code requirements.

KEYWORDS

Offshore wind farm, HVAC, voltage stability, dynamic simulation

1 INTRODUCTION

Offshore wind energy plays a crucial role in the development of wind power in Europe. At the end of 2009 the total installed offshore wind power in Europe was about 2 GW, and EWEA predicted that it will reach 40 GW by 2020 and 150 GW by 2030 [1]. In Germany the offshore wind power is expected to reach 20 GW by 2020 according to a prognosis [2]. The wind power capacity penetration in Europe was about 9.1% in February 2010. One of the major issues of offshore wind farms is how to integrate the large amount of wind energy into the onshore power system. The stability and security of the power system operation have to be ensured in spite of large wind power penetration. Currently there are two types of technologies available to connect the offshore wind farm to the power grid. One is high voltage direct current (HVDC) and the other high voltage alternating current (HVAC) technology. The HVAC transmission systems will continue to be the preferred choice as long as they are technically feasible for offshore wind farms due to their advantages such as lower investment costs, smaller required areas, and higher reliability as compared with the HVDC

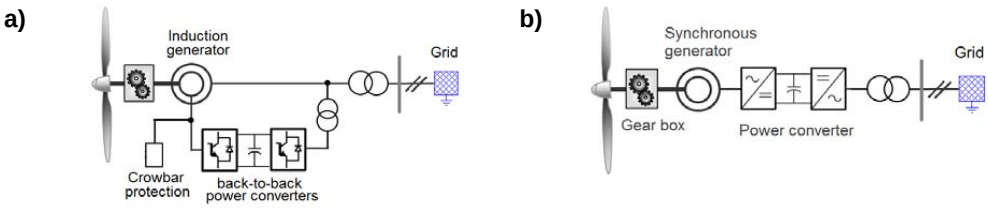

Figure 1: Wind turbine – DFIG and SG with power converter

transmission systems [3]. In this paper the impact of the wind park operation during grid faults on the voltage stability will be investigated by the means of numerical simulations. For this purpose an adequate model for offshore wind farm will be employed, which is based on the Alpha Ventus wind farm.

Generally, the stability of wind farms depends mainly on the wind turbine concept, the chosen interconnection system of the wind farm and the the strength and configuration of the power network to be connected. Furthermore, it can be classified as rotor angle stability, frequency stability and voltage stability, respectively [4]. For an offshore wind farm equipped with DFIG (Figure 1a) or a power converter connected Synchronous Generator (SG) (Figure 1b) the rotor angle stability is not critical because the power electronic converter decouple the frequency of wind farm and grid. The wind farm with DFIGs provides more controllability and is able to contribute to frequency stability by using proper control strategy. Voltage stability is the most critical factor among the stability issues, in fact most of the TSOs in Europe specify the requirement of Low Voltage Ride Through (LVRT) capability [5]. This means that large wind farms have to remain connected to the grid during voltage dips for a specified duration in order to support the voltage recovery. In this study the voltage stability will be taken as the focus.

2 MODELING OF AN OFFSHORE WIND FARM

2.1 System modelling and description

The model of the offshore wind farm and its periphery is implemented in the simulation tool PSS®NETOMAC. Figure 2 shows the one-line diagram of the wind farm and its connection to the grid. It consists of 12 dynamic DFIG-type models, wind turbine transformers, an HVAC cable (70 km), shunt reactors “Comp.1” and “Comp.2”, local loads “Load 1” and “Load 2”, etc. “T1” (30/110 kV) is the offshore transformer; “T2” (110/220 kV) is the transformer on land, its high-voltage side is connected to the PCC (Point of Common Coupling). The HVAC submarine cable is completely compensated with two shunt reactor banks at both ends, each has 35 Mvar. The power is transferred by transformer “T2” through the transmission line

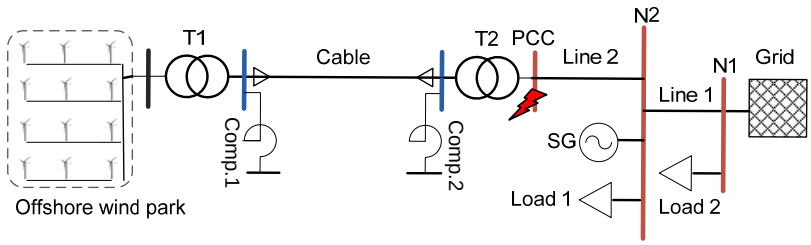

Figure 2: Brief one-line diagram of the offshore wind farm

"Line2" to node "N2" where there is a local "Load 1" and generation "SG". The node "N2" will be connected to node "N1" through "Line 1" to the grid.

2.2 Control of the wind turbine generator

In the wind farm model the voltage control and rotor speed control are applied to the wind turbine generators. The terminal voltage of a DFIG can be controlled by varying its reactive power output of the converter. Figure 3 shows the voltage control schema of the DFIG in PSS®NETOMAC. To prevent the over-voltage and over-current in the rotor side of the DFIG during fault condition, an active crowbar protection has been modelled. This makes it possible for the DFIG to provide the grid with reactive power to support the voltage recovery during a fault in the grid.

3 STUDY CASE AND SIMULATION

In order to observe the transient voltage stability of the wind farm under fault conditions, a three-phase fault is assumed to take place at the PCC (Figure 2) with critical clear time for 150 ms. In this case the LVRT capability is investigated. Fig. 4 shows the simulation results. During the disturbance the voltage at PCC drops severely from 1 p.u. to 0. The reactive power output from wind farm increases rapidly to support the voltage (Figure 4d). A fast

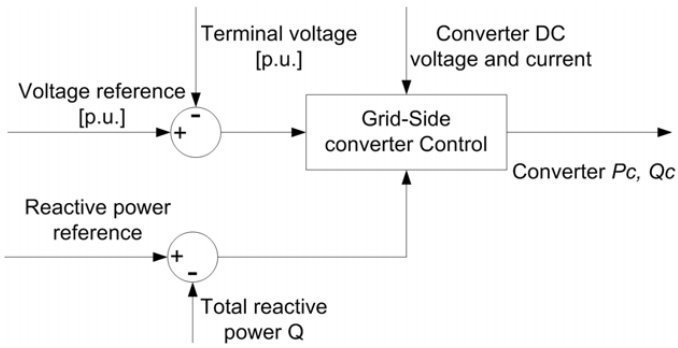

Figure 3: Voltage controller of the DFIG Model

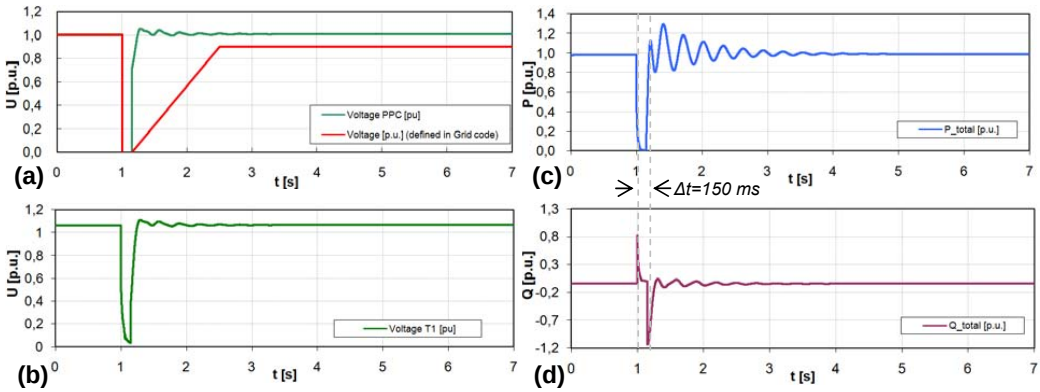

Figure 4: System response of three-phase fault at PCC

voltage recovery can be seen in Figure 4a, where the red curve shows the LVRT capability defined in the German grid code [6]. As can been seen the voltage performance fulfils the requirement on LVRT. After a dynamic oscillation (about 3 s) the power output becomes stable.

4 CONCLUSION

In this study the impact of an offshore wind farms with DFIG on voltage stability is analyzed. The investigation of these issues is especially important since offshore wind farms are interconnected by long HVAC cables that can significantly influence the behaviour of the system regarding its stability. Thus, the adequate control strategies are necessary that can adapt to the current operating situation and support the system voltage stability, e.g. by applying reactive power and voltage control.

BIBLIOGRAPHY

[1] Information from www.ewea.org.

[2] "Planning of the Grid Integration of Wind Energy in Germany Onshore and Offshore up to the Year 2020", Consortium DEWI/E.ON Netz/EWI/ REW Transport Grid, Electricity /VE Transmission, Summary, 2005.

[3] H. Brakelmann, "Efficiency of the HVAC Power Transmission from Offshore-Windmills to the Grid", 2003 IEEE Bologna Power Tech Conference, Italy.

[4] Kundur P. "Power System Stability and Control", New York: McGraw-Hill, Inc, 1993.

[5] Project Report, "REALISEGRID", REseArch, methodoLogies and technologieS for the effective development of pan-European key GRID infrastructures to support the achievement of a reliable, competitive and sustainable electricity supply, 2008.

[6] TransmissionCode 2007 – Network and System Rules of the German Transmission System Operators, August 2007.

European Academy of Wind Energy

Norwegian University of Science and Technology

Dynamic Modelling of Wind Turbine and Power System for Fault Ride-through Analysis

Fan Zhang[1)], W.E. Leithead[1)], Olimpo Anaya-Lara[1, 2)]

[1)] Department of Electronic and Electrical Engineering, University of Strathclyde, Glasgow, UK

[2)] DNV Visiting Professor, Faculty of Engineering Science and Technology, NTNU, Norway

ABSTRACT

This paper presents a Simulink model of a wind power system for the holistic analysis of wind turbine and power grid during grid faults, aiming to investigate wind turbine Fault Ride-Through performance. The model comprises a highly detailed dynamic model of a 2MW wind turbine and a generic electrical network model. The simulation result shows the behaviour of both wind turbine and power grid when grid faults occurs. The impact that a grid fault has on wind turbine components and grid transients is illustrated and discussed.

KEYWORDS

Wind turbine, DFIG, Fault Ride-Through

1 INTRODUCTION

As one of the most promising renewable energy, wind power is growing rapidly around the world. Grid Codes have been revised to cope with the high penetration level of wind power. The integration of large-scale wind turbines into power system needs to be investigated to meet the new requirements raised by power system operators. The challenge for wind power integration is focused on wind turbine Fault Ride-Through and grid support capability.

The objective of this paper is to present a detailed wind power system that allows analysing the wind turbine and power network in an integral way. The wind turbine model consists of the dynamic model and the control system of a 2 MW wind turbine. A doubly-fed induction generator model is attached to the wind turbine model because of its popularity in the wind energy industry. A generic power system model including a main system generator and a conventional power plant equipped with synchronous generator is developed to represent the electrical network dynamics.

This paper is organised as follows. First, the wind turbine model is briefly described. Then, the model of the DFIG using decoupled current-mode control is explained, followed by the

description of the power system model. Simulations are carried out with grid faults applied and results are presented.

2 WIND TURBINE AND ITS CONTROL SYSTEM MODEL

2.1 Dynamic models

The dynamic model of a wind turbine consists of the aerodynamics and drive-train dynamics. When the wind turbine is running, the wind produces an aerodynamic torque on the rotor. The torque is

$$F_1 = \frac{1}{2} \cdot \frac{\rho \pi C_p(\lambda, \beta) R^2 v^2}{\lambda}$$

where the tip-speed ratio is $\lambda = \frac{R\Omega}{v}$, R is the rotor radius, Ω is the rotor speed, v is the effective wind speed, ρ is the air density, β is the pitch angle and Cp is the aerodynamic power coefficient. This implies the wind turbine can be controlled by regulating the rotor speed or adjusting the pitch angle.

The wind turbine drive-train is composed by rotor hub, low-speed shaft, gearbox, high-speed shaft and generator rotor. To study the interaction between the wind turbine and the power grid, the behaviour of the drive-train needs to be investigated as it is connected directly to the generator and affected by the power fluctuation in the grid. It should be noted that the drive-train of wind turbine is lightly damped therefore it is very sensitive to torque variations caused by grid faults. A two-mass drive-train model is used as a simpler model does not provide clear transients for wind turbine fault ride-through studies.

2.2 Wind turbine control system

The wind turbine is controlled by defining the relationship between the rotor speed of the wind turbine and the wind speed. The generator reaction torque is adopted to regulate the rotor speed in below-rated wind speed, while the blade pitch angle is varied to control the rotor speed in above-rated wind speed. Different controllers are used under different wind speeds. A controller switching method is implemented to guarantee the smooth switching between different control modes.

3 DFIG SYSTEM MODEL

A DFIG is basically a wound rotor induction generator coupled with the grid through power electronics. The DFIG controller developed in [3] is adopted. The generator torque and reactive power generation are controlled by d and q axis rotor currents respectively.

4 GENERIC NETWORK MODEL

The generic network model presented in [2] is used to represent the dynamics of the power system. The layout of the system is shown in Figure 1

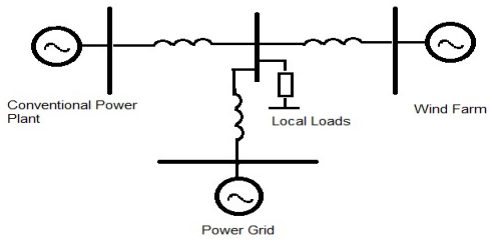

Figure 1: Generic network

The wind farm is represented by a DFIG wind turbine. The conventional power plant uses a synchronous generator with PSS and AVR installed. The power grid is modelled by a synchronous generator and a load. The generator represents the total generation on the grid and the load represents the aggregated loads in the power system. Grid faults are set at both the wind farm side and the power network side to test the fault response of the system.

5 SIMULATION RESULTS

A 3-phase symmetrical fault is applied near the wind farm. Figure 2 illustrates the generator torque during and after the fault. Due to the voltage drop in the grid, the DFIG loses magnetisation. Thus, the output torque drops significantly during grid fault.

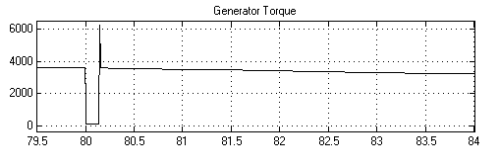

Figure 2: Generator torque

The generator speed keeps increasing during the fault because of the torque imbalance on the drive-train as shown in Figure 3. From the simulation result we can see the drive-train is very lightly damped.

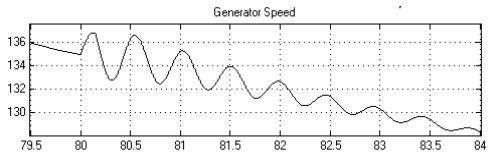

Figure 3: Generator speed

The torque drop is transferred through the drive-train and affects the wind turbine hub torque as shown in Figure 4. The hub torque oscillation increases wind turbine loads and therefore reduces turbine lifetime.

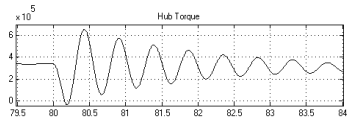

Figure 4: Hub torque

The grid voltage is illustrated in Figure 5. The DFIG output current rises during the grid fault trying to maintain the generator torque. The over current causes grid voltage sag.

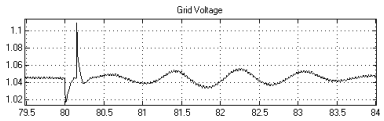

Figure 5: Grid Voltage

6 CONCLUSIONS

This paper used a detailed model of a wind turbine and power network to study dynamic interactions in a holistic manner highlighting the need for combined controllers. The model is developed for further research on improving wind turbine Fault Ride-Through and grid support ability. The modelling of wind turbine, conventional generator and power grid were briefly presented. Simulation results show the dynamic response of the system when a grid fault occurs. The advantage of this model is that the dynamics of both the mechanical system and the electrical system are modelled in detail, which allows accurate investigation on the interaction between them. How the electrical system disturbance affects the operation of wind turbine is clearly shown in the simulation results. In conclusion, both the wind turbine and power system dynamics are accurately modelled.

BIBLIOGRAPHY

[1] W.E. Leithead and M.C.M. Rogers Drive-train Characteristics of Constant Speed HAWT's: Part I, II, Wind Engineering, Volume 20, No. 3, 1996.

[2] Olimpo Anaya-Lara, F. Michael Hughes, Nicholas Jenkins, Goran Strbac, Rotor Flux Magnitude and Angle Control Strategy for Doubly Fed Induction Generators, Wind energy. 2006; 9:479-495.

[3] L. Holdsworth, X.G. Wu, J.B. Ekanayake and N. Jenkins, Comparison of fixed speed and doubly-fed induction wind turbines during power system disturbances, IEE Proc-Generation, Transmission and Distribution, Vol. 150, No.3, May 2003.

European Academy of Wind Energy

Norwegian University of Science and Technology

Large Scale energy storage for a 100% renewable electricity system in Germany

Amany von Oehsen[1)], Carsten Pape[1)], Yves-Marie Saint-Drenan[1)], Norman Gerhardt[1)], Mareike Jentsch[1)], Michael Sterner[1)]

[1)] Fraunhofer Institute for Wind Energy and Energy Systems Technology, Kassel, Germany

ABSTRACT

This paper presents results of a study commissioned by the German Federal Environment Agency on possible ways to realise a 100% renewable electricity supply of Germany by 2050 [1]. In the scenario presented here, 94% of the electricity demand are met by national renewable energy sources, about two thirds being provided by wind energy and about 19% by PV. Heat demand is covered mainly by electric heat pumps with the option of demand side management. Half of the energy demand for road transport is supplied by electricity (for electric and hybrid-electric vehicles) with the possibility of load management. Large momentary deviations between supply and demand remain and the available pump hydro storage power plants in Germany are not sufficient to balance supply and demand. About 43 TWh_e of storage capacity and considerable storage power is needed. This could be supplied by underground storage of hydrogen or so-called “renewable power methane” in northern Germany.

KEYWORDS

100% renewable energy supply of Germany, load management, long-term storage, renewable power methane.

1 INTRODUCTION

With its study “100% renewable electricity supply by 2050” the German Federal Environment Agency (UBA) has presented a way how Germany could reduce its greenhouse gas emissions by 80 to 90% until 2050. Currently accounting for 40% of Germany’s greenhouse gas emissions, the decarbonisation of the electricity sector is crucial for reaching this goal. Through introduction of electric heat pumps in the heat sector and electric vehicles in the transport sector renewable electricity can also help to lower emissions in these sectors. UBA investigates several scenarios how to decarbonise the German electricity sector by renewable energies, for the scenario presented here 94% of the electricity demand are met

by national renewable energy sources. UBA comssioned the Fraunhofer Institute for Wind Energy and Energy Systems Technology to perform a simulation with hourly time-resolution of the renewable energy feed-in, the electricity demand and storage power dispatch to test the feasibility of supply-demand matching and supply-security. Data of four meteorological years (2006-2009) was used to simulate renewable energy feed-in to account for meteorological variations among years.

2 RENEWABLE ENERGY FEED-IN, ELECTRICITY DEMAND AND NEED FOR ENERGY STORAGE

2.1 Renewable energy production

In a first step the available technical potentials of renewable energies in Germany in-line with sustainability criteria are analysed. As Table 1 shows, they are sufficient to provide the scenario electricity demand of 506 TWh. However, in the scenario 5% of the electricity demand are met by imports. Based on assumed regional distributions of the installed capacities (as given in Table 1), meteorological data of spatial resolution 14 x 14 km^2, and hydrological data, renewable energy feed-in time series are simulated.

Table 1: Estimated sustainable national renewable potentials, installed capacities and power production

	Conservatively estimated sustainable technical potential (GW)	Installed power (GW)	Delivered energy (TWh)
Onshore wind	60	60	170
Offshore wind	45	45	177
PV	275	120	104
Geothermal energy	6,4	6,4	50
Hydro	5,2	5,2	22
Biomass	[1]	23,3	11

2.2 Momentary electricity excesses and deficits: required storage capacity and power

The time series of the hourly electricity demand is generated by scaling-down the German electricity demand of the years 2006-2009 (as published by ENTSO-E) to the assumed “base” electricity demand of the year 2050. Then the time series of electricity demand for

[1] Most of the biomass energy is used in road transport sector and not quoted in terms of installed power here

heat pumps and electric cars are added. For both, load management is simulated: heat pump systems are equipped with a hot water thermal storage tank and for electric cars the charging of batteries may be shifted during the day or within several days depending on individual driver habits. 50% of the assumed pump-hydro storage power of 8.6 GW in 2050 and 30% of their storage capacity is used for further balancing supply and demand. Because of the large share of wind and PV energy, the deviations of renewable energy supply from the demand cannot be balanced by pump-hydro storage and load-management alone. Figure 1 shows the time series of production minus load for the meteorological year 2009, deficits are depicted in red, surplusses in blue. Surplusses add up to about 78.5 TWh, deficits to 82.6 TWh. A maximum of 26 TWh of electricity imports with a maximum power of about 10 GW is allowed as well as the use of 20 GW biogas plant power. After dispatching them, the residual needed storage capactity is 43 TWh_e , the needed storage "turbine" power is on the order of 30 - 33 GW. So in total, a positive balancing power of nearly 64 GW is needed (including pump hydro storage power).

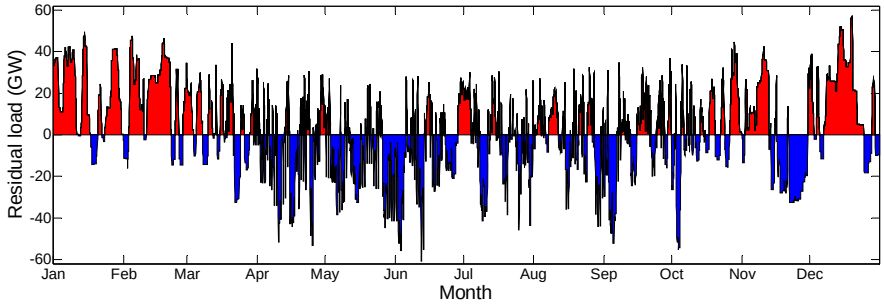

Figure 1: Balance of electrcity demand and supply for the meteorological year 2009 [1]

3 LARGE-SCALE STORAGE POTENTIALS IN GERMANY

3.1 Storage capacity for hydrogen or renewable power methane in Germany

Hydrogen has long been discussed as a candidate for large scale power storage in renewable energy systems: renewable electricity is used for electrolysis of water in times of electricity surplus to produce hydrogen. Hydrogen can be converted back to electricity in times of electricity shortage by fuel cells or by combustion in combined cycle or simple gas turbine plants. In this study, alcaline electrolysis and combustion in combined-cycle power plants with an overall round-trip efficiency of 42% are simulated. Recently, it has been suggested to convert hydrogen and carbon dioxide to methane as a storage medium [2]. The required carbon dioxide can be taken from biomass or the atmosphere to make the burning of this so-called "renewable power-methane" CO_2 - neutral. The assumed average round-trip

efficiency for methane production and conversion back to electricity in combined cycle power plants is 35%. Methane has the advantage that the existing natural gas infractructure can be used, whereas for hydrogen a lot of new infrastructure would have to be built.

Table 2 gives the "net usable" storage capacity potential in salt caverns and pore-space storages in Germany and the storage volume required for balancing in the simulated scenario (a large fraction of the gross available volume is needed for "cushion gas" which is needed to prevent that pressures drop below the minimum working pressure, but which cannot be used for power production). The potential is sufficient and leaves a reserve margin, which may be needed for storing natural gas for other uses. Necessary electrolyser power in this scenario amounts to 44 GW. This way 90% of the energy surplusses can be used.

Table 2: Storage potential for underground hydrogen and methane storage and required volumes

	Estimated sustainable potential of net usable storage capacity (at standard conditions)	Required storage volume
Hydrogen	37×10^9 m^3 = 110 TWh$_{th}$[2]	28×10^9 m^3
Methane	$51{,}4 \times 10^9$ m^3 = 514 TWh$_{th}$[1]	$7{,}5 \times 10^9$ m^3

4 CONCLUSIONS

A 100% electricity supply of Germany based on national renewable energy is possible from the point of view of available renewable energy potential and large-scale power storage potential within Germany. Hydrogen or renewable power meathne can serve as chemical storage medium. This study did not analyse the necessary enhancement of the electricity grid, an aspect which needs to be studied further. A 100% renewable electricty supply with a high degree of international cooperation (see for example [3], [4]) is likely to be more cost-effective than a purely national supply because advantage of low production or storage costs in countries with good resources could be taken (e.g. import of solar energy from North-Africa or import of storage hydro power from Scandinavia and export of wind energy to Scandinavia to balcance out wind power fluctuations). Furthermore, meteorological smoothing effects which occur when areas are larger than single weather systems can be

[2] at the necessary working pressure of 60 -180 bar

exploited to lower the required storage capacity and power which mostly will also lead to a reduction of overall costs.

BIBLIOGRAPHY

[1] German Environmental Agency 2010: “100% renewable electricity by 2050 , downloadable at http://www.uba.de/uba-info-medien-e/3997.html “

[2] Sterner, M. 2009: “Bioenergy and renewable power methane in integrated 100% renewable energy systems“, Renewable Energies and Energy Efficiency, Vol. 14, Kassel University Press, Kassel.

[3] Czisch,G. 2005: “Kostenoptimierten Variationen zur Stromversorgung Europas und seiner Nachbarn mit erneuerbaren Energien”, Dissertation, Kassel

[4] SRU 2010: „100% Erneuerbare Stromversorgung bis 2050: Klimaverträglich, sicher, bezahlbar at http://www.umweltrat.de/SharedDocs/Downloads/DE/04_Stellungnahmen/2010_05_Stellung_15_erneuerbareStromversorgung.html

Part 9

Session 6A - Wind Field Measurements and Simulations II

- The 2D lid-driven cavity - Validation of CFD code to model non-Neutral Atmospheric Boundary Layer Conditions
  Tilman W. Koblitz, Risø DTU
- Forest Winds in Complex Terrain
  Ilda Albuquerque, GL Garrad Hassan
- Physical and Numerical Modelling of Flow over a Real Complex Terrain
  Domingo Muñoz-Esparza and Boris Conan, von Karman Institute for Fluid Dynamics
- Modelling of atmospheric boundary layer: Generation of shear profile in wind tunnel
  Tee Seong Yeow, Universidad Politécnica de Madrid

European Academy of Wind Energy

Norwegian University of Science and Technology

The 2D lid-driven cavity – Validation of CFD code to model non-Neutral Atmospheric Boundary Layer Conditions

T. W. Koblitz[1], A. Bechmann[1], N. N. Sørensen[1]

[1)] Wind Energy Dep., Risø National Laboratory, DTU, DK-4000 Roskilde, Denmark

ABSTRACT

In order to improve existing models for wind resource assessment on complex terrain, the effect of thermal stratification in the atmospheric boundary layer (ABL) should be included in the Reynolds Averaged Navier-Stokes (RANS) methodology.

The existing in-house CFD code (Risø DTU) EllipSys3D provides the starting point for the present work. Under neutral conditions the code has been validated against large scale field experiments [2]. In the present study 2D simulations including the effect of thermal stability are conducted and validated against previous benchmark simulations of a differentially heated lid-driven square cavity (LDC).

KEYWORDS

CFD, Lid-driven square cavity, Mixed convection, RANS, Temperature gradient

1 INTRODUCTION

The diurnal cycle of heating and cooling of the ground surface strongly influences the wind conditions in the earth atmosphere. Wind industry is increasingly relying on CFD and the RANS approach but temperature stratification is mostly ignored in state-of-the-art CFD models for wind resource assessment. For predicting these geophysical transport phenomena it is essential to understand the effect of buoyancy on the shear flow in the ABL. The differentially heated LDC is an excellent candidate to gain insight into the involved fluid mechanical phenomena and to validate our incompressible flow solver. This standard CFD test case is dynamically very complex and displays almost all fluid mechanical phenomena. It has been studied extensively and a vast amount of benchmark literature is available. The simple geometry shown in fig. 1 with its regular boundary conditions provides an appealing setting to study the combined forced and natural convection (mixed convection). The forced convection is induced by a shear force from the motion of the upper lid, whereas natural convection is induced by the differentially heated horizontal walls. Except for the lid, all walls are stationary (no-slip tangential and zero normal velocity boundary condition) and the vertical walls are adiabatic. Three cases are considered: 1) horizontal walls at same temperature (neutral case a) 2) top wall heated, bottom wall cooled (gravitationally stable

tiko@risoe.dtu.dk

case b) 3) top wall cooled, bottom wall heated (gravitationally unstable case c). The steady, laminar, 2D numerical simulations are performed for the following non-dimensional governing parameters: Reynolds number: $316 < Re < 5000$, Grashof number: $Gr = 10^6$, Prandtl number $Pr = 0.71$ representative of air, Richardson number $0.1 < Ri < 10$. The governing incompressible Navier-Stokes equations (Boussinesq approximation employed) are solved numerically using the finite-volume code Ellipsys2D [9-11].

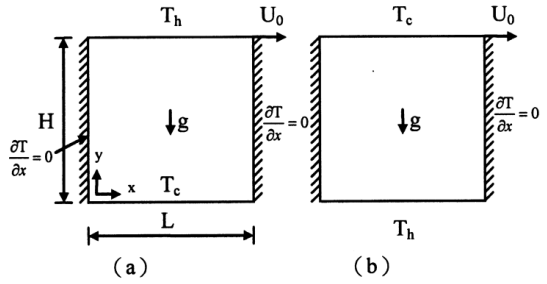

Figure 1: Physical domain and boundary conditions for cases (a) stable and (b) unstable [5]

2 RESULTS

The code was tested and validated by means of grid sensitivity and convergence studies. Therefore a mesh resolution of 128x128 was found to be sufficient for the present problem, and a convergence criterion of $\left|\phi^{k} - \phi^{k-1}\right| < 10^{-5}$ was used for all variables. Hence, iterations were terminated when the maximum between two successive iterations was smaller than 10^{-5}. The streamlines and isothermal lines of the conducted simulations are visualized and qualitatively compared against the results from [1,5,7,8] in fig. 2. For reasons of brevity only $Re = 1000$ is presented. As the Ellipsys code employs the primitive variable formulation (velocity and pressure) to describe the flow, the streamfunction Ψ was generated from the axial velocity components by integrating over the physical domain in order to compare our results with earlier studies that used the vorticity-streamfunction formulation.

$$u = \frac{\delta\Psi}{\delta y}, v = -\frac{\delta\Psi}{\delta x} \tag{1}$$

The top left plot shows the steady state streamlines of case (a). The driven-lid generates a primary vortex that dominates the entire cavity, with small secondary eddies in the lower corners. Table 1 presents the quantitative comparison of the primary vortex for the neutral case. For case (b), shown in the second column of fig. 2, the stable temperature gradient limits the main motion of the fluid to the upper region, resulting in an almost stagnant bottom region with vertically-linear isotherms (middle plot). The unstable case (c) promotes natural convection in the lower half of the cavity while the upper part is dominated by forced convection. The interaction of both results in the formation of two counter-recirculating eddies

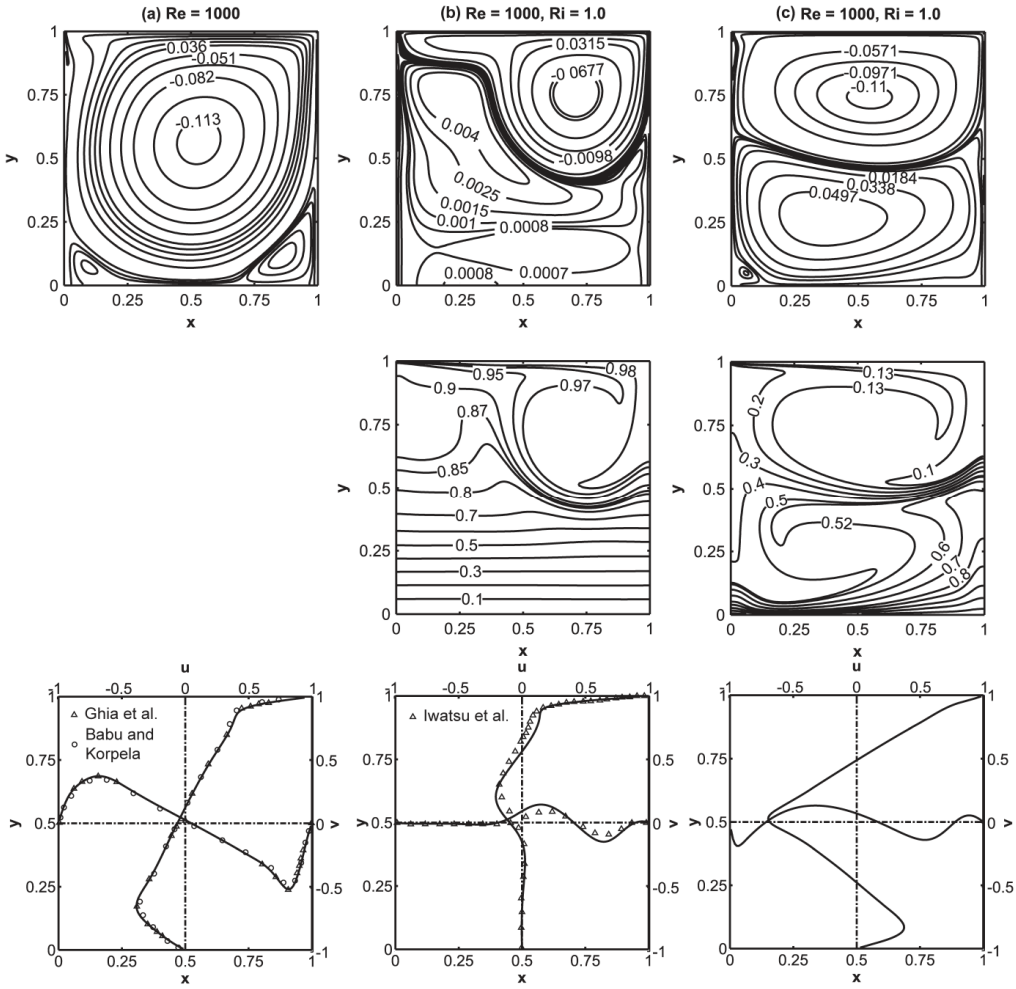

Figure 2: Visualization of streamlines (top), isothermal lines (middle) and mid-plane velocity profiles (bottom) for cases (a) neutral, (b) stable and (c) unstable

Table 1: Comparison of primary vortex to benchmark simulations (neutral case): streamfunction Ψ, vorticity Ω, location X, Y and error $\Delta[\%]$

Re	Reference	Grid	Ψ	Δ	Ω	Δ	X	Δ	Y	Δ
1000	Erturk and Gökçöl [6]	601 x 601	0.118938	1.70	2.067760	0.23	0.53000	0.48	0.56500	0.29
	Ghia et al. [7]	128 x 128	0.117929	0.86	2.049680	0.65	0.53130	0.72	0.56250	0.74
	Zhang [12]	128 x 128	0.118806	1.59	2.066777	0.18	0.53125	0.72	0.56250	0.74
	Botella and Peyret [3]	128 x 128	0.118937	1.70	2.067750	0.23	0.53080	0.63	0.56520	0.26
	Bruneau and Saad [4]	128 x 128	0.117860	0.80	2.050800	0.60	0.53125	0.72	0.56250	0.74
	Bruneau and Saad [4]	1024 x 1024	0.118920	1.69	2.067400	0.21	0.53125	0.72	0.56543	0.22
	Cheng and Liu [5]	128 x 128	0.116874	0.03	2.064753	0.08	0.53125	0.72	0.56250	0.74
	Present	**128 x 128**	**0.116912**		**2.063036**		**0.527450**		**0.566660**	
3200	Ghia et al. [7]	128 x 128	0.120377	2.03	1.988600	3.30	0.51650	0.60	0.5469	0.69
	Zhang [12]	128 x 128	0.120157	1.86	1.948934	1.33	0.515625	0.77	0.539063	0.76
	Cheng and Liu [5]	128 x 128	0.119845	1.60	1.947966	1.28	0.515625	0.77	0.539063	0.76
	Present	**128 x 128**	**0.117928**		**1.922957**		**0.519607**		**0.543135**	
5000	Erturk and Gökçöl [6]	601 x 601	0.122216	3.99	1.940547	2.81	0.51500	0.63	0.53500	0.05
	Ghia et al. [7]	256 x 256	0.118966	1.37	1.860160	1.39	0.51170	0.01	0.53520	0.02
	Zhang [14]	128 x 128	0.118121	0.66	1.906214	1.06	0.515625	0.75	0.539063	0.70
	Bruneau and Saad [4]	256 x 256	0.120640	2.74	1.912500	1.38	0.51562	0.75	0.53516	0.02
	Bruneau and Saad [4]	2048 x 2048	0.121970	3.80	1.932700	2.41	0.51465	0.56	0.53516	0.02
	Cheng and Liu [5]	128 x 128	0.118224	0.75	1.909011	1.20	0.515625	0.75	0.539063	0.70
	Present	**128 x 128**	**0.117338**		**1.886077**		**0.511764**		**0.535292**	

having a large temperature gradient between them.

3 CONCLUSIONS

The modified finite-volume code Ellipsys2D that now accounts for thermal stratification has been validated by solving the incompressible Navier–Stokes equations of the coupled convective heat transfer problem in a differentially heated LDC for three different cases. Qualitative comparisons of the flow patterns with earlier studies show good agreement, while quantitative comparison shows better than 96 % agreement for the strength and position of the primary vortex of case (a). This positive agreement shows that the solver is adequate to solve the mixed convection problem like the one presented. As a next step we are currently working on validating the code for 2D atmospheric flows over flat terrain including a modified k-ε turbulence model that accounts for buoyancy effects. The long-term goal of the ongoing work is to use the code to simulate atmospheric flow over complex terrain including the diurnal effect of thermal stratification and to compare it against large scale field experiments.

BIBLIOGRAPHY

[1] Babu V, Korpela SA. On the direct solution of Poisson's equation on a non-uniform grid, *J Comput Phys* 1993;104:93-8.

[2] Bechmann A, Presentations from "The Bolund experiment: Workshop" 3-4th December 2009. Technical Report Risø-R-1745(EN), Risø National Lab., Roskilde, Denmark, 2010.

[3] Botella O, Peyret R. Benchmark spectral results on the lid-driven cavity flow. *Comput Fluids* 1998;27:421–33.

[4] Bruneau CH, Saad M. The 2D lid-driven cavity problem revisited. *Comput Fluids* 2005;35:326–48.

[5] Cheng TS, Liu WH. Effect of temperature gradient orientation on the characteristics of mixed convection flow in a lid-driven square cavity. *Comput Fluids* 2010;39-6: 965-78.

[6] Erturk E, Gökçöl C. Fourth-order compact formulation of Navier–Stokes equations and driven cavity flow at high Reynolds numbers. *Int J Numer Methods Fluids* 2006;50:421–36.

[7] Ghia U, Ghia KN, Shin CT. High-resolutions for incompressible Navier–Stokes equation and a multigrid method. *J Comput Phys* 1982;48:387–411.

[8] Iwatsu R, Hyun JM. Three-dimensional driven-cavity flows with a vertical temperature gradient. *Int J Heat Mass Transfer* 1995;38:3319–28.

[9] Michelsen JA. Basis3d—a platform for development of multiblock PDE solvers. Technical report AFM 92-05, Technical University of Denmark, 1992.

[10] Sørensen NN. General purpose flow solver applied to flow over hills. Technical Report Risø-R-827(EN), Risø National Lab., Roskilde, Denmark, 1995.

[11] Michelsen JA. Block structured multigrid solution of 2D and 3D elliptic PDE solvers. Technical report AFM 94-06, Technical University of Denmark, 1994.

[12] Zhang J. Numerical simulation of 2D square driven cavity using fourth-order compact finite difference schemes. *Comput Math Appl* 2003;45:43–52.

Forest Winds in Complex Terrain

Ilda Albuquerque [1)]

[1)] GL Garrad Hassan – CREST, UK

ABSTRACT

Presently wind conditions assessment in complex topography is a major challenge for the wind energy industry. Nevertheless current used techniques were originally developed for mildly complex terrain under neutral atmospheric conditions; which have lack of reliability in areas of complex terrain, including complex orography, forests, or a combination of both.

The PhD thesis is expected to develop an improved CFD modelling for "Forest winds in complex terrain", using a commercial CFD platform - ANSYS CFX. Due to the project's early stage main topics and foreseen work are presented in this paper.

KEYWORDS

WIND, COMPLEX TERRAIN, FOREST, CFD

1 INTRODUCTION

The PhD Thesis is inserted in the European WAUDIT (Wind Resource Assessment Audit and Standardization) project, an ITN (Initial Training Network), funded under the EU FP7-PEOPLE program. WAUDIT aims the development of state-of-the-art wind resource assessment methodologies with added value to the Wind Energy Industry. This project, inserted in the Work Package 2, aims to develop a numerical model, using a commercial CFD (Computational fluid dynamics) platform, of wind flow over forested complex terrain.

There is a shortage of ideal sites for wind farms, which will be flat and with low vegetation ones. [3] This situation leads to the increasing consideration of sites that present both complex topographic features and forest, is then a priority to this field to enhance the understanding and accurate prediction of the wind flow in such conditions.

2 SECTION A: FORESTED COMPLEX TERRAIN

2.1 Subsection A1: Forest Complex Terrain Physical Description

Wind flow over forested hills is characterized by large scale horizontal pressure gradient due to topography [4], which induces a distortion of the mean flow and generates specific turbulent eddies. Streamlines are distorted by the presence of the hill and the separated region on the lower lee side of the hill is verified [14]. Streamlines enter the canopy on the upwind slope as the vertical pressure gradient is negative in that area, and go out from the

canopy just behind the summit. In [4] the author sums up as the main observations: an acceleration of the wind flow within and above the canopy, with a quasi-disappearance of the inflexion point in the streamwise wind profile at the canopy top and enhancement of turbulent kinetic energy and momentum flux in the canopy, indicating that turbulent structures penetrate deeper within the canopy. The author also acknowledged the presence of a wake region behind the hill where wind velocity is reduced and it is capped by an elevated shear layer. In [1] it was observed: strong intermittent reversal of flow with length scales imposed by a combination of outer layer eddy scale and hill scale pressure perturbations; influence of drag within the canopy where speeds were significantly reduced by canopy drag; strong spatial variation in streamwise component of the flow in the canopy scale turbulence created by the interaction between the canopy and the free moving flow just above the canopy.

2.2 Subsection A2: Forest Complex Terrain Numerical Models

According to [1] with increased computational power, models used in forested complex terrain have moved from being linear to nonlinear and the treatment of surface boundary conditions have moved from simple roughness length parameterisations to distributed drag formulations in which momentum is absorbed through a finite depth at the lower surface. Nevertheless a number of challenges persist in modelling scales of turbulent motion that are near those of the main topographic features.

In the case of canopy representation [1] stated that a canopy typical description is the one where it is assumed that momentum is absorbed through an infinitely thin layer at a height of z_0 or z_0 + d, maintaining the logarithmic profile. The author alerts, that the real profile in and above a canopy shows a strong departure from the logarithmic profile and suggests a distributed drag parameterization in modelled vegetative canopy flows. An alternative is the implicitly inclusion of the canopy length, via a dissipation equation incorporating canopy drag. In [4] the author refers that most numerical airflow models of forested hills, using a drag-force approach for the canopy, with a first order turbulence scheme, are able to simulate satisfactorily the mean flow field but the turbulence and momentum fluxes are overestimated on the lee of the hill. The same happens with models using roughness-length approach. There were also some simulations using 3D virtual canopy geometries.

The main approaches in CFD currently in use within wind field predictions are RANS (Reynolds-averaged Navier-Stokes) and LES (Large eddy simulations). [6] Alerts that the flow over trees can be seen as made up of large vortex structures that depend on the pattern, size, and type of trees. The large size and relatively low time scale of them, like strong intermittent interaction with the flow above may exclude the use of gradient diffusion

models, steady state and Reynolds averaged formulation of the fluid flow equations. In the same way [1] suggest that eddies formed in the lee of the hill have time and length scales much larger than those represented in a Reynolds average model, and they can affect the mean flow further downstream. Large eddy simulations of flows over hills with and without forest canopies showed a strong coupling between intermittently separated flows in the lee of a hill with perturbations in the outer-layer flow [1], [6]. This reaffirms difficulties in modelling the effects of these motions in Reynolds averaged Navier–Stokes (RANS) models, in which there are no mechanism for representing this type of connection between the inner and outer layers of the flow. A recent comprehensive study of flows in forested complex terrain was presented by [1]. In this study the flow was modelled using a nested LES on an isolated two dimensional hill, in a neutrally stratified atmosphere. It reproduced accurately the main forest features, confirming the intermittency of recirculation region behind the hill and the domination of sweep motions in momentum transfer at the canopy top along the hill. The streamwise wind velocity upwind from the summit was shown not to be correlated with the flow within the wake region, only with the flow above it. In the other hand at the wake region the streamwise wind velocity at the canopy top was only correlated with the flow within the wake region. The author referred that this result suggests that turbulence within the wake region results from a superposition of various turbulent structures: large turbulent structures induced by elevated shear layer that may result from the rolling over of Kelvin-Helmholtz instabilities, structures induced at the lee side foot of the hill by an adverse pressure gradient and structures induced by the canopy presence. [5] Used LES to investigate spatial perturbations of the first and second moments of the velocity and pressure fields over a train of gentle hills covered by either sparse or dense vegetation. Increase in the canopy density was able to provoke recirculation inside the canopy on the lee side of the hill. In the latter case zones of intense shear stress originated near the canopy atmosphere interface persisted all the way up to the middle layer contaminating much of the middle and outer layers with shear stress gradients. For the upper canopy layers, wake predictions increased with increasing leaf area density. The simulation confirms that the minimum mean pressure shifts downstream from the hill crest. Also [1] in his LES simulations of a single hill, showed signs of a intermittent mean separation in the lee, parcels accelerating toward a pressure minimum at the hill crest as they move up the windward side of the hill. The parcels then enter in the adverse pressure gradient area on the lee side of the hill, in this area they decelerate and may reverse direction. Parcels of flow over a roughness surface will have less momentum near the surface and will separate easily. Also steeper slopes will create a stronger adverse pressure gradient and provoke separation easily.

Recently [2] presented a hybrid RANS/LES method for wind flow over complex terrain, a concept that fit to the characteristic flow within forested complex terrain. In the hybrid model the near wall eddies were modelled with RANS, and the outer flow was modelled with LES. The k-epsilon turbulence model used in RANS automatically switches to a k-epsilon subgrid scale stress model in the LES region. It uses stochastic backscatter model to avoid unphysical transition regions between the two layers.

3 SECTION B: FORSEEN WORK

From the previous stated, according to most authors a CFD approach based in LES should be used to simulate both the forest and the complex terrain. Although this is acknowledged, the project will start by using RANS, simulating several case tests from published data. At a later stage LES and even DES approaches could be applied. Another consideration is the close physical representativeness with the inclusion of stratification effects in the model.

4 CONCLUSIONS

Main topics on wind flow over complex terrain are presented as well as foreseen work.

5 BIBLIOGRAPHY

[1] Ayotte, K. W. (2008). Computational modelling for wind energy assessment. Journal of Wind Engineering and Industrial Aerodynamics, 96(10-11), 1571-1590.

[2] Bechmann, A., & Sorensen, N. N. (2010). Hybrid RANS/LES method for wind flow over complex terrain. Wind Energy, 13(1), 36-50.

[3] Brodeur, P., & Masson, C. (2008). Numerical site calibration over complex terrain. Journal of Solar Energy Engineering (Transactions of the ASME), 130(3), 031020 (12 pp).

[4] Dupont, S., Brunet, Y., & Finnigan, J. J. (2008). Large-eddy simulation of turbulent flow over a forested hill: Validation and coherent structure identification. Quarterly Journal of the Royal Meteorological Society, 134(636), 1911-1929.

[5] Palma, J. M. L. M., Castro, F. A., Ribeiro, L. F., Rodrigues, A. H., & Pinto, A. P. (2008). Linear and nonlinear models in wind resource assessment and wind turbine micro-siting in complex terrain. Journal of Wind Engineering and Industrial Aerodynamics, 96(12), 2308-2326.

[6] Kim, H. G., & Patel, V. C. (2000). Test of turbulence models for wind flow over terrain with separation and recirculation. Boundary-Layer Meteorology, 94(1), 5-21.

European Academy of Wind Energy

Norwegian University of Science and Technology

Physical and Numerical Modelling of Flow over a Real Complex Terrain

Domingo Muñoz-Esparza, Boris Conan, J.P.A.J. van Beeck
von Karman Institute for Fluid Dynamics
Environmental and Applied Fluid Dynamics Department,
Chaussée de Waterloo 72, B-1640 Rhode-St-Genèse, Belgium

ABSTRACT

In the fast development of wind energy, more and more wind turbines are placed in complex terrains. As an alternative to the costly field measurement campaigns, this study shows two different and complementary modelling approaches: CFD and wind tunnel.

Numerical simulations are performed using the OpenFOAM v1.6 open source code. Wind tunnel measurements are carried out with PIV and hot-wire anemometry on a 1/5000 scaled model. Comparisons are done on a 2D plane and different inlet and boundary conditions are investigated. A good agreement is found between numerical computations and wind tunnel measurements. Finally, limitations and future improvements are discussed.

KEYWORDS

Complex terrain, physical modelling, wind tunnel, PIV, *k*-ε turbulence closure, ABL flows.

1 INTRODUCTION

The test case is a real terrain of more than 600m height. In this first approach on the assessment of wind potential on the top of the mountain, only one of the two predominant wind directions, with flat upstream terrain, is studied (figure 1). The modelled area is chosen to be stretched over 15km x 14km real scale, allowing to include the complete mountain and the inlet cliff. The large

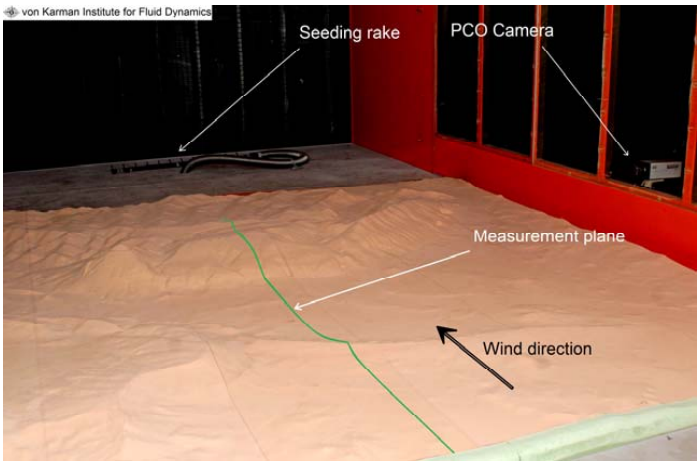

Figure 1: View of the model in the test section

boris.conan@vki.ac.be
domingo.munoz.esparza@vki.ac.be

modelled area induces a very large scaling factor (1/5000). The objective of this study is to compare wind resource assessment by physical and numerical modelling and to assess key parameters for the modelling of complex terrains.

2 NUMERICAL MODELLING

2.1 Turbulence modelling and wall treatment

The numerical simulations presented hereafter are performed using the open source code OpenFOAM v1.6 ®, based on the Finite Volume Method [1]. The differential operators were implemented up to second order accuracy in space. Steady state was assumed and the standard *k*-ε model was applied to account for the turbulence effects. Second order moments are diagnosed by means of a so called eddy viscosity concept, which relates the turbulent stresses to the mean flow gradients trough the turbulent viscosity. The Semi-Implicit Method for Pressure-Linked Equations (SIMPLE) was used to introduce the pressure term in the continuity equation. A standard wall function based on the equivalent sand-grain roughness height, k_s, was applied [2].

2.2 Domain and boundary conditions

The computational domain is a 2D slot of the wind tunnel model. The incoming ABL is generated by an empty rough fetch of 3 m length upstream of the modelling area. The inlet profile and roughness are obtained from hot-wire measurements with the following characteristics of friction velocity, u*=0.6753 m/s and roughness length,$z_0=1.0575\cdot10^{-4}$ m. The model is considered as smooth. Three different approaches are considered to generate appropriate inlet boundary conditions: Richards & Hoxey, [3], Experimental Data [4] and Parente et al. [5]. The height of the domain was set to 1.85 meters to get domain independence and to avoid blockage effects, where a symmetry condition was applied. At the outlet boundary the pressure was fixed to the atmospheric one. A grid independence study in both streamwise and spanwise directions showed that a mesh with 93.100 elements is fine enough to obtain grid independent results. With that configuration, the resolution in the mountain area is about 36 m x 11m in streamwise and spanwise directions, respectively.

3 PHYSICAL MODELLING

3.1 Experimental set-up

Experiments are carried out in the VKI L1 low-speed wind tunnel in the Atmospheric Boundary Layer configuration. The ABL is simulated with a grid, a fence and an adapted 12m

boris.conan@vki.ac.be
domingo.munoz.esparza@vki.ac.be

long cups surface able to simulate different types of roughness length. The mock-up is a representation of the real mountain at 1/5357 scale machined at 1/10mm precision with a provided 3D mesh.

3.2 Measurement techniques

The study is an opportunity for the implementation of 2D-2C PIV [6] in the VKI low speed wind tunnel for wind engineering applications. A double pulsed laser is placed on the sealing of the test section for the lightening of the area of interest. Seeding is realized by a smoke generator placed downstream the model to avoid a perturbation of the incoming velocity profile. Thanks to the closed return circuit of the wind tunnel, an homogeneous particle dispersion is ensured. Several successive planes are recorded along the measurement plane and data are linked afterwards in mean quantities. Additionally to PIV, 1-C hot-wire anemometry (CTA) [7] traverses are carried out to provide time series along the measurement plane. The agreement between PIV and hot-wire anemometry is good, velocity magnitude profiles are matching very well (<2% in average) and turbulence intensity are very close. An uncertainty analysis concludes that both techniques are giving a similar error on the mean velocity, below 2%, and more than 10% for turbulence intensity.

4 COMPARISON

Experiments and numerical simulations are in a good agreement. The velocity profiles at the top of the hill (P4 position) are showed as example in fig. 2. However, there exist differences in the first 100 meters a.g.l., where numerical simulations under predicts the over-speed obtained with the experimental approach. No strong deviation is obtained in the CFD calculations for the different inlet conditions. In terms of turbulent kinetic energy, k, more spreading is found. For z>400 m, the Experimental Data inlet (green line) matches accurately the hot-wire results whereas PIV values are slightly underestimated. Close to the surface, numerical simulations produce more turbulent kinetic energy. Parente et al. and Richards &

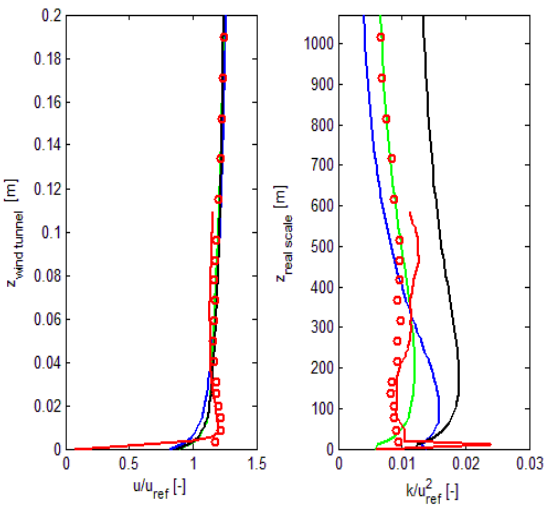

Figure 2: Comparison of wind tunnel measurement with CFD calculation at P4 (see legend of fig. 3)

boris.conan@vki.ac.be
domingo.munoz.esparza@vki.ac.be

Hoxey give in general a higher level of turbulent kinetic energy, which is about two times higher for the Richards & Hoxey case. The peak close to the ground is not reproduced for any of the different inlet conditions.

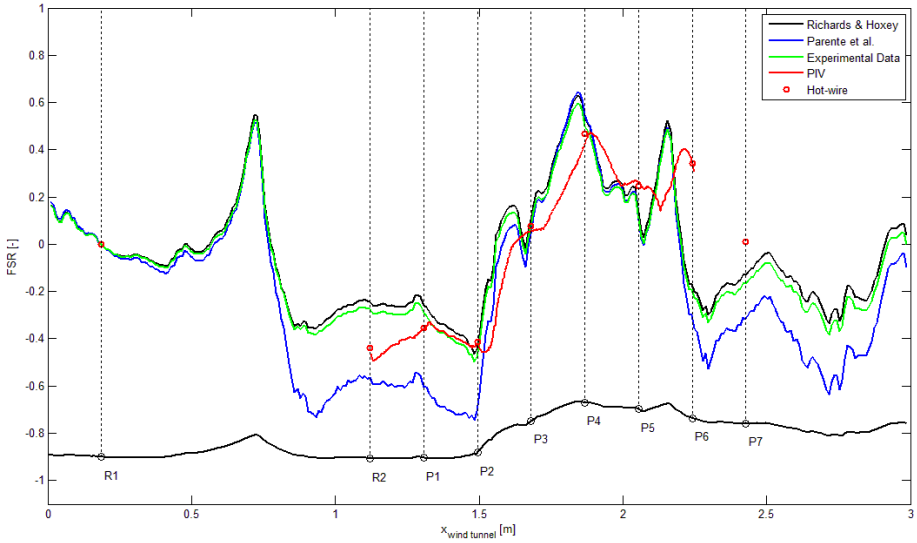

Figure 3: Fractional speed-up ratio at 90m a.g.l.

The Fractional Speed-up Ratio (FSR) gives lots of information about the effect of the topography. In fig. 3, this factor is computed using the velocity at R1 and z=90m a.g.l. as reference velocity. Observations show a wind speed reduction upstream the obstacle, a very important rise on the obstacle slope and a dramatic drop after the top followed by a region where fully developed conditions are recovering. Similar observations were made by Kondo et al. [8], on a parametric study of flow around simplified 2D obstacles. Both experimental and numerical simulations are producing similar flow behaviour but with an offset in x direction, mainly attributed to the use of a 2D domain for the numerical computations. As shown in figure 3, the upstream cliff creates an important speed up and reduces dramatically the velocity approaching the main mountain. The cliff seems to damp the wind speed increase induced by the main mountain. The speed-up ratio is of the same order as on the top of upstream cliff. The inlet conditions only present differences for the case of Parente et al., which is the only scenario in which the flow recirculates after the first hill (x≈0.75m) and the deficit of velocity does not recuperate until P2 location is reached. That recirculation is not observed experimentally.

boris.conan@vki.ac.be
domingo.munoz.esparza@vki.ac.be

5 CONCLUSIONS AND PERSPECTIVES

Numerical and experimental modelling results are satisfactory for a first approach however many effects that affect the modelling are not completely mastered (effect of roughness, high down-scaling factor, etc.). Results are still under post-processing and a comparison with field measurements would allow a real validation. Another conclusion of these simulations is the strong effect of far-field topography; further investigation will be carried out in this direction. Numerical simulations over the 3D domain and URANS methods will be the next steps of the investigation, in cooperation with the wind tunnel analysis.

ACKNOWLEDGMENTS

This work was realized with the financial support of the European Commission within the Marie Curie ITN-WAUDIT program. Partners CENER and UPM are gratefully acknowledged for providing test-case and mock-up, respectively. VKI students S. Buckingham and E. Croonenborgs are sincerely thanks for their considerable implication in the success of this work.

BIBLIOGRAPHY

[1] J. Ferziger, M. Perîc. Computational Methods for Fluid Dynamics. Springer-Verlag Berlin and Heidelberg. New York, 2002.

[2] B. Blocken, T. Stathopoulos, J. Carmeliet. CFD simulation of the atmospheric boundary layer: wall function problems. Journal of Atmospheric Environment, 41 (2007) 238 – 252.

[3] P.J. Richards, R.P. Hoxey. Appropriate boundary conditions for computational wind engineering model using the k-ε turbulence model. Journal of Wind Engineering and Industrial Aerodynamics, 46 & 47 (1993) 145 – 153.

[4] C. Gorlé, J. van Beeck, P. Rambaud, G. Van Tendeloo. CFD modelling of small particle dispersion: The influence of the turbulence kinetic energy in the atmospheric boundary layer. Journal of Atmospheric Environment, 43 (2009) 673 – 681.

[5] A. Parente, C. Benocci. On the RANS simulation of neutral ABL flows. Proceedings of 5th International Symposium on Computational Wind Engineering, 2010.

[6] Raffel M., Willert C., Wereley S., Kompenhans J. (2007) Particle Image Velocimetry: A practical guide. Second Edition Springer ISBN: 978-3-540-63683-0

[7] Bruun H. H. (1995) Hot-wire anemometry, principles and signal analysis. Oxford University Press ISBN: 0-19-856342-6

[8] K. Kondo, M. Tsuchiya, S. Sanada Evaluation of effect of micro-topography on design wind velocity. J. Wind Eng. Ind. Aerodyn. 90(2002)1707-1718

boris.conan@vki.ac.be
domingo.munoz.esparza@vki.ac.be

European Academy of Wind Energy

Norwegian University of Science and Technology

Modelling of atmospheric boundary layer: Generation of shear profile in wind tunnel

Yeow, T.S.[1)], Cuerva, A.[2)] Pérez, J.[3)] Conan, B.[4)], Buckingham, S.[5)] Beeck, J.V.[6)]

[1) 2) 3)] Universidad Politecnica de Madrid, ETSI Aeronauticos, Instituto Universitario Ignacio Da Riva, IDR-UPM, Spain,

[4) 5) 6)] Von Karman Institute, Belgium

ABSTRACT

Roughness length, z_0 and friction velocity, u_* are the defining parameters of wind log profile that must be matched in wind tunnel simulation. To fully understand the role of these parameters, the basics and review from the primitive equations and its relation to the logarithmic profile obtained for wind tunnel conditions were discussed. The problem of roughness, although well known, still needs to be addressed more rigorously especially when determining values of z_0 and u_* from wind tunnel data and their relation to the roughness element geometry. A review of classic literature and new published material were carried out, focusing on the applicability to wind tunnel modelling.

KEYWORDS

log profile, roughness length, roughness height, friction velocity

1 INTRODUCTION

1.1 Logarithmic Profile

In describing the atmosphere, the set of seven equations configured by the Navier-Stokes ones plus continuity, energy, state equation and conservation of humidity is the most rigorous model known. The full set of equations, while giving the best solution, is practically impossible to solve due to non-linearity and large number of complex initial and boundary conditions that need to be considered. Starting from these equations, performing the ensemble averaging and applying the corresponding averaging rules to obtain the RANS equations, and confining the problem to wind tunnel conditions (channel flow hypothesis, see Schlichting and Gersten, 2000 and Wyngaard, 2010), therefore adopting a few assumptions; isentropic flow, dry air considered and incompressibility (density, ρ = constant); the problem is reduced to a much simpler approximation though still leaves much to be solved. The classic logarithmic profile equation is attained in the case of a flow on a smooth, flat surface,

for the mean value of the longitudinal component of the wind speed, U (see expression (0.1)), in terms of the well known non-dimensional "+" variables, after using as characteristic length, $l_+ = \nu/u_*$, being ν the kinematic viscosity, and as characteristic velocity, the friction velocity, u_* (u_* is a reference velocity applied to the motion near the surface where the shear stress is not a function of the distance from the wall and defined as $u_* = \sqrt{\tau/\rho}$, where τ is the Reynolds stress and ρ is the density of the fluid).

$$U(z_+) = \frac{u_*}{\kappa}\ln(z_+) + Bu_* \qquad (0.1)$$

z_+ is the non-dimensional distance from the wall, κ is the von Karman constant (taken as 0.4) and B is an integration constant. In the considered case of smooth wall, B is usually taken to be 5.1 though experimental values give a range 5.0 – 5.5 (Raupach, 1991). In the figure 1, the theoretical result (0.1) (log law in the figure) is included along with experimental data from different authors, the viscous region (viscous sub-layer in the figure, where $U = u_* z_+$) and the buffer region (buffer layer in the figure, adapted from Garratt, 1992). For a deeper explanation on the viscous and buffer regions, see Jimenez (2004) and Durbin & Pettersson Reif (2001).

1.2 Rough Wall Boundary Layer

For rough walls, the logarithmic law can be written as

$$U(z_+) = \frac{u_*}{\kappa}\ln(z_+) + B_h(h_+)u_* \qquad (0.2)$$

where the constant B is replaced by a function B_h that depends on the non-dimensional roughness geometry. A basic dependency on the roughness geometry for B_h can be defined in terms of the non-dimensional equivalent sand grain roughness height $h_+ = h/l_+$ (being h the dimensional equivalent sand grain roughness height, see Durbin & Peterson-Reif, 2001). The equation above can also be written as

$$U(z_+) = \frac{u_*}{\kappa}\ln(z_+) + \tilde{B} \qquad (0.3)$$

where $\tilde{B}$ is a function of roughness height in the form of

$$\tilde{B}(h_+) = \frac{1}{\kappa}\ln(h_+) + B_h(h_+) \qquad (0.4)$$

The logarithmic profile for rough wall can now be rewritten alternatively as

$$U(z) = \frac{u_*}{\kappa}\ln\left(\frac{z}{z_0}\right) \qquad (0.5)$$

with z_0 the hydrodynamic roughness length (also known as aerodynamic roughness length or simply roughness length), which is defined from (0.3) and (0.5) as:

$$z_0 = h\exp(-\kappa\tilde{B}) \qquad (0.6)$$

For smooth walls, expressions (0.1) and (0.5) give the minimum value of hydrodynamic roughness length, $z_{0,min} = \exp(-\kappa B)\,\nu/u_* \approx 0.14\nu/u_*$. For fully rough surface values $\tilde{B} = 8.5$ and $z_0 = 0.033h$ are obtained (see Ligrani & Moffat, 1986). This practice of defining roughness influence was first introduced by Schlicting (1936). The effect of roughness on the logarithmic profile is a matter of intense study since the pioneering work of Schlicting (1936). As an example, in figure 2, the measurements obtained by Schultz and Flack (2007) are shown. It can be observed that the higher the roughness height, h_+ the lower the wind speed in the log region. This is a common result but it is not universal since some types of roughness geometry can lead to flow acceleration (see Jimenez, 2004).

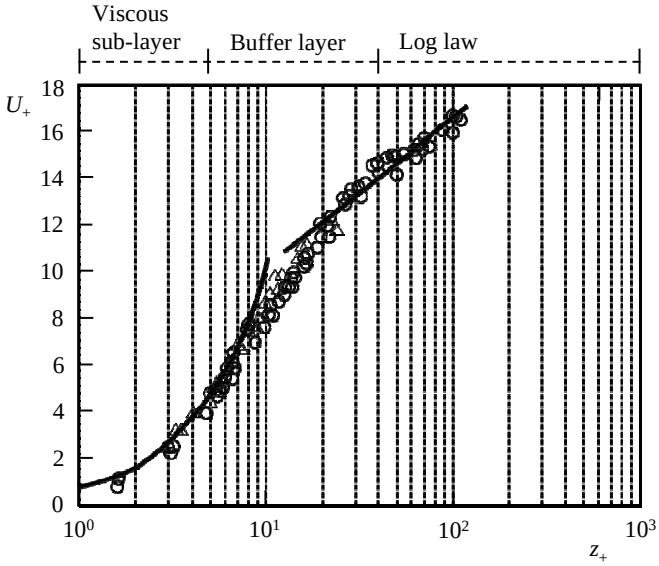

Figure 1: Velocity distribution above a smooth surface, from laminar flow to fully turbulent flow (viscous sub-layer to log law regions). Experimental data represented by symbols. The curve at low Re number represents a linear velocity profile while at higher Re. represents the logarithmic law. (Schlichting, 2000, Garratt, 1992). Observe that $z_+ = zu_*/\nu$ can be interpreted as a Reynolds number based on the friction velocity and the height on the wall.

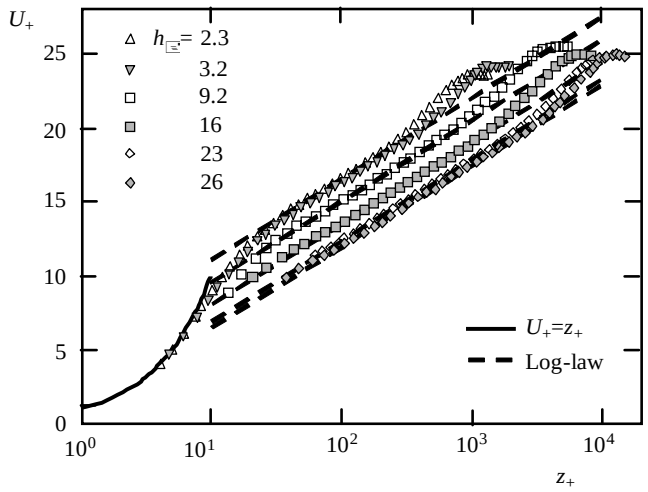

Figure 2: Mean velocity profile for different roughness heights compared to logarithmic profile of McKeon et al. (2004). (Schultz and Flack, 2007)

The relation between the hydrodynamic roughness length, z_0, and the roughness geometry has been an issue of main concern up to know. In the figure 3, the so called roughness function, $\Delta U/u_*$ (see Jimenez, 2004), which is related to the hydrodynamic roughness length by (see Raupach et al. 1991)

$$z_0 = \frac{\nu}{u_*}\exp\left(-B\kappa + \frac{\Delta U}{u_*}\kappa\right) \qquad (0.7)$$

is presented for different values of non-dimensional roughness height in lab and the free atmosphere.

Studies of different roughness elements by Lettau (1969), Wooding (1973) and Raupach et al. (1991), amongst others, established a relation between the hydrodynamic roughness length, z_0, roughness height, h, and roughness density, λ, which is the total projected frontal roughness area per unit area on the wind tunnel floor corresponding to a single roughness element of a homogenous roughness layout, in the form

$$z_0 / h = 0.5\lambda \qquad (0.8)$$

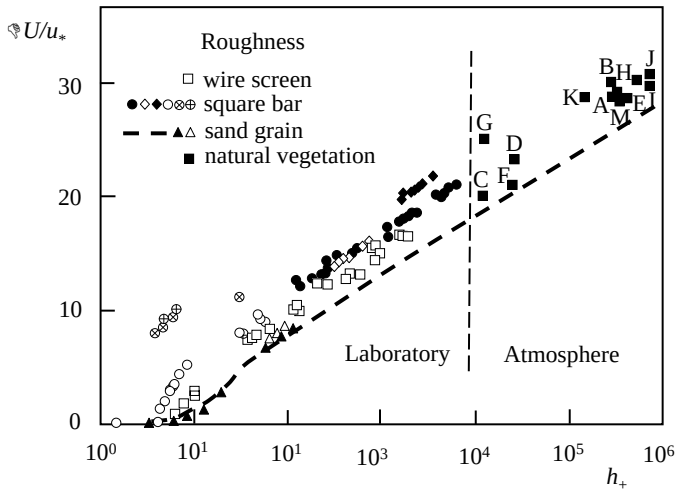

Figure 3: Roughness function, $\Delta U/u_*$, as a function of the roughness Reynolds number, $h_+=hu_*/\nu$ for different types of roughness elements in the wind tunnel and in the atmosphere (from Raupach et al., 1991). Codes for natural vegetation are described in the reference.

The relation (0.8) is widely used to define the density, λ, and height, h, of homogeneously distributed roughness elements to match a given value of hydrodynamic roughness length, z_0. (Dyrbye and Hansen, 1996) A scheme on the definition of roughness density, λ, is presented in figure 4.

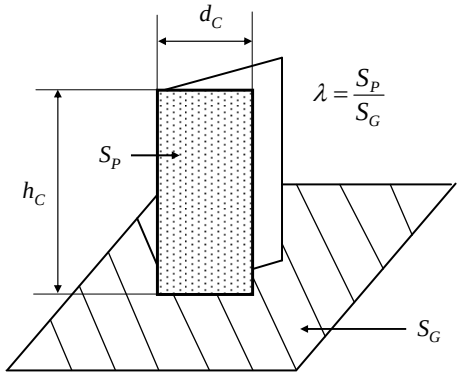

Figure 4: Schematic for determining the roughness density, λ with S_P being the projected frontal area to the averaged wind speed, and S_G being the unit area on the wind tunnel floor corresponding to a single roughness element.

Therefore, with this method, a simple estimation of roughness element needed to generate the required value of z_0 can be obtained. Here there is a maximum value of λ_{max} where the equation holds which has been studied to be ≈0.15. Beyond λ_{max}, z_0/h decreases with further increase of λ, which is attributed to the mutual sheltering of roughness elements (Wooding, 1973). However, changes of the value of λ_{max} depending on the roughness geometry, suggest a need to study different aspect ratios or additional characteristic lengths (Raupach et al. 1991), see figure 5. Lettau (1969) who first proposed equation (0.8), also remarked that a sufficient extent of roughness in the upwind direction is needed for the equation (0.8) to be valid. This was confirmed by Counehan (1971) who suggested a minimum length of 1000*h* needed to achieve an almost equilibrium boundary layer in the wind tunnel.

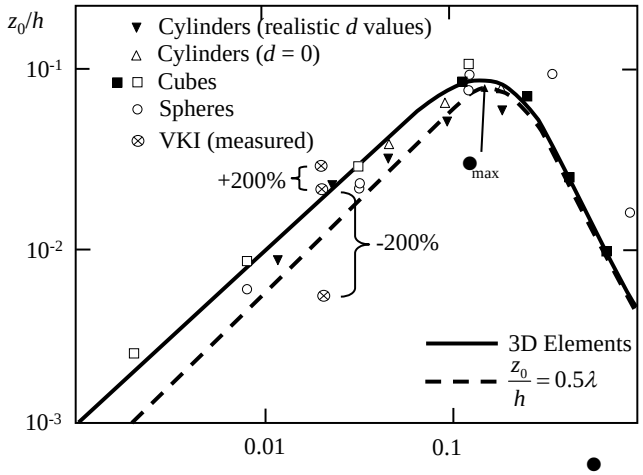

Figure 5: Normalized roughness length z_0/h as a function of roughness density, λ for three dimensional elements. The empirical correlation z_0/h = 0.5 λ, is shown by the dashed line. Measured values of z_0/h from VKI initial wind tunnel tests (Buckingham, 2010) are included along with the uncertainty levels due to different methods of determining z_0 from Iyengar & Farell (2001).

Some authors have also paid attention to the limits related to the geometrical roughness height, *h*, for instance Jimenez (2004) remarks that the ratio of the total boundary layer height, δ, to the roughness element height, *h*, must satisfy $\delta/h > 80$ if one wants to apply the previous considerations. For larger heights, the flow must be better analysed as flow over obstacles.

2 FRICTION VELOCITY AND ROUGHNESS LENGTH DETERMINATION

Some studies have been devoted to compare the different methods to estimate the friction velocity, u_* and hydrodynamic roughness length, z_0 in wind tunnel flows (see for instance, Iyengar & Farell, 2001). These authors compared indirect methods of obtaining z_0, u_* and d, zero-displacement height, (Schlichting, 2000) (using Hama's law fits and log-power law fits) with values obtained from direct measurements of u_* (from Reynolds shear stress and balance measurements). Estimates by indirect methods, used successfully in smooth wall flow studies, can give differences of up to 200% in rough wall cases due to the possibility of having several sets of values z_0, u_* and d giving comparable fits to the same velocity profile (Iyengar & Farell, 2001). Direct measurements give errors of up to 15 % which is mainly due to the X-wire probe errors in measuring turbulent flows. The predicted value of z_0/h from the roughness elements (33mm cups with base to top diameter variation of 40mm to 30mm) used in the initial wind tunnel study in VKI is shown in the figure 5 along with possible value range of z_0/h according to the indirect method uncertainty factor of 2 documented in (Iyengar & Farell, 2001).

2.1 Scaling Factor Effects

After deciding the model scale, S, at the beginning and considering an objective value for $z_{0(real)}$, the value of the required hydrodynamic roughness length in the wind tunnel, $z_{0(WT)}$ is determined. As a preliminary attempt, the relation (0.8) can be used for determining the geometry of the roughness element and its density to be used in the wind tunnel. By taking $\lambda = S_P/S_G$ as shown in figure 5, a range of possible roughness element dimensions can be calculated (see figure 6).

Considering the Alaiz site, the large scaling factor proposed for wind tunnel modelling posed a new challenge as most wind tunnel modelling have been done to a scale of S <500. Considered the minimum value reproducible in the wind tunnel $z_{0,min} = 0.14\nu/u_*$ a minimum real value for the hydrodynamic roughness length can be estimated as $z_{0,min(real)} = 0.14S\nu/u_*$. If the free upflow to the Alaiz site is assumed to be between Type II and Type III terrain type according to the Eurocode classification, which corresponds to a $z_{0(real)}$ range of 0.05-0.3m, choosing the model scale to be $S \approx 5000$, the $z_{0(WT)}$ needed to be reproduced in the wind tunnel can be calculated (see table 1).

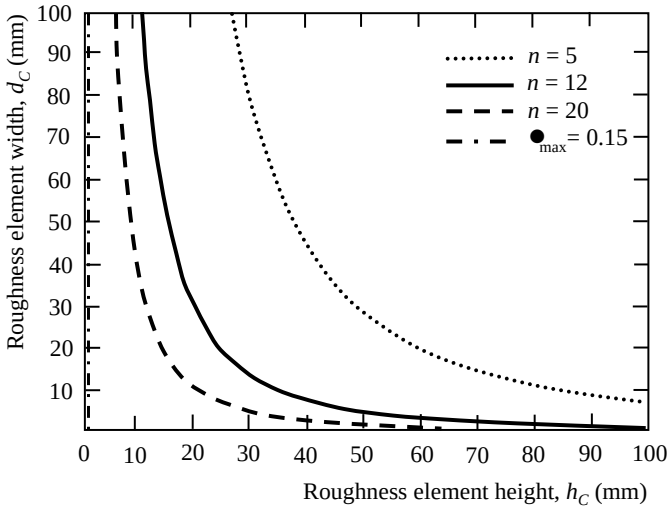

Figure 6: Relation roughness element dimensions, d_C and h_C, and roughness density λ for a chosen model scale, S, and hydrodynamic roughness length, $z_{0(real)}$ (in the figure, S=500 and $z_{0(real)}$= 50mm, therefore $z_{0(WT)} = z_{0(real)}/S$ = 0.1mm). A homogenous distribution of roughness elements in wind tunnel has been assumed, lines plotted are from the different number of elements in a row, n perpendicular to the mean flow speed. The limit λ = 0.15 is shown with the right side of this line for $\lambda << \lambda_{max}$.

Table 1: z_0 of real terrain and wind tunnel model with a model scale, S= 5000.

	Terrain	Model
Type II: z_0 (m)	0.05	1×10^{-5}
Type III: z_0 (m)	0.3	6×10^{-5}

For flat and smooth wall boundary layers, it is quite well established that the viscous region (the region close to the wall where the log profile is no applicable) extends to non-dimensional values of height, $z_+ \in [0, \approx 40]$. In case of using large scale models, such as the one for Alaiz ($S \approx$1:5000) this range of non-dimensional heights could correspond to values comparable to the hub height in the real case.

Roughness and non-homogeneity of the terrain lead to variations of this interval of height for which the log profile is not applicable (see figure 2). Taking as valid the estimation for smooth and flat wall, and considering typical values of kinematic viscosity and friction velocity (ν = 1.5×10^{-5} m^2/s, u_* = 0.5 m/s) the viscous limitation in the case of Alaiz might range in the

interval $z \in [0, 1.2mm]$, which corresponds to an interval in the real terrain $z \in [0, 6.5m]$. So no-conclusions about the log profile from the wind tunnel model could be obtained for height values less than 6.5m in the reality. Hence, a rough estimation on the minimum analyzable height is $z_{min,(real)} = 40S\nu/u_*$.

Table 2: Wind turbine height and distance from model with scaling.

	Wind Turbine	Distance from model surface
Height: (m)	70	0.014
Height: (m)	100	0.02

The distances shown in the table above indicate that measurements taken on a model with scale S = 1:5000 are well into the logarithmic region of the wind profile (non viscous region). In this case the limitation would be associated to the precision of the traverse system used in the case of a hot-wire system.

3 CONCLUSIONS

This paper presents a preliminary study to conduct a modelling of complex terrain in wind tunnels with large scales (≈5000). The analysis is focussed on the generation of a required log profile for the mean wind speed. The relation between the hydrodynamic roughness length and the roughness geometry has been analysed particularly for the case of large scale models. Two issues are outlined, first the fact that a large scale factor might provoke that viscous sub-layer on the model extends to heights that in the real field correspond to distances from the ground comparable to the hub height, being the minimum analyzable height $z_{min,(real)} = 40S\nu/u_*$. Secondly, there is a limit for the generation of the hydrodynamic roughness height in the wind tunnel which establishes a minimum reproducible value for the real value $z_{0(real)} = 0.14S\nu/u_*$.

BIBLIOGRAPHY

[1] Buckingham,S. 2010. Wind park siting in complex terrains assessed by wind tunnel simulations. Master's thesis, VKI, Brussels, Belgium

[2] Counehan, J. 1971. Wind tunnel determination of the roughness length as a function of the fetch and the roughness density of three-dimensional roughness elements. Atmospheric Environment (1967) 5, 637-642.

[3] Drybye, C., Hansen, S.O. 1996. *Wind Loads on Structures*. Wiley, West Sussex, 229 pp.

[4] Durbin, P. A., Pettersson Reif, B. A. 2001. *Statistical Theory and Modelling for Turbulent Flows*. Wiley, West Sussex, 302 pp.

[5] Garratt, J. R. 1992. *The Atmospheric Boundary Layer*. Cambridge Atmospheric and Space Science Series, New York, 336 pp.

[6] Iyengar, A.K.S., Farell, C. 2001. Experimental issues in atmospheric boundary layer simulations: roughness length and integral length scale determination. Journal of Wind Engineering and Industrial Aerodynamics 89, 1059-1080.

[7] Jimenez, J. 2004. Turbulent flows over rough walls. Annual Review of Fluid Mechanics 36, 173-196.

[8] Lettau, H. 1969. Note on aerodynamic roughness-parameter estimation on the basis of roughness-element description. Journal of Applied Meteorology 8, 828-832.

[9] Ligrani, P.M., Moffat, R.J. 1986. Structure of Transitionally Rough and Fully Rough Turbulent Boundary-Layers. Journal of Fluid Mechanics 162, 69-98.

[10] Raupach, M.R., Antonia, R.A., Rajagopalan, S. 1991. Rough-wall turbulent boundary layers. Applied Mechanics Review 44, 1-25.

[11] Schlichting H. 1936. Experimentelle Untersuchungen zum Rauhigkeits problem. Ing-Arch 7, 1-34; NACA Tech Mem 823.

[12] Schlichting H. 2000. *Boundary Layer Theory*, 8th ed. McGraw-Hill, New York, 801 pp.

[13] Schultz, M.P., Flack, K.A. 2007. The rough-wall turbulent boundary layer from the hydraulically smooth to the fully rough regime. Journal of Fluid Mechanics 580, 381-405.

[14] Wooding, R., Bradley, E., Marshall, J. 1973. Drag due to regular arrays of roughness elements of varying geometry. Boundary-Layer Meteorology 5, 285-308.

[15] Wyngaard, J.C. 2010. *Turbulence in the Atmosphere*. Cambridge University Press, New York, 406 pp.

ACKNOWLEDGEMENT

The work has been carried out with funding from the EU FP7-PEOPLE program, under WAUDIT Marie-Curie Initial Training Network.

Special acknowledgements to Boris Conan, Sophie Buckingham and Jeroen van Beeck from VKI for carrying out initial experiments in wind tunnel on a model of Alaiz and sharing the results.

Part 10

Session 6B - Electrical Power Production and Transmission

- Wet Mateable Connectors for Flexible Offshore Installations
  Majid Hasheminezhad, NTNU
- The Effect of Wind Energy
  Ayobami Olanrewaju Makinde, Jubilee Comm
- Analysis of Switching Transients in Offshore Wind Parks with Focus on Prevention of Destructive Effects
  Amir Hayati Soloot, NTNU
- Worst Asymmetrical Short-Circuit Current
  Ivan Arana, DONG Energy

European Academy of Wind Energy

Norwegian University of Science and Technology

Wet Mateable Connectors for Flexible Offshore Installations

Majid Hasheminezhad

Department of Electric Power Engineering, NTNU

ABSTRACT

This paper presents the results from experimental examinations of the breakdown strength of interfaces between XLPE samples. The influence of water droplets on the AC breakdown voltage is described. In addition, by introducing the existence of solid-solid interface at wet mateable connector, the proper insulating materials for subsea application is demonstrated.

KEYWORDS

Offshore power distribution system, Wet mateable connector, interface, Dielectric strength

1 INTRODUCTION

The contact area between different insulating materials is called “interface” in high voltage equipment. Concerning electrical strength, the breakdown strength is dramatically reduced if the electrical stress is applied in parallel with the interface. Such critical interfaces will occur, for example, in subsea high voltage wet-mateable connectors. The voltage of central core is applied across PEEK and insulation of cones (see Fig. 1). The existence of water droplet and foreign particles on the surface of interface between insulation cones (polymer) is extremely detrimental and field enhancement is caused due to the high permittivity and conductivity of water droplet and contamination. This will result in initiation of partial discharges and surface tracking at the interface. Several studies described the electrical behaviour of interface [1-2]. It is, however, many unknown issues: What role do mechanical pressure and surface roughness play in breakdown? What is the effect of water droplet at the interface? In the following, the volume of trapped water droplets at the interface is estimated. Then, investigations are presented on the tangential AC breakdown strength of interfaces.

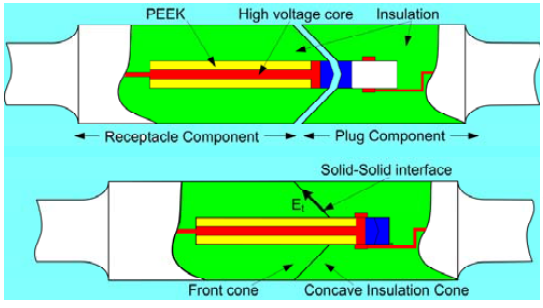

Fig.1: Illustration of wet mateable connector

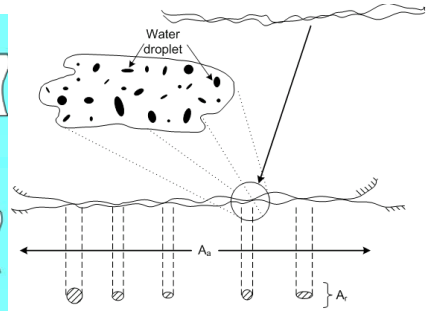

Fig. 2: Schematic representation of an interface

2 PROBLEM FORMULATION

When two nominally flat surfaces are placed in contact, surface roughness causes contact to occur at discrete contact spots. The sum of the areas of all the contact spots constitutes the real area of contact, and for most materials with applied load, this will be only a small fraction of the apparent area of contact. The ratio of real contact area to nominal area versus the apparent pressure, $p_a = \frac{F}{A}$, for plastic contact is derived from [3]

$$\frac{A_{re}}{A} \approx \frac{P_a}{H} \quad (1)$$

where A_{re} and A are the real area and the nominal area of contact, respectively; H is the hardness of the material. Assuming H=3 MPa for the elastomer used in subsea connector and a high engagement pressure of 10 bar, it is observed that there is contact between two surfaces only at 33% of nominal area. Therefore, on engagement of subsea connector parts under water, water droplet is trapped in the rest of apparent area at the interface between two insulating solids (see Fig. 2). In order to evaluate the total volume of the trapped water, the separation between reference planes of two surfaces should be estimated. From a surface profile, it is a simple matter to find the area of surface above any given height, or vice versa, via bearing area curve (BAC) [3]. Assuming a triangular profile across the surface and pyramid shape cavity, the total volume of water needed to fill the free space at the contact is approximately 0.1 μL for the smooth surface specimen used in this study.

If electric field at the tip of a droplet exceeds the discharge inception field, it can trigger discharges. With rises in voltage, PDs can induce an excessive increase in temperature leading to thermal degradation of the surrounding materials, and then erosion and possible tracking of the material appear. The process often is referred to as “aging”.

3 EXPERIMENT

In this experiment, two rectangular prisms of XLPE samples ($4\times55\times2.5\text{mm}^3$) were placed on top of each other between two horizontally placed Rogowski shaped electrodes as indicated in Fig 3. A single water drop with a definite volume (1, 2.5, 5 or 10 μL) and conductivity (500 $\mu\text{S/cm}^{-1}$) was placed on the surface of interface (with the aid of a micro-pipette) before assembling the interface. The equipment and methods used for PD inception and breakdown voltage measurement have been described previously [2].

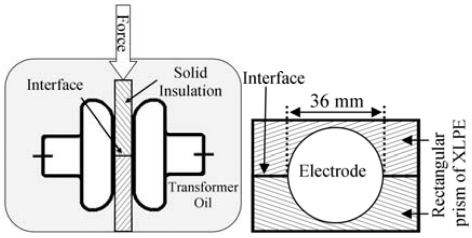

Fig. 3: Sample mounted between electrodes

4 RESULTS

Figure 4 shows the breakdown strength versus the applied mechanical pressure for different volume of the deposited drop water. It can be inferred that the breakdown field strength decreases with increasing water drop volume. A water drop with a larger volume likely reduces the insulation path between the electrodes more significantly, thus increasing the risk of flashover. Further, the higher is the applied pressure, the higher is the electric field. It is interesting that the influence of water drop volume is more significant at lower pressure than higher pressure. A possible explanation for this resides in the fact that, by applying more interfacial pressure, the real area of contact increases and the available space for water droplets reduces. Therefore, regardless of water drop volume, the limited fraction of drop volume is trapped at the interface while the rest is ejected to neighbouring region.

The breakdown strength versus volume of deposited water droplet are presented in Fig. 5 for the rough and smooth surfaces (applied pressure = 5 bar). It is interesting that volume of water drop has trivial effect on the flashover voltage. It is concluded that even a single drop with a volume of few μL might result in initiation of partial discharges and likely flashover. It is also observed that field strength is around 3.5 kV/mm in average which is approximately a third of values presented in [2] for the interfaces without the presence of water droplet.

5 DISCUSSION

The following are the important issues regarding dielectric properties, which relate to the interface design and performance:

- How do changes in polymer structure relate to dielectric properties such as conductivity and permittivity?
- Is dielectric strength of interface affected by changes in polymer properties?

The following is a summary of some studies to answer some of the above questions:

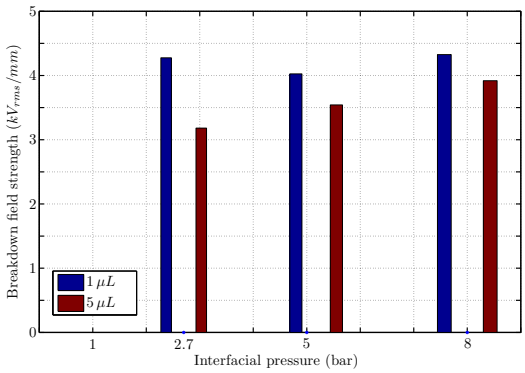

Fig. 4: Dielectric strength of interface as a function of the applied mechanical pressure

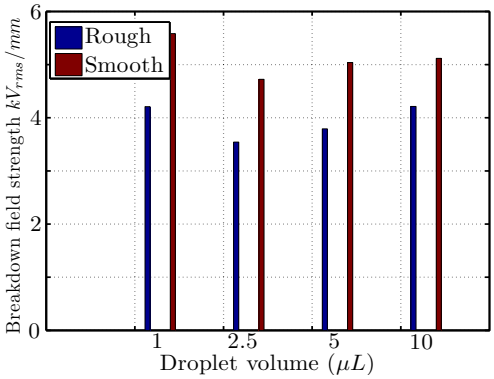

Fig. 5: Dielectric strength of interface versus the volume of the deposited drops

Having decided that the elastomer would be ideal (due to its low Young modulus [2]) as a cone insulation, the next choice to be made is that of the type of elastomer that should be used and dielectric strength of material become number one criteria.

It has also been demonstrated [1] that surface erosion due to water droplet can be avoided when insulator surface parallel to the electric field are not stressed more than 0.4-0.6 kV/mm. The maximum electrical field at the inner part of interface in Fig. 1 is reduced if a material with higher dielectric constant is used. On the other hand, the dielectric loss factor and the dielectric strength of elastomer do also matter. It is known that the Nitrile butadiene rubber (NBR) has a high dielectric constant ($\varepsilon' \approx 12$) but other dielectric properties are poor. The considerably high dielectric loss value ($\varepsilon'' = 1.3 \sim 3.5$) contributes to lowering its insulating properties. Thus, it is aimed to fill it with filler particles to reduce the dielectric loss values while not adversely affecting both the mechanical properties and the permittivity of the end product. To understand the effect of filler particles on electrical properties of polymer, Fig. 6 shows the variation of ε' and ε'' versus mica content [4].

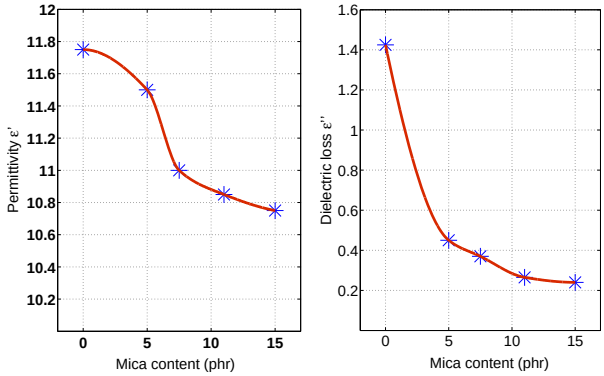

Fig. 6: Permittivity and dielectric loss vs. mica content

6 CONCLUSIONS

A detailed investigation into the influence of various factors on the dielectric strength of interface has shown that moisture clearly plays an important role at the interface. Permissible quantities of PD and leakage current are still missing, but are needed for the assessment of appropriate aging tests on subsea wet mateable connector. Furthermore, investigation is on the way aiming an analysis of the dielectric strength of an interface assembled in water.

BIBLIOGRAPHY

[1] A. Phillips et al. “Aging of non-ceramic insulators due to corona from water drops,” IEEE Transactions on Power Delivery, vol. 14, no. 3, pp.1081–1089, 1999.

[2] M. Hasheminezhad et al., “Breakdown strength of solidjsolid interface,” in Proc. 10th IEEE International Conference on Solid Dielectrics (ICSD), Potsdam, Germany, 2010

[3] Greenwood, J.A., “The area of contact between rough surfaces and flats”, ASME Journal of Lubrication, Vol. 89, 1967, pp. 81-91

[4] D.E.El-Nashar et al. “Physico-mechanical and dielectric properties of nitrile rubber filled with silica and mica,” Kautsch. Gummi Kunsts, vol. 9, pp. 434–440, 2009.

The Effect of Wind Energy

Ayobami Olanrewaju Makinde

Jubliee Comm, Electrical, Ibadan, Nigeria

ABSTRACT

Wind energy has emerged as the leading renewable energy generation method, currently producing a power yield equivalent to 20 GW, with an estimated projection of 40-60 GW by 2010. In order to successfully integrate wind energy with traditional generation supplies it is necessary to have the ability to accurately forecast the available yield of a wind park over a given period. This paper presents a wind power and subsequently an energy yield forecast tool which is based on a multi-layered perceptron. The tool produces energy yield forecasts which can be used for two main purposes; firstly, delivery of wind (energy) yield estimations and secondly to assess the suitability of a given location for development into a wind park site. The tool makes use of a Multi-layered Perceptron which has been trained with historical data to produce a set of predicted wind speed data for a given period. This data is then processed in conjunction with independent variables, including Wind Turbine Generator (WTG) type and altitude to give an estimated power yield and expected uncertainty of the forecast (in terms of percentage capacity factor). Results indicate that by using a neural network approach the accuracy of the tool is sufficiently accurate to be considered as a feasible method for short to medium term (wind speed) power yield estimation for wind energy producers and utility operators.

European Academy of Wind Energy

Norwegian University of Science and Technology

Analysis of Switching Transients in Offshore Wind Parks with Focus on Prevention of Destructive Effects

Amir Hayati Soloot[1)], Hans Kristian Høidalen[2)]

[1)] ,[2)] Electric Power Engineering / NTNU, Norway

ABSTRACT

Switching transients are one of the main phenomena which excite resonance overvoltages on transformer terminals in Offshore Wind Farms (OWFs). Since the maintenance and repair costs of OWFs are noticeable, the investigation of possible failures in OWF equipments such as cables, transformers and power converters are of main importance.

In this paper, the high frequency model of a typical Medium Voltage (MV) transformer is employed to assess the potential of resonance overvoltages in OWF. It is shown that remarkable resonance overvoltages can be observed in low voltage side of transformers.

KEYWORDS

Offshore Wind Farm, Switching Transient, Transformer Resonance Frequency, Black Box Modeling.

1 INTRODUCTION

The application of renewable sources for electricity production has been raised in the last decade. Among the renewable sources, wind energy has been mainly focused. In addition, the suitable places for the installation of big clusters of wind mills are uninhabited islands and offshore platforms, because they offer high, uniform wind speed and acceptable visual impact [1]. The cumulative capacity of installed offshore wind energy in Europe, amounting to 800 MW at the end of 2006, grew to 2056 MW at the end of 2009, i.e. 150 % increase in three years [2]. In 2020, European Wind Energy Association (EWEA) expects between 40 and 55 GW of power production by offshore wind farms [2].

In order to connect the offshore wind mills, large undersea cable connections are required. Since each windmill has a step-up transformer, a windmill row configuration is cable-transformer sections which are linked in series. There are similarities and differences between the connection grid of OWFs and Medium Voltage (MV) underground cable systems [3]. Although the energization of both systems deals with similar equipments, more considerations should be taken into account for energization of OWFs due to higher cost of maintenance and repair and accessibility issues for OWFs.

Transformers installed in every windmill can be exposed to dielectric failures due to overvoltages, e. g. energization overvoltages, current chopping, and voltage escalation and reignition of VCB during disconnection. Many studies have investigated and analyzed dielectric failures in transformers [4]-[9].

Overvoltages on the secondary side of transformer terminal due to resonance phenomenon is assessed in [4] for cable-transformer interaction. Therefore, resonance overvoltages on transformer terminal and along transformer winding should be taken of great importance.

In this paper, Overvoltages along a cable in a row of windmill is simulated and analyzed in ATP. The potential of resonance overvoltages on transformer terminals are assessed for wind mill energization.

2 OFFSHORE WIND FARM MODELING

Main components in OWFs for the switching transient investigations are Wind Turbine Transformers (WTTs), cables and VCBs. In this paper, the OWF system considered for simulation is illustrated in Fig. 1. It consists of five WTTs which are connected in row with five cables interconnections. There are five VCBs to switch the WTTs and one VCB for switching the row.

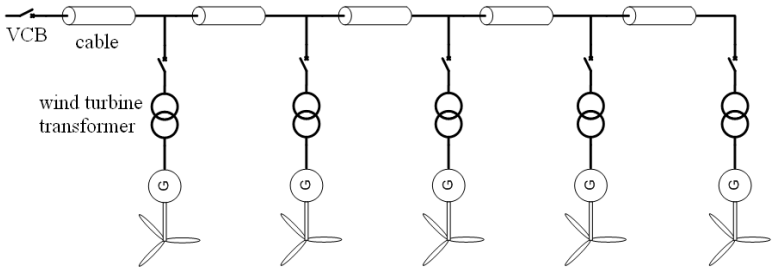

Figure 1: Offshore wind farm system

For modeling WTTs in ATP, the following steps are taken:

1. 6×6 admittance matrix of 11.4kV/235V transformer is achieved by measurements as functions of frequency from 10 Hz to 10 MHz. Connected coaxial cables were compensated for.
2. The black box model [10]-[11] of the transformer is obtained. Black box model is based on vector fitting [10]-[11] and the online available routine “Matrix Fitting Toolbox” with enhanced open circuit response representation is applied. (http://www.energy.sintef.no/produkt/VECTFIT/index.asp).

3. Transformer RLC lumped parameters are implemented in “User Specified Library” elements.

For cable modelling, JMarti model is used. Since JMarti model considers transformation matrix as a frequency independent matrix and computes it for a known frequency, “Frequency matrix” is adjusted according to travelling wave frequency which is subsequently in relation with cable length. The cable geometry data are shown in table I.

Table I: cable geometrical parameters

Parameter	Value
core inner radius (m)	0
core outer radius (m)	0.02
core resistivity (ohm×m)	1.72×10^{-8}
core-sheath insulation permittivity (F/m)	2.671
sheath inner radius (m)	0.035
sheath outer radius (m)	0.038
sheath resistivity (ohm×m)	2.2×10^{-7}
sheath insulation permittivity (F/m)	2.3

3 SIMULATION RESULTS

In this section, the energization of wind farm shown in Fig. 1 is simulated in ATP and shown in Fig. 2-a. The transient voltages of phase A on HV and LV sides of transformers are shown in Fig. 2-b and Fig. 3, respectively.

The traveling wave phenomenon due to energization at voltage peak and the duplication of the voltage at the end of wind mill row can be observed in Fig. 2-b. Since the main transformer resonance frequency [12] is 2 MHZ in this case, the superposition of 2 MHz oscillation on the traveling surge can be seen in the rising edge of HV side of transformers.

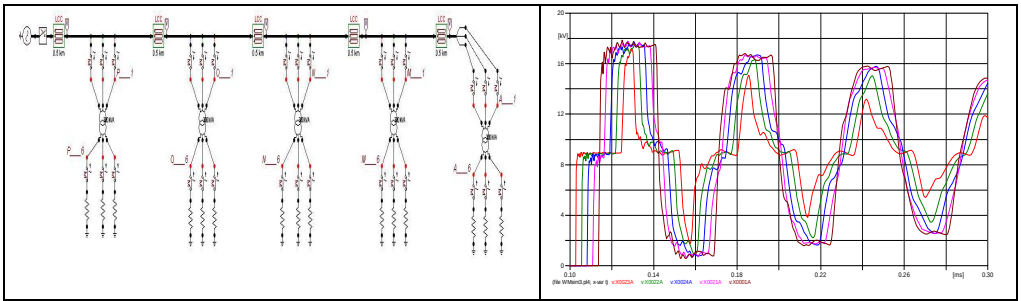

(a) (b)

Figure 2: a) Offshore wind farm simulation circuit in ATP. b) Transient overvoltages in phase A of HV side of transformers, P___1 (red plot), O___1 (green plot), N___1 (blue plot), M___1 (pink plot), A___1 (brown plot).

In Fig. 3-a, this high frequency resonance phenomenon can be obviously seen on LV side of transformers. The decrement of overvoltage amplitude in transformers along the row is due to traveling wave dissipation in cables. Although it is not distinguishable in Fig. 2, it can be well understood from Fig. 3-a and Fig. 3-b. The current obtained from cable by each transformer is directly related to overvoltage amplitude at transformer terminal. Therefore, the first current surge amplitude decreases from the first transformer to the last one.

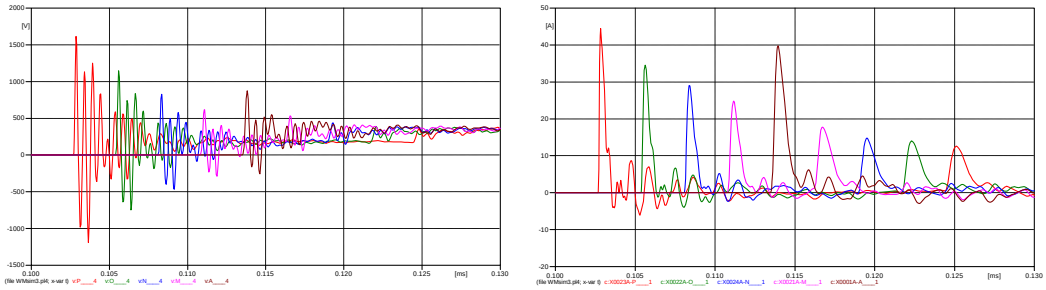

(a) (b)

Figure 3: a) Transient overvoltages in phase A of LV side of transformers, P___4 (red plot), O___4 (green plot), N___4 (blue plot), M___4 (pink plot), A___4 (brown plot). b) Current surges in phase A of HV side of transformers, P___1 (red plot), O___1 (green plot), N___1 (blue plot), M___1 (pink plot), A___1 (brown plot).

4 CONCLUSIONS

The overvoltages in HV and LV side of transformers in a row of wind farm are containing two main frequencies; the dominant resonance and traveling frequency. Since the prominent resonance frequency has influenced the overvoltage amplitude and waveform on transformer terminals, the design of cable-transformer system should be performed in a way to minimize the effect of resonance overvoltages in offshore wind farm.

BIBLIOGRAPHY

[1] X. I. Koutiva; et al.: Impact of Large Offshore Wind Farms on Power. IEEE Trans. On Power Delivery, vol. 21, no. 2, pp. 987-994, April 2006.

[2] Annual report of the European Wind Energy Association (EWEA):“The European Offshore Wind Industry- Key Trends and Statistics 2009”, Jan. 2010. Available online: http://www.ewea.org/fileadmin/emag/statistics/2009offshore/pdf/offshore%20stats%2020092.pdf

[3] L. Liljestrand; et al.: Transients in Collection Grids of Large Offshore Wind Parks. Wiley Inter science, Volume 11 Issue 1, Pages 45 – 61, 2008.

[4] B. Gustavsen : Study of Transformer Resonant Overvoltages Caused by Cable-Transformer High Frequency Interaction. IEEE Trans. on Power Delivery, vol. 25, no. 2, April 2010.

[5] E. Bjerkan, H.K. Høidalen, High frequency FEM-based power transformer modelling: Investigation of internal stresses due to network-initiated overvoltages", Electric Power Systems Research, vol. 77, no. 11, pp. 1483–1489, 2007.

[6] M. Popov; et al.: Analysis of very fast transients in layer-type transformer windings. IEEE Trans. on Power Del., vol. 22, no. 1, pp. 238–247, Jan. 2007.

[7] S. M. H. Hosseini; et al.: Comparison of transformer detailed models for fast and very fast transient studies. IEEE Trans. Power Del., vol. 23, no. 2, pp. 733–741, Apr. 2008.

[8] M. Popov; et al.: Evaluation of surge transferred overvoltages. Elect. Power Syst. Res.,vol. 78, no. 3, pp. 441–449, 2008.

[9] A. Borghetti; et al.: Lightning-induced overvoltages transferred through distribution power transformers. IEEE Trans. Power Del., vol. 24, no. 1, pp. 360–372, Jan. 2009.

[10] B. Gustavsen : Wide band modelling of power transformers. IEEE Trans. Power Del., vol. 19, no. 1, pp. 414–429, Jan. 2004.

[11] B. Gustavsen and A. Semlyen : Rational approximation of frequency domain responses by vector fitting. IEEE Trans. Power Del., vol. 14, no. 3, pp. 1052–1061, Jul. 1999.

[12] A. H. Soloot, H. K. Høidalen : High Frequency Modeling of Transformers in ATP for Investigation of Resonances in Offshore Wind Park, in proc. Of EEUG meeting , pp. 164-175, August 2010.

Worst Asymmetrical Short-Circuit Current

I. Arana[1)], O. Holmstrøm[1)], L. Grastrup[2)] and J. Holbøll[3)]

[1)] DONG Energy, Denmark, [2)] Burmeister & Wain Scandinavian Contractor A/S, Denmark and [3)] Technical University of Denmark, Denmark

ABSTRACT

In a typical power plant, the production scenario and the short-circuit time were found for the worst asymmetrical short-circuit current. Then, a sensitivity analysis on the missing generator values was realized in order to minimize the uncertainty of the results. Afterward the worst asymmetrical short-circuit current was analyzed in order to compare the results with the allowable DC current component based in the IEC. Finally the normal operating condition for the power plant was modeled.

Index Terms

IEC, synchronous generators, armature DC component time constant for three-phase short-circuits, first zero-axis crossing

1. POWER PLANT

A digital model of a Power Plant was created in Power Factory/DigSILENT, based on typical information. Power Factory/DigSILENT is a Windows´ based simulation tool, with special functions for electromagnetic transient (EMT) simulations.

The information from:

- the 132 kV grid
- HV cable connecting the 132 kV grid
- step-up transformers (75MVA 142/11kV)
- cable connecting the step-up transformer
- cable connecting 20 MVA generator
- 20 MVA generator
- cable connecting 9 MVA generator
- 9 MVA generator

were entered into the model in Power Factory. However, missing values in several components were set to generic values based on DONG Energy experience.

The Power plant grid under normal operating conditions can be seen in Fig. 1. The power plant is connected to a 132kV grid through a HV cable. Below the HV busbar two step-up

75MVA transformers are connected, each though a cable connecting the step-up transformers to a MV busbar. Then, connected to each MV busbar the 9 MVA and 20MVA generators are connected though cables. There are three generators connected to each MV busbar. However in the simulations only three 20MVA generators are connected in the MV busbar 1 and one 9MVA generator in the MV busbar 2. In all simulations the three-phase short-circuit to ground was simulated in the MV terminal of the 75MVA transformer.

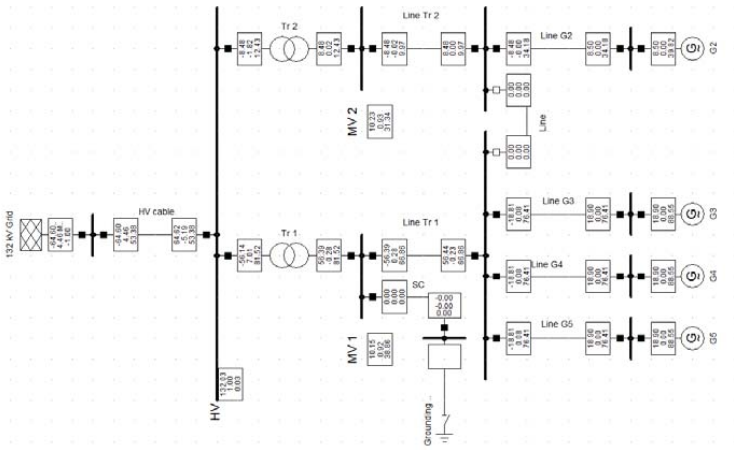

Fig. 1 Power plant single line diagram. Power flow for full power production with unity power factor.

2. WORST ASYMMETRICAL SHORT-CIRCUIT CURRENT

The maximum DC component of the short-circuit current as shown in figure 1 and 2 in [1], may be calculated with sufficient accuracy by equation:

$$i_{d.c.} = \sqrt{2} I_k^{"} e^{-2\pi f t R/X} = i_{d.c.\max} e^{-t/Ta} \qquad (1)$$

where

$I_k^{"}$ is the initial symmetrical short-circuit current;

f is the nominal frequency;

t is the time;

X/R is the ratio between the imaginary and real part of the equivalent impedance of the system as seen from the short-circuit location;

Ta is the armature DC component time constant for three-phase short-circuits.

The phenomenon of DC short-circuit current components was explained by [2]. For three-phase short-circuit current on synchronous machine terminals, it was clarified that:

To avoid discontinuity, initial DC component will appear in each faulted phase in the case of a short-circuit occurrence.

The initial DC component in each phase will be equal to the instantaneous value of the current of that particular phase at the moment of a short-circuit occurrence, but with an opposite sign.

The DC component will decay to zero in all three phases and their rate of decay will be similar in all three phases regardless of the initial DC component value.

Since typical X/R rations for “far-from-generator” faults in typical distribution systems may be in the order to 15, the corresponding time constant will be 45 to 50ms for 50Hz system. On the other hand, a mid-size generator system may have a X/R ratio in the order of 80, which yields a 255ms time constant in a 50Hz system; and if the fault is located close to the generator terminals this is called a “near-to-generator” short-circuit. Fig. 2 shows the corresponding DC component decay for cases where X/R equals 125, 80, 55, 48 and 15 based on (1). It should be noted that at a time equivalent to 60ms after the initial moment of the fault occurrence, the DC current component will decay to approximately 30% of its initial value for the system with X/R=15. The DC component will decay to approximately 70% for a system with X/R=55 and to about 85% for the system with X/R=125. These noticeable differences in DC components’ decay should be taken into account when selecting the circuit breaker.

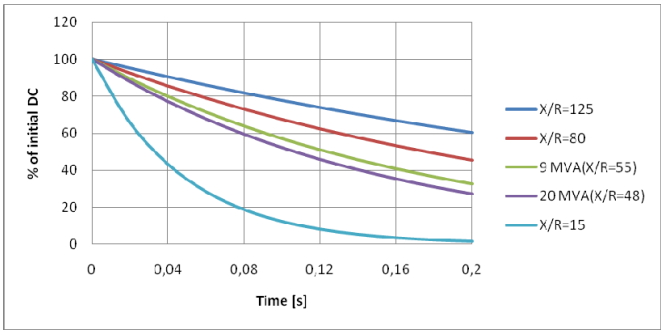

Fig. 2 Effects of X/R ratio on DC component decay (50Hz systems)

During a “near-to-generator” short-circuit, there is a possibility of the first zero-axis crossing occurring several periods after the short-circuit occurred [1]. Hence, it is necessary to describe the short-circuit current as a function of time when determining the moment of the first zero-axis crossing. Unfortunately, [1] does not provide guidance for this phenomenon.

It is possible to determine the fist zero-axis crossing of a synchronous generator short-circuit current by using

$$i(t) = E\sqrt{2}\left[\left(\frac{1}{X''d} - \frac{1}{X'd}\right)e^{\left(\frac{-t}{T''d}\right)} + \left(\frac{1}{X'd} - \frac{1}{Xd}\right)e^{\left(\frac{-t}{T'd}\right)} + \frac{1}{Xd}\right]\sin(\omega t) - \frac{E\sqrt{2}}{X''d}e^{\left(\frac{-t}{Ta}\right)} \quad (2)$$

where

$i(t)$	short-circuit current;
E	rms phase voltage at generator terminals;
t	time;
$X''d$	d-axis subtransient reactance;
$X'd$	d-axis transient reactance;
Xd	d-axis synchronous reactance;
$T''d$	d-axis subtransient time constant;
$T'd$	d-axis transient time constant;
Ta	armature time constant
ω	angular frequency

The calculation using (2) can easily be performed on a computer spreadsheet and does not require network analysis software. The external reactance, such as a transformer or reactor, can be incorporated into a modified version of this equation which adjusts both the reactances and time constants [3].

It is important to remember that standards for power systems and equipment such as [1] and [4] specify requirements and testing of equipment based on normal configurations that represents about 90% of the applications in the industrial and public distribution sectors. Some of this application guides are designed for front-end engineering phase, where it is necessary to examine various possible solutions involving different voltage levels, short-circuit currents, etc. This must be done using available manufacturers' data based on IEC/IEEE standards [2]. For applications not described by these standards, such as the current report, a method based on EMT simulations should be used in order to determine the worst asymmetrical short-circuit current.

Previous work has been done where the IEC and IEEE standards have been compared against EMT simulations [5]. First a comprehensive survey of uncertainties regarding the arc fault resistance, circuit breaker arc resistance, asymmetrical short-circuit current and first zero-axis crossing were examined. Then a system was analyzed using the IEC, ANSI/IEEE and EMT simulations, where the asymmetry factor for a generator with Ta=0.33s using IEC

was 112%, 135% using ANSI/IEEE and 131% using EMT simulations. Afterwards the effect of the generator power factor before the short-circuit was simulated, and the asymmetry factor was further increased to 142% with the generator lightly loaded and 0.29 leading power factor.

3. SIMULATIONS

In order to take into account the operating condition of the power plant, two study scenarios were defined: the full load and no load scenario. In the full load scenario, four generators were connected, but only three of them 100% loaded and the remaining one with only 60%. In the no load scenario, only one generator was connected at 30% load.

Three production levels were also defined for both scenarios where the power factor was varied from 0.9 lagging unity, and 0.9 leading.

In both scenarios with all production levels, eleven different times of the short-circuit were varied in order to find the worst short-circuit angle.

3.1. Full load scenario

In this scenario, the four generators are connected, but only three of them 100% loaded and the remaining one with only 60%.

Fig. 3 presents the currents for the full load scenario with leading power factor. It is possible to see that the current crosses zero value right after the short-circuit happens, even with the initial DC current, in all the times of short-circuit. The closest current not to cross zero after the short-circuit occurs is the phase B current in the generator G2 when the short-circuit appears at 20ms (red line in all curves). It is important to remember that this generator is only 60% loaded.

The rest of the simulations for the full load scenario with lagging and unity power factor were not presented because all current crossed the zero axis after the short-circuit occurs.

3.2. No load scenario

In this scenario only one generator is connected with 30% load. The worst short-circuit time was found with the lagging, leading and unity power factor.

In the lagging power factor, the closest current not to cross zero after the short-circuit occurs is the phase B current in the generator when the short-circuit appears at 20ms. The maximum instantaneous current is 1.6kA and is very dependent on the phase angle when the short-circuit occurs.

In the unity power factor, the phase A current does not cross zero the first cycle when the short-circuit happens at 23 and 24ms; phase B current does not cross zero the first cycle

when the short-circuit happens at 20 and 21ms; and finally phase C current does not cross zero the first cycle when the short-circuit happens at 26 and 27ms. The maximum instantaneous current is 1.4kA and is very dependent on the phase angle when the short-circuit occurs.
In the leading power factor, the phase currents does not always cross zero right after the short-circuit happens, depending on the short-circuit time. The maximum instantaneous current is only 1.25kA, which corresponds to a time of the firs zero crossing of 400ms.

The maximum asymmetry short-circuit current from the generator was found to be in the no load scenario where the generator consumes reactive power (leading power factor).
Fig. 4 shows the comparison of the highest current asymmetry for no load (left plot) and full load (right plot) scenarios; for leading, lagging and unity power factor. Here it is possible to see that the initial conditions, the power factor and the loading are really important for this kind of study.

3.3. Sensitivity analysis

Once the worst scenario with the short-circuit angle was found, a sensitivity analysis on the uncertain values was realized. Here the X/R grid ratio, generator inertia, stator leakage reactance, stator resistance, mechanical damping, generator saturation, excitation control and capacitances in the generator and the transformer were varied.
First the X/R ratio from the grid was varied without mayor changes in the short-circuit current contribution from the generator.
Then the inertia of the generator was decreased, and this caused acceleration on the machine and an angle shift in the current during the short-circuit duration; however, the current amplitude, initial asymmetrical component and asymmetrical decay remained unchanged.
The stator leakage reactance were increased and decreased from the standard values, and small variations were presented, however, no major changes were achieved.
When the stator resistance was increased two times and ten times with respect to the generator data, the asymmetrical decay increased proportionally to the resistance. However, it should be mentioned that this value is normally available from the generator datasheet.
The mechanical damping from the generator was increased two and ten times with no significant change in the short-circuit current.
The generator main flux saturation was defined based on the open circuit test of a 35MVA 0.85PF 10.5kV 50Hz 1500rpm generator, in order to show a more realistic machine. However, the generator short-circuit current did not presented any significant variation.

In order to account for the excitation of the generator, the excitation voltage was set from an initial value of 0.8p.u. to 0p.u. and 1.2p.u., after the short-circuit occurred. This variation had an effect on the amplitude of the generator short-circuit current, where the highest amplitude was presented when the excitation voltage was increased to 1.2p.u. during the short-circuit, and this caused the current to cross zero at 300ms, instead of 400ms at the base case. When the excitation voltage was decrease to 0p.u., the current amplitude decreased and the first zero crossing time was longer than 500ms. Hence, in reality where the AVR and excitation system is supposed to increase excitation voltage during faults, positive effect should be expected. A more detailed investigation using AVR dynamic model has not been made

The capacitors in the transformer and generator were included in the no load scenario with leading power factor, in order to find the short-circuit current dependence in these values. The capacitances did not show any important effect on the generator short-circuit contribution.

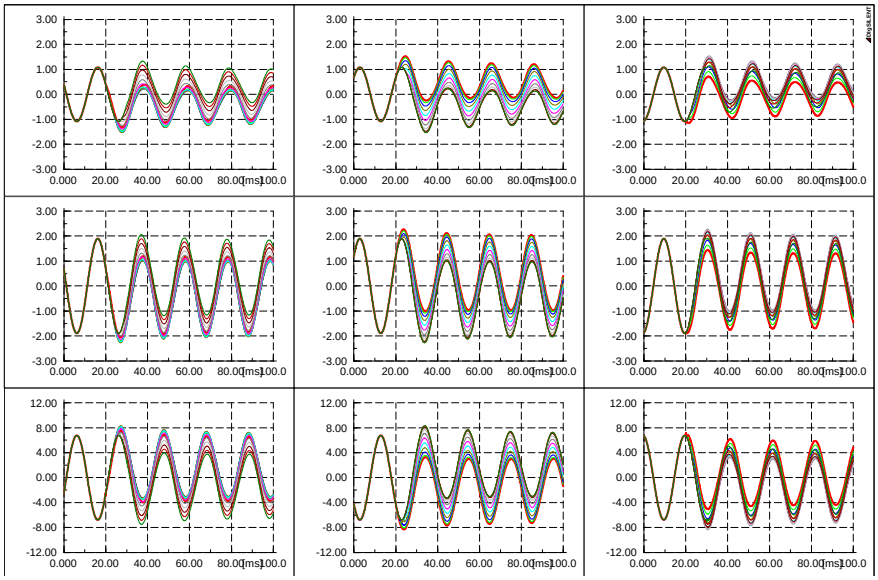

Fig. 3 Simulated currents for a three phase short-circuit by 1ms time sweep for 10ms, full load scenario with leading power factor. The phase A currents are plotted in the left column, the phase B currents in central column and phase C currents in right column. The currents from the G2 generator are in the top row, while the mid row presents the current from the G5 generator and the lower row the MV transformer circuit breaker current. The different curves in each plot refers to 11 times of short-circuit, from 20ms to 30ms.

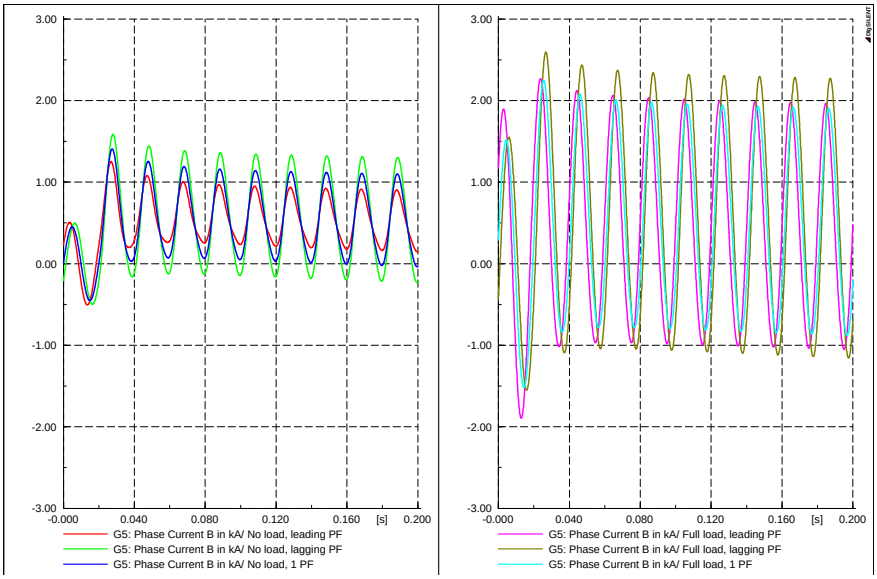

Fig. 4 Comparison of highest current asymmetry for no load (left plot) and full load (right plot) scenario; for leading, lagging and unity power factor.

3.4. Worst asymmetrical short-circuit current

Once the worst asymmetrical short-circuit current has been found to appear in the no load scenario with leading power factor, and the uncertain parameters in the generator have been confirmed; the analysis of the current in order to calculate the DC component as a specific ratio of the breaking current can be done.

From the instantaneous current the r.m.s. current, DC current and current amplitude can be calculated. Then based on the IEC definition with a breaking current at 80ms, for 60ms delay between the short-circuit and the contact separation, taking into account that the short-circuit occurred at 20ms. The decay of the DC contents is shown in Fig. 5. A maximum of 160% DC component was found.

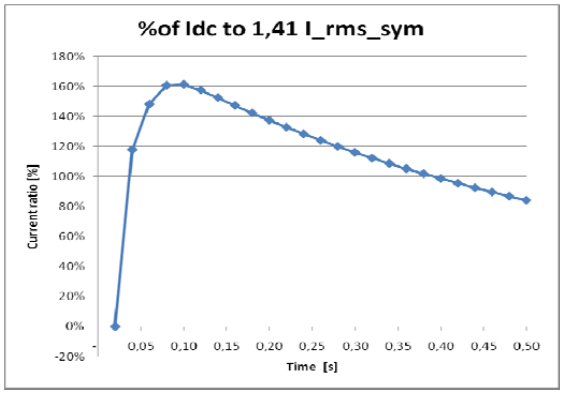

Fig. 5 DC component as a specific ratio of the breaking current, from the worst asymmetrical short-circuit current.

3.5. Normal Operating condition

Finally the normal operating condition for the Power Plant was modeled with three generators 80% load and 0.8 lagging power factor. From the instantaneous short-circuit current contribution from each generator, the r.m.s. currents, DC current and current amplitude can be calculated. It was found a maximum of 45% DC component.

4. CONCLUSIONS

Several simulations were performed in the digital model of a typical power plant under different operating condition, production levels and short-circuit times. Then, a sensitivity analysis on some missing parameters was also performed in order to account for uncertainties. Finally, it was found that the no load scenario with leading power factor and short-circuit time at 20ms would yield the worst asymmetrical short-circuit current. Here, a maximum of 160% DC component was found.

For the normal operating condition with three generators at 80% load and 0.8 lagging power factor and short-circuit time of 20ms, only a maximum of 45% DC component was reach.

5. DISCUSSION

The procedure to find the worst asymmetrical short-circuit current in a typical power plant was shown. This information could be used to select appropriate equipment, specifically generator circuit breakers. However, this comprehensive procedure is based on well known models of synchronous generators, industrial experience and accepted standards and recommendations; information not yet developed for the design offshore wind power plants.

Offshore wind power plants are based on extensive MV submarine cable collection networks connecting tens to hundreds of usually identical WTs placed in regular patterns with certain

interspacing and connected to a transformer station which in large wind farms is usually also placed offshore at which the voltage is raised to high voltage for transmission via a submarine export cable to a connection point in the public power system on land. Such arrangements are unusual as compared to a typical expansion of a power system in several ways such as: the lateral sizes of the systems, the large number of identical sub systems: generators, power converters, transformers, and switchgears in the WTs and collection network cable network; and also unusual compared to other power system´s operating conditions and environmental constrains.

Due to the demand of wind turbines, there are many different manufacturers with different technologies, and each year new wind turbines are developed. Hence, there are no standard values yet to compare wind turbine models, or the models available are not designed for EMT simulations.

6. REFERENCES

[1] IEC 60909-0, “Short-circuit Currents in Three-Phase AC Systems”, 2001-07.

[2] Kimbark, E.W. “Power system stability. vol. III. Synchronous machines”, an IEEE Re-issue, IEEE Press Power Systems Engineering Series (1995), Originally Published: New York: Wiley, 1956.

[3] Cosse, R.E., Jr.; Hazel, T.G.; Thomasset, G. “IEC medium-voltage circuit-breaker interrupting ratings-unstated short-circuit considerations”, IEEE Transactions on Industry Applications, vol. 36, issue.3 , pp. 884-892, 2000.

[4] IEEE Std. C37.09, “IEEE Standard Test Procedure for AC High-Voltage Circuit Breakers rated on Symmetrical Current Basis”, 1999 (R2007).

[5] Das, J. C. “Study of Generator Source Short-Circuit Currents with Respect to Interrupting the Duty of Generator Circuit Breakers, EMTP Simulation, ANSI/IEEE and IEC Methods”, International Journal of Emerging Electric Power Systems, vol. 9, issue.3, Berkeley Electronic Press, 2008.

Part 11

Postersession P1 - Wind Field Measurements and Simulations

- Flow Measurements in complex terrain using a 3D LIDAR Windscanner
  Nikola Vasiljevic, Risø DTU
- Lidar (Light Detection and Ranging) Measurement uncertainty in complex terrain
  Fernando Borbón Guillén, CENER
- Yaw Error Estimation Using Spinner Based LIDAR
  Knud Abildgaard Kragh, Risø DTU
- MCMC simulation of wind speed time series
  Jakov Krstulović Opara, University of Split
- New Model Development Concerning Turbulence and Wakes
  Thomas Ternisien, CRES
- Assessing wind energy potential using the high resolution meso-scale model RAMS
  Nicolas Barranger, University of Athens
- Simulation and Prediction of Wakes and Wake Interaction in Wind Farms
  Søren J. Andersen, DTU
- Downscaling of extreme wind using CFD
  Martin Vanandruel, CENER

Flow Measurements in complex terrain using a 3D LIDAR Windscanner

Nikola Vasiljevic[1)]

[1)] Risø DTU, Denmark

ABSTRACT

Many onshore wind turbines are being erected in hilly and mountainous areas. In terms of flow and resource modelling, such areas are described as 'complex' since sophisticated mathematical models are required to describe the mean flow and the turbulence. By using a Windscanner, which is a system comprising three individual lidar systems each with a modified scanner head, it is possible to measure 3D flow vector. This is done by steering the three beams to meet at a point, and by moving the beam intersection over an area of interest, a complete 3D flow field can be measured. The measured flow field can then be compared to model predictions.

KEYWORDS

Lidar, Complex Terrain, CFD

1 INTRODUCTION

Remote sensing techniques bring other dimension in measurements. One of the differences is the way the measurement is done. Standards point measurements are obtained from a mast-mounted cup anemometer, the volume-averaged wind vectors are obtained from a profiling wind lidar or sodar.

The oldest remote sensing technique for wind energy application is sodar [1]. This technique is based on sensing Doppler shift of sound waves in order to measure wind speed profiles. Due to the diffraction of sound and the relatively low speed of sound waves, the accuracy of sodars is inherently limited. Their price is lower comparing to lidars. Therefore, hybrid system consisting tall mast and a relatively low power sodar is often choice of wind farm planers since the high accuracy and availability of the cup anemometer complements the less accurate but highly relevant vertical resolution obtained by sodar.

The second remote sensing technique is lidar. Even they are been used for long period of time in meteorological applications such as measurement of thickness of boundary layer, or concentration of aerosols, recently they have been utilized for wind energy applications. The problem for utilizing was in high demand of accuracy (0.1 m/s) in order to be applicable for

niva@risoe.dtu.dk

wind energy. The first commercial versions of lidars appeared during the 2006. Lidars are using same principle of Doppler shift like sodars, this time light is the medium and shift of frequency of light is measured. Bending of beam due to wind isn't present. Since laser light travels very fast, almost 1 million times faster than a sound, drastically higher data sampling rates are achieved in contrast to sodars. With increase in temporal resolution, noise is decreased, while the potential accuracy is significantly increased.

Having high accuracy lidar will replace cup anemometers in near future. This will be achieved by fully certification and accreditation of lidars to industry standards. New and revised IEC lidar standards must be set and come into effect in order to achieve that.

2 HOW LIDARS MEASURE

Aerosols in the atmosphere move at the same speed as the wind, with exception during the rain. Having beam of coherent laser light at certain frequency 'shoot' in to the sky, lidar measure returned signal which is backscattered by the aerosols. This signal is the carrier of information of the wind speed along the line of the sight. Hence, this wind speed is extracted based on the Doppler shift information in returned signal. In coherent detection lidar, the signal is mixed with a local oscillator beam (un-shifted laser light) then detected with a photodetector. The resulting beat signal is a radio frequency (RF) photocurrent whose frequency, which can be estimated using digital or analog frequency discriminator techniques, is a direct measure of the Doppler shift. For estimation of wind velocity vector (u, v, w) it is required to measure three radial velocities from three independent Lines-Of-Sight (LOS). The most accurate approach to obtaining a vector wind measurement at a given point in space is to view that same point from three or more directions. For short-range measurements, this can be accomplished by using multiple apertures from the same lidar system, but for longer-range measurements multiple lidar systems are typically required (Windscanner). One widely used approach for measuring the vector winds is the velocity-azimuth display (VAD) or conical scan pattern (Figure 1). In a VAD scan, three or more independent LOS are achieved by scanning the beam in azimuth at a fixed elevation angle (conical angle). Conical scan technique is accurate for flat terrain. As the complexity of terrain increase this drives the appearance of distortions in flow leading to decrees of homogeneity in flow. By-product is large bias on the horizontal wind speed estimated from the lidar up to 10% in horizontal wind speed measurements [2]. Some of the lidar producers present smaller cone angle (Leosphere, 2009) or custom scan regimes (SgurrEnergy, 2009) as one of the possible solution to overcome the problem caused by inhomogeneous flow. The hypothesis that the lidar conical scan error due to inhomogenity of the mean flow is

independent of the cone angle on the horizontal components has been supported with experimental results from moderately-complex terrain site measurements [3].

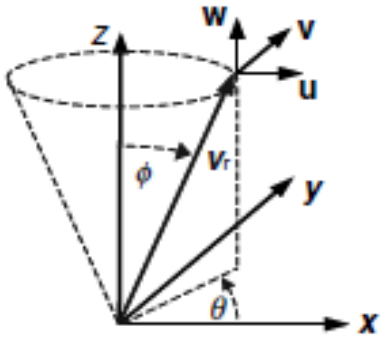

Figure 1: VAD technique, 3D scanning geometry.

Lidars can be used in complex terrain with support of flow models which should include well defined flow separation predictions. It is important to note that modelling must be accompanied by flow analysis before and after the measurements. Prior to the measurements, models should be used to detect possible suitable locations for lidar placement. This can be done with linearised or advanced CFD models because any of these can perform a simple assessment based on tough calculations of error values. Thus, majority of sub-optimal locations can be eliminated. Subsequently, any attempt to correct the lidar data must be performed with an advanced flow model, preferably a CFD model that has already been tested in complex terrain with measurements.

3 WINDSCANNER

As previously discussed, in order to solve the problem of complex terrain, one solution is to measure desired point/volume from three independent lines of sight. One of possibility to that is to use Windscanner, developed by Risø DTU [4]. Aim of this device is to measure real-time 3D wind vector. Hence, fully understanding of flows upstream of the turbine, near turbine, wakes of the turbine rotors and wind field. Creating database of measurements can lead at first stage in evaluation of CFD codes (EllipSys) and at the end their improvement. First prototype device consists of three ZephIR's wind lidars modified with fast adjustable focus length and equipped with 2D prism-based scan heads, in conjunction with a Windcube wind lidar for extended vertical profiling range. Two different designs are under development. Short-range is based on prototype design, considered to be in use for scanning around wind turbine since the CW lidars has high temporal resolution together with short probe length at the range of interest (near turbine). On the other hand long-range will have pulsed lidars in its

design, this gives the possibility to actually scan complete wind field of interest and to see how the wind flow behave on various types of terrain. Also it will be possible to see effects of large wind farms on wind flow in the terms of wakes.

4 CONCLUSION

Modelling the flow is encompassing certain sets of assumptions, averaging, and limitations. In order to enrich models capability to simulate “real” world, necessary is to supply representative database of measurements. Best practice doesn’t exist. After all, the major question since the Askervein hill project throughout Bolund experiment is still present: “**How to compare model results with measurements?”**

In order to compare models results with measurements in complex terrain first task is to supply sufficient quantity of data, not just temporal but furthermore spatial. By building and testing long-range Windscanner it is assumed that is possible to scan large volumetric portion of field of interest.

The important issues are:

- How to scan terrain in order to extract efficiency enough data per time/space?
- How to average this data (10 or 30 minute’s averages)?
- How from this set of measurements to create representative database?

Hence, using lidars for field measurement from start is introducing some amount of averaging effects, which in contrast to point measurements are giving outputs much more similar to models (i.e. WAsP). Also, scan will not have point to point movement; it will be more natural, measuring continuously, catching changes in wind field as whole, and actually “seeing” wind as it passes area. It is important to bypass randomness in ABL and unstable conditions of it during the measurements. Hopefully some level of measurements under same ABL condition (similar wind speeds, wind directions, temperature, etc.) is preferable.

BIBLIOGRAPHY

[1] G. H. Crescenti, "A look back on two decades of Doppler sodar comparison studies," *Bulletin of the American Meteorological Society,* vol. 78, pp. 651-673, Apr 1997.

[2] F. Bingöl*, et al.*, "Lidar performance in complex terrain modelled by WAsP Engineering," presented at the EWEC 2009, Marseilles, France, 2009.

[3] F. Bingöl, "Complex Terrain and Lidars," *Remote Sensing for Wind Energy, Risø-I-3068(EN)* vol. 1, pp. 118-135, 2010.

[4] T. Mikkelsen*, et al.*, "Wind Scanner: A full-scale Laser Facility for Wind and Turbulence Measurements around large Wind Turbines " presented at the EWEC 2008, Brussels, Belgium, 2008.

Lidar (Light Detection and Ranging)
Measurement uncertainty in complex terrain

Fernando Borbón Guillén[1)]

[1)] National Renewable Energy Centre (CENER) – CENER-CIEMAT Foundation.
Ciudad de la Innovación, nº 7; 31621 Sarriguren (Navarra), Spain.
fborbon@cener.com

ABSTRACT

Wind velocity measurements obtained with lidar devices rely on the assumption of homogeneous wind flow. However, in complex terrain conditions, the wind flow suffers from variations caused by the terrain orography. As a result, lidar measurements present higher uncertainty when compared to cup anemometer data. The aim of this research work is to reduce lidar measurement uncertainty in complex terrain by developing a data processing methodology to improve the measurement accuracy. Additional improvements are expected when considering wind vector information obtained by CFD simulations. By reducing lidar uncertainty, this technology is expected to have performance comparable to standard cup anemometry.

KEYWORDS

Remote sensing, lidar, complex terrain, measurement uncertainty, wind resource.

1 Introduction

Currently, lidars offer a mobile, easy-to-install wind remote sensing alternative, able to measure wind velocity at several heights. The most relevant assumption that lidar anemometry techniques lie on is the homogeneity of the air flow. This means the wind velocity vectors are considered to not change (very much) throughout the volume where lidar scans.

Literature indicates that lidar technologies have close correlation to standard cup anemometer measurements in flat terrain conditions. However, in complex terrain, the performance is degraded. Errors in the mean wind speed are in the order of 5% to 10%. Bingöl et al. [1] have appointed the vertical wind speed gradient as the main source of deviation in lidar measurements. Still, some considerable work has to be done in order to reduce the lidar uncertainty [2].

2 Experimental location: CENER's Alaiz experimental park

2.1 Terrain conditions

CENER's Alaiz experimental park is located at the top of a mountain of approximately 1000m height above surrounding plateaus. The mountain has a uniform slope facing north which extends nearly parallel to the west-east direction. The wind speed measurement instruments are positioned on the ridge top, as seen in Figure 1. The mountainous compound extends to the south-east direction where the orography becomes more complex.

2.2 Instrumentation

The met mast has been equipped with cup anemometers to sense the horizontal wind speed component, propeller anemometers to sense the vertical wind speed component and with wind vanes to sense the horizontal wind direction.

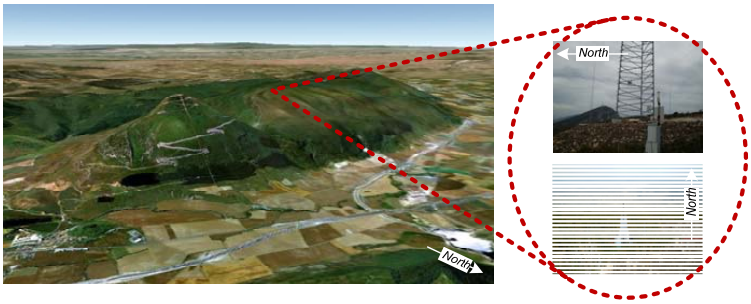

Figure 1. CENER's Alaiz experimental park. Lidar and met mast location indicated.

Sets of this instrumentation have been installed evenly at several heights. Correspondingly, the lidar was programmed to measure at four different heights coinciding with those from the met mast instrumentation. Measurements have been recorded during a period of approximately seven months.

3 Theory

Lidar devices scan wind velocity component parallel to the laser beam direction (so called radial or line of sight velocities). These measurements are spatially located in the perimeter of a horizontal circle situated at the desired height, as indicated by the points A and B in Figure 2. There, the actual wind vectors where drawn. Based on these measurements, an internal algorithm estimates the wind velocity by adjusting a weighting function using the previously obtained data. In flat terrain conditions where the wind flow is supposed to be

highly spatially homogeneous (see wind flow streamlines in Figure 2); the calculated wind vector (indicated by C in the same figure) is not so different from the measured wind vectors. Conversely, in complex terrain conditions, the uniform wind flow is disturbed by the irregular terrain orography. Therefore, changes in direction, vertical tilt, turbulence and flow acceleration are present. Subsequently, the measured vectors at points A and B can be considerably different both in direction and magnitude and do not necessarily represent properly the wind vector at the circle centre. As expected, the calculated wind velocity (based on the assumption of a homogeneous wind field) results in more discrepancy when compared to point measurements at the desired height; obtained with a cup anemometer installed in a met mast.

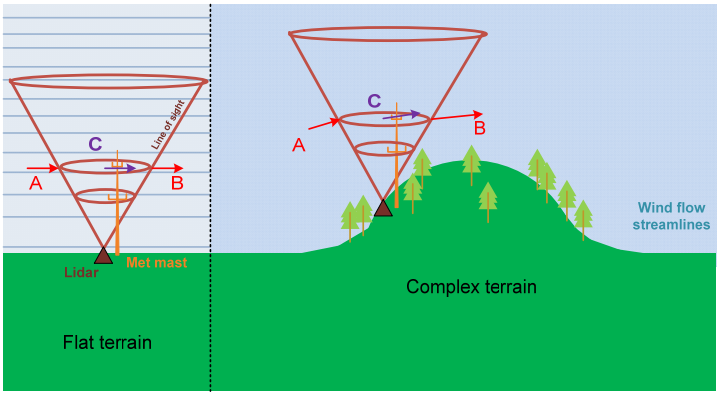

Figure 2. Lidar and met mast located in flat terrain and complex terrain conditions. Wind flow streamlines are shown. The wind velocity vector is drawn in locations A and B at spatial points where the lidar scans the radial velocity component. The velocity vector calculated by the lidar is drawn at the circle centre marked as C.

4 Lidar performance

The horizontal velocity averaged every 10 minute periods obtained with the lidar and the cup anemometer is plotted in Figure 3. Here, all wind directions where included and the values correspond to a height of 78 m. If the tendency line is plotted and forced to cross the coordinate system origin, a slope value of 0.91 is obtained, with a corresponding coefficient of determination of 0.991. As can be seen, despite using several quality filters, still there exist a considerable dispersion, with some values clearly distant from the main tendency. These values need further analysis in order to determine their causes.

Another source of comparable information is the vertical tilt angle sensed by the lidar and the one obtained based on the horizontal and vertical anemometers. As can be seen in Figure 4, for measurements at the shortest and largest heights, the ratio between lidar vs. cup measurements tends to be close to one. The biggest discrepancy occurs when the wind

blows from the direction range between 55º to 125º. Currently, several other parameters are being studied in order to identify what are the most relevant parameters that influence the correlation between cup anemometer and lidar measurements in complex terrain conditions.

5 Conclusions

Results from the CENER's Alaiz experimental park reveal the correlation between lidar and standard cup anemometer measurements in complex terrain conditions. High dispersion was found in the correlation graph, encouraging further research to determine the sources of discrepancy between the two instruments. The aim of this research works to develop a methodology to reduce the lidar uncertainty in complex terrain. For this reason, it is necessary a good understanding of what are the sources of discrepancy and their sensitivity in lidar vs. cup comparisons.

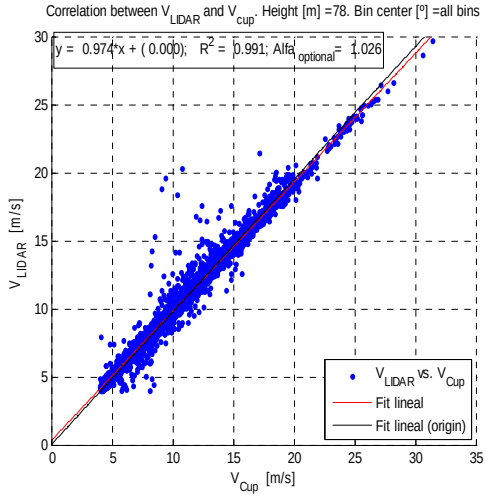

Figure 3. Horizontal wind speed

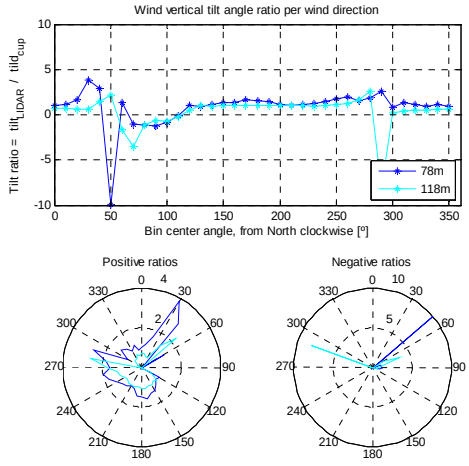

Figure 4. Vertical tilt angle ratio: lidar/cup.

BIBLIOGRAPHY

[1] Bingöl, F. et al. Lidar performance in complex terrain modelled by WAsP Engineering. EWEC 2009 Proceedings. Marseille, France, March 2009

[2] Lindelöw, P et al. Wind shear proportional errors in the horizontal wind speed sensed by focused, range gated lidars. IOP Conf. Series: Earth and Environmental Science 1 (2008) 012023

European Academy of Wind Energy

Norwegian University of Science and Technology

Yaw Error Estimation Using Spinner Based LIDAR

Knud A. Kragh[1)], Morten H. Hansen[1)], Torben Mikkelsen[1)]

[1)] Risø DTU, Wind Energy Department, Denmark

ABSTRACT

In this study a method for estimating the yaw error of a wind turbine based on measurements from a LIDAR mounted in the spinner is suggested. Simulations are performed in turbulent wind flows at one seed number, using the aeroelastic code HAWC2. Results show that with the spinner based LIDAR it is possible to estimate yaw errors in turbulent wind flows. Two scan patterns were tested and results show that a linear scan pattern gives the most precise estimates. The influence of turbulence intensity on the yaw error estimates was explored and a significant drop in the precision of the yaw error estimates was observed at increasing turbulence intensities.

KEYWORDS

LIDAR, yaw error, turbulence, yaw control, HAWC2

1 INTRODUCTION

When extracting energy from the wind using horizontal axis wind turbines, the ability to align the rotor axis with the dominating wind direction is crucial. This alignment is referred to as the yaw alignment and the rotational movement of the nacelle around the axis of the tower is the yaw of the turbine. Today's yaw alignment is mainly based on indirect measurements of the incoming wind flow, e.g. wind vanes or sonics atop the nacelle. T. Mikkelsen et. al[1] have demonstrated the experimental capabilities of Light Detection and Ranging, LIDAR, technology for measuring inflow, and demonstrated that it is not uncommon for a wind turbine in normal operation to exhibit a yaw misalignment above 10˚. For a perfectly aligned wind turbine, the maximum available energy in the wind P_{max} is defined as [2]:

$$P_{\max} = \frac{1}{2}\rho A_r V_0^{\,3} \qquad (1)$$

where ρ is the density of air, A_r is the projected area of the rotor, and V_0 is the free wind speed. If the turbine is misaligned by an angle of θ_{Err}, the wind speed perpendicular to the rotor plane is reduced to $V_p = V_0\cos(\theta_{Err})$. Hence the available energy is reduced by a factor of $\cos^3(\theta_{Err})$ and at $\theta_{Err}=10^{\circ}$, approximately 5 % of the available energy is lost. An improved yaw alignment could therefore have a considerable impact on the turbine power output.

In the present study the potential of LIDAR based yaw error estimation using a spinner based LIDAR is assessed. The study is based on a simulation of a 5MW turbine [4]

performed using the HAWC2 aeroelastic code developed at Risø DTU. A spinner based LIDAR with two different types of scan patterns has been implemented in the HAWC2 code and will provide simulated wind speed measurements. In the present study only the turbulence box used in HAWC2 will influence the results. A dedicated turbulence-modeling tool could have been used instead of HAWC2, but to enable later studies of inflow measurement based control strategies, the simulations were performed in HAWC2.

2 LIDAR MODEL, SCAN PATTERNS, AND YAW ERROR ESTIMATION

The basic principle of LIDARs is to measure the relative velocity of airborne particles in the atmosphere. In the planetary boundary layer these consists primarily of dust, smoke, pollen, etc.. It is assumed that the particles are carried with the wind at the instantaneous wind velocity. The velocity of the particles is estimated by analyzing the backscatter signature of a laser pointed in the desired measurement direction [5]. The implemented LIDAR extracts a line of sight measurement from a Mann turbulence box[6] in the direction of the laser beam.

Two scan patterns have been implemented; a circular and a linear, see Figure 3 and 4. For the circular scan pattern, the position of the focus point in the nacelle coordinate system is: $(x,y,z)=(-L_f sin(\theta_{meas})sin(\theta_{LIDAR}),-L_f sin(\theta_{meas}),-L_f\, sin(\theta_{meas})sin(\theta_{LIDAR}))$, where θ_{meas} is constant and θ_{LIDAR} is the azimuth angle of the beam and varies at a constant rate. For the linear scan pattern $(x,y,z)=(-L_f\, sin(\theta^{xy}_{meas}),-L_f\, cos(\theta^{xy}_{meas}), 0)$, where θ^{xy}_{meas} varies at a frequency.

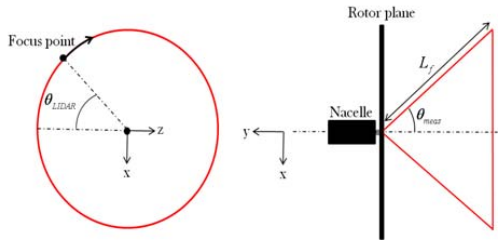

Figure 1: Circular scan pattern, $\dot{\theta}_{meas} = 0$ and $\dot{\theta}_{LIDAR} \neq 0$, in the nacelle coordinate system. Right: Top-view, left: View in the direction of the wind

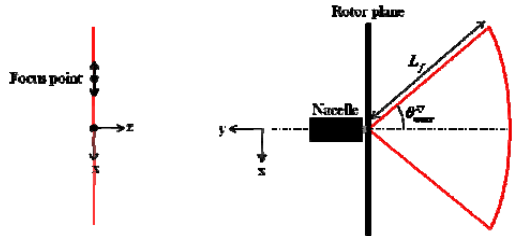

Figure 2: Linear scan pattern, $\dot{\theta}_{meas} \neq 0$ and $\dot{\theta}_{LIDAR} = 0$, in the nacelle coordinate system. Right: Top-view, left: View in the direction of the wind

For both scan patterns the yaw error is estimated by projecting the measured wind speeds into the x-y plane at the centre of the rotor plane, V_{xy}. For the linear scan this corresponds to the actual measured velocities. For the circular scan, a projection is necessary to estimate the in-plane wind speed and the in-plane measurement angle, θ^{xy}_{meas}. The transformations are given as:

$$V_{xy} = V(\theta_{meas}, \theta_{LIDAR}) \frac{1}{\cos(\theta_{meas} \cos(\theta_{LIDAR}))}, \qquad \theta^{xy}_{meas} = \theta_{meas} \sin(\theta_{LIDAR}) \tag{2}$$

As seen from Equation (2) the transformation assumes that the true wind speeds are in the x-y plane.

To estimate the yaw error, V_{xy} is evaluated as a function of θ^{xy}_{meas}. It is assumed that the largest value of V_{xy} will be measured at the θ^{xy}_{meas} aligning the LIDAR beam with the mean wind direction; hence the estimated yaw error is the θ^{xy}_{meas} maximizing V_{xy}. Since the simulations are performed in turbulence, time averaging is necessary for the estimates to converge. The measured/estimated V_{xy} is averaged at each θ^{xy}_{meas} and the curve used for finding the maximum value of V_{xy} is the curve consisting of the averaged values of V_{xy}.

3 RESULTS

The yaw error estimation method and scan patterns were tested at yaw errors from 0 to 25 deg., turbulence intensities from 1 to 20%, with and without wind shear (power law coefficient: 0.05) and with a turbulence seed number of 5. The results are shown in Figures 4 and 5 as root mean square errors of the estimates at actual yaw errors of 0-25 deg.. All the simulations had durations of 10 min, the LIDAR sampling frequency was 40 Hz and the estimated yaw errors where obtain from 10 minute averages.

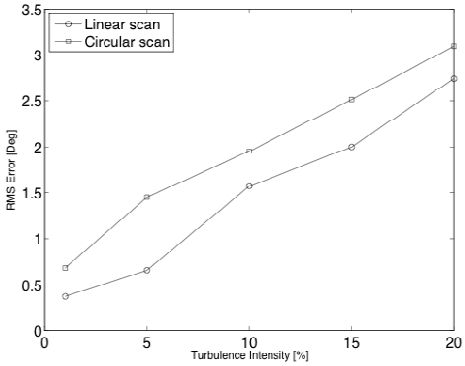

Figure 3: RMS error of the yaw error estimates for the linear and circular scan pattern as a function of turbulence intensity, mean wind speed: 12 m/s, no shear, $\theta^{xy}_{meas} \in [-15;15]$deg, L_f=100m, scan sweep period: 2 sec..

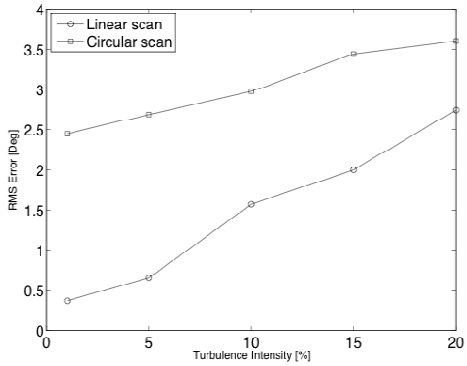

Figure 4: RMS error of the yaw error estimates for the linear and circular scan pattern as a function of turbulence intensity, mean wind speed: 12 m/s, shear, $\theta^{xy}_{meas} \in [-15;15]$deg, L_f=100m, scan sweep period 5 sec..

The simulations showed that the precision of the yaw error estimates were independent of the magnitude of the actual yaw error. From Figures 4 and 5 it is seen that for turbulence

intensities below 20% and without wind shear, the RMS error of the yaw error estimates of the linear scan pattern is below 3 degrees and 3.5 degrees for the circular pattern. In the situation with wind shear, the performance of the linear scan is unaffected while the performance of the circular scan is decreasing, even at a very modest level of shear. The affect of the shear on the circular scan results is due to a bias in the transformation.

4 CONCLUSIONS

In this preliminary study, a LIDAR mounted in the spinner of a wind turbine has been tested through simulations. It has been shown that the yaw error can be estimated with a precision below 3.5 degrees for turbulence intensities up to 20%, using the LIDAR measurements. Furthermore, it was shown that both with and without wind shear the linear scan pattern out-performed the circular scan pattern. The yaw error estimates from the linear scan was shown to be unaffected by the wind shear, while the precision of the estimates decrease when the circular scan pattern was used.

5 FUTURE WORK

Further studies are needed to establish a control strategy for the yawing of the turbine. The necessary averaging time as well as yawing threshold will be assesses by studying the statistics of the simulated measurements.

Further studies will also focus on exploiting the inflow measurements for pitch control. It is believed that the inflow measurements will provide information regarding wind shear, gusts and wakes, which can be used for load alleviation based on individual pitch control.

BIBLIOGRAPHY

[1] Mikkelsen, T., Hansen, K., Angelou, N., and Sjöholm, M., “LIDAR measurements from a rotating spinner,” Proceedings of EWEC2010, EWEC, 2010.

[2] Hansen, M. O. L., Aerodynamics of Wind Turbines, James & James, 2000.

[3] Harris, M., Bryce, D. J., Coffey, A. S., Smith, D. A., Birkemeyer, J., and Knopf, U., “Advance measurement of gusts by laser anemometry,” Journal of Wind Engineering and Industrial Aerodynamics, Vol. 95, No. 12, 2007, pp. 1637 – 1647.

[4] Jonkman, J., “NREL 5 MW baseline wind turbine”, Technical Report, NREL/NWTC, 1617, Cole Boulevard; Golden, CO 80401-3393, USA, 2005.

[5] Driggers, R. G., “Encyclopedia of Optical Engineering – Volume 2 of 3”, CRC, 2003.

[6] Mann, J. “Wind Field Simulation”, Probabilistic Engineering Mechanics, Vol. 13, No. 4, 1998, pp. 269-282.

European Academy of Wind Energy

Norwegian University of Science and Technology

MCMC simulation of wind speed time series

Jakov Krstulović Opara[1)], Ranko Goić[1)], Damir Jakus[1)]

[1)] Faculty of Electrical Engineering, Mechanical Engineering and Naval Architecture, University of Split, Croatia

ABSTRACT

Power system design issues require stochastic simulation methods in order to derivate synthetic time series for the stochastic source modelling. In this paper, essential aspects about the use Markov chain Monte Carlo (MCMC) method for wind speed activity simulation, are analyzed. Emphasis is given to simulation of multiple, spatially correlated wind speed time series. The modified MCMC simulation method is introduced, aimed to capture the stochastic dependency between the series, in conjunction with individual persistence.

KEYWORDS

Monte Carlo simulation, Markov chain, time series, stochastic dependency

1 INTRODUCTION

Designing a wind farm requires installing a meteorological station at a potential location and recording all the relevant wind data series. Respective time series obtained from mast measurements are usually not long enough in order to capture wind stochasticity and may lead to biased conclusions regarding system design issues and analysis of impacts on power system operation. Therefore, it becomes necessary to use simulation techniques for the derivation of synthetic time series for the modelling of wind activity. Since wind speed is conditioned with lots of climatologic, atmospheric and environmental parameters, such phenomena are impossible to deterministically describe, so various probabilistic and stochastic methods appears as more appropriate. In the case when certain persistency exists in a generated time series, the MCMC simulation method is appropriate to apply. In this paper, besides the basics of MCMC method for wind speed time series simulation, the emphasis is given to the simulation of multiple wind speed time series, measured on geographically spread wind farms, according to the method proposed in [1].

2 MARKOV CHAIN MONTE CARLO SIMULATION

The basic idea of using Markov chain Monte Carlo method, in order to generate wind speed time series base on measured pattern, intends to model wind speed data as a Markov chain, while the Monte Carlo simulation is used as a tool for generating new data.

jakov.krstulovic-opara@fesb.hr

2.1 Markov chain

The Markov chain of n^{th} order is a mathematical model of a discrete-time random variable, where the future state depends on the n previous states of the process. The probability of the transition to state j for the n^{th} order Markov chain is defined with [2]:

$$\Pr\{X_t = j \mid X_{t-1} = i_1, ..., X_{t-n} = i_n\} = p_{i_n i_{n-1} \ldots i_1 j} \quad (1)$$

The probabilities are obtained by computing all appropriate transitions in the time series:

$$p_{i_n i_{n-1} \ldots i_1 j} = \frac{n_{i_n i_{n-1} \ldots i_1 j}}{\sum_{j=1}^{m} n_{i_n i_{n-1} \ldots i_1 j}}, 0 \le p_{i_n i_{n-1} \ldots i_1 j} \le 1, \sum_{j=1}^{m} p_{i_n i_{n-1} \ldots i_1 j} = 1, \forall i = 1, \ldots m \quad (2)$$

Since these probabilities are constant in time and divided by equal time steps, it is possible to formulate a transition probability matrix, which is generally size $(mxm)^n$, where m is the number of defined states of variable, and n order of the chain.

2.2 MCMC simulation

Markov chain Monte Carlo methods are a class of algorithms used for sampling from probability distributions based on Markov chain. The first step in an MCMC simulation is to define the states and the transition probability matrix of the associated Markov chain. A further simulation step requires construction of the cumulative probability transition matrix so that each row corresponds to the discrete cumulative distribution function (*cdf*) for the next transition. For the first order MCMC the simulation starts with arbitrarily assumed initial wind speed (e.g. state *i*), and the next state is obtained comparing randomly generated number between 0 and 1 with elements of the *i*th row of the cumulative probability transition matrix. Assuming this number falls between elements *j*-1 and *j*, the subsequent element of the process is defined as a random number between the boundaries of the state. To sample the next transition, the same procedure is repeated for the row *j*. In case of a n^{th}-order Markov chain, the simulation procedure is analogous, but with n initial assumed states. When defining the states, it is important to note that a higher resolution of the states definition leads model to better accuracy, but significantly increases complexity. It is interesting to note thet higher values in the transition probability matrix are gathered around the main diagonal generally indicate high chronological persistence of the wind speed [3].

3 MCMC SIMULATION RESULTS

In this paper MCMC simulation is used in order to synthetically generate wind speed time series based on measured dataset of 10 min wind speed averages, over one year period (52560 data). The results shown on the Figure 1 shows very good matching of probability

density function (*pdf*) between original and generated data by all first, second and third order Markov chain models.

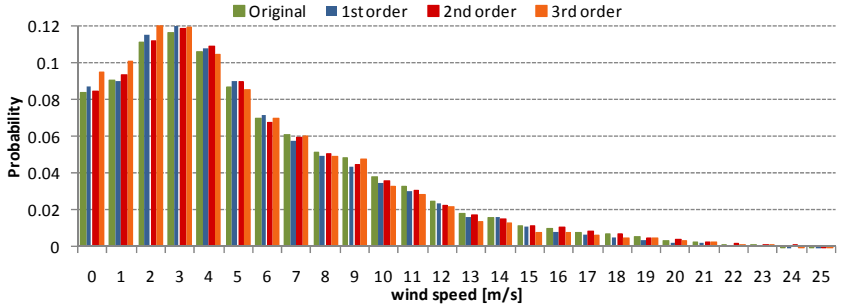

Figure 1: Probability distribution of observed and synthetically generated wind speed

Additionally, in order to determine the persistency structure in the measured and the generated wind speed data series, the autocorrelation function (*acf*) is used. Figure 2 shows that all generated data series keeps persistence in the short term lag, but for the longer time scales fail to retain the persistence of the original data. Also, the exponential fall of autocorrelation is faster for the first order, while for the higher orders Markov chain it slows, matching closer the original. Consequently, since the *acf* reveals wind variations on different time scales, observed simulation model can adequately simulate only short-term variations, while the longer term variations could significantly mismatch the original ones. However, better representation of the *acf* and longer term variations could be obtained using a longer wind speed averaging window [3]. Furthermore, if the aim of the simulation is the power output of the wind farm, direct generation of wind power appears to be superior to indirect generation via wind speeds, since it leads to a reduced number of states and a lower order Markov chain, at equal power data resolution [3].

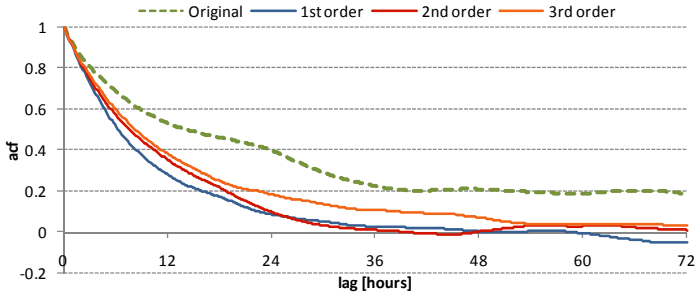

Figure 2: The autocorrelation functions of the original and generated wind speed data series

4 SIMULATION OF MULTIPLE TIME SERIES

Wind farm production analysis mostly includes multiple wind speed (power) time series. Namely, since the geographical spreading of wind power reduces variability and

intermittency and increases predictability, it is relevant to take into account all relevant wind farms. Generally, simulation of multiple time series presents an extra challenge for the model, if the stochastic mutual dependence between the series is required. According to the recent paper [1], modified MCMC simulation method is proposed, aimed to generate multiple time series, while preserving individual persistence, as well as their mutual dependency. The idea is to model all time series as one Markov process, but with separate transition probability matrices for each series. Transition probabilities are defined in such a way that the future state of one time series depends on it's previous state and on recent states in all other time series. Therefore, the order of the Markov chain and number of transition probability matrices needs to be at least equal to the number of the considered time series.

Table 1: Correlation matrix of original and simulated time series

			Site		
			1	2	3
Site	1	Original	1,00	0,65	0,58
		Model	1,00	0,66	0,56
	2	Original		1,00	0,63
		Model		1,00	0,57
	3	Original			1,00
		Model			1,00

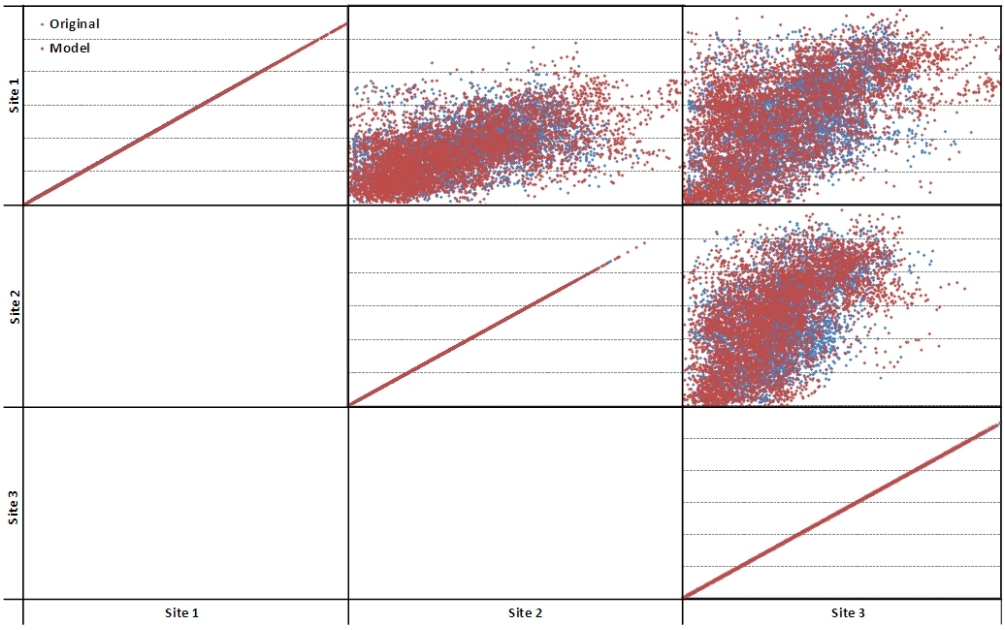

Figure 3: Scatter diagrams of original and generated time series

In order to verify time series simulated for three wind farm sites, the spatial correlation is represented using correlation square matrix (Table 1). Each row of the correlation matrix shows the correlation between one site and all the other sites, so that the diagonal is

composed of ones and the other elements are cross-correlation between sites. Also, scatter diagrams on the Figure 3 show very good match between the data simulated by introduced model and the original data. The main limitation of the presented simulation method lies in potentially high memory space requirements, since the size of the transition probability matrix exponentially grows with order of the Markov chain, i.e. number of wind farms sites.

5 CONCLUSIONS

Since the power systems are more frequently based on stochastic sources, system design issues require various simulation methods for power series generation, based on a measured data. In this paper, Markov chain Monte Carlo simulation method is discussed, as an appropriate representation of wind speed regarding probability density function and the persistency on the certain time lag range. Wind power production analysis and impact on power system operation, requires considering multiple wind farms on larger geographical area. Therefore, in order to simulate multiple time series the modified MCMC simulation method is presented, which allows modelling of mutual dependency of time series, in conjunction with preserving individual statistical parameters.

BIBLIOGRAPHY

[1] R. Goić, J. Krstulović; D. Jakus - Simulation of Aggregate Wind Farm Short-term Production Variations, Renewable Energy 2010 Volume 35, Number 2602-2609

[2] S.P. Meyn, R.L. Tweedie, Markov Chains and Stochastic Stability, first ed., Springer-Verlag, London, 1993.

[3] G. Papaefthymiou, B. Klöckl, MCMC for Wind Power Simulation, IEEE transactions on energy conversion, 23 (2008), no. 1.

European Academy of Wind Energy

Norwegian University of Science and Technology

New Model Development Concerning Turbulence and Wakes

T.TERNISIEN [1], J.PROSPATHOPOULOS[1] , P.K.CHAVIAROPOULOS [1]

[1] Center For Renewable Energy Sources CRES, Pikermi,Greece

ABSTRACT

As all turbulent closure models based on the Boussinesq approximation, the k–ω one cannot account for the anisotropic part of the Reynolds stress tensor and, thus, cannot properly split the turbulent kinetic energy to its diagonal components. Improving the Reynolds stresses modelling will also improve the overall accuracy of our code CRES–flowNS, in particular when secondary flows are dominant due to highly complex terrain. The objective of the proposed work is, therefore, to implement an atmospheric EARSM model in CRES-flowNS building upon the currently available k–ω model.

KEYWORDS

Wakes, atmospheric, CFD, Turbulence models, EARSM.

1 INTRODUCTION

Wind energy community has an increasing interest in wake modelling for two main reasons. Obviously, accurately quantifying power losses due to wind turbine wakes is an important part of the overall wind farm economics. In parallel, the need for maximizing the deployment of wind energy leads to installing machines at the closest possible distances, increasing thus the interaction phenomena and affecting the performance of the downstream turbines by reducing their power output and increasing the fluctuating loads.

More accurate models of the wakes are so needed.

2 CODE DETAILS

The 3–D incompressible Navier-Stokes equations are numerically integrated by means of an implicit pressure correction scheme [1]. A matrix-free algorithm for pressure updating is introduced, which maintains the compatibility of the velocity and the pressure field corrections, allowing for practical unlimited large time steps within the time integration process. Spatial discretization is performed on a computational domain, resulting from a body-fitted coordinate transformation, using finite difference/finite volume techniques. The convection terms in the momentum equations are handled by a second order upwind

ternisien@cres.gr

scheme bounded through a limiter. Centred second order schemes are employed for the discretization of the diffusion terms. The Cartesian velocity components are stored at grid-nodes. On the contrary, pressure is computed at mid-cells. This staggering technique allows for pressure field computation without any explicit need of pressure boundary conditions. A linear fourth order dissipation term is added into the continuity equation to prevent the velocity-pressure decoupling. To accommodate the large computational grids needed in most applications for a fair discretization of the topography at hand, a multi-block version of the implicit solver has been developed.

3 TWO-EQUATION TURBULENCE MODELS

3.1 Boussinesq Hypothesis

In the context of two-equation modelling, the Reynolds stress tensor $\overline{u'_i u_j}'$ is assumed to be an algebraic function of the local mean-velocity gradient and two turbulent scale variables:

$$\overline{u'_i u_j}' = -2\nu_T S_{ij} + \frac{2}{3}k\delta_{ij} \quad (1)$$

Where, for the most popular models, the so-called eddy viscosity ν_T is a function of k and ω or k and ε. [2]

3.2 Overestimating

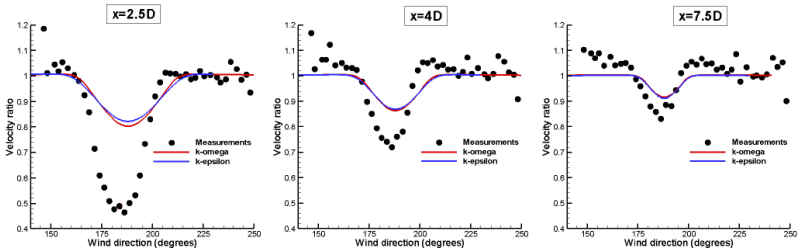

Figure 1: Comparisons of axial velocity profiles of the two-equation models k- ω , k-ε, with measurements, in the wake of a wind turbine at 2.5, 4 and 7.5 diameters downstream of the wind turbine [3] .

Especially in the near wake of the wind turbine, *Figure 1* shows an overestimating of the axial velocity for both turbulence models using the Boussinesq approximation.

The assumption of velocity linearity over the turbulent length scale may not be valid in the wake boundary region; a more accurate modelling of the Reynolds stress tensor is needed.

4 NON LINEAR REYNOLDS STRESS MODELLING

4.1 ARSM (Algebraic Reynolds Stress Model)

The Reynolds stress components can be divided into an isotropic part and an anisotropic part a_{ij} defined as:

$$a_{ij} = \frac{\overline{u'_i u_j'}}{k} - \frac{2}{3}\delta_{ij} \tag{2}$$

We can derive the equation of transport of the anisotropy tensor a_{ij} from the equation of transport the Reynolds stress tensor [4].

The idea of the ARSM is that the convection and diffusion of a_{ij} may be neglected; we then obtain an equation taking the following form:

$$a_{ij}\left(\frac{P}{\varepsilon} - 1\right) = \frac{P_{ij}}{\varepsilon} - \frac{\varepsilon_{ij}}{\varepsilon} + \frac{\phi_{ij}}{\varepsilon} + C_{ij} \tag{3}$$

Where P_{ij} is the production term and $P = P_{ii}/2$, ε_{ij} is the dissipation rate tensor, ϕ_{ij} the redistribution term and C_{ij} the Coriolis term.

P_{ij} and C_{ij} can be computed directly, only ε_{ij} and ϕ_{ij} need modelling.

We can find the expression of the implicit equation form of (3) in the document of Rodi [4].

4.2 EARSM (Explicit Algebraic Reynolds Stress model)

However the implicit ARSM relation for the Reynolds stress anisotropy tensor has been found to be numerically and computationally cumbersome since there is no damping present in the equations. A more simple way to calculate a_{ij} can be found.

Indeed, it can be mathematically proved that the most general form for the Reynolds stress tensor a_{ij} in terms of **S** and **Ω**, (which are respectively the strain rate tensor and the vorticity tensor), can be written in a compact form as [5]:

$$\mathbf{a} = \beta_1\mathbf{S} + \beta_2(\mathbf{S}^2 - \frac{1}{3}II_S\mathbf{I}) + \beta_3(\mathbf{\Omega}^2 - \frac{1}{3}II_\Omega\mathbf{I}) + \beta_4(\mathbf{S\Omega} - \mathbf{\Omega S}) + \beta_5(\mathbf{S}^2\mathbf{\Omega} - \mathbf{\Omega S}^2)$$

$$+ \beta_6(\mathbf{S\Omega}^2 + \mathbf{\Omega}^2\mathbf{S} - \frac{2}{3} IV\mathbf{I}) + \beta_7 (\mathbf{S}^2\mathbf{\Omega}^2 + \mathbf{\Omega}^2\mathbf{S}^2 - \frac{2}{3} V\mathbf{I}) + \beta_8(\mathbf{S\Omega S}^2 - \mathbf{S}^2\mathbf{\Omega S})$$
$$+ \beta_9(\mathbf{\Omega S\Omega}^2 - \mathbf{\Omega}^2\mathbf{S\Omega}) + \beta_{10}(\mathbf{\Omega S}^2\mathbf{\Omega}^2 - \mathbf{\Omega}^2\mathbf{S\Omega}^2) \quad (4)$$

Where II_S, II_Ω, IV, and V are invariants of **S** and **Ω**.

Inserting (4) in equation (3) and using the appropriate models for ε_{ij} and ϕ_{ij} we obtain the complete EARSM system of equations [5].

5 CONCLUSIONS

Current models using the Boussinesq approximation fail to properly simulate the physical mechanisms that occur in the near wake of wind turbines.

Our goal is here to increase the accuracy of already existing turbulence models without excessively increasing the computational costs. We so suggest implementing an atmospheric EARSM (Explicit Algebraic Reynolds Stress Models) as an intermediate model in between two-equation models and LES (Large Eddy Simulation) scheme.

BIBLIOGRAPHY

[1] PK Chaviarapoulos and DI Douvikas. Mean flow field simulations over complex terrain using a 3-D Reynolds Averaged Navier-Stokes solver. *Computational fluid dynamics'98*, pages 842_848, 1998.

[2] D.C. Wilcox, Turbulence Modelling for CFD, *DCW Industries Inc., La Canada,* California, IBSN 0-9636051-0-0, 1993.

[3] JM Prospathopoulos, ES Politis, and PK Chaviaropoulos. Modelling wind turbine wakes in complex terrain. Proceedings EWEC 2008, Brussels, Belgium, 2008.

[4] W. Rodi. A new algebraic relation for calculating the Reynolds stresses. *Z. angew. Math. Mech.,* 56:219–221, 1976. [5] Wallin

[5] S. Wallin. Engineering turbulence modelling for CFD with a focus on explicit algebraic Reynolds stress models. *KTH Doctoral thesis*, 2000.

European Academy of Wind Energy

Norwegian University of Science and Technology

Assessing wind energy potential using the high resolution meso-scale model RAMS

Nicolas Barranger

University of Athens, Greece

ABSTRACT

The regional atmospheric model RAMS has been developed for meteorological purpose. It solves the unsteady dynamical equations governing the atmospherics physics from the synoptic scale down to mesoscale and microscales. Its last evolution include particle and pollutant dispersion as far as an elaborate parametrisation of cloud physics.

The aim of this study is to use it as a tool for wind farm sitting and focus on the microscale physics of the so called atmospheric boundary layer. A special attention will be devoted to the interaction between the topography and the induced turbulence. A clear assessment of the turbulent scheme will be detailed and its limitations and improvement will be discussed.

KEYWORDS

Mesoscale model, turbulence, wind sitting.

1 INTRODUCTION

Generally, advanced CFD is used as a model to study the flow structure over complex terrain[1]. The alternative proposed here is to use a meteorological model to catch the microscale effect such as turbulent flux and wind speeds near the surface.

RAMS model is a regional meteorological model that can provide a complete description of the mesoscale effects of turbulence. The usual low resolution turbulence models(Mellor-Yamada) is often applied blindly at higher resolutions that does not fit to microscale turbulence characteristics[2]. Two equation turbulence model E-epsilon and one equation E-l has been implemented this last decade[3]. This last development enables the use of very high grid resolution(order of meters) and models very precisely particle dispersion in complex area such as urban canopy[4]. The effort that have been deployed to “tune” this mesocale model in order to solve turbulence on smaller scale is an asset in modelling wind speed and turbulent kinetic energy for wind sitting purpose.

The advantages of using this model is a complete description of the thermodynamic equations and the study of interaction between mechanically forced wind over stable unstable or neutral conditions.

nbarranger@mg.uoa.gr

A complete parametrisation of radiation and moisture processes allows a better description of the microscale physics. Several other capabilities are implemented such as data assimilation and nudging[5]. Models prediction can be significantly improved using stochastic methods such as Model output statistics[6] or recently developed Kalman filters[7,8].

2 TURBULENT SCHEME AND THEIR IMPLEMENTATION IN RAMS

RAMS allows the use of 4 different turbulent schemes which are or Yamada 2.5 Level[9,10], Deadorff[11],E-l and E-epsilon[12]. It solves the Navier Stokes equation using finite difference method and use a first order approximation to compute turbulent flux using K-theory.

Mellor Yamada Level 2.5 scheme is aimed to calculate vertical diffusion coefficients and therefore horizontal diffusion terms are neglected. The diffusion coefficient is computed as follow: $K_m = S_m l \sqrt{2}\, E^{1/2}$ where l is the master turbulent length scale, Sm is a function that depends on empirical constants related to shear stress. The master length scale is computed using the Blackadar[13] formulation. A prognostic equation is set up in order to calculate turbulent kinetic energy E in the boundary layer approximation. The diffusion coefficient for turbulent kinetic energy are computed in the same way as the momentum one, the two coefficients differs from a constant.

The Deadorff scheme is a large eddy simulation model. It means that it solves the subgird scale model using subgrid filter. Here the filter is the grid itself. There we consider the turbulent length scale l to be the equal to the grid box length. In other words $l = \Delta x$.

The turbulent momentum coefficient is computed using the formula: $K_m = 0.1 l \sqrt{2}\, E^{1/2}$

The prognostic equation for the TKE is the same as mentioned for the Mellor Yamada scheme. The shear production is now computed in all direction.

The E-l scheme is also based on a complete TKE equation and the turbulence is also defined as anisotropic. It means that turbulent diffusion coefficients are the same in each directions. Practically, it has to be pointed out that this scheme represent well small scale turbulence and that the grid domain size must be equal in each direction.

The E-ε scheme is a two equation turbulence scheme that use prognostic equation from turbulent kinetic energy and its dissipation rate. It is well adequate for small scale anisotropic turbulence for the same reasons mentioned in the two previous schemes.

3 ADVANTAGES OF EACH MODEL

On smooth surfaces, the four schemes represent well the turbulent kinetic energy and wind speed and is coherent with data observations. However, on complex terrain each model gives significant deviation from data experiments[14]. The Mellor yamada Level 2.5 is generally used for low resolution simulation. It uses the boundary layer approximation that is not well suited for three dimension topography. However it has been pointed out that It catches well recirculation immediately down a hill and gives correct values of wind speed. The three other schemes better predict turbulent kinetic energy profiles in complex topography. The Deadorff scheme is very sensitive to the grid generation since the filter used (large eddy simulation theory) is the grid itself and assumes that over the grid scale the turbulence is developed by the bulk motion. For E-l model a correct boundary layer parametrisation is essential since it uses one equation for turbulent prognostic but its implementation into RAMS gives the best values of turbulent kinetic energy profiles. E-ϵ provide a complete equation system for turbulence closure and provide a good transport of turbulent kinetic energy towards higher level.

4 CONCLUSIONS

This paper covers the state-of-the-art in using the regional model RAMS on high resolution. Details about turbulent parametrisation have been presented. It clearly shows that Mellor Yamada model has some limitation concerning high resolution simulation and is not appropriate for isotropic small scale turbulence.

The E-ε scheme is the most advanced high resolution turbulent scheme available and still needs further development in its implementation into RAMS. E-l and Deadorff scheme have been demonstrated to be the most reliable schemes and are a good basis for validation purpose.

The future works will be to improve the turbulent schemes and to assure that they are working in a large range of situation such as a multiple choice of topography in agreement with complex terrain diversity. In facts, E- ε model is highly influenced by topography and the closure hypothesis needs to be double checked for each case.

Implementation of other turbulent schemes will be discussed as it could be better for comparison of high resolution turbulence. K-ω model will be an advantage. Even if this model is not common in atmospheric physics, it is often used in CFD models and seems to be more adequate than E- ε in modelling the atmospheric boundary layer. A step further will be to take advantage of RAMS possibilities such as running simulations in non-neutral conditions, use grid nesting and Lagrangian particle tracer for wind turbines wakes.

BIBLIOGRAPHY

[1] Stangroom P., CFD modelling of wind flow over complex terrain, 2004, PhD thesis University of Nothingham.

[2] Hara T., Trini-Castelli S., Obha R., Tremback C., 2009: Validation of turbulence closure schemes for high resolution in mesoscale meteorological models- A case of gas dispersion at the local scale, Atmosheric environements 43 3745-3753.

[3] Trini Castelli S., Ferrero E. and Anfossi D., 2001: Turbulence closure in neutral boundary layer over complex terrain. Boundary layer Meteorology, n. 100, 405-419.

[4] Trini Castelli S. and Reisin T. G., 2008, Application of a modified version of RAMS model to simulate the flow and turbulence in presence of buildings: the must COST732 exercise, International Journals of Environment and Pollution, in press

[5] Trini Castelli S., Reisin T. G. and Tinarelli G., 2008, Development and Application of MicroRMS Modelling System to Simulate the Flow, Turbulence and dispersion in the Presence of buildings. Air Pollution Modelling and its Applications XIX, Ed., 81-89

[6] Alessandrini S., Decimi G., Palmieri L., Ferrero E.,2009: A wind power forecast system in complex topographic conditions, EWEC 2009 Marseille

[7] Galanis G., Louka P., Katsafados P., Kallos G., Pytharoulis I., 2006: Application of Kalman filters based on non-linear functions to numerical weather predictions, Annales Geophysicae.

[8] Von Bremen L.,2007: Combination of Deterministic and Probabilistic Metorological Models to enhance Wind Farm Power Forecasts: 2007, Journal of Physics: Conference Series 75.

[9] Mellor G., Yamada T.,1982: Devellopement of a turbulent closure model for geophysical fluid problems, Rev. Geophysics. Space Physics. 20 , 851-875.

[10] Mellor G., Yamada T.,1974: A hierarchy of turbulence closure models for planetary boundary layers, Journal of atmospheric Science 31, 1791-1806.

[11] Deadorff J., 1980: Stratocumulus-capped mixed layers derived from a three-dimentional model, Boundary layer meteorology, 18, 495-527.

[12] Trini Castelli S., Ferrero E., Anfossi D. and Ohba R., 2005: Turbulence closure models and their applications in RAMS. Environmental Fluid Mechanics, 5, 169-192.

[13] Blackadar A., 1962: The vertical distribution of wind and turbulence exchange in a neutral atmosphere, Journal of Geophyscics 67, 3095-3102

[14] Ferrero E., Tritelli S., Anfossi D., 2003: Turbulence fields for atmospheric dispersion models in horizontally non-homogeneous conditions. Atmospheric environments.

European Academy of Wind Energy

Norwegian University of Science and Technology

Simulation and Prediction of Wakes and Wake Interaction in Wind Farms.

Søren J. Andersen[1)], Stefan Ivanell[2)], Robert Mikkelsen[1)], Jens N. Sørensen[1)]

[1)] DTU Mechanical Engineering, Technical University of Denmark

[2)] University of Gotland, Sweden

ABSTRACT

The present paper gives a brief overview of previous work at DTU Mechanical Engineering using the actuator disc and actuator line methods in CFD modelling to simulate flows around wind turbines. Future investigations will focus on CFD simulations of wakes and wake interaction in wind farms through a parametric study, investigating such effects as sheared inflow, incoming turbulence, wake meandering, stability of the atmospheric boundary layer and spacing of wind turbines.

KEYWORDS

Wind farms, wakes, turbulence modelling, CFD modelling, actuator line, parametric study.

1 INTRODUCTION

The Navier-Stokes based actuator disc method was introduced by Sørensen and Myken, (1992) to simulate axisymmetric flows about wind turbines. An extension to full 3-dimensional flows was later introduced by the actuator line technique developed by Sørensen and Shen (2002). Later Mikkelsen (2003) implemented the actuator disc and line methods in the CFD modelling code, EllipSys3D, which is a finite-volume, multi-block general purpose Navier-Stokes code developed as a collaborate work between DTU (Michelsen, 1992) and Risø (Sørensen, 1995). Previously, in their PhD work, Troldborg (2008) and Ivanell (2009) used the actuator line technique to simulate single and multiple wind turbines clustered in wind farms. The present work is a continuation on previous work using EllipSys and the actuator line technique to perform large eddy simulations to simulate and optimize wind farms.

2 PREVIOUS RESULTS

2.1 General Wake Development

The conceptual development of the wake from a rotating wind turbine is illustrated in Figure 1. The wake includes three individual tip and root vortices stemming from each blade, which moves downstream as distinct helical structures before eventually collapsing.

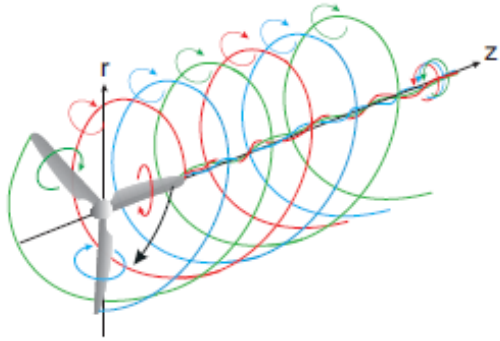

Figure 1: Development of a wake behind a wind turbine (Ivanell, 2009).

2.2 Large wind farms

Ivanell (2009) modelled an idealized Horns Rev wind farm using the actuator disc method and periodic boundary conditions to simulate an infinitely large wind farm consisting of two central rows of 10 wind turbines. Figure 2 shows velocity plots for nine wind turbines at hub height for different inflow directions for both laminar and turbulent inflow, top and bottom row respectively. Introducing ambient turbulence (bottom row) has a significant impact on the velocity experienced by downstream wind turbines as the turbulence ensures mixing with the ambient velocity, hence increasing the velocity in the wake. Similarly, it is seen how the velocity experienced by the downstream wind turbines differ significantly between the various inflow directions depending on how the downstream turbine is positioned relative to the incoming wake.

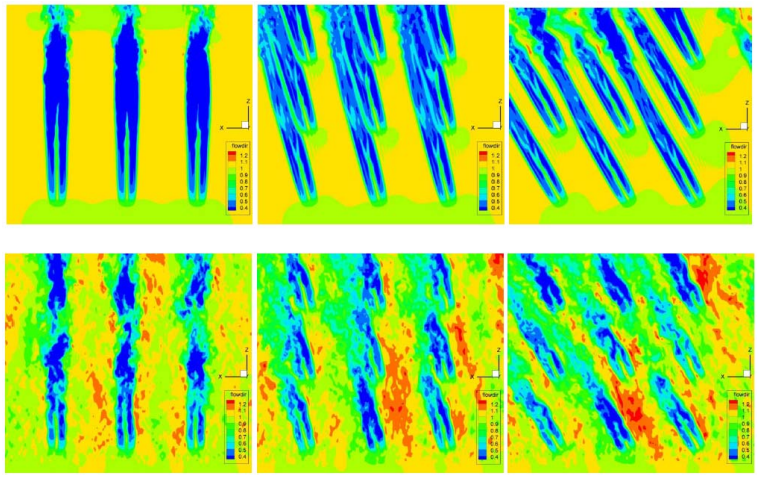

Figure 2: Contours of the inflow velocity at hub height and different flow directions: a) 265°, b) 270°, c) 285°, and laminar and turbulent flows. Reproduced from Ivanell et al., 2008.

Figure 3 shows simulated and measured power production normalized by the power production of the first wind turbine. Overall, the agreement is fair, and it is good for +5, +10, and +15 degrees, validating the overall performance of the model and giving valuable information on design optimization for wind farms.

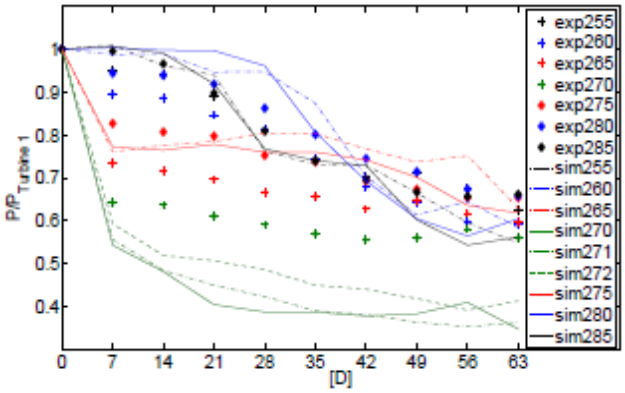

Figure 3: Comparison between computed and measured power performance shown for inflow angles between 255 and 285 degree, i.e. ±15 degrees from the westerly direction. Reproduced from Ivanell, 2009.

2.3 Future work

The future work will focus on extending the previous findings of wind farm simulations by utilizing the actuator line method, since the increase in available computational power makes it possible to simulate entire wind farms with sufficient details. The actuator line method increases the level of detail by including tip vortices in the simulations. A comprehensive parametric study will investigate the influence of effects such as stability and shear of the atmospheric boundary layer, vortex collapsing and transition between near and far wake, ambient turbulence, spacing of the turbines and wake meandering on the overall power production and loads on clustered wind turbines. The aim of the parametric study is to update guidelines and recommendations for the design and layout of future wind farms.

3 CONCLUSIONS

The present paper has presented a brief overview of previous work conducted on numerical simulations of wind turbine wakes using the actuator disc/line technique. The increase in computational power makes it possible to push the limits of numerical investigations, as it is now possible to simulate medium to large scale wind farms with sufficient details of the individual wind turbines, represented by actuator discs or lines. A thorough parametric study will aim at updating guidelines and recommendation for the design of future wind farms.

BIBLIOGRAPHY

[1] Sørensen, J.N. and Myken, A. (1992) "Unsteady Actuator Disc Model for Horizontal Axis Wind Turbines". Journal of Wind Engineering and Industrial Aerodynamics**,** vol. 39, pp. 139-149.

[2] Sørensen, J.N. and Shen, W.Z. (2002), “Numerical Modelling of Wind Turbine Wakes”, Journal of Fluids Engineering, vol. 124, no. 2, pp. 393-399.

[3] Ivanell, S., Mikkelsen, R., Sørensen, J. N., Henningson, D. (2008) – Three-dimensional actuator disc modelling of wind farm wake interaction. European Wind Energy Conference and Exhibition, Brussels.

[4] Ivanell, S. S. A. (2009) – Numerical Computations of Wind Turbine Wakes. Doctoral Thesis, Engineering Sciences, KTH Royal Institute of Technology, Stockholm.

[5] Michelsen, J. A. (1992) – Basis3d – A Platform for Development of Multiblock PDE solvers. Tech. Rep. AFM 92-06. Dept. of Fluid Mechanics, Technical University of Denmark, Lyngby,

[6] Mikkelsen, R. (2003) – Actuator Disc Methods Applied to Wind Turbines. PhD Thesis, Dept. of Fluid Mechanics, Technical University of Denmark, Lyngby.

[7] Sørensen, N. N. (1995) – General Purpose Flow Solver Applied to Flow over Hills. PhD thesis, Risø National Laboratory, Roskilde.

[8] Troldborg, N. (2008) – Actuator Line Modeling of Wind Turbine Wakes. PhD Thesis, Dept. of Fluid Mechanics, Technical University of Denmark, Lyngby.

Downscaling of extreme wind using CFD

Martin Vanandruel[1)]

[1)] Waudit FP7 PhD hosted in
CENER-Ciemat Fundación
Ciudad de la Innovación, 7
31621 Pamplona

ABSTRACT

Extreme wind characterization is of primary importance for wind turbine dimensioning. Simulation of extreme wind as obtained by the mesoscale models gives satisfactory results in flat terrain but it may underestimate the extremes in moderate to highly complex terrain. Microscale CFD model permit to accurately solve the flow at those scales. The aim of this work is to develop dynamical coupling between mesoscale and microscale. Whatever the physical coupling used to transmit physics it is necessary to improve the precision of the present methodology in order to obtain valuable departure from the mesoscale model. The characterization of meshing error and the Reynolds stress modelling will be inquired. Classical test cases of Sierra of Alaiz and Bolund island will permit to validate mesh and turbulent model while applying the dynamical coupling for extreme wind series.

KEYWORDS

Reynolds stress modelling, a-priori mesh assessment, dynamical coupling

1 INTRODUCTION

Since a decade the wind modelling discipline has taken a new turn by the use of Computational Fluid Dynamics (CFD) adapted to atmospheric boundary layer as a tool of assessment. While mesoscale models have a resolution of the order of the kilometre CFD models can resolve scales of the order of 100 meter. The terrain geometry and roughness being more resolved in the case of CFD the model can capture small-scale features like fractional speed-up that are invisible to mesoscale. The inclusion of the microscale model within the mesoscale model can permit to simulate episodes of extreme wind values with a increased precision of the order of 10%. This will permit to provide better estimation for the extreme wind characterisation necessary for IEC61400-1 caracterization. Indeed the current approach of CENER is to simulate a 10 year wind forecasting model for the studied wind park. For the moment the CENER CFD model methodology CFDWIND2.0 [2] is not directly

mvanandruel@cener.com

usable for such a dynamical downscaling of extreme winds. To be valuable it lacks an a-priori mesh and turbulent scheme residual indicator and representation of the turbulence anisotropy.

1.1 Mesh and Turbulent modelling

The approach in CENER, CFDWIND2.0 [2] is to represent the zone of interest using a parallelepiped domain through mesoscale Skiron model and the CFD calculation with Fluent 12.0 through a representation of the in-site topology with the generation of a uniform wind profile and the simulation carried on a parallelepiped domain. Provided H_x and H_y the horizontal and V the vertical length scales the dimension of the box must be at least of ($5H_x * 5H_y * V$) to avoid physical and numerical blockage effects. Ansys ICEM structured hexagonal elements are used as this kind of elements are necessary because of the advective dominated nature of the flow and ease the specification of the inlet boundary conditions. The mesh is more refined in the zone of interest where wind turbines will be implanted. Following Apsley and Castro [2] idea a maximum limitating length is employed to limit destruction term in turbulent dissipation rate equation and Coriolis term is added to the momentum equations. Those equations are resolved in Fluent 12.0 solver. The top is symmetric and the inlet is precised as velocity-inlet and outlet pressure and the lateral boundary conditions are periodical. To give an order of magnitude the turbulence error above than 5m committed when applying CFDWIND2.0 was observed to be of the order of 10% in the case of Bolund island which could be dramatically reduced providing the present computational power.

1.2 Coupling

At present CFDWIND2.0 is linked to mesoscale by two key parameters. In fact the domain is fed by entry wind profile characterized by the geostrophic wind speed and the surface Monin-Obukhov length. Those two entry values are used to generate an entry profile obtained by a k-epsilon corrected following Apsley and Castro [2] turbulence model. The simulation is resolved only in space and not in time obtaining the microscale related effects corresponding to the time of the entry from the mesoscale in a static manner.

2 IMPROVEMENT

2.1 Meshing improvement

The fact is that the residual introduced when defining the mesh has to be precisely known in order to a-priori determine the quality of the simulation is obtained. First the analytical expression for the residual introduced when specifying the mesh will be obtained. For the sake of simplicity and practical application it will be expressed as a function of the ruggedness (RIX), the streamwise and spanwise concavity of the terrain and the difference of altitude. As a result the formula must be applied to determine the error introduced by the numerical scheme simulating simple and complex terrain with elevated ruggedness factor (RIX). The meshing and numerical correlation term can be inferred from the comparison with a third intermediate case.

As mentioned residuals introduced by the equation representing the turbulence is still important in complex terrain. More specifically CFDWIND2.0 current isotropic formulation using k-epsilon is questionable in complex terrain where this model overestimates turbulence close to the ground. The replacement of isotropic by anisotropic turbulence model through a Reynolds Stress Modelling constitutes a central point of this research work. The numerous questions posed by the use of the wall function the calibration to obtain equilibrium the boundary conditions treatment and the initial conditions to be used will be largely investigated. Stability and accuracy analysis are to be carried on. The implementation of the CFD under Mercure Saturne code will permit to facilitate the dynamical coupling under linux and use of the mesoscale model skiron.

2.2 Transient, Solver implementation and data-flow management

The improvement of the existing state-of-the-art consists of resolving the equations in time. Therefore the dynamical downscaling of extreme wind is not only convenient because it permits time-efficiency but also because typical physical scales occurring in those complex terrain would be of the order of

$$\tau \approx \frac{V}{U} \approx \frac{10m}{10m/s} \approx 1s$$

which would be computationally too expensive for the mesoscale model but with the CFD model physically meaningful using a mesoscale model. Notwithstanding of this an output of the mesoscale model of the order of 10 seconds used with the backward-forward semi-implicit scheme with a precision of 5 kilometre. Development of time resolved computation

and data flow coupling in an elegant way from the microscale to the mesoscale will permit to simulate a complete extreme wind event in a single shot.

2.3 Test cases

The validation of the new mesh procedure and turbulent model will be carried on the island of Bolund in Denmark and the Sierra de Alaiz. Alaiz and Bolund test cases will be used to downscale a storm scenario. The microscale correction factors will be directly used to obtain a 10-minutes averaged extreme hub height wind speed. Bolund island is equipped with 9 measurement masts sonic anemometers besides of 20 sonic anemometers, 10 cup anemometers and two lidar aircraft laser measurement while Sierra de Alaiz is instrumented with 6 masts each with 24 sonics 24 cup anemometers and one lidar. Both sites are thus extremely well documented and furthermore possess clean boundary conditions permitting to obtain a well-defined problem.

3 CONCLUSIONS

Extreme wind analysis can benefit from the advance of CFD as a tool for microscale simulations. In order to dynamically implement downscaling of extreme wind for long episodes better standard precision is required for meshing. The model employed being k epsilon which resolves only isotropic turbulence this PhD aims to move from steady k-epsilon to transient and anisotropic turbulence permitting to capture intermittent effects. Last but not least the dynamical coupling will be validated during a 24 h extreme simulation event episode in Bolund and Alaiz sites.

BIBLIOGRAPHY

[1] Castro F.A., Palma J.M.L.M, et.al., 'Simulation of the Askervein Flow. Part 1: Reynolds Averaged Navier-Stokes Equations (k-epsilon turbulence model)', Boundary Layer Meteorology 107:501-530, 2003

[2] Sanz J., Cabezon S., Marti I., Parameterization of the atmospheric boundary layer for offshore wind resource assessment with a limited-length-scale k-espilon model, Proceedings of the European Wind Energy Conference 2009, Marseille

[3] Alinot C., Masson C., k-epsilon Model for the Atmospheric Boundary Layer Under Various Thermal Stratifications, Journal of Solar Energy Engineering, Vol 127, november 2005

Part 12

Postersession P2 - Electrical Operation, Structural Design and Maintenance

- State of the Art on Generator Technology for Wind Power Plants
  Zhang Zhaoqiang, NTNU
- Contribution to Study of Doubly-Fed Induction Generators: Operation under Network Disturbances
  Jean Patric da Costa, Fraunhofer IWES and University of Kassel
- A model based controller for Hybrid HVDC using in Offshore Wind Farms
  Raymundo E. Torres, NTNU
- Loads and dynamics in lattice tower support structures for offshore wind turbines
  Daniel Zwick, NTNU
- Novel coating system for rotating parts in offshore wind turbines
  Fahmi Mubarok, NTNU

State of the Art on Generator Technology for Wind Power Plants

Zhang Zhaoqiang
Norwegian University of Science and Technology, Norway

ABSTRACT

This paper presents an overview of the state of art on generator technology for wind power plants. It is found that in present market, DFIG is the dominate solution. PM machine is supreme over others in term of system cost, annual energy production, annual energy production per cost and cost of energy. But it is not clear which PM machine and associate drive train more promising in future large wind power application.

KEYWORDS

Generator Drive Train Wind Power

1 INTRODUCTION

In the past decade, global wind industry has seen an annual increase of above 25% (Figure 1), and the installed capacity is expected to increase by 160% over the next five years [1]. The average power of generators in global wind power plant is just under 1.6MW, and variable speed system is the normal solution for megawatt wind turbine. In market, generators in the range of 1.5MW-2.5MW make up nearly 82% [2]. And many manufactures are developing turbines in 4MW-6MW, even 10MW.

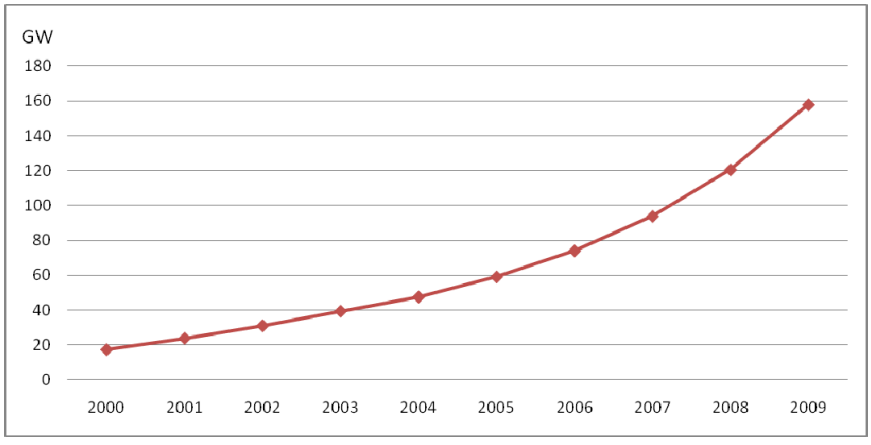

Figure 1: Global cumulative installed wind capacity

2 GENERATORS FOR WIND POWER PLANTS

Figure 2 shows the mainstream generator types. Doubly fed induction generator (DFIG) is the dominated generator type, then followed by squirrel cage induction generator and wound rotor induction generator (SCIG & WRIG), direct drive electrically excited synchronous generator (EESGDD), and permanent magnet synchronous generator (PMSG).

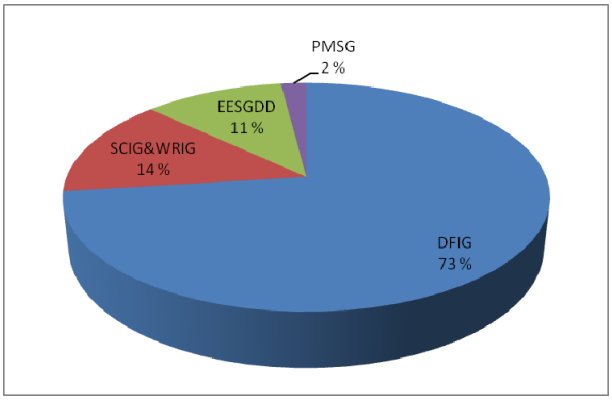

Figure 2: 2008 market analysis by generator type [3]

2.1 Drive trains

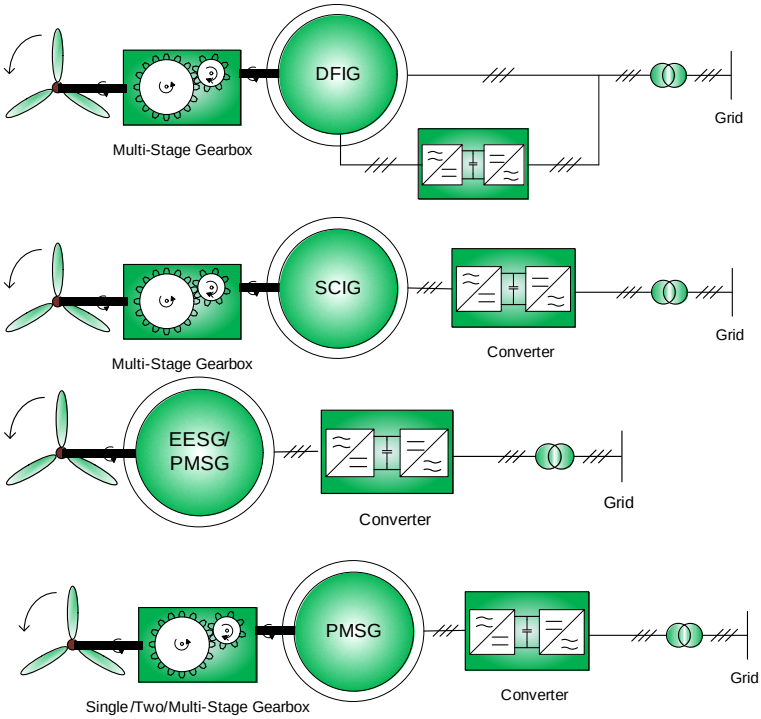

Figure 3: Mainstream drive train schemes

2.2 Generator Characteristics

Table 1: Characteristics of different generators in present market

Generator	Feature	Advantages	Disadvantages
DFIG	Stator gird-connected Rotor connected to partial scale converter; High speed; Up to 6MW;	Light weight; Low machine cost; Low cost of coupling converter; Capable to meet grid code; Proven technology; Available from standard industry machine;	Reliable problem due to gearbox, slip ring and brushes; Directly affected when grid fault; Complicated control to meet grid code;
SCIG	No rotor winding; Full scale converter needed; High speed; Up to 3.6MW;	Light weight; Low cost of machine, O&M; Simple and robust construction; Decoupled with the grid; Capable to meet grid code; Proven technology; Available from standard industry machine;	Relative low efficiency in light load;
WRIG	Stator grid-connected; Rotor connected to external resistor; Needs capacitor banks and soft starter High speed; Up to 2.1MW;	Light weight; Low machine cost;	Semi-variable speed operation; Low efficiency; Incapable to meet grid code;
EESGDD	Rotor connected to external excitation source; Full scale converter needed; Large diameter and short length; Low speed; Up to 6MW;	Simple drive train; Decoupled with the grid; Proven technology; Capable to meet grid code;	Efficient discount due to rotor losses; Heavy weight; High machine cost; Problems in transportation and Installation; Reliable problem due to slip ring and brushes;
PMSG	High energy PM material used for excitation; Full scale converter needed; Different topologies; Up to 5MW;	Light weight; Simple construction; High power density; High efficiency; Decoupled with the grid; Adapted to different drive trains; Capable to meet grid code;	PM material sensitive to hash environment; Difficulty to install PM poles; High machine cost;

3 COMPARISION

It makes sense to evaluate and compare different generators for WECS in the level of the drive train. System cost, AEP, AEP/C and COE are normally used as the criteria for comparison and written as [4-5]:

$$C_{system} = C_{Gear} + C_{gen} + C_{conver} + C_{other} \quad (1)$$

$$AEP = \int_0^{36\times24}\left[\int_{v_i}^{v_o} P_{WECS}(v)\cdot f(v)dv\right]dt \quad (2)$$

$$AEP/C = \frac{AEP}{C_{system}}\ kWh/Euro \quad (3)$$

$$COE = \frac{FCR\cdot ICC + AOM}{AEP}\ Euro/kWh \quad (4)$$

where P_{WECS} is WECS output power, $f(v)$ is Weibull density distribution, FCR is fixed charge rate, ICC is initial capital cost, AOM is annual operation & maintenance, AEP is annual

energy production. References [4-6] compare different drive trains with system cost, AEP, AEP/C and COE. Conclusions are summarized bellow (for 3MW system).

- In term of system cost,PMSG1G(DFIG3G)<PMSG3G<SCIG3G<PMSGDD<EESGDD
- In term of AEP, PMSGDD>EESGDD>PMSG1G>DFIG3G
- In term of AEP/C, PMSG1G>DFIG3G>PMSG3G>SCIG3G>PMSGDD>EESGDD
- In term of COE, PMSG1G<PMSGDD(DFIG3G)

As it can be seen, PMSG with single-stage gear box tends to be supreme over drive trains with other machines. But the performance of different drive trains based on PM machine varies. And no one is supreme than others in all the aspects. Considering the different machine topologies and the design concern of light weight and high reliability for large power application, especially for offshore, it is not clear which PM machine and associate drive train more promising in future large wind power application.

4 CONCLUSIONS

This paper presents an overview of the technology state of art on generator for wind power plants. In present market, DFIG is the dominate solution. PM machine is supreme over others in term of system cost, annual energy production, annual energy production per cost and cost of energy. But it is not clear which PM machine and associate drive train more promising in future large wind power application.

BIBLIOGRAPHY

[1] Appleyard, D.: Bigger blades and better designs in wind energy. Renewable Energy World International Magazine. Vol.13, Issue 4, 2010.

[2] Milford, E.: BTM wind market Report. Renewable Energy World International Magazine, Vol.13, Issue 4, 2010.

[3] Sakki, R.: Technology trends of wind power generators. Nordic Conference R8 Power Chapters Leadership Workshop and IAS Technical Seminar on Wind Power Technologies, 2009.

[4] Bywaters, G.; et al.: Northern power systems WindPact drive train alternative design study report. National Renewable Energy Laboratory 2004; NREL/SR-500-35524.

[5] Li, H.; Chen, Z.: Design optimization and evaluation of different wind generator systems. ICEMS, China, 2008.

[6] Polinder, H.; et al.: Comparison of direct-drive and geard generator concepts for wind turbines. IEEE Transactions on Energy Conversion 2006, 21(3):725-733.

European Academy of Wind Energy

Norwegian University of Science and Technology

Contribution to Study of Doubly-Fed Induction Generators: Operation under Network Disturbances

Jean Patric da Costa

Fraunhofer IWES and University of Kassel, Germany

Federal University of Santa Maria, Brazil

ABSTRACT

This paper presents a high performance stationary frame controller for DFIG, which improves the steady state and transient behaviour of the grid connected wind turbines especially under unbalance voltage dips resulting from network unbalance faults. A controller design procedure that guarantees the DFIG stability under uncertainties and disturbances at grid side is presented in details. Furthermore, it is demonstrated in the paper that with the proposed controller different goals such as control of grid side active and reactive power and improvement of the FRT capability can be achieved. Simulations and experimental results are given to illustrate the good performance of a grid connected DFIG with the proposed controller.

KEYWORDS

Wind Turbines, Doubly-Fed Induction Generator, Reactive Current Support, FRT.

1 INTRODUCTION

The doubly fed induction generator (DFIG) are one of the most used concept especially in large size grid connected wind turbines (>1.5 MVA) [1]. When compared with the full scale power converter wind turbine concept, WT with DFIG offer some advantages, such as: reduced inverter and output filter costs due low rotor power converters rating (25-30%). It is well known that the DFIG performance with PI controllers in synchronous reference frame oriented to the stator flux or stator voltage or resonant controllers is good in normal grid conditions, allowing independent control of active and reactive power. Since grid operators are requiring wind turbines to remain connected during grid faults, resulting in low voltage fault ride through capability (LVRT) with only 15% voltage at the PCC [2] or even less [3], as well as to contribute to system stability during and after fault clearance [3], the transient behavior of the DFIG and its controllers design have become a challenge to WT manufactures. This paper presents a high performance stationary frame controller for DFIG which improves the behaviour of the grid connected wind turbines especially during voltage

dips resulted from unbalanced faults in the grid. The block diagram of the proposed controller is shown in Figure 1. A controller design procedure that guarantees the DFIG stability under uncertainties and disturbances at grid side. Furthermore, it is demonstrated that with the proposed controller different goals such as control of grid side active and reactive power, minimization of torque pulsation under unbalance operation and improvement of the FRT capability can be easily achieved.

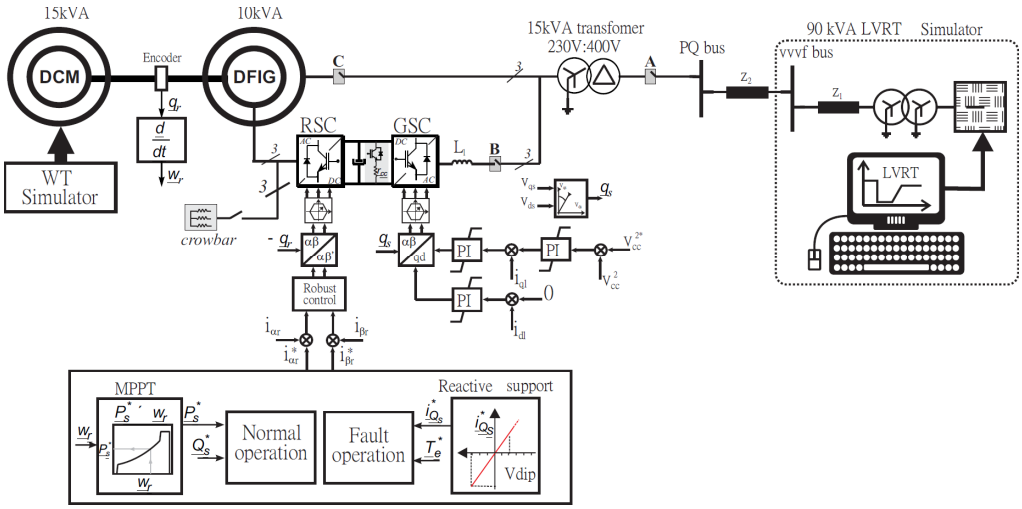

Figure 1: Block diagram of the proposed DFIG controller for grid connected WT.

2 DOUBLY FED INDUCTION GENERATOR MODEL IN STATIONARY REFERENCE FRAME

The nominal part of DFIG dynamic model has been obtained considering the following hypotheses: The DFIG has symmetrical phases and sinusoidally distributed phase windings, the permeability of the fully laminated core is assumed to be infinite and saturation, iron losses, end winding and slot effects are neglected. In addition, it is considered that the perturbation **w**(t) and its derivatives are continuous and bounded in norm. On the other hand, in order to account for the uncertainties in the system a perturbed term added to nominal model. As a result the grid connected DFIG dynamic model can be obtained according to flux and voltage equations in αβ-coordinates, and it is possible to obtain a state-space model:

$$\dot{\mathbf{x}} = \mathbf{A}\mathbf{x} + \mathbf{B}\mathbf{u} + \mathbf{F}\mathbf{w} + \Delta(\mathbf{x}, \mathbf{u}, \mathbf{w}) \tag{1}$$

where the state and input vectors have been chosen as:

$$\mathbf{x} = \begin{bmatrix} i_{\alpha s} \\ i_{\beta s} \\ i_{\alpha r} \\ i_{\beta r} \end{bmatrix};\ \mathbf{u} = \begin{bmatrix} v_{\alpha r} \\ v_{\alpha r} \end{bmatrix};\ \mathbf{w} = \begin{bmatrix} v_{\alpha s} \\ v_{\alpha s} \end{bmatrix} \tag{2}$$

The objective here is to define a control law, which ensures that the trajectories of the system (1) move toward reference and reach it in finite time, even in presence of uncertainties. So, the next section presents the controller design.

3 HIGH PERFORMANCE CONTROL: DESIGN AND STABILITY

The design procedure can be summarized in two main steps that are:

3.1 Design the Sliding Surface

Let us introduce the control vector surface **e** defined by:

$$\mathbf{e} = \begin{bmatrix} e_1 \\ e_2 \end{bmatrix} = \begin{bmatrix} \mathbf{i}_r^* - \mathbf{i}_r \end{bmatrix} = \left[\begin{bmatrix} i_{\alpha r}^* \\ i_{\beta r}^* \end{bmatrix} - \begin{bmatrix} i_{\alpha r} \\ i_{\beta r} \end{bmatrix} \right] = 0. \tag{3}$$

As long as the state trajectories are kept on the surface **e** = 0, then the rotor currents will track their references.

3.2 High Performance Controller Design

The control action **u** is designed to bring the error **e** to zero in a finite time and then maintain **e** = 0 for all future time. The rotor current error dynamic equation is:

$$\dot{\mathbf{e}} = \mathbf{A}_{22}\mathbf{e} - \mathbf{B}_2\mathbf{u} + \mathbf{g} \tag{4}$$

where **g** is given by:

$$\mathbf{g} = \dot{\mathbf{\imath}}_r^* - \mathbf{F}_2\mathbf{w} - \mathbf{A}_{21}\mathbf{i}_\mathbf{s} - \mathbf{A}_{22}\mathbf{i}_\mathbf{r}^* - \Delta_\mathbf{2}(\mathbf{x}, \mathbf{u}, \mathbf{w}). \tag{5}$$

Taking the control **u** as

$$\mathbf{u} = (\mathbf{B}_2)^{-1}(\mathbf{A}_{22}\mathbf{e} + \mathbf{g}_1 - \mathbf{u}_\mathrm{n}) \tag{6}$$

where $\mathbf{B}_2$ is non-singular for all time in the domain of interest, and $\mathbf{g}_1$ is given by:

$$\mathbf{g}_1 = \dot{\mathbf{\imath}}_r^* - \mathbf{F}_2\mathbf{w} - \mathbf{A}_{21}\mathbf{i}_\mathbf{s} - \mathbf{A}_{22}\mathbf{i}_\mathbf{r}^*. \tag{7}$$

Now, by substituting (7) into (6) yields:

$$\dot{\mathbf{e}} = \mathbf{u}_n - \mathbf{g}_0 \tag{8}$$

where $\mathbf{g}_0 = -\mathbf{\Delta}_2$. Under the assumption that $\mathbf{\Delta}_2$ has limited energy, it is possible to design **u** to force the rotor current error **e** toward the surface **e**=0 by choosing an appropriate Lyapunov function candidate. Let us consider

$$V(\mathbf{e}) = \frac{1}{2}\mathbf{e}^T\mathbf{e} \tag{9}$$

the derivative of V along the trajectories of the e is given by

$$\dot{V}(\mathbf{e}) = \mathbf{e}^T\dot{\mathbf{e}} = \mathbf{e}^T(\mathbf{u}_n - \mathbf{g}_0) \tag{10}$$

Now, by selecting the control law $\mathbf{u}_\mathrm{n}$ as

$$\mathbf{u}_n = -k\begin{bmatrix} \mathrm{sgn}(e_1) \\ \mathrm{sgn}(e_2) \end{bmatrix} \tag{11}$$

ensures that the derivative of V will be negative if $k > ||\mathbf{g}_0||$.

4 EXPERIMENTAL RESULTS

Simulations and experimental results are shown Figure 2 and Figure 3. In the simulation, a 5% error in parameters was considered. Figure 2 shows the DFIG behavior during an asymmetrical voltage dip with 25% of unbalance factor (VUF) and without disconnection from the grid. However, accord with the new grid requirements in Germany [3], the wind farm must be able to feed reactive current during fault aiming to improve the voltage profile. Figure 3.(a) shows again simulation and (b) experimental results where the reactive support required to comply with Germany grid code has been included.

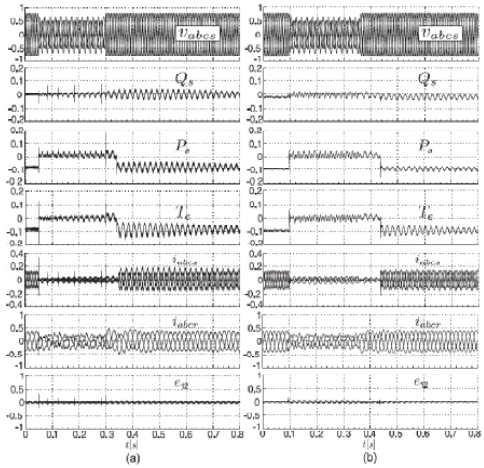

Figure 2: Behaviour of a DFIG during an asymmetrical voltage dip (a) simulation and (b) experimental result without reactive support.

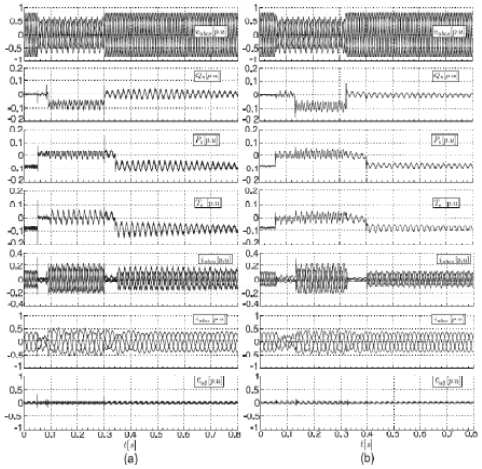

Figure 3 Behaviour of a DFIG during an asymmetrical voltage dip (a) simulation and (b) experimental result with reactive support.

5 CONCLUSIONS

This paper proposes a high performance stationary frame controller for DFIG which improves its behaviour under unbalance voltages as well as its FRT capability. In addition, a dynamic model of the DFIG including the controllers is derived and the controller design procedure that guarantees the DFIG stability under uncertainties and disturbances at grid side is presented. The experimental results demonstrate the DFIG behaviour and confirm the theoretical analysis presented.

BIBLIOGRAPHY

[1] WWEA, World Wind Energy Report, 2008.
[2] AESO, Wind Power Facility - Tecnical Requirements, Alberta Electric System Operator-AESO, http://www.aeso.ca.
[3] BDEW, Generating Plants Connected to the Medium Voltage Network, Bundesverband der Energie und Wasserwirtschaft e.V., http://www.bdew.de, 2008.

A model based controller for Hybrid HVDC using in Offshore Wind Farms

Raymundo E. Torres [1)], Marta Molinas[1)],Tore Undeland[1)]

[1)] Norwegian University of Science and Technology, Norway

ABSTRACT

In this paper, a model-based controller is proposed for Hybrid HVDC, Hybrid comprising a Voltage Source converter (VSC) using in the sending side and Line-commutated Converter (LCC) using in the receiving side. This type of HVDC may be applied when power is only in one direction for example HVDC for offshore wind farm applications. It also proposed in this paper, when AC grid is weak, to replace the LCC for a capacitor commutate converter (CCC) because of the additional commutation voltage reduces the risk of commutation failure. PSCAD/EMTDC simulations are provided to illustrate the performance of the proposed controller under normal operation and severe disturbance such as three phase-to-ground AC and DC faults.

KEYWORDS: Hybrid HVDC, VSC, LCC.

1 INTRODUCTION

Nowadays there are two different HVDC transmission technologies, i.e. Line-Commutated Converter (LCC), using partially controllable switches, thyristors and Voltage Source Converter (VSC), using controllable switches like Insulated gate bipolar transistors (IGBT) [1]. LCC HVDC has been widely used by more than 40 years because of the reliability, availability and the feasibility for very high power levels.

However when the LCC is connected to weak AC systems presents some difficulties to operate, for instance frequent commutation failures [2].

Now VSCs have attracted more attention due to the beneficial features such as [2] [3] :

- Independent active and reactive power control
- VSC can operate into a passive network, whereas LCC requires a voltage source
- VSC is about 60 % of the site of LCC station
- No commutation failure problem
- No communications required between two stations.

However the VSC, compared with LCC, is costly, has a limited range of power, more losses and is defenceless against DC faults (because their anti-parallel diodes operate as rectifier

feeding power directly into the fault. In LCC the DC faults are cleared operating both converter as inverter [2]). Hybrid HVDC, which can be seen in Fig. 1, is composed by a VSC and a LCC connected on the same DC link. The Hybrid option is aimed at combining advantages of both HVDC technologies. Among the advantages [2]:

- LCC converter can handle high power levels
- VSC converter can overcome the problem of the LCC in connection with weak AC system
- No fast communication is required in Hybrid HVDC.
- Less cost, losses and lower cost in Hybrid HVDC compared with VSC HVDC.

In spite of the above mentioned advantages, the Hybrid HVDC cannot reverse the power flow easily because LCC requires changing the polarity of the DC voltage while VSC requires changing the direction of DC current. Therefore the reverse of the power flow in the Hybrid requires the reconnection and discharge of the DC link. However, Hybrid HVDC may be suitable for specific applications for example in offshore wind farms where the power flow is always unidirectional [2].

The state of the art of the Hybrid HVDC is composed by [2]-[4].

2 HYBRID HVDC

The Hybrid HVDC configuration is shown in Fig. 1; VSCs are connected to the wind turbines all together in the same DC bus. The onshore LCC makes the connection with AC grid. It is expected that VSCs can handle the active and reactive power, while is expected to exploit the great capacity of the LCC.

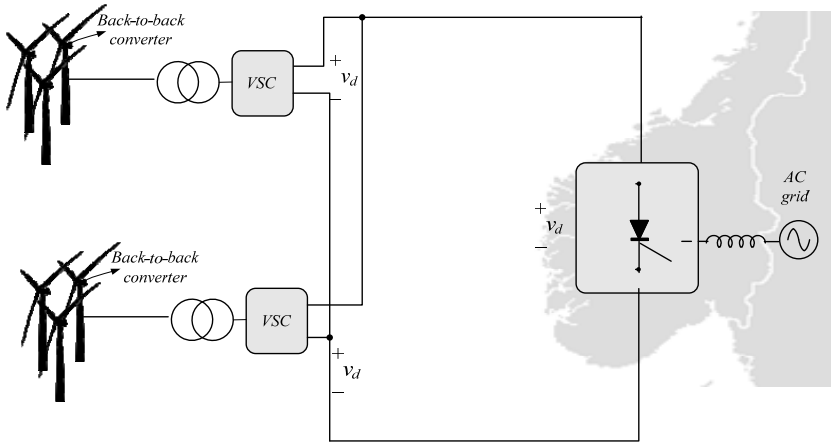

Fig. 1 Hybrid HVDC configuration

2.1 System Description

The Fig. 2 shown the scheme of VSC connected with LCC through the equivalent model of a DC line. Based on this scheme, the model of the system in d-q synchronous reference frame to the VSC is

$$L\frac{di_{Sdq}}{dt} = v_{Sdq} - -u_{dq} + \omega L J i_{Sdq}$$

$$C\frac{dv_{C1}}{dt} = i_{dq}{}^{T} u_{dq} - i_{DC1}$$

Where the vector i_{Sdq} represents the line currents (d-q coordinates), v_{Sdq} represents line voltages, u_{dq} is the control input, v_{C1} is the voltage in the DC line and i_{DC1} is the DC current in the DC link.

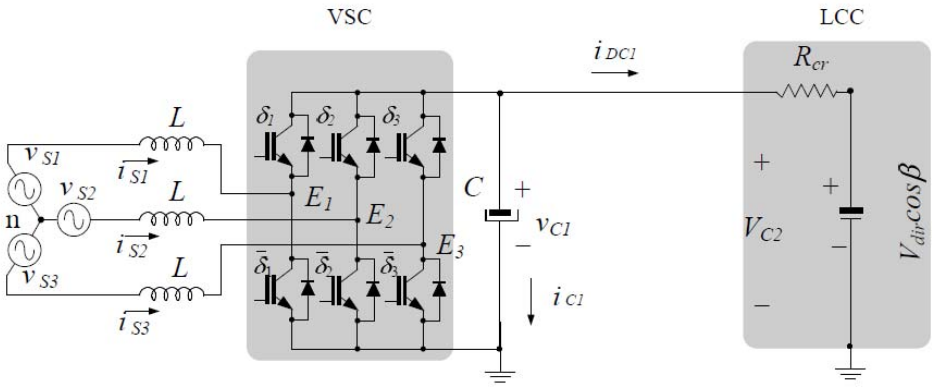

Fig. 2 Scheme of the Hybrid HVDC

While to the model of the LCC is

$$V_d = \frac{3\sqrt{2}}{2} v_{LL}\cos\beta - \frac{3}{\pi}\omega L_c i_{DC1}$$

Where the vector V_d represent DC voltage in DC link, v_{LL} is rms of line to-line voltage, β is the advance firing angle and Lc is the commutation inductance.

2.2 Control Design

Based on the model, the controller shown in the Fig. 3 is chosen to VSC. This control scheme can regulate both d and q component of the line currents in order to control the active and reactive power. For the LCC is proposed the PI controller which is shown in the Fig.3 This PI scheme can regulate the DC voltage toward its reference.

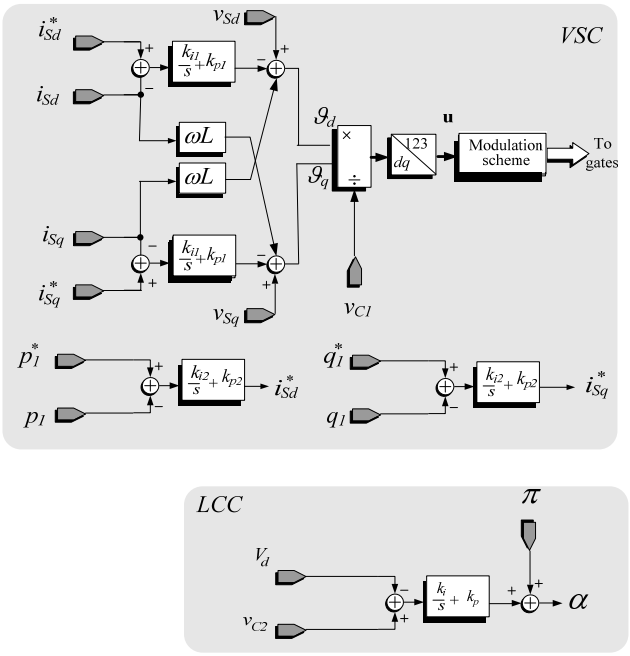

Fig. 3 Block diagram of the proposed controller

3 SIMULATION RESULT

The Hybrid HVDC system, shown in Fig. 2, has been implemented using PSCAD/EMTDC to illustrate the performance of the proposed controller. The system, which is rated at 1000 MW and 500 kV, is composed of a two-level VSC connected to a 12 pulses LCC through a long DC cable. It is important to remark that for comparison purposes the parameters were selected identical to the CIGRE benchmark HVDC model parameters, except for the modifications in VSC [5]. In this section, the Hybrid HVDC is simulated in different conditions, these are start-up, steady state, single phase-to ground fault in the inverter side, three phase-to-ground fault in the inverter side and DC fault Conventional LCC inverters have a serious limitation when is connected to weak grid. Any lowering in the inverter AC voltage produces a larger current with a lower voltage in the thyristor valves. Eventually the overlap angle is increased, thus the extinction angle is decreased which implies a smaller margin to commutation failure. The CCC utilizes series capacitors to generate the necessary portion of the voltage required for a successful commutation. This paper proposes to replace the LCC for a CCC in the Hybrid HVDC when the AC network is weak. . Fig. 4 shows the system time response of the hybrid HVDC during start-up. It shows that Hybrid system settles to steady state in about 1 s. Fig. 5 shows the time response in the hybrid HVDC when a single phase-to-ground fault is applied in the receiving side (CCC).

The system returns is recover, the recovery time is defined from fault clearing to the instance at 90% of the DC pre-fault is recover, after about 300 ms. Fig. 6 shows the time response when a three phase to ground fault occurs at the AC terminal of the CCC. Notice that the system returns to the pre-fault operation, after about 500 ms. Fig. 7 shows the time response of Hybrid HVDC when a DC fault occurs at the DC link The fault starts at t = 2 s and last 100 ms. Notice that the system returns to stable operation after about 600 ms.

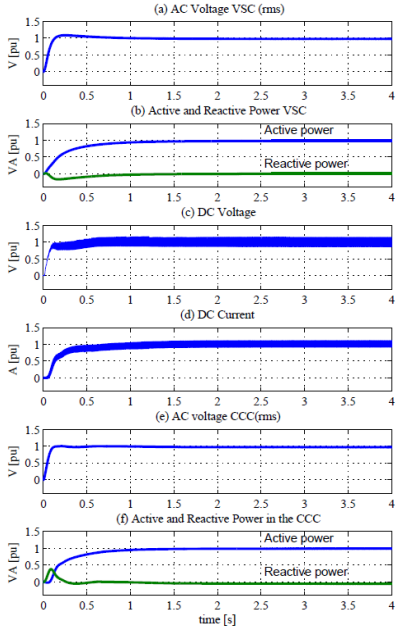

Fig. 4 Start up of the hybrid HVDC

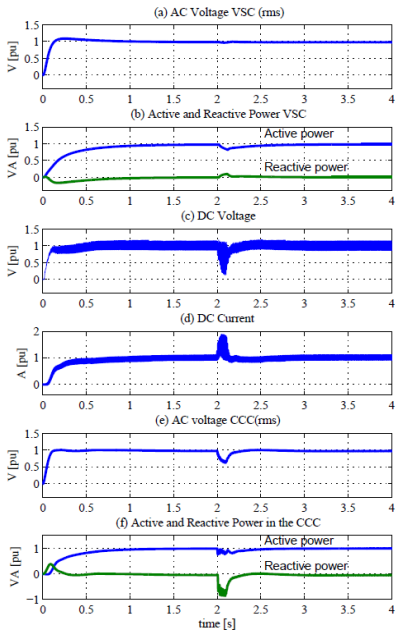

Fig. 5 Time response when single fault to-ground occurs

. (a) AC voltage in the rectifier, (b) Active and reactive power in the rectifier, (c) DC voltage, (d) DC current, (e)AC voltage in the inverter, (f) Active and Reactive power in the inverter

4 CONCLUSIONS

In this paper was presented a model-based controller for Hybrid HVDC. The controller consisted of a d-q synchronous reference frame controller for the VSC which regulates directly the active and reactive power and PI controller for the LCC which regulates the DC voltage. The controller for Hybrid HVDC demonstrated good performance under normal conditions however has serious limitations when the LCC is connected to a weak grid and a fault is applied. In this paper, it proposed using a new Hybrid consisting of a VSC and CCC when the network is very weak.

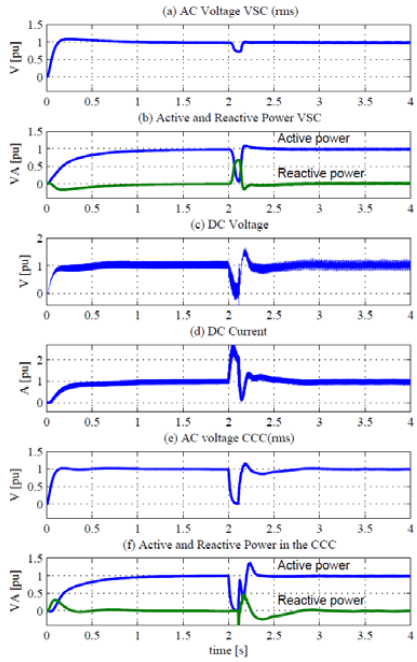

Fig. 6 Time response when three phase fault to-ground occurs.

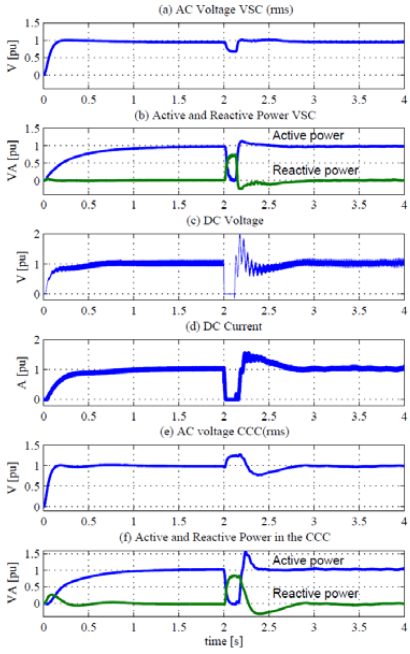

Fig. 7 Time response when DC fault occurs

(a) AC voltage in the rectifier, (b) Active and reactive power in the rectifier, (c) DC voltage, (d) DC current, (e)AC voltage in the inverter, (f) Active and Reactive power in the inverter

BIBLIOGRAPHY

[1] L Xu and B.R. Andersen. Grid Connection of Large Offshore Wind Farms using HVDC. Wind Energy, 9: 371-382,2006.

[2] Z. Zhao and MR Iravani. Application of GTO voltage source inverter in a hybrid HVDC link. IEEE Transactions on Power Delivery, 9(1):369–377, 1994

[3] W. Pan, Y. Chang, and H. Chen. Hybrid Multi-terminal HVDC System for Large Scale Wind Power. In 2006 IEEE PES Power Systems Conference and Exposition, 2006. PSCE'06, pages 755–759, 2006.

[4] Y. Iwata, S. Tanaka, K. Sakamoto, H. Konishi, and H. Kawazoe. Simulation study of a hybrid HVDC system composed of a selfcommutated converter and a line-commutated converter. Sixth International Conference on AC and DC Power Transmission,. pages 381–386, 1996.

[5] M. Szechtman, T. Wess, and CV Thio. A benchmark model for HVDC system studies. In AC and DC Power Transmission, 1991., International Conference on, pages 374–378, 1991.

Loads and dynamics in lattice tower support structures for offshore wind turbines

Daniel Zwick, Geir Moe

Department of Civil and Transport Engineering, NTNU

ABSTRACT

Lattice tower support structures for offshore wind turbines are used in the intermediate water depth of 30-70m. Today's concepts are mainly based on a lattice tower sub-structure combined with a traditional tubular tower for the support of nacelle and rotor. In this study, a full lattice tower from the sea bead up to the nacelle was investigated. Loads in all nodes of the structure were calculated with the aeroelastic code HAWC2 and analysed under varying loading, focusing on dynamics and fatigue of the joints.

KEYWORDS

Offshore wind, support structure, lattice tower, fatigue loading

1 INTRODUCTION

The extremely ambitious political goals concerning extensive use of offshore wind energy result in an intense demand of research and development in this field. As an example, round 3 in UK could mean a need to install several thousands of offshore wind turbines within the next ten years. To be able to fulfil this goal, components for offshore wind farms has to be produced by mass production techniques and within reasonably short fabrication time.

New node concepts might be of interest for more automated production of lattice towers. As a basis for such an investigation, loading and dynamic response by focusing on design of the nodes has been analysed with HAWC2 [1] in this study.

2 SUPPORT STRUCTURES FOR OFFSHORE WIND TURBINES

2.1 Support structure concepts

Where offshore wind turbines are planned to be installed in the intermediate water depths of 30-70m, bottom-fixed support structures as shown in Figure 1 might be used. One promising concept is the lattice tower type, due to less material use compared to other concepts like monopile or tripod structures. A lattice topology could be used for the entire support structure between sea bottom and turbine nacelle or for the lower part of the tower. While so-called

hybrid concepts with half lattice/half tubular tower has been installed in different projects ([2], [3]), the fully lattice tower concept is still a relatively new proposal for support structures for offshore wind turbines in intermediate water depth.

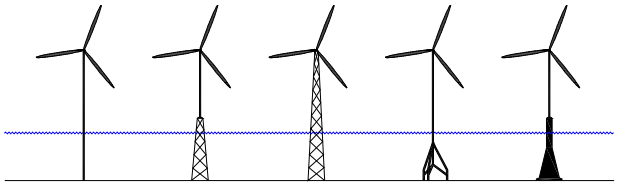

Figure 1: Bottom-fixed support structure concepts for the intermediate water depth of ca. 30m

2.2 Lattice towers

Lattice towers are assembled from steel tubes, where legs and bracings are welded together in tubular joints. Legs and bracings are connected in K-joints (Figure 2), while bracings in the planes between the legs are connected in X-joints. Today's lattice towers, known from the offshore oil and gas industry, are mainly fabricated by manual welding due to the complex geometry of the joints, which is varying in size and angle around the pipe. This results in time-consuming and expensive fabrication of the support structure.

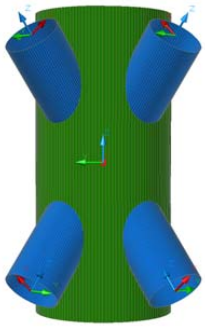

Figure 2: Joint geometry of nodes in lattice towers

New ways to fabricate the lattice tower nodes are of interest to facilitate mass production techniques for the assembling of lattice tower members to a structure. For the design and evaluation of new node concepts, load distributions in the nodes and over the tower height have to be known.

3 LOADS AND DYNAMICS IN LATTICE TOWERS

For a detailed analysis of loads and dynamics in lattice tower nodes, a HAWC2 model of a lattice tower support structure with 84 beam elements was established. Wind turbine and rotor configuration were taken from the NREL 5MW baseline turbine [4]. Results from HAWC2 are obtained in time domain and further analysed with MATLAB.

3.1 Node member forces

An overview over varying forces of a complete K-joint, as shown in Figure 2, is given for a specific node in one leg in Figure 3. Forces in x- and y- direction are varying in a more stable manner around their mean, while forces in the z-direction, which is the axial direction of the members, are varying more irregularly over a larger range between minimum and maximum value. The dynamic behaviour of the load leads to a high fatigue loading of the structure.

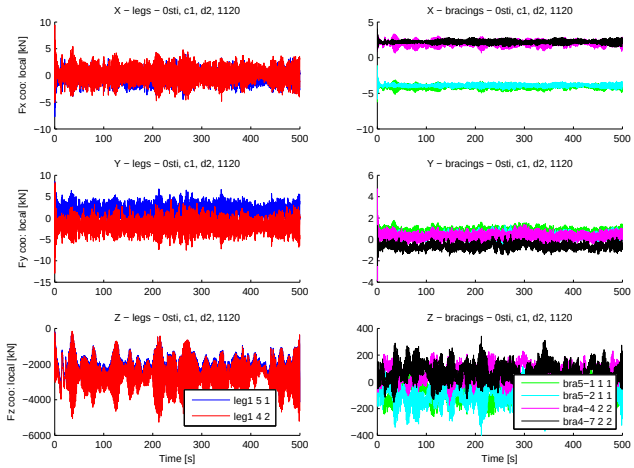

Figure 3: Node member forces in one leg at a specific node

3.2 Force distribution

The distribution of forces over the tower height is interesting for the design of the member dimensions. Figure 4 shows a plot of the mean forces in the z-direction in one leg with appropriate standard deviation (std) and min/max range. The absolute value of the mean forces and the range of variations around the mean are both decreasing from sea bottom towards the tower top.

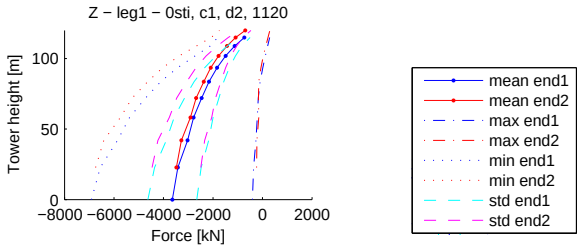

Figure 4: Force distribution in one leg over the tower height

The initial design of this study is based on a former PhD work of the department, where constant leg and bracing dimensions over the tower height were used.

3.3 Fatigue analysis

For the fatigue analysis of the initial tower design, a MATLAB-program with steps shown the in Figure 5 was written. Results for each beam element end in the time domain were processed with a rainfall counting algorithm and evaluated with the Palmgren-Miner rule. To be able to estimate the lifetime of the joints, S-N-curves from DNV [5] were used.

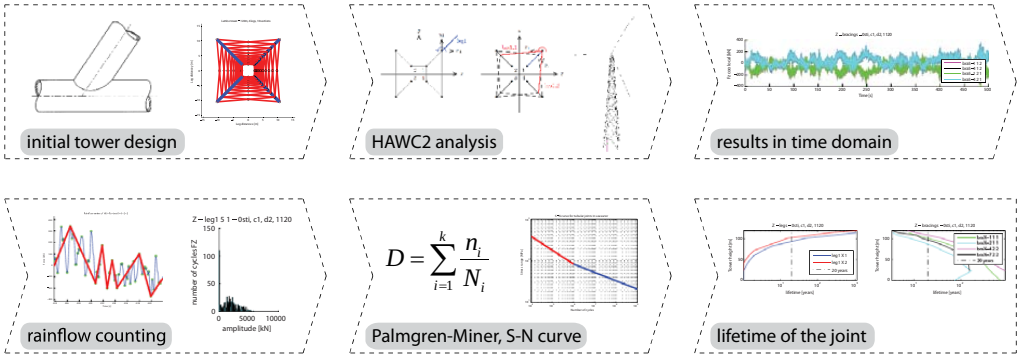

Figure 5: Fatigue analysis of lattice tower nodes

4 CONCLUSIONS

This paper gives an overview over the analysis of loads and dynamics in lattice tower support structures for offshore wind turbines. Highly varying loads in the structure leads to fatigue loading, which was analysed by a rainflow counting algorithm and the Palmgren-Miner rule. As a result, structural members and components may be redesigned to obtain the required lifetime of the structure. The obtained results can also be used for the development of new node concepts, suitable for mass production of lattice towers.

BIBLIOGRAPHY

[1] Juul Larsen, T.; How 2 HAWC2, the user's manual, Risø National Laboratory, Denmark Sept 2009.

[2] http://www.beatricewind.co.uk

[3] http://www.alpha-ventus.de

[4] Jonkman, J., Butterfield, S., Musial, W., Scott, G.; Definition of a 5-MW Reference Wind Turbine for Offshore System Development, Technical Report NREL/TP-500-38060, National Renewable Energy Laboratory, February 2009.

[5] Recommended Practice, DNV-RP-C203, Fatigue Design of Offshore Steel Structures, April 2008.

European Academy of Wind Energy

Norwegian University of Science and Technology

Novel coating system for rotating parts in offshore wind turbines

F. Mubarok[1], S. Armada[2], R. Johnsen[1], N. Espallargas[1]

[1] Department of Engineering Design and Materials-NTNU
Richard Birkelandsvei 2B, 7491 Trondheim, Norway
[2] SINTEF Materials and Chemistry, Department of Applied Mechanics and Corrosion,
Richard Birkelandsvei 2B, 7465 Trondheim, Norway

ABSTRACT

Rotating parts in offshore wind turbines such as gears or bearings will be subjected to high static and dynamic loads coming from the turbine blade and wind alteration. As the turbine goes up to large rating of 10-20 MW, these components will be induced to higher stresses and can worn-out within shorter period than is designed. Thus, it is important to improve the wear resistance of these parts either by introducing coatings and/or renewing its lubrication system. There is a lot of research available in the literature regarding coating materials for rotating systems, however the challenge in offshore wind turbines also include seawater harsh environment and abrupt change of temperature that these components can face in the offshore. The service lifetime is also one of the most important issues since offshore wind turbines are expected to serve for minimum 20 years. This PhD work is carried out to propose a new method by introducing novel coatings for tribological purposes in offshore wind turbines by utilizing suspension plasma spray coating techniques. These coatings consist of embedded nano-lubricants in a ceramic or metallic matrix to increase service life of the rotating parts. This embedded nano-lubricant systems is expected to be of great importance to reduce wear and in the case where the rotating system lacks of lubrication.

KEYWORDS

Coating, suspension plasma spray, lubrication, wind turbine

1 INTRODUCTION

Wind turbine has gained widespread acceptance as promising low cost and clean renewable source of energy. The recent trend of wind turbine technology is to install larger turbines offshore with power capacities in between 10-20 MW. Having larger turbines will reduce the number of installed turbine in offshore wind farms to produce equal power output compared to small turbine. This in turn, will reduce the number of expensive tower, foundation, turbine component and power collection cable needed. However, weight will be a major constrain in

large turbines as the wind turbine will be very heavy and this tends to lead on higher stresses induced in the components of wind turbine which later can result in high wear [1].

Rotating parts in wind turbine such as gears and bearings are critical components in wind turbine that experience tribological condition and encountered extreme loads coming from turbine rotor weight and wind alteration. The extreme static and dynamic loads will affect fatigue life of the components to meet their expected service life of a minimum 20 years. Moreover, these parts should be corrosion resistant since it will expose to harsh sea water environments. Experience from early installed wind turbine system had shown that these components were repaired or replaced over significantly smaller time intervals than which is intended [2]. In order to ensure that all wind turbine tribological system running smoothly, they should come with specific materials, having effective lubrication system installed and superior tribological properties.

2. COATING FOR LARGE PARTS

The rotating components installed in large rating wind turbine are massive and thus need special technique of surface treatments to enhance its surface properties. Diffusion techniques such as carburizing, nitriding, pulse plasma nitriding and shot peening are widely used for treatment of gears and bearings steel surfaces. Surface modification such as ion implantation and laser surface processing also considers as a viable process. Coating deposition such as thermal spray coating, electroplated coating and PVD or CVD coating are also used to improve near-net surface properties of these tribological components.

Among them, thermal spraying is considered as one of the most versatile techniques available for the application of protective coatings within large surface area. It uses wire, rod, powder or suspension/solution feedstock which passed through a high temperature regime generated by plasma or gas flame where they fully or partially melted and accelerated in gas stream and impinge the substrate to form coating layer by layer [3].

There are several different types of plasma spray methods that distinguished by the type of the surrounding atmosphere or feedstock materials. In recent year much research effort was expanded to develop new spray facilities to apply new materials with nano or submicrometric sized powders. One of the processes that gaining interest is suspension/solution thermal spray. This process used liquid suspension or liquid precursors having nanometric (<100 nm) or submicrometric (100 nm - 1µm) sized particles as a feedstock material in order to obtain finely structured coatings [4-5].

3. SUSPENSION/SOLUTION PLASMA SPRAY

The nanoparticles used in the SPS process are dispersed in a solvent such as water or ethanol. In order to avoid agglomeration of fine particles during milling and transport, the dispersants or deflocculating agents are added to the formulated suspension. The suspension is then injected into the plasma torch where the liquid will evaporate and agglomerated nanoparticles will melt and upon impacting the substrate, coating with nanostructured sizes will form. For solution plasma spray, the liquids feedstock is prepared by dissolving the precursor chemical in a solvent. The liquid precursors consist of nano- or submicrosized particles, aqueous or organic solvents and effective dispersing agents that develop repulsive forces to prevent agglomeration of particles.

The suspensions or liquids are transported into plasma flow either using pneumatic injection or mechanical injection (pressurized vessel). In pneumatic system, a secondary atomization of liquid stream is injected by secondary plasma gas flow within a dedicated nozzle, while in mechanical system continuous jet of liquid stream is injected within the plasma flow.

4. NOVEL COMPOSITE COATING CONTAINING NANO-LUBRICANTS

This PhD research will utilize suspension/solution plasma spray with d.c plasma jets to form nanostructured silicon carbide (SiC) coatings embedded with nano-solid lubricants on the substrate. Silicon carbide material has known for its excellent mechanical, thermal and chemical properties. However, the use of non-oxide ceramic material such as SiC in the thermal spray is less common since in high temperature, SiC tends to decompose and to react with all transient metals. Additives or binder phases is required to suppress oxidation and to avoid formation of silicides during spraying of SiC-based composites [6].

There are two routes that will be explored to produce dense nanostructured SiC coatings. The first route performed through applying SiC powder mixed with binder phase Al_2O_3/Y_2O_3. The mixture of powders is ball-mixed with ethanol or isopropanol in agitator ball mill to produce fine, non-agglomerated and homogenous composite suspensions. The suspension is stabilized by the addition of a dispersant. The optimum content of SiC in the suspension will be investigated with limit up to 80% vol.[7].

The second route will utilize liquid precursor of polycarbosilanes or chlorocarbodisilane dissolved in ethanol to produce silicon carbide coatings. These precursors has been extensively studied for SiC synthesis with the aid of CH_4 gases [8]. During the spraying

process, raw materials are rapidly decomposed and dissociated to various species in plasma flame and these species reacted with each other or recombined to the raw material in a short time. Gaseous products and by-products will impact the substrate and solidified forming a layer of coatings.

For this research, there are three different kinds of solid lubricant that will be added to the suspension or liquid precursor. Two of the solid lubricant, graphite and WS_2, are known as friction modifiers commonly added to liquid lubricant. These lubricants have hexagonal layered structure with weak bonding between planes of atoms that provides low shearing of the bonds in the direction of sliding. The third solid lubricant is teflon-based material encapsulated in ceramic shell to protect the teflon from thermal degradation during spraying [9]. Teflon have very weak bonding between neighbouring teflon molecules the may slide easily along each other at low shear stresses similar the hexagonal planes of solid lubricants with lamellar structure**.**

The spraying process will be carried out on martensitic stainless steel disk substrates. Prior to deposition, the surface is sand-blasted with Al_2O_3 grit to enhance coating adhesion. Structural and morphological characterization of the working surfaces will be performed by surface roughness testing, light microscopy, X-ray diffraction analysis and SEM microscopy. The tribological behavior of the novel coating system will be assessed in a CSM Pin on Disk Tribometer using martensitic stainless steel as a pin (ASTM G99).

5. CONCLUSIONS

Novel coating system with SiC-composite coating embedded graphite, WS_2 or teflon solid lubricant will reduce the friction and lower the wear rate and kept the wind turbine rotating parts running smoothly. The formulated suspensions and liquid precursors will be sprayed to produce thick coating around 10 to 50 µm. Since this process requires a very careful suspension/solution preparation and very tight control of the plasma operating condition, the effect of main parameters will be observed throughout the experiments.

REFERENCES

[1] D. Milborrow, "Wind energy technology—the state of the art," *J. Power Energy* pp. 23-30, 2002.

[2] AGMA, "Standard for design and specification of gearboxes for wind turbines. ANSI/AGMA/AWEA 6006-A03," ed. United States: American Gear Manufacturer's Association, 2004.

[3] R. B. Heimann, *Plasma spray coating : principles and applications*, 2nd rev. and enl. ed. Weinheim: Wiley-VCH, 2008.

[4] F.-L. Toma*, et al.*, "Nanostructured photocatalytic titania coatings formed by suspension plasma spraying," *Journal of Thermal Spray Technology,* vol. 15, pp. 587-592, 2006.

[5] J. Berghaus*, et al.*, "Suspension plasma spraying of nanostructured WC-12Co coatings," *Journal of Thermal Spray Technology,* vol. 15, pp. 676-681, 2006.

[6] B. Wielage*, et al.*, "Production of SiC-composite Coatings by HVOF," in *The 1st GTV Conference*, Luckenbach, Germany, 2000, pp. 51-56.

[7] B. Wielage*, et al.*, "Development and investigation of SiC-based thermal spray powders with alumina-yttria binder matrix," in *ITSC 2007, International Thermal Spray Conference & Exposition*, Beijing, China, 2007, pp. 1140-1144.

[8] E. Bouyer*, et al.*, "Thermal Plasma Chemical Vapor Deposition of Si-Based Ceramic Coatings from Liquid Precursors," *Plasma Chemistry and Plasma Processing,* vol. 21, pp. 523-546, 2001.

[9] J. Voyer and B. R. Marple, "Tribological performance of thermally sprayed cermet coatings containing solid lubricants," *Surface and Coatings Technology,* vol. 127, pp. 155-166, 2000.

Part 13

Postersession P3 - Rotor Design, Control and General Aspects

- Root flapwise moment on downwind and upwind rotors with truss and tubular towers
  Marit Reiso, NTNU
- Models for global and local loads on wind turbines
  Roberto Longo, University of Genoa
- A numerical and analytical investigation of blade fatigue loads on the NREL 5MW wind turbine
  Mads Døssing, Risø DTU
- A Framework for Integrated Control System and Aeroelastic Design of Wind Turbines
  Fabiano Daher Adegas, Aalborg University
- Temporary Rotor Inertial Control of Wind Turbine to Support the Grid Frequency Regulation
  Bing Liu, NTNU
- Dynamic analysis of wind turbines from an integrated perspective
  Braulio Barahona Garzon, Risø DTU
- Space-related conflicts over offshore wind farms
  David Rudolph, University of Edinburgh

European Academy of Wind Energy

Norwegian University of Science and Technology

Root flapwise moment on downwind and upwind rotors with truss and tubular towers

Marit Reiso[1)]

[1)] NTNU, Norway

ABSTRACT

The present work compares the root flapwise moment, RFM, on a 5-MW downwind and upwind, truss and tubular tower wind turbine. In order to do an appropriate comparison, all experimental designs use the NREL Offshore 5-MW Reference Wind Turbine blade. Preliminary calculations show promising results for adjusting stiffness properties on blades for downwind rotor.

KEYWORDS

Wind turbine, downwind rotor, truss tower, root flapwise moment, damage equivalent load

1 INTRODUCTION

From the start of the modern wind turbines up until today the growth in wind turbine size has been tremendous, ranging from the smaller kW size into todays MW size. The trend has been to up-scale existing technology into larger MW-size wind turbines. In addition to increasing power output this has contributed to a substantial weight increase, as the weight scales to the cube while the power at the same time only scales to the square [1]. Due to this substantial weight increase it is understandable that the up-scaling cannot continue without changing the wind turbine design itself.

Lighter blades will reduce the weight and at the same time make the blades more flexible. More flexible blades have the advantage of being more compliant in gusts and impact loading than the stiffer upwind blades [2] but they also run a higher risk of hitting the tower. If using a downwind rotor instead of an upwind rotor the risk will be smaller.

The problem with the downwind rotor is the tower shadow that can give unwanted loads onto the blades passing behind the tower. One option might be to use a more transparent truss tower instead of the conventional tubular tower.

In the present paper the effect of using downwind and upwind rotors with truss and tubular towers have been investigated with respect to root flapwise moment, RFM. The RFM has also been shown for the downwind truss tower using different blade stiffness.

marit.reiso@ntnu.no

2 METHODS

In this paper root flapwise moment, RFM, for a downwind and upwind wind turbine is compared. The downwind and upwind rotors are combined with both a truss and tubular tower.

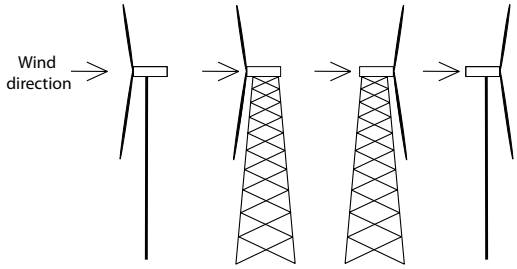

Figure 1 Sketch of the experimental setup. From left to right; Upwind tubular tower, upwind truss tower, downwind truss tower and downwind tubular tower. Wind direction from left.

The bottom-fixed NREL offshore 5-MW baseline wind turbine has been used in these calculations, detailed information can be found in reference [3]. Changes have been applied to the NREL 5-MW baseline wind turbine for the rotor mounting (refer Table 1 in reference [8]) as well as for the tower layout for both the truss and tubular towers [4], [5]. A sketch of the experimental setup is shown in Figure 1, and tower dimensions can be found in Figure 2. The fatigue calculations have been carried out according to the IEC61400-3 standard using design load case 1.2 for power production and design load case 6.4 for idling case [6]. Wind and wave data has been taken from a site in the Dutch North Sea [7].

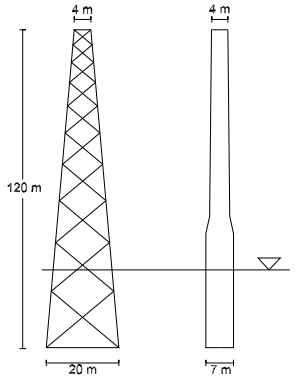

Truss Tower	
Main leg diameter/thk [mm] Angle wrt horizontal [degrees]	900/35 85.95
Brace diameter/thk [mm] Angle wrt horizontal [degrees]	360/14 49.51
Number of sections	10
Tubular Tower	
Bottom diameter/thk [mm] Angle wrt horizontal [degrees]	7000/70 90
Top diameter/thk [mm] Angle wrt horizontal [degrees]	3870/19 89.02
Tower height	120

Figure 2 Truss and tubular tower dimensions, sketch not to scale.

3 RESULTS

The following results show how the root flapwise moment, RFM, differs depending on type of tower and rotor mounting.

From a power production point of view there is no preference towards truss or tubular tower, or downwind or upwind rotors, as they all show the same power production [8].

Figure 3 shows the RFM as a function of rotor azimuth where 180 degrees corresponds to the blade pointing vertically downwards. The most obvious finding is that both upwind rotors show a much higher mean RFM than the two downwind rotors. But the downwind rotors show a larger dip at about rotor azimuth 180 degrees, caused by the tower shadow.

To see if the downwind rotor can be a better option than the upwind rotor a rainflow count has been carried out to compare the damage equivalent loading, DEL, on the different rotor-tower combinations. Figure 4 shows the rainflow count for the different rotor-tower combinations. The result is plottet against the inverse SN-slope, where composite blades have an inverse SN-slope around 10. The lowest DEL is found for the upwind truss tower while the downwind tubular tower shows the largest DEL. This means that the larger dip in RFM for the downwind rotors has a more severe impact on the DEL on the blades than the higher mean RFM for the two upwind rotors.

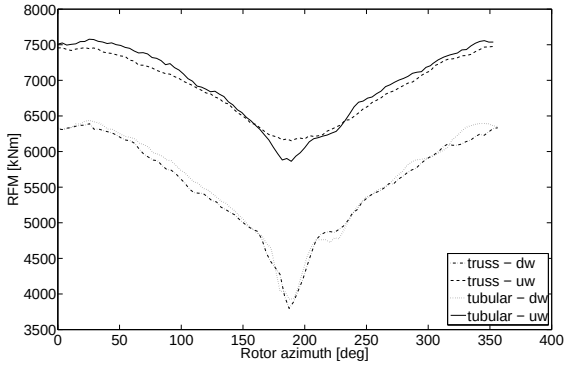

Figure 3 RFM as a function of rotor azimuth for different rotor-tower combinations (truss – dw/truss – uw; truss tower with down- and upwind rotor respectively, tubular – dw/tubular – uw; tubular tower with down- and upwind rotor respectively).

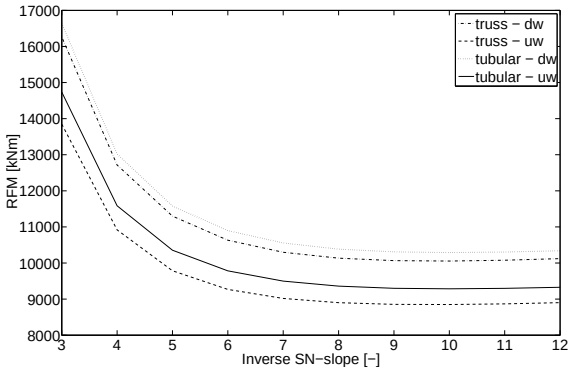

Figure 4 Rainflow count, RFM vs inverse SN-slope for the different rotor-tower combinations.

It should be investigated how the blade can be better adapted for a downwind rotor. Figure 5 shows the downwind truss tower with three different blade stiffnesses. The *NREL 5-MW blade* shows the NREL 5-MW blade without any changes to the stiffness. The *modified stiffness 1* and *2* show how the RFM changes as the stiffness is reduced. A more flexible blade, as shown with the *modified stiffness 1* can reduce and smoothen out the RFM and maybe also improve the DEL for the blade. But if the blade becomes too flexible, refer *modified stiffness 2* the effects of the adjusted stiffness can be the opposite.

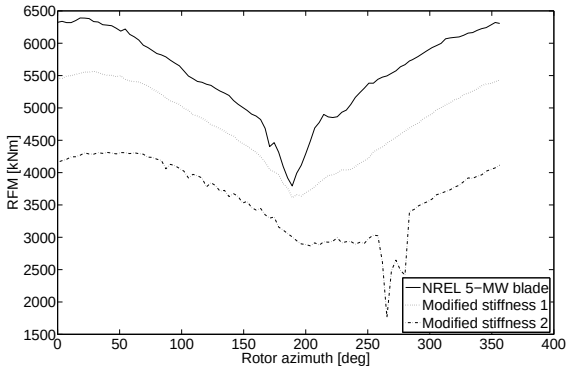

Figure 5 RFM vs rotor azimuth for varying blade stiffness on the downwind truss tower.

4 FURTHER WORKS

- The RFM DEL need to be further investigated to see if they have any significant impacts on the total lifetime of the wind turbine blade.
- More detailed investigations into the blade stiffness for the blade on the downwind truss tower to obtain a blade which will give the same or lower DEL compared to the blade on the upwind tubular tower.

BIBLIOGRAPHY

[1] Moe, G., 2007. What is the optimum size for a wind turbine? In Proceedings of the 26th International Conference on Offshore Mechanics and Arctic Engineering, OMAE2007-29035.

[2] Lee, A., and Flay, R., 1999. Compliant blades for wind turbines. IPENZ Transactions, 26(1), pp.7-12.

[3] Jonkman, J., Butterfield, S., Musial, W., and Scott, G., 2009. *Definition of a 5-MW reference wind turbine for offshore system development.* NREL.

[4] Long, H., Fischer, T., and Moe, G., 2009. Design methodology and optimization of lattice towers for offshore wind turbines in 35m water. In Proceedings of EWEC Marseilles.

[5] Fischer, T., 2009. Private communication Tim Fischer SWE – Endowed Chair of Wind Energy at the Institute of Aircraft Design Stuttgart University.

[6] International Standard, 2009. *IEC 61400-3. Wind Turbines – Part 3 : Design requirements for offshore wind turbines.* IEC, ISBN 2-8318-1025-2.

[7] Fischer, T., de Vries, W., and Schmidt, B., 2010. UpWind Project, Design Basis, K13 Shallow Water Site, WP4 – Offshore Foundations and Support Structures.

[8] Reiso, M., and Moe, G., 2010. Blade response on offshore bottom fixed wind turbines with downwind rotors. In Proceedings of OMAE2010 the ASME 29th International Conference on Ocean, Offshore and Arctic Engineering, OMAE2010-20586.

European Academy of Wind Energy

Norwegian University of Science and Technology

Models for global and local loads on wind turbines

R. Longo[1], S. Gaggero[2]

[1] PhD student, School of Science and Technologies for Engineering, Univ. of Genoa, Italy

[2] Department of Naval and Electric Engineering (DINAEL), University of Genoa, Italy

ABSTRACT

In wind turbine design, a widely used approach for predicting the steady loads on the rotor is the Blade Element Momentum Theory (BEMT). This simplified method is useful for computing the global loads but it may be not enough precise in predicting the load distribution on the blade, that is needed for structural verifications. In the present work a comparison is presented between global and local loads estimation obtained by BEMT and a theoretically more precise panel method. Different blade geometries and kinematic conditions are considered in order to assess in which range the BEMT method can be regarded as enough accurate.

KEYWORDS

Blade Element Momentum Theory, Panel Method, Loads on wind turbines.

1 INTRODUCTION

Blade Element Momentum Theory (BEMT) for the analysis of conventional axial turbines is based on a few assumptions which simplify the model, but limits its physical representativeness [1]. A key limiting assumption is represented by the decomposition of the blades into 2D profiles acting independently from each others. This imply to neglect the end effects of the blade, at root and tip, and the interaction between blades.

2D performances of the profiles, on the other hand, can be derived from other experimental or theoretical investigations, possibly including viscous and/or stall effects.

Empirical corrections are proposed in literature to account for some of the interaction effects, like the Prandtl correction for the tip effects, but also the accuracy of such corrections is object of the investigation.

With the aim of identifying the effects of these inaccuracies on global and local loads estimation, in the present work a comparison is presented between the results obtained by the BEMT and by a potential panel method which, in principle, should account properly for

the 3D effects above mentioned. On the other hand, panel methods are unable to model viscous and rotational effects in the flow (in particular in stall conditions).
The comparison reported in the present paper is therefore confined to low wind speed conditions, for which the viscous effects are less relevant and the local angles of attack at all blade sections result to be far enough from the stall value.
The panel code used for the comparison has been developed at the University of Genoa, (Department of Naval and Electric Engineering: DINAEL) originally for the analysis of marine propellers [2] and it is here adapted for the case of wind turbine rotors.

2 CASE STUDY FOR THE COMPARISON

As a first step, the results from the DINAEL panel method (PM) were validated by comparison with the data available from [4] regarding a stall regulated horizontal axis wind turbine (HAWT), having three blades and a radius of 50m. The comparison showed a good agreement in the low speed range, whereas, for wind speeds exceeding in that case about 9 m/s, the PM tends to overestimate the power respect to the experimental results. This was justified with stall phenomena starting to occur in some of the blade sections. From this first comparison, the criterion of checking the angle of attack of the various sections and avoiding angles close to stall has been established and applied in the following comparisons.
For the present study, the considered configuration is represented by three-bladed horizontal axis wind turbines (HAWTs), with radius R, rotating at constant angular velocity ω and subjected to a uniform wind flow at steady velocity V_0.
Three different rotor geometries are taken into account, whose principal geometrical and kinematic data are summarized in table 1. The twist and chord radial distributions adopted correspond in all cases to those presented in [4] but, because no experimental data were available for the NACA 632xx airfoil series employed in [4], the NACA 44xx series was used instead, maintaining along the radius the same maximum t/c distribution of the reference rotor. Experimental polar data for the NACA 44xx series were obtained from the classical reference [5]. The chosen rotational speeds and radii were adjusted in order to guarantee that the three rotors work at the same tip speed ratio, λ, for the various wind velocity considered.

Table 1: Summary of the geometrical and kinematic data

Case	R [m]	r_{HUB} [m]	ω [rpm]	V_0 [m/s]	λ
1	50	11.20	10.50	4.5, 5.0, 5.5, 6.5	12,11,10,9
2	65	14.56	8.08	4.5, 5.0, 5.5, 6.5	12,11,10,9
3	35	7.84	15.00	4.5, 5.0, 5.5, 6.5	12,11,10,9

3 COMPARISON BETWEEN BEMT AND PM RESULTS

The comparison was performed in terms of total thrust and total torque generated on the rotor and of the radial distribution of the same quantities along the blades. Figure 1 and 2 report results for case 1. Figure 1 shows on the left the thrust radial distribution vs. the radial position *r*/*R* for different kinematic conditions, represented by the tip speed ratio, $\lambda = \omega R / V_0$, and on the right the total thrust, *T*, as a function of the wind speed. Analogously, in Figure 2 the torque radial distribution, *q*(*r*/*R*), and the total torque, *Q*, are reported. The continuous and dashed lines are referred to BEMT results, respectively with and without the application of the Prandtl tip loss correction, whereas the dotted lines represent the PM results.

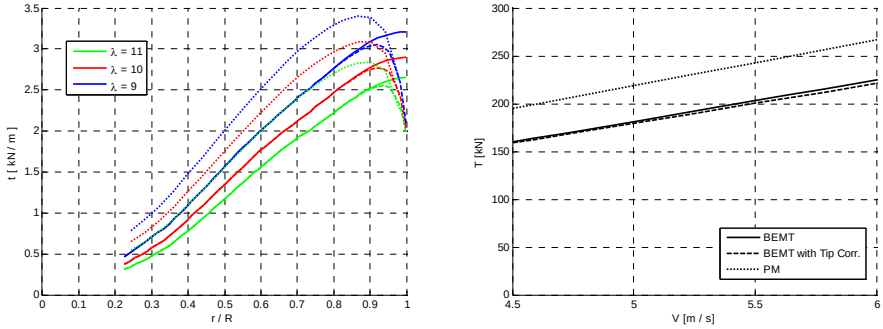

Figure 1: Total thrust Vs. wind velocity (left) and thrust radial distribution (right)

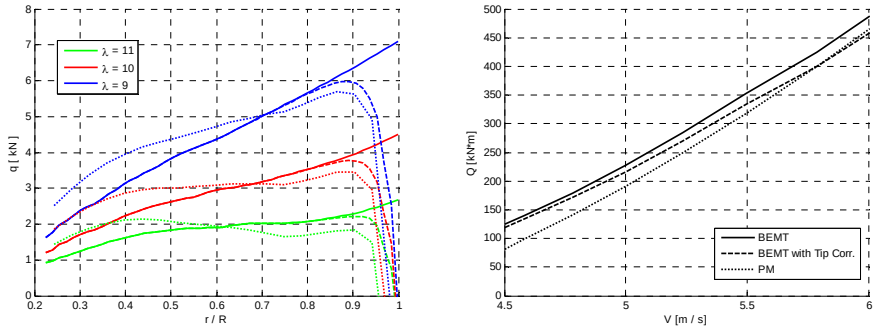

Figure 2: Total torque Vs wind velocity (left) and torque radial distribution (right)

In the present case the thrust distribution shows a pattern quite similar with the two methods if the Prandtl correction is applied, but a general underestimation of about 20% is present in the BEMT results. This is reflected also in the total thrust figure in which the differences do not show dependency on the flow speed. The end effect correction shows little influence.

The torque radial distribution is quite well captured at tip by BEMT if the Prandtl correction is adopted, but a certain underestimation by BEMT is present at lower radii. The total torque is

generally overestimated by BEMT but, in this case, the Prandtl correction tend to improve the comparison at higher wind speed.

Other results, not reported here, show that the bending load on the root of the blade is underestimated by BEMT, particularly with Prandtl correction; this effect increases with speed.

What reported above was found for case 1 but analogous results were obtained for the other two study cases.

4 CONCLUSIONS

As regards the 3D effects, not accounted for in BEMT, results show that the Prandtl correction is quite effective in capturing the end effect at the tip of the blade. This is achieved despite the fact that the correction doesn't account for the precise geometry of the blade. The effect of the hub, for which corrections are not available, seems to have a role in affecting the torque radial distribution while the influence on the thrust distribution is less evident.

Significant deviations are found between BEMT and PM in terms of thrust and thrust distribution on one side and torque and torque distribution on the other side. Trends are different for the two quantities, but the general effect on the bending moment on the blade root results to be an underestimation by BEMT.

All the results presented are however inherent to the specific geometries investigated and therefore cannot be automatically generalized.

The present work represents a first step in a wider research project covering the dynamics of an entire floating wind turbine unit.

BIBLIOGRAPHY

[1] Hansen M.O.L., "Aerodynamics of Wind Turbines", Harthscan 2007, ISBN: 978-1-84407-438-9

[2] Gaggero S. & Brizzolara S., "Exact Modelling of Trailing Vorticity in Panel Method for Marine Propeller", Proceedings of ICMRT 2007, Ischia (Italy)

[3] Brizzolara S., Villa D. & Gaggero S., "A systematic comparison between RANS and Panel Methods for Propeller Analysis", Proceedings of ICHD 2008, Nantes (France)

[4] Lain S., Quintero B. & Lopez Y., "Aerodynamic and Structural Evaluation of Horizontal Axis Wind Turbines with Rated Power over 1 MW", Proceedings of ICREPQ 2007, Sevilla (Spain)

[5] Abbott I.H. & von Doenhoff A.E., "Theory of Wing Sections: Including a Summary of Airfoil Data", Dover Publications 1959.

European Academy of Wind Energy

Norwegian University of Science and Technology

A numerical and analytical investigation of blade fatigue loads on the NREL 5MW wind turbine

Mads Døssing[1)], Christian Bak[2)]

[1) 2)] Risø DTU National Laboratory for Sustainable Energy, Wind Energy Division, Aeroelastic Design Group, Denmark.

ABSTRACT

The design of blades for horizontal axis wind turbines relies heavily on numerical optimization methods. Estimating the fatigue damage requires aeroelastic simulations in the time domain. This is very time-consuming and simplified methods are much needed. We determined time simulations and resulting fatigue loads on the NREL 5MW reference turbine using HAWC2. We then derived analytical expressions which captured the most important fatigue generating-effects. The results show that gravity and turbulence generate the edgewise fatigue loads. The flapwise loads are mainly caused by turbulence. A number of other factors are also important, but the resulting equations provide a simplified means of predicting fatigue loads which should lead to improvements in blade design as well as a general understanding of the important parameters.

KEYWORDS

Wind turbine, rotor, atmospheric turbulence, gravity-loads, material-fatigue.

1 INTRODUCTION

Wind turbine blades are designed for a lifetime of typically 20 years during which they operate in the atmospheric turbulence and under cyclic gravitational loading. This causes the loads on the blade to vary in time and thereby causing fatigue damage. Control strategies and stability issues are also important but will not be studied in detail here. Besides from aerodynamic efficiency and production price, the survivability to fatigue is a main design driver and it is therefore extremely important to calculate the fatigue damage and component lifetime when designing wind turbine blades.

We have derived an analytical expression which describes the fatigue loads on the wind turbine blades in the blade root. The results are given in terms of equivalent fatigue loads for the edge- and flapwise bending moments. The equivalent load has the advantage that the fatigue damage, due to a complicated load history, can be quantified using a minimum of

mads@risoe.dtu.dk

material- and structural data. The equivalent loads has been calculated numerically and compared to the analytical predictions in order to validate the theory. The NREL 5 MW fictitious reference turbine [1] was used as a test case which is representative for modern wind turbines in the MW range. The numerical simulations of the wind turbine were made using HAWC2 [2], which is an aeroelastic code developed at RISØ DTU National Laboratory for Sustainable Energy.

We had two reasons for deducing the analytical expression. 1) It would provide a simplified means for predicting fatigue damage and is useful for initial design purposes. 2) Given success of the analytical model we would have established the important parameters which influence the fatigue damage. This knowledge was needed because it clearly shows designers how they can improve the design.

The structural design requirements for blades are described in standards (IEC 61400-x). An appropriate fatigue analyses based on 10 min aeroelastic time series must be carried out using e.g. the Palmgren-Miner rule, for a number of design load cases (DLC). The DLC's corresponds to typical operating conditions described by the wind speed, turbulence intensity, wind shear etc. We used DLC 1.2 in [3] as the numerical reference case and it corresponds to normal operation from cut-in to cut-out wind speed in atmospheric turbulence using a normal turbulence model (NTM).

Previous work has mainly been focused on the development of aeroelastic codes and the correct numerical estimation of fatigue damage – i.e. a completely numerical approach which is carried out routinely in the design and certification of wind turbines. Some good examples of the results can be found in [4]. Such results are based on heavy calculations and since wind-turbines differ very much from one manufacturer to the next it is hard to generalize the results. A general qualitative introduction to wind turbine design and optimization is found in Fuglsang [5]. The possibility of fast engineering models for fast estimation of fatigue damage is mentioned and a semi-empirical model is suggested in Fuglsang [6]. This model is based on a linear relation between the variations in blade bending-moments and the turbulence standard deviation and this is in agreement with the result from this work. Fuglsang approximated the linear-coefficient using empirical data and the windspeed-derivative of bending moments in steady state operation. The procedure had to be repeated if the overall dynamics or rotational speed changed.

2 METHODS

Variations in wind speed relative to the rotating blade are related to variations in bending moments by taking the blade aerodynamic layout into consideration. We used an analytical expression to describe operation in shear and an engineering model in the case of turbulence. The fatigue damage is expressed using equivalent loads. The variation in bending moment due to gravity is taken as the difference in the static moments in the horizontal blade positions.

2.1 Equivalent flap-wise load due to wind-shear

The case where the wind-turbine operates without turbulence in a power-law-shear is simple because the binned RFC as function of radius r can be determined analytically

$$R_{eq}^{m} = \frac{\Omega}{2\pi f_{eq}}\left(\Omega\tfrac{1}{2}\rho \mathrm{V}_0 \int_{\mathrm{r}}^{\mathrm{R}} (1-\mathrm{a})\left[\left(1+\frac{\mathrm{r}'}{\mathrm{z_{hub}}}\right)^{\alpha} - \left(1-\frac{\mathrm{r}'}{\mathrm{z_{hub}}}\right)^{\alpha}\right](\mathrm{r}'-\mathrm{r})\,\mathrm{r}'\frac{dC_l}{d\alpha}c\,dr'\right)^{m} \quad (1)$$

2.2 RFC of axial velocities in turbulent windfield

Let n'_{tip} denote the distributed RFC of the turbulent, undisturbed wind seen from the blade tip, with ranges Δv (range from min to max). Other important parameters are the turbulence standard deviation σ_1 at hub height, the rotational speed Ω, rotor radius R, a characteristic turbulence length scale l, the power-law shear factor α and the hub heigh z_{hub}. A dimensionless analysis yields the functional relationship

$$\frac{\sigma_1 n'_{tip}}{\Omega} = f\left(\frac{\Delta v}{\sigma_1}, \frac{\Omega l}{\sigma_1}, \frac{\Omega R}{\sigma_1}, \frac{R}{z_{hub}}, \alpha\right)$$

Figure 2 shows RFC's calculated using HAWC2. The results can be approximated using only the first dimensionless group:

$$\frac{\sigma_1 n'_{tip}}{\Omega} = 3.0e^{\frac{-\Delta v}{\sigma_1}} = f\left(\frac{\Delta v}{\sigma_1}\right) \quad for\ \frac{\Delta v}{\sigma_1} \in [0, 8.0] \quad (2)$$

2.3 Equivalent flap-wise load due to turbulence

Assume n'_{tip} is valid on a major part of the blade so that $n' = n'_{tip}$. The equivalent load for M_f is found

$$R_{eq}^{m} = \frac{1}{f_{eq}} 3.0\Omega(1-\mathrm{a})\left(\sigma_1 \Omega\tfrac{1}{2}\rho \int_{r}^{R} (\mathrm{r}'-\mathrm{r})\mathrm{r}'\frac{dC_l}{d\alpha}c\,dr'\right)^{\mathrm{m}} \int_{0}^{8.0} y^m e^{-y}\,dy \quad (3)$$

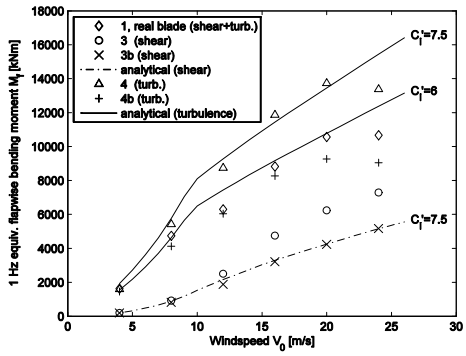

Figure 1: 1 Hz equivalent *flapwise* root-bending-moment. Equations: Analytical (shear) (1). Analytical (turbulence) (3)

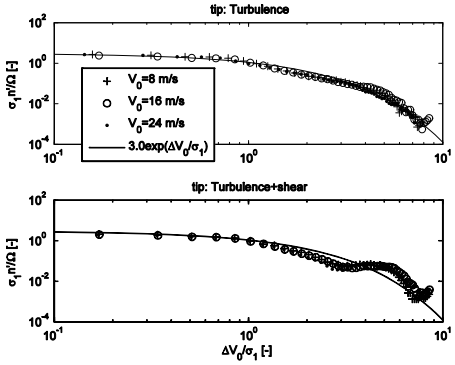

Figure 2: Distributed RFC plotted using dimensionless groups

3 CONCLUSIONS

The fatigue caused by the flapwise bending moment can be predicted by the presented theory. The accuracy is best in the case of rotation in shear which shows that the assumptions, used in the analytical approach, are valid and that the important fatigue generating effects have been identified. However, the fatigue damage is much higher when turbulence is present and the fatigue loads are described by (3). Important parameters include the dynamic-lift-curve-slope, turbulence standard deviation, the chord-distribution and the rotational speed (the latter increases both cycles and load).

BIBLIOGRAPHY

[1] J. Jonkman, S. Butterfield, W. Musial, and G. Scott. *Definition of a 5-MW Reference Wind Turbine for Offshore System Development*. 2009.

[2] Torben Juul Larsen. *How to HAWC2, the user's manual*. 2009.

[3] IEC 61400-1. *International Standard, Wind Turbines – Part 1 : Design requirements (Third edition)*. IEC 61400-1:2005(E), 2005.

[4] Torben J. Larsen, Helge Aa. Madsen and Gunnar C. Larsen. *Comparison of Design Methods for Turbines in Wake*. In *Research in Aeroelasticity EFP-2007*. 2008.

[5] P. Fuglsang. *Aerodynamic Design Guidelines for Wind Turbine Rotors*. 2002.

[6] P. Fuglsang and H.A. Madsen. *Optimization method for wind turbine rotors*. 1999.

European Academy of Wind Energy

Norwegian University of Science and Technology

A Framework for Integrated Control System and Aeroelastic Design of Wind Turbines

Fabiano Daher Adegas, Jakob Stoustrup, Torben Knudsen

Automation and Control, Dept.of Electronic Systems, Aalborg University, Denmark.

ABSTRACT

A proper control system design mitigates the mechanical stresses suffered by wind turbines' components. A proper design of wind turbines' aerodynamics and mechanical structure also aims the avoidance of stresses. Ideally, control system, aerodynamics and structure designs should be smartly integrated to result in a more (cost) efficient wind turbine. This paper brings a basic overview of a preliminary framework for integrated control systems and aeroelastic design of wind turbines based on advanced systems and control techniques.

KEYWORDS

Control systems, aeroelasticity, linear fractional transformation, linear matrix inequalities.

1 INTRODUCTION

The design of controlled systems is usually done in two steps. In the first step, the system to be controlled (plant) is designed to satisfy static and dynamic requirements. In the second step, a controller is designed to provide robustness and to satisfy closed-loop performance specifications. The state-of-the-art procedures for wind turbine design are not exceptions to this approach. The plant is designed according to aeroelastic objectives such as structural integrity, avoidance of modal excitation due to the rotor rotary movement, and increased damping to reduce vibrations [1]. A controller is designed afterwards based on the predefined aeroelastic plant aiming at objectives such as closed-loop stability and robustness, increased energy production and active vibration and moment suppression [2]. This two-step approach does not result in a total optimal system. The design parameters of both plant and controller have to be simultaneously adjusted to optimize closed-loop performance. A Ph.D. thesis entitled "Integrated Control and Aeroelastic Design of Wind Turbines" is addressing this issue by applying advanced systems and control engineering techniques. A basic overview of a preliminary framework for integrated control and aeroelastic design is described, including: the environment and data transfer between modules; how control and aeroelasticity are modelled within the same system description; the structured control design arising when synthesizing controller and aeroelastic parameters, and the tools for optimization.

fda@es.aau.dk

2 OPTIMIZATION FRAMEWORK

2.1 Interconnection Environment

To make possible the exploitation of different integrated design strategies, a flexible structure and control system interconnection environment was conceived inspired on [3]. One of the objectives of the interconnection environment is to reduce the human intervention on the design phases. An increased level of automation when designing model-based controllers or/and improving aeroelasticity is pursued.

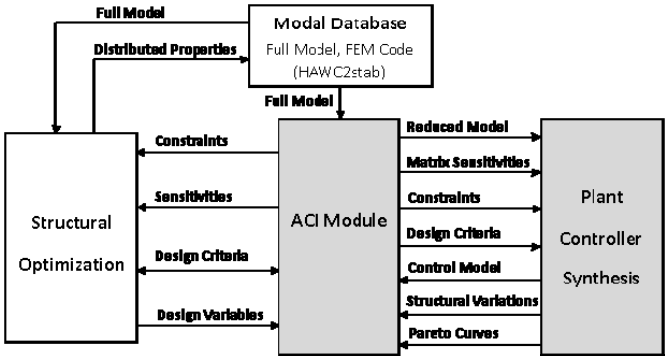

Figure 1: Structural and control system interconnection environment.

The core of the Modal Database is the HAWC2stab finite element code under development by a partner institution. It generates linearized full-order aeroelastic models. The Structural Optimization module contains shapes and distributed properties of the structural components and is responsible for the quasi-static aerodynamics and structural design. The present Ph.D. thesis focuses on the development of the Aeroelastic-Control Interface (ACI) module the Plant-Controller Synthesis (PCS) module. The ACI module is responsible for the modelling, sensitivity analysis, and data transfer between the other modules. In the PCS module, control systems and aeroelasticity are simultaneously designed for improvement of dynamics. The ACI module supplies the following data to the PCS module:

- Reduced-size versions of the vector second-order matrices for nominal and extreme design cases.
- Sensitivities of these matrices and their maximum allowed variations with respect to structural design variables.
- Design constraints and criteria depending on the design case of interest.

The ACI module supplies the following data to the Structural Optimization module:

- Control system model.
- Values of optimal structural variations computed by the PCS.

- Definition of control design variables as changeable gains in the quasi-static structural design process, and the associated allowable variations.
- Control design constraints to be satisfied in the structural optimization.
- Pareto-optimal curves relating wind speed to rotational speed (or electrical power) RMS disturbance attenuation, maximum pitch angle rate, and maximum damping of modes.

2.2 System Modelling

2.2.1 Linear Fractional Representation

An important operator in systems and control theory called Linear Fractional Representation (LFR) [4] is utilized to unify the control and aeroelastic systems models. Figure 2(a) illustrates the LFR as a block diagram. The LFR is a natural formulation to describe feedback systems, as *M* can be seen as the system to be controlled and Δ as the controller. Parameter variations of lumped mechanical systems, even for finite element models, can be represented as LFR interconnections [5]. In this case, *M* is the nominal system and Δ are variations from nominal values of mass, stiffness and damping, or natural frequency and damping of modes. Δ can also represent variations of structural dimensions, e.g. spar thickness. Interconnections of LFRs are again LFRs as illustrated in Figure 2(b). A simple reorganization of the diagram, by grouping all the known systems together, and grouping the unknown Δ_i's, results in a single LFR as seen on the diagram of Figure 2(c).

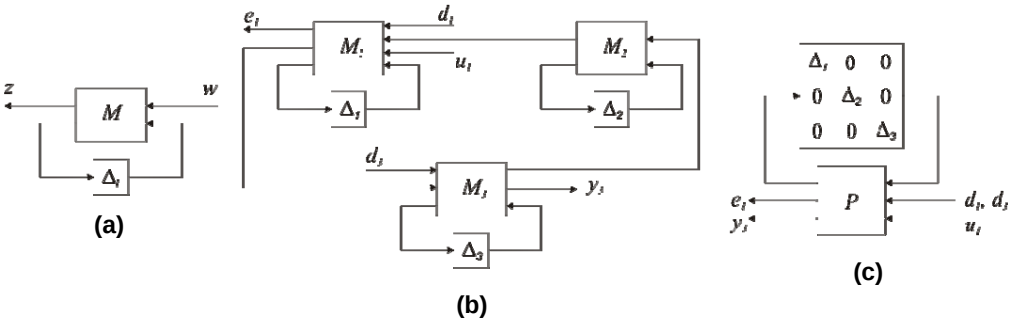

Figure 2: Block diagrams of Linear Fractional Representation.

2.2.2 Structured Control Design

Our particular interest lies in the structured state-space system (1).

$$\begin{aligned} x_{k+1} &= A(\delta,K)x_k + B(\delta,K)d_k \\ e_k &= C_e(\delta,K)x_k + D_{ed}(\delta,K)d_k \\ y_k &= C_y(\delta,K)x_k + D_{yd}(\delta,K)d_k \end{aligned} \tag{1}$$

Where x_k is the state, e_k the error, y_k the measurements, and d_k the disturbance vectors. $A(\ )$, $B(\ )$, $C(\ )$, $D(\ )$ are matrices originated from a realization of the "grouped" LFR. K is the controller and $\Delta = \delta = diag(\delta_1, \delta_2, \ldots \delta_n)$ are the plant parameters. The simultaneous design of plant parameters δ and controller K, to be done by the PCS module, is a *structured control design* problem which can be solved by optimization algorithms.

2.3 Linear Matrix Inequalities

A variety of problems related to system and control theory can be formulated to standard convex and quasiconvex optimization problems that involve matrix inequalities (LMI) [6]. The resulting optimization problems can be solved numerically very efficiently using interior-point methods. A *structured control design* is originally a non-convex problem and therefore can have several local minimal points. The present thesis is developing algorithms to turn this non-convex problem into a convex one with optimality guarantees by sequentially solving optimization problems with LMI constraints. Papers with recent results within this subject are expected to be published in the upcoming 2011 control conferences.

3 CONCLUSIONS

This paper briefly described a preliminary framework for integrating control and aeroelastic design of wind turbines. Advanced procedures for analysis and synthesis of dynamical systems are being developed to simultaneously design control and aeroelastic parameters. LFR and LMI-constrained based optimization, along with recent developments in structured controller design carried out during the Ph.D. thesis, are the main tools for accomplish such task.

BIBLIOGRAPHY

[1] Hansen, M. H. "Improved Modal Dynamics of Wind Turbines to Avoid Stall-induced Vibrations". In: Wind Energy, Vol. 6, 2003.

[2] Bossanyi, E., "The Design of Closed Loop Controllers for Wind Turbines". In: Wind Energy, Vol.3, 2000.

[3] Moulin, B. ; Idan, M. ; Karpel, M. "Aeroservoelastic Structural and Control Optimization Using Robust Design Schemes". Journal of Guidance, Control and Dynamics, Vol. 25, No 1, 2002.

[4] Doyle, J.; Packard, A.; Zhou, K. "Review of LFTs, LMIs, and μ". In: IEEE CDC, 1991.

[5] Lind, R.; Brenner, M. "Robust Aeroservoelastic Stability Analysis". Springer-Verlag.

[6] Boyd, S. ; El Ghaoui, L. ; Feron, E. ; Balakrishnan, V. "Linear Matrix Inequalities in System and Control Theory". SIAM, Philadelphia.

Temporary Rotor Inertial Control of Wind Turbine to Support the Grid Frequency Regulation

Bing Liu

Department of Electric Power Engineering, Norwegian University of Science and Technology, Norway

ABSTRACT

This paper describes control approach of variable speed wind turbine to provide inertial response, which support grid primary frequency control. During a frequency disturbance, the magnitude of the change in wind power generation is proportional to the magnitude of the increase in the error between the system frequency reference and the actual system frequency. Furthermore, the inertial response capability of a baseline variable speed wind turbine is quantified by PSCAD simulations.

KEYWORDS

Inertial control, wind turbine, frequency regulation

1 INTRODUCTION

The rapid increasing portion of wind energy calls for wind turbines' inertial response characteristics to facilitate primary frequency control. System frequency, as signal of balance between load and generation, need to be kept stable during major disturbance. Conventional power generation units with synchronous generators provide inertial response, which contributes to the system transient stability significantly. However, wind turbine with partial or full size power converter by default will not provide any inertial response. Therefore, the displacement of wind energy might reduce the power system total inertia with consequence of more and faster frequency variation, which might limit the further wind energy penetration level. The situation is more serious in isolated grids.

The utilities have realized the need of wind generation's contribution to frequency stability. In Nordic grid code 2007, it is required that 'Automatic control of the wind turbine active production as a function of the system frequency must be possible. The control function must be proportional to frequency deviations and must be provided with a dead-band.' In UK grid guidance to wind park there is also similar requirement. Furthermore, Hydro-Québec requires wind farm to have the capability to reduce large frequency deviation (0.5 Hz) up to 10

seconds. These regulations require wind turbine's inertial response, which can utilize stored rotating energy temporarily to support power system frequency stability.

In the variable speed wind turbine, partial or full size power converter decouples the generator from the network. So the control strategy needs to be revised to enable the inertial response, as presented in several recent papers [3] - [5]. Two control strategies were compared in [3], and the primary frequency control strategy used by conventional power plants shows a better performance. In the primary frequency control strategy, the magnitude of the change in power generation during a frequency disturbance is proportional to the magnitude of the increase in the error between the system frequency reference and the actual system frequency. In [6] and [7], the control theme of extra control loop responding proportionally to the system frequency deviation was verified by simulation results.

A wind turbine inertial response control application in the hydro dominated system was presented and modelled in [1], which shows significant improvement in the system temporary minimum frequency. The opposite initial power surge of hydro power will bring undesirable frequency variation, and the situation will be even serious in isolated grids.

The main objectives of this paper are to present a variable wind turbine model with inertial response ability, and to investigate its temporary active support capability. Furthermore, a configuration and model of isolated grid containing hydro and wind energy will be presented. Basing on this configuration, a case study for primary frequency control strategy will be investigated to stabilize the active power fluctuation.

The structure of this paper is as follows. First, Wind turbine model will be presented briefly. Second, the extra control loop will be introduced both in partial load and full load operating modes. Third, the inertial response capability will be investigated and quantified. At last, a case study of primary frequency control in isolated island configuration will be demonstrated by both control strategy and simulation results.

2 VARIABLE-SPEED WIND TURBINE MODELLING

A double-fed induction generator (DFIG) wind turbine model is presented in [10], which consists of air dynamic and mechanical model, generator and power converter control. A wind turbine sized at 2 MW is selected as baseline of modelling.

The DFIG is a wound rotor induction generator whose rotor is fed via slip rings by a frequency converter. The network frequency is decoupled from the mechanical speed of the machine by the frequency converter. Since power ratings are a function of slip, normally the DFIGs operate over a range of speeds typically between about 0.75 and 1.25 pu of synchronous frequency, which requires converter power ratings of approximately 25%.

Another great advantage of the DFIG wind turbine is that it has the capability to control active and reactive power independently.

According the definition, the inertia of any object consisting of N point masses (with respect to a given axis of rotation) can be expressed as:

$$J = \sum_{i=1}^{N} m_i r_i^2 \quad (1)$$

Where m is mass and r is the perpendicular distance to the axis of rotation. And the power stored in rotating objective is given by: $E = \frac{1}{2} J\omega^2$, where omega is angular rotating speed.

3 INERTIAL RESPONSE CONTROLLER IMPLEMENTATION AND QUANTIFICATION

For the variable speed, pitch control wind turbine control, two different control stages are implemented according the wind speed. Below-rated wind speed (partial load), torque control will be implemented to track the maximal power from wind. Above-rated wind speed (full load), pitch regulation dominates the power control [9].

Figure 1 shows a typical wind turbine control schematic during partial load mode. To enable the inertial response, an extra power command is added into the reference power, which is originally decided by speed-power relationship curve. Normally pitch angle will keep at -2 to 0 degree during the partial load operation.

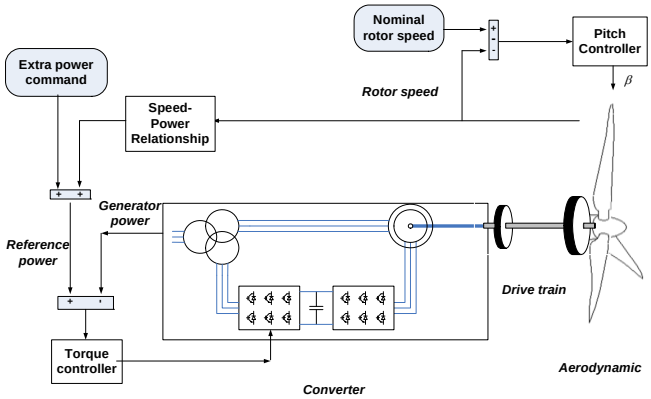

Figure 1: typical wind turbine control schematic during partial load mode

The figure 2 shows a typical wind turbine control schematic during full load mode, which is adopted from [1]. When wind turbine operates at full load mode, the pitch will limit the power tracking from wind to achieve desirable rotating speed. Theoretically, wind turbine can submit extra power by decrease the pitch angle. Practically, extra power value and duration will be limited by the stresses of wind turbine drive-train components.

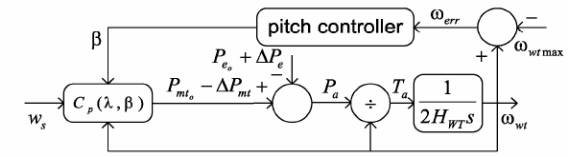

Figure 2: typical wind turbine control schematic during full load mode [1]

This paper will focus on the quantification of wind turbine inertial response capability in partial load mode. In the following simulation case, the wind turbine is operating at constant wind speed 8 meter per second. Figure 3 demonstrates that the wind turbine is able to give 10% extra power by stored energy in the rotor for 43 seconds, before it reaches minimal allowable 70% of rated rotating speed rotor speed.

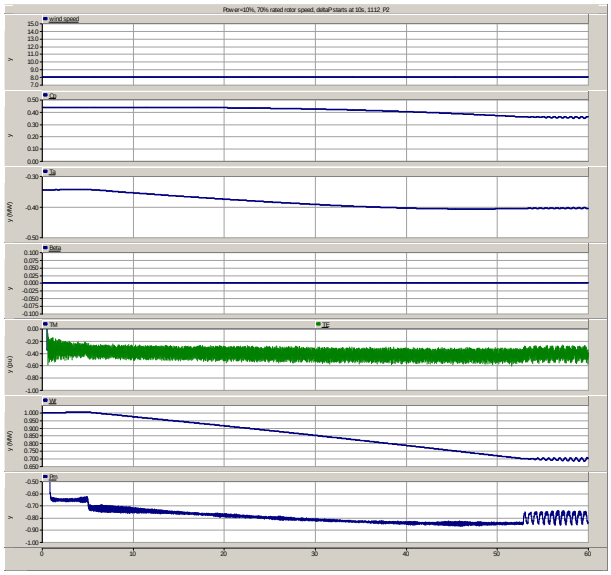

Wind speed (m/s)

Power co efficiency

Air dynamic torque (PU)

Pitch angle

Generator mechanic torque (PU)

Rotor speed (PU)

Power output (MW)

0 s Time (s) 60 s

Figure 3: Wind turbine parameters when Power reference=110%, starts at 10s.

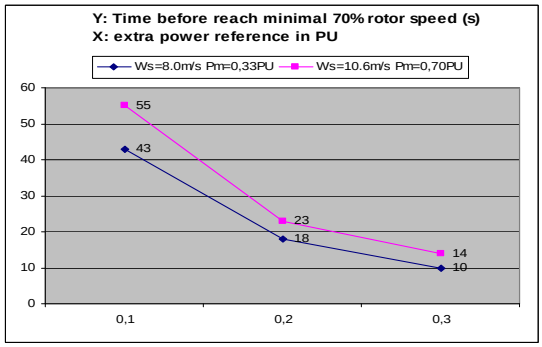

Figure 4: Time before wind turbine rotor speed reaches 70% PU

Similarly, the time before wind turbine rotor speed reaches 70% PU with 10%, 20%, and 30% extra power reference was presented in the figure 4. The more extra power submitted, the sooner wind turbine reaches the minimal rotor speed. The higher wind speed wind turbine operates at, the later wind turbine reaches the minimal rotor speed.

4 CONCLUSION:

This paper presented control approach of variable speed wind turbine to provide inertial response, which support grid primary frequency control. After brief introduction of inertial response control implementation during partial load and full load, the inertial response capability of a variable speed wind turbine was qualified by simulation.

BIBLIOGRAPHY

[1] Ullah NR, Thiringer T, Karlsson D. Temporary primary frequency control support by variable speed wind turbines—potential and applications. IEEE Transactions on Power Systems 2008; 23: 601–612.

[2] Suul, J.A.; Uhlen, K.; Undeland, T., "Wind power integration in isolated grids enabled by variable speed pumped storage hydropower plant," Sustainable Energy Technologies, 2008. ICSET 2008. pp.399-404, 24-27 Nov. 2008

[3] Johan Morren, Jan Pierik, Sjoerd W.H. de Haan, Inertial response of variable speed wind turbines, Electric Power Systems Research, Issue 11, July 2006, Pages 980-987

[4] Mullane, A.; O'Malley, M., "The Inertial Response of Induction-Machine-Based Wind Turbines," Power Systems, IEEE Transactions on , vol.20, no.3, pp. 1496-1503, 2005

[5] PSCAD® / EMTDC™ user's guide, 2004.

[6] Rogério G. de Almeida, J. A. Peças Lopes, Primary frequency control participation provided by doubly fed induction wind generators, 15th PSCC, Liege, August 2005

[7] James F. Conroy, Rick Watson, Frequency Response Capability of Full Converter Wind Turbine Generators in Comparison to Conventional Generation, Power Systems, IEEE Transactions on , VOL. 23, NO. 2, MAY 2008

[8] Eek, Jarle; Uhlen, Kjetil; Gjengedal, Terje, Wind power contribution to primary frequency response in the Nordel power system. NWPC'2006.

[9] Abram Perdana, Ola Carlson, Jonas Persson, Dynamic Response of Grid-Connected Wind Turbine with Doubly Fed Induction Generator during Disturbances., NORDIC WORKSHOP ON POWER AND INDUSTRIAL ELECTRONICS. TRONDHEIM – 2004.

[10] Bing Liu, The Implementation of Variable Speed Wind Turbine Aerodynamic and Drive Train Modeling for Transient Analysis, The 4th EAWE PhD Seminar on Wind Energy in Europe, Magdeburg, Germany, October 2008.

European Academy of Wind Energy

Norwegian University of Science and Technology

Dynamic analysis of wind turbines from an integrated perspective

Braulio Barahona and Poul Sørensen

Risø DTU, Denmark

ABSTRACT

This work presents a mapping of the dynamical phenomena on the structural loads of a wind turbine using a multi-domain simulation platform that combines state-of-the-art aeroelastic and structural software, with commercial software for dynamic systems and control. A fixed-speed wind turbine is analyzed to investigate frequency coupling between electrical and structural subsystems.

1 INTRODUCTION

Given the increased amount of electricity produced by wind turbines in modern power systems, the analysis of wind turbines needs to integrate dynamic aspects of the power system, control systems, and electrical components with the dynamics of the wind turbine structure and the aeroelastic phenomena. For example, in [1] the coupling between wind turbine structural modes, and the generator electromechanical mode is studied in a fixed-speed wind turbine. The work in [2, 3] investigates the impact of voltage faults on the structural loads in variable-speed (DFIG), and in fixed-speed wind turbines respectively. In [4], the impact of wind turbulence, and tower shadow on the capability of DFIG wind turbines to provide network support is investigated.

As the complexity of the model that represents appropriately the desired integrated dynamics of wind turbines increases, one approach is to couple sub models of different domains. This can be done in a block fashion, where the blocks representing subsystems can be simulated in different software. Such approach is taken in [5] using the software FAST and Simulink, where the impact of electrical transient on mechanical loads is illustrated. In [6], investigations regarding the impact of the limits of electrical systems and control on wind turbine design is illustrated using the software Bladed.

The present work uses HAWC2 and Simulink, as described in [7], the aim is to observe the frequency coupling between electrical and structural subsystems. The system under study is a fixed-speed wind turbine, directly connected to a infinitely stiff grid. The aim is to investigate the frequency coupling between the asynchronous generator dynamics, and the structural dynamics of the wind turbine. Section 2 presents numerical and analytical analysis

braulio.barahona@risoe.dk

of the asynchronous generator dynamics. Section 3 describes the numerical simulations and presents the spectrum of structural loads and generator torque. Conclusions are presented in Section 4.

2 ANALYSIS OF ASYNCHRONOUS GENERATOR DYNAMICS

A dynamic model of an asynchronous generator in dq-frame [8, 9], can be expressed in state-space form using fluxes λ as state variables by Eq. 1.

$$\begin{bmatrix}\dot{\boldsymbol{\lambda}}_{dqs}\\ \dot{\boldsymbol{\lambda}}_{dqr}\end{bmatrix} = \boldsymbol{\mathcal{M}}\begin{bmatrix}\boldsymbol{\lambda}_{dqs}\\ \boldsymbol{\lambda}_{dqr}\end{bmatrix} + \begin{bmatrix}\mathbf{v}_{dqs}\\ \mathbf{v}_{dqr}\end{bmatrix} \tag{1}$$

where the vectors of stator and rotor fluxes ($\boldsymbol{\lambda}_{dqs}$, $\boldsymbol{\lambda}_{dqr}$) and input voltages ($\mathbf{v}_{dqs}$, $\mathbf{v}_{dqr}$) are Eq. 2,

$$\begin{bmatrix}\boldsymbol{\lambda}_{dqs}\\ \boldsymbol{\lambda}_{dqr}\end{bmatrix} = [\lambda_{ds} \quad \lambda_{qs} \quad \lambda_{0s} \quad \lambda_{dr} \quad \lambda_{qr} \quad \lambda_{0r}]^{\mathrm{T}} \tag{2}$$

$$\begin{bmatrix}\mathbf{v}_{dqs}\\ \mathbf{v}_{dqr}\end{bmatrix} = [v_{ds} \quad v_{qs} \quad v_{0s} \quad v_{dr} \quad v_{qr} \quad v_{0r}]^{\mathrm{T}}$$

and the system matrix $\boldsymbol{\mathcal{M}}$ is defined by a diagonal matrix of winding resistances **R**, an inductance matrix in dq-frame $\mathbf{L}_{dq}$, and a matrix $\boldsymbol{\Omega}$ that relates to the speed voltages.

$$\boldsymbol{\mathcal{M}} = -\left(\mathbf{R}\mathbf{L}_{dq}^{-1} + \boldsymbol{\Omega}\right) \tag{3}$$

The electromagnetic torque of the generator with balanced input voltages is given by Eq. 4.

$$T_{em} = \frac{3}{2}\frac{p_f}{2}\frac{\mathcal{L}_m}{D}\left(\lambda_{qs}\lambda_{dr} - \lambda_{ds}\lambda_{qr}\right) \tag{4}$$

The state-space model Eq. 1 can be simplified when input voltages are balanced, in that case the zero components of state variables, and inputs are always zero. Therefore, the full order state-space model can be expressed as in Eq. 5.

$$\begin{bmatrix}\dot{\lambda}_{ds}\\ \dot{\lambda}_{qs}\\ \dot{\lambda}_{dr}\\ \dot{\lambda}_{qr}\end{bmatrix} = \begin{bmatrix}\frac{R_s\mathcal{L}_r}{D} & -\dot{\beta}_s & \frac{-R_s\mathcal{L}_m}{D} & 0\\ \dot{\beta}_s & \frac{R_s\mathcal{L}_r}{D} & 0 & \frac{-R_s\mathcal{L}_m}{D}\\ \frac{-R_r\mathcal{L}_m}{D} & 0 & \frac{R_r\mathcal{L}_s}{D} & -\dot{\beta}_r\\ 0 & \frac{-R_r\mathcal{L}_m}{D} & \dot{\beta}_r & \frac{R_r\mathcal{L}_s}{D}\end{bmatrix}\begin{bmatrix}\lambda_{ds}\\ \lambda_{ds}\\ \lambda_{dr}\\ \lambda_{qr}\end{bmatrix} + \begin{bmatrix}v_{ds}\\ v_{qs}\\ v_{ds}\\ v_{dr}\end{bmatrix} \tag{5}$$

Using the definition of electromagnetic torque Eq. 4, and the equation of conservation of angular motion Eq. 6

$$T_{em} - T_L = J\dot{\omega}_{rm} \tag{6}$$

the change in rotor speed $\dot{\omega}_{rm}$ in terms of the states variables of Eq. 5 yields Eq. 7.

$$\dot{\omega}_{rm} = \frac{1}{J}\frac{3}{2}\frac{p_f}{2}\frac{\mathcal{L}_m}{D}\left(\lambda_{qs}\lambda_{dr} - \lambda_{ds}\lambda_{qr}\right) - \frac{1}{J}T_L \tag{7}$$

The linear system in Eq. 5, and Eq. 7 that relates non-linearly fluxes to rotor speed, are coupled. This can be expressed in matrix form, as shown in Eq. 8.

$$\begin{bmatrix}\dot{\lambda}_{ds}\\ \dot{\lambda}_{qs}\\ \dot{\lambda}_{dr}\\ \dot{\lambda}_{qr}\\ \dot{\omega}_{rm}\end{bmatrix}=\begin{bmatrix}\frac{R_s\mathcal{L}_r}{D} & -\dot{\Theta}_{ar} & \frac{-R_s\mathcal{L}_m}{D} & 0 & 0\\ \dot{\Theta}_{ar} & \frac{R_s\mathcal{L}_r}{D} & 0 & \frac{-R_s\mathcal{L}_m}{D} & 0\\ \frac{-R_r\mathcal{L}_m}{D} & 0 & \frac{R_r\mathcal{L}_s}{D} & \omega_{re}-\dot{\Theta}_{ar} & 0\\ 0 & \frac{-R_r\mathcal{L}_m}{D} & \dot{\Theta}_{ar}-\omega_{re} & \frac{R_r\mathcal{L}_s}{D} & 0\\ -\mathrm{A}\lambda_{qr} & A\lambda_{dr} & 0 & 0 & 0\end{bmatrix}\begin{bmatrix}\lambda_{ds}\\ \lambda_{ds}\\ \lambda_{dr}\\ \lambda_{qr}\\ \omega_{rm}\end{bmatrix}+\begin{bmatrix}v_{ds}\\ v_{qs}\\ v_{ds}\\ v_{dr}\\ -\frac{1}{J}T_L\end{bmatrix} \tag{8}$$

with

$$A=\frac{1}{J}\frac{3}{2}\frac{p_f}{2}\frac{\mathcal{L}_m}{D} \tag{9}$$

The dynamics of this system of equations are illustrated in Fig. 1a, where a steady-state torque characteristic (circles), together with the dynamic response (black dotted line) to a change in load are plotted in the slip-torque plane. The change in load is a step change that is kept until the system reaches steady-state, then another step back to the previous load is done. Therefore, it can be seen in Fig. 1a, a loop going from one steady-state point to another and back again.

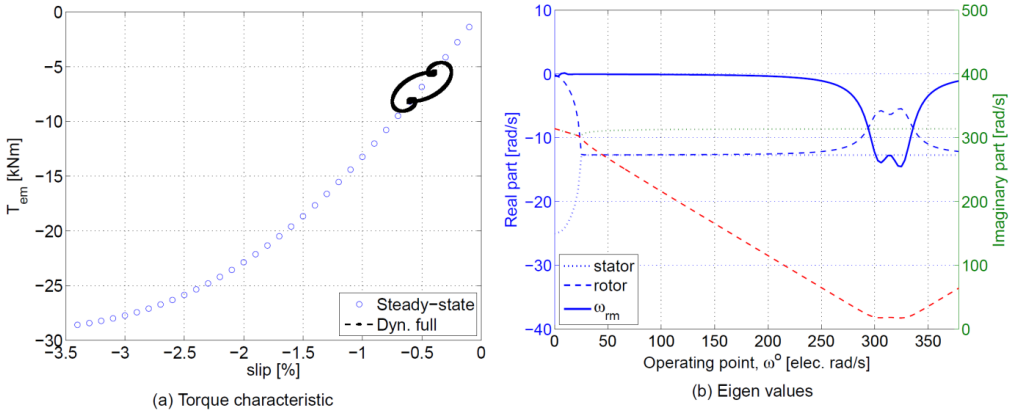

(a) Torque characteristic (b) Eigen values

Figure 1: Dynamics of asynchronous generator

In order to observe the natural frequencies of the system in Eq. 8 at different operating points, the system is linearized. Linearizing around a given operating point (ω_{re}^{o}), yields the following linear system Eq. 10. The eigen values of the system matrix at different ω_{re}^{o}, are the natural frequencies corresponding to the state variables of the system. Noticed that the eigen values of fluxes are complex conjugated pairs. For example, the eigen value of the stator flux in d-axis is the complex conjugate of the eigen value of the stator flux in q-axis. Fig. 1b shows the eigen values of stator flux (small dotted lines), rotor flux (dotted lines) and rotor speed (solid line). The left axis of Fig. 1b reads the real parts or real eigen values (blue lines), and the right axis reads the positive imaginary parts of eigen values (red lines).

$$\begin{bmatrix} \Delta\dot{\lambda}_{ds} \\ \Delta\dot{\lambda}_{qs} \\ \Delta\dot{\lambda}_{dr} \\ \Delta\dot{\lambda}_{qr} \\ \Delta\dot{\omega}_{rm} \end{bmatrix} = \begin{bmatrix} \frac{R_s\mathcal{L}_r}{D} & -\dot{\Theta}_{ar} & \frac{-R_s\mathcal{L}_m}{D} & 0 & 0 \\ \dot{\Theta}_{ar} & \frac{R_s\mathcal{L}_r}{D} & 0 & \frac{-R_s\mathcal{L}_m}{D} & 0 \\ \frac{-R_r\mathcal{L}_m}{D} & 0 & \frac{R_r\mathcal{L}_s}{D} & \omega_{re}^o - \dot{\Theta}_{ar} & \lambda_{qr}^o \\ 0 & \frac{-R_r\mathcal{L}_m}{D} & \dot{\Theta}_{ar} - \omega_{re}^o & \frac{R_r\mathcal{L}_s}{D} & \lambda_{dr}^o \\ -A\lambda_{qr}^o & A\lambda_{dr}^o & A\lambda_{qs}^o & -A\lambda_{ds}^o & 0 \end{bmatrix} \begin{bmatrix} \Delta\lambda_{ds} \\ \Delta\lambda_{ds} \\ \Delta\lambda_{dr} \\ \Delta\lambda_{qr} \\ \Delta\omega_{rm} \end{bmatrix} + \begin{bmatrix} \Delta v_{ds} \\ \Delta v_{qs} \\ \Delta v_{ds} \\ \Delta v_{dr} \\ -\frac{1}{J}\Delta T_L \end{bmatrix} \quad (10)$$

3 NUMERICAL SIMULATION OF FIXED SPEED WIND TURBINE

This section presents the numerical simulations run with HAWC2-Matlab/Simulink model. The system under study is a 2 MW, pitch-regulated fixed-speed wind turbine directly connected to the grid. The dynamic sub models simulated in HAWC2 are: the stochastic wind input (3D-coherent turbulence, logarithmic shear profile), aeroelastic phenomena (tower shadow, dynamic and yawed inflow), and structural phenomena (large deflections, gyroscopic and centrifugal effects). The generator sub model, 4th order dynamic model described by Eq. 1, is modeled in Matlab.

The system is simulated for 600 s, under rated wind speed operation 12 m/s, with turbulence intensity of 10%. The following Fig. 2-4 (page 4) present the spectrum of structural loads (light colors), and electromagnetic torque (blue). This spectra have been normalized with the minimum value of each signal, therefore the spectral magnitude cannot be compared across signals, the reason is to make it simpler to compare frequencies of peak values. In every figure, one can observe the main P-frequencies in most of the signals very clearly. On the other hand the structural modes are seen in the corresponding signals, and in some cases across the structure. The focus of this work is to observe the structural signals in the frequency range of the natural frequency of the generator rotor speed, this is around 2 Hz for operation at rated speed (Fig. 1b).

In Fig. 3, the side-wise tower moment spectra shows a mode at 2.067 Hz. The electromagnetic torque shows a mode at 2.017 Hz, this would be the natural frequency of the generator rotor speed. Observing the time domain response of the structural loads under a grid fault in [7], the sidewise tower moment was the most affected, this can be explained by the coupling of tower side-wise and generator rotor speed modes. In [2], the impact of a voltage fault on sidewise tower moment is also remarked.

4 CONCLUSIONS

An analysis of the dynamics of an asynchronous generator was presented, the natural frequencies of the generator fluxes and rotor speed were mapped for different operation points. Numerical simulations of a fixed-speed wind turbine showed that a sidewise tower

mode is very close to the generator rotor speed torque, which supports the fact that voltage faults have a realtively large impact on the sidewise tower moment of fixed-speed, and DFIG wind turbines.

ACKNOWLEDGMENTS

The Wind Energy Division of Risø DTU is acknowledge for supporting the Ph.D. project 'Integrated Design of Wind Power Systems'.

REFERENCES

[1] T. J. Larsen, M. H. Hansen, and F. Iov, "Generator Dynamics in Aeroelastic Analysis and Simulations," tech. rep., Risø DTU, 2003.

[2] R. Fadaeinedjad, G. Moschopoulos, and M. Moallem, "Investigation of voltage sag impact on wind turbine tower vibrations," Wind Energy, 2008.

[3] A. D. Hansen, N. A. Cutululis, H. Markou, and P. Sørensen, "Impact of fault ride-through requierements on fixed-speed wind turbine structural loads," Wind Energy, 2010.

[4] F. M. Huges, O. Anaya-Lara, G. Ramtharan, N. Jenkins, and G. Strbac, "Influence of Tower Shadow and Wind Turbulence on the Performance of Power System Stabilizers for DFIG-Based Wind Farms," IEEE Transactions on Energy Conversion, vol. 23, pp. 519–528, 2008.

[5] R. Fadaeinedjad, M. Moallem, and G. Moschopoulos, "Simulation of a wind turbine with doubly fed induction generator by fast and simulink," IEEE Transactions on Energy Conversion, vol. 23, pp. 690–700, 2008.

[6] G. Ramtharan, N. Chris, and B. Ervin, "Importance of advanced simulations of electrical transients in wind turbines," in European Wind Energy Conference, April 2010.

[7] B. Barahona, L. C. Henriksen, A. D. Hansen, N. A. Cutululis, and P. Sørensen, "Coupling of hawc2 and matlab: Towards an integrated simulation platform," in European Wind Energy Conference, April 2010.

[8] C.-M. Ong, Dynamic Simulation of Electric Machinery using Matlab/Simulink. Prentince Hall PRT, 1998.

[9] P. C. Krause, O. Wasynczuk, and S. D. Sudhoff, Analysis of Electric Machinery and Drive Systems. IEEE Press Series on Power Engineering, WileyBlackwell, 2002.

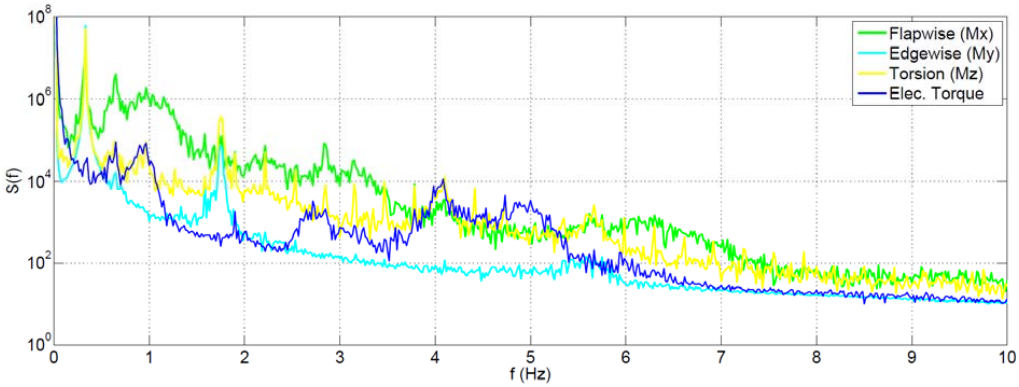

Figure 2: Spectrum of blade root bending moments and electromagnetic torque

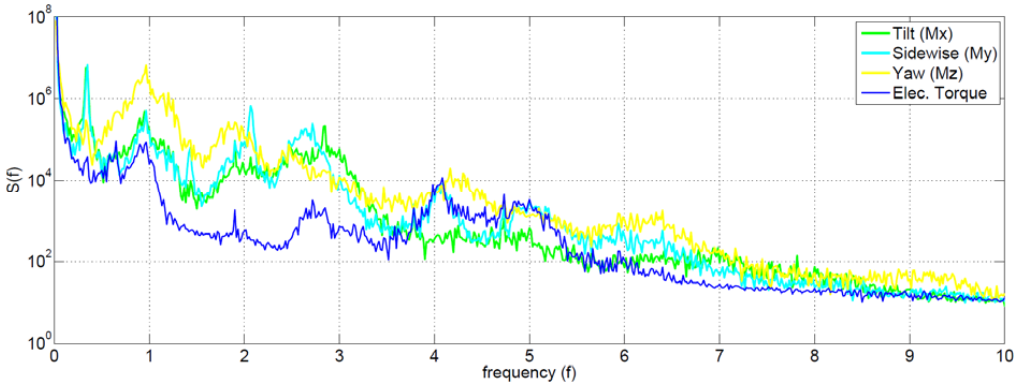

Figure 3: Spectrum of tower bottom bending moments and electromagnetic torque

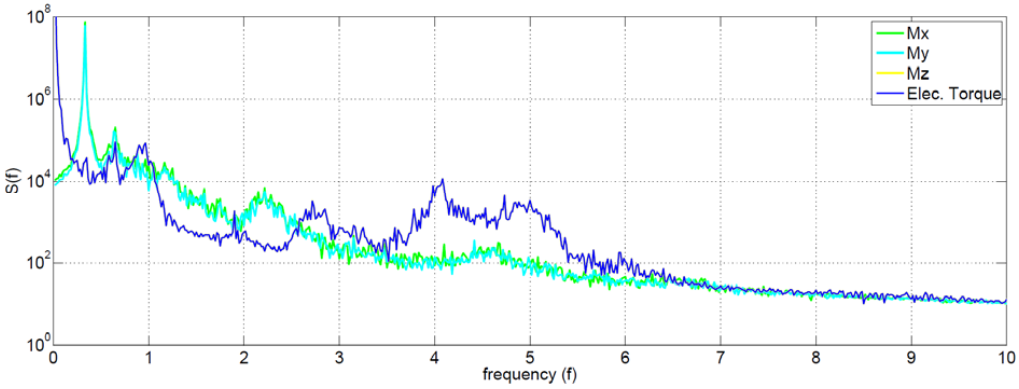

Figure 4: Spectrum of shaft bending moments and electromagnetic torque

European Academy of Wind Energy

Norwegian University of Science and Technology

Space-related conflicts over offshore wind farms

David Rudolph[1)]

[1)] University of Edinburgh, School of Geosciences, Human Geography Research Group, Scotland, United Kingdom

ABSTRACT

The ambitious expansion of offshore wind requires attention to a number of pertinent issues, not just technical and operational aspects. This research examines the conflicts over the use of offshore spaces which have been increasingly accompanying and hindering the implementation of offshore wind farms. The goal is to reveal and comprehend the background of multi-level conflicts over offshore wind farms. By focusing on case studies in Germany and Scotland, the research particularly explores conflicting interests, motivations, arguments, discourses and actions by affected stakeholders as well as various meanings ascribed to the offshore space that are supposed to determine the conflict situation.

KEYWORDS

offshore wind farms, stakeholders, space-related conflicts, Scotland, Germany

1 INTRODUCTION

Developing offshore wind farms has the benefits of exploiting better and continuous wind resources, overcoming the increasing scarcity of suitable onshore sites, and avoiding the growing criticism, land use conflicts and resistance which have accompanied onshore wind farms. All of these reasons have provided an increasing impetus for orientating towards the offshore area for the production of wind power during the last decade. However, the initial offshore projects have revealed that the assumption of a problem-free expansion of offshore wind farms is far from reality. The relocation of wind farms off the coast causes new and different problems. Thus, the development of offshore wind farms is likewise contested and accompanied by conflicts [1]. Such new types of obstacles need to be addressed if the intended expansion of offshore wind energy is to be fulfilled. This research is looking at previously neglected space-related conflicts and its significance in implementing offshore wind farms in different policy contexts. Perceptions, motivations, interests and practices of affected stakeholders as well as subjective interpretations and discourses of the offshore space are at the focal point of the research to gain further comprehension of the formation of

d.p.rudolph@sms.ed.ac.uk

resistance to offshore wind farms. These investigations – on what are described as 'space-related conflicts' – are being conducted and comparatively analysed for case studies in Germany and Scotland.

2 CONFLICTS OVER OFFSHORE WIND FARMS

Although the bulk of resistance to offshore wind farms seems to stem from local stakeholders and the community level, opposition to wind farms cannot simply be explained by the so called NIMBY-syndrome (not-in-my-backyard), which refers to a general support of projects unless someone is affected personally. The NIMBY-description has been commonly rejected [2] [3] and numerous different and more profound explanations have been applied in order to elucidate opposition to wind farms onshore and recently also offshore. So it is vital to deal with the wider context of resistance and oppositions to offshore wind energy projects to question and understand its formation.

2.1 From spatial conflicts to space-related conflicts

This research attempts to follow and expand previous efforts by looking explicitly at conflicts as a particular sort of obstacle for the realization of offshore wind farms, as concrete conflicts have widely been neglected for scrutinizing the generation of opposition. Conflicts as obstacles can be conceived as originating from various clashing spatial utilizations of the offshore area, which compete with each other. These spatial land use interests are claimed by a variety of stakeholders from different national and local levels, which cause multi-level conflicts. In detail, traditional interests in and use of the offshore space, such as shipping, recreation, fisheries, environmental protection etc., contend with the novel and growing wind energy sector for terrain in the offshore area. So, it can be argued that these land use or spatial conflicts are nothing else than conflicts of interest. This conception allows the opportunity to understand spatial conflicts as conflicts of utilization of different stakeholders, which are aimed at the offshore space. Since the starting point of examining spatial conflicts is not space but rather intersecting interests aimed at space [4], it is argued that the term 'space-related conflicts' is the most apt and useful here. Pursuing and enforcing the conflicting space-related interests causes obstacles during planning and approving procedures and, thus, often decelerates the realisation of offshore wind farms. Further implications and actual objectives of investigating space-related conflicts over offshore wind farms can be derived from these considerations, which also lead to novel insights in obstacles to offshore wind farms.

2.2 Objectives of research

The issues of space-related conflicts and the approval procedures are combined in the research objective of examining how conflicts shape and are dealt with in the institutional implementation of offshore wind farms. Accordingly, supplementary questions – which new conflicts emerge from moving wind farms offshore, who are the stakeholders and what interests they pursue, how they enforce their goals as well as the question of the role and meaning of spatial conditions – can be concluded from the overarching problem. Pursuing these particular questions is regarded as helping to widen the comprehension of the relationship between space-related conflicts and obstacles to offshore wind energy. In order to meet these requirements and to uncover conflicts the research project is directed to and examines the divergent space-related motivations, interests, arguments and strategies of stakeholders as well as the relevance of subjective meanings of the offshore space, which both create the conflict context. Turning attention towards different space-related interests, practices and discourses is crucial for understanding the conflict context, since the deployment of offshore wind farms is a process of transforming spatial conditions, which engenders different perceptions and results in active oppositions to wind farm projects. Hence, the research requires knowledge of divergent perceptions of offshore wind energy issues.

3 METHODOLOGY

In order to gain knowledge of space-related conflicts this research follows a qualitative methodology, which looks at a subjectively perceived world rather than objectively conceived realities [5]. A qualitative approach is preferred as individual positions, experiences, perceptions and interpretations of the conflict situation are at stake. The conflict situations of certain case studies are comparatively investigated.

3.1 Data acquisition & analysis

With the purpose of obtaining data of human interpretations, perceptions and practices, problem-centred and semi-structured interviews with affected stakeholders, as case-sensitive experts, are in the centre of the data acquisition. These conversations can help to reconstruct diverging positions of and disputes between stakeholders. Documents, statements and newspaper articles evidencing the conflict situation are additionally consulted. These data will be analysed using methods of stakeholder and discourse analysis in order to reveal underlying discourses of argumentations about offshore wind farms.

3.2 Case studies

The research presents an analytical insight into specific case studies. The contemplation of various case studies contributes to the examination and comparison of the conflict formation in different contexts and, thus, enables a focus on particularities, differences and commonalities of space-related conflicts. For this purpose offshore wind farms in Germany and Scotland are being investigated. Germany and Scotland have been selected as both countries have similar ambitious goals in promoting offshore wind energy, but are likewise at the beginning of their efforts. Despite parallel objectives of incorporating a large share of energy from offshore sources, the respective plans of both countries are embedded in different energy and environmental policies as well as decision-making and approval procedures, which also imply distinctions in dealing with potential conflict situations. At this point, case studies of planned and currently constructed wind farms are located at the western coast of Scotland (County Argyll) and in the Baltic Sea off the coast of Germany.

4 CONCLUSIONS

This research, which is empirically being conducted in Scotland and Germany, attempts to provide new insights in obstacles to the establishment of offshore wind farms by focusing on space-related conflicts. Drawing on space-related interests and practices, as well as on spatial conditions, is deemed to be worthwhile to understand the formation of resistance and opposition, which have been a major impediment of gaining wind energy from offshore sites. The findings of the research are anticipated to give suggestions for coping with or mitigating future conflicts.

BIBLIOGRAPHY

[1] Haggett, C. (2008): Over the Sea and Far Away? A Consideration of Planning, Politics, and Public Perception of Offshore Wind Farms. Journal of Environmental Policy & Planning, 10, 3, 289-306.

[2] Bell, D.; et al. (2005): The “Social Gap” in wind farm siting decisions: explanations and policy responses. Environmental Politics 14, 4, 460-477.

[3] Devine-Wright, P. (2005): Beyond NIMBYism: Towards an integrated framework for understanding public perceptions of wind energy. Wind Energy 8, 125-139.

[4] Werlen, B. (2007): Sozialgeographie alltäglicher Regionalsierungen. Vol.2. Globalsierung, Region und Regionalisierung. 2nd Edition.

[5] Flick, U. (2004): Constructivism. Flick, U.; et al.: A companion to qualitative research. Sage. London, 88-94.

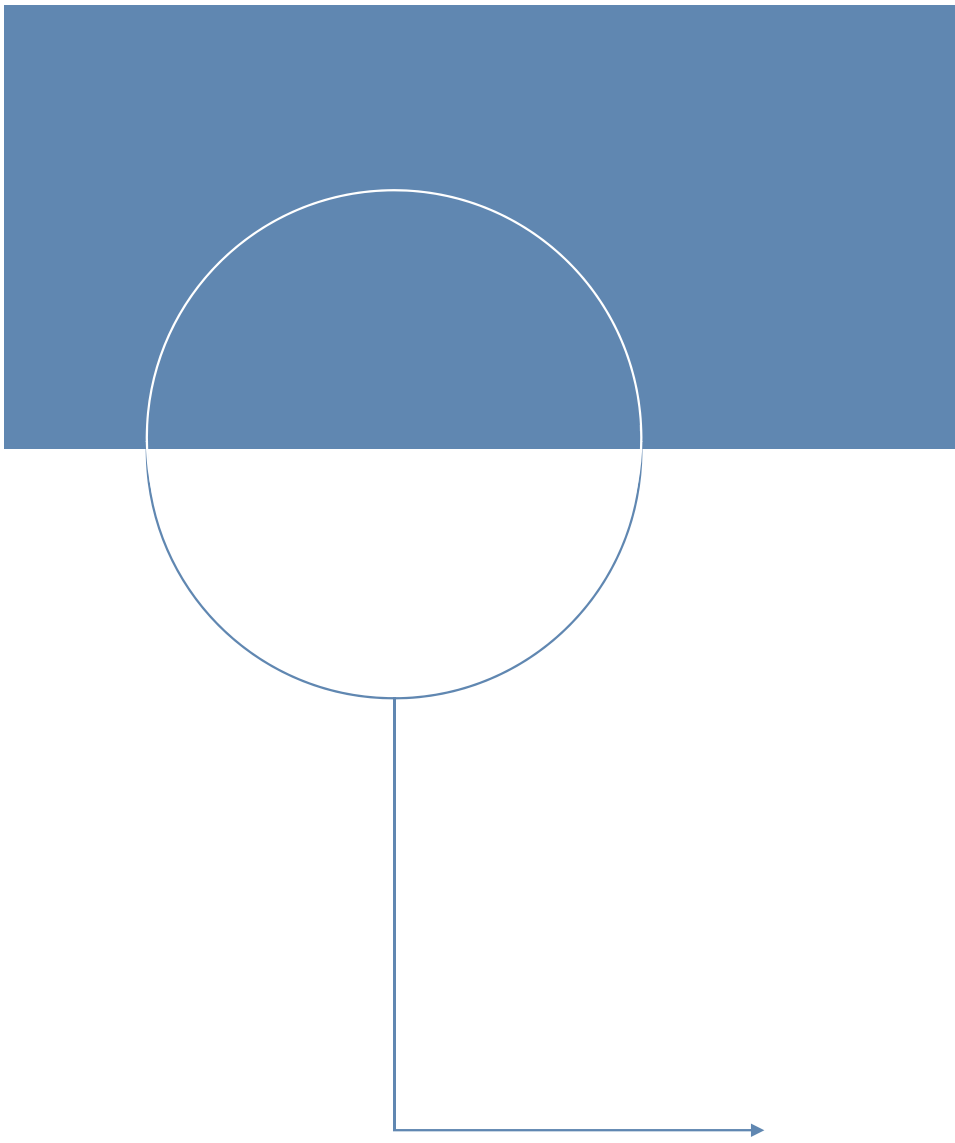

NTNU

Norwegian University of
Science and Technology